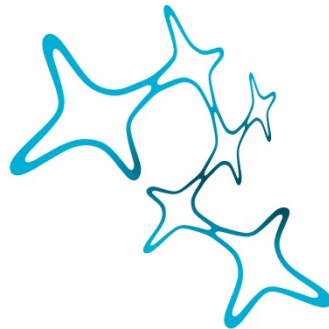

THE ROLE OF GRANULINS IN REGULATING ADULT ZEBRAFISH BRAIN HOMEOSTASIS AND REGENERATION

Alessandro Zambusi



Graduate School of
Systemic Neurosciences

LMU Munich



Dissertation der
Graduate School of Systemic Neurosciences
der Ludwig-Maximilians-Universität München

16th August, 2021

Supervisor
Prof. Dr. Jovica Ninkovic
Biomedical Center (BMC)-Institute for Cell Biology and
Anatomy
Faculty of Medicine
LMU Munich

Helmholtz Zentrum München
Institute of Stem Cell Research

First Reviewer: Prof. Dr. Jovica Ninkovic
Second Reviewer: Dr. Tim Czopka

Date of Submission: 16th August, 2021
Date of Defense: 16th December, 2021

Index

Abstract	5
Introduction	7
Hallmarks of brain aging	8
CNS responses to TBI	15
Cellular stress and liquid-liquid phase separation as sources of chronic neuroinflammation in the CNS	18
Zebrafish as model to study aging kinetics in the CNS	20
Zebrafish as model to study CNS regeneration	22
Neurogenic niches and neural stem cells in the adult zebrafish telencephalon..	23
Glial cells in the adult zebrafish telencephalon	24
Cellular and molecular responses to TBI in the adult zebrafish telencephalon..	26
Inflammation as positive contributor to restorative neurogenesis in the adult zebrafish telencephalon.....	29
Progranulin structure and expression in the CNS.....	31
PGRN as risk factor for aging and brain pathologies.....	31
PGRN as regulator of neuroinflammation and immune cell functions in the CNS	32
Four granulins (Grns) in the zebrafish brain	35
Results	36
Aim of the study I.....	37
Aim of the study II	69
Aim of the study III.....	103
Aim of the study IV	147
Discussion	202
Granulins regulate aging kinetics and neuroinflammatory state in the adult zebrafish telencephalon.....	203
Granulin-mediated regulation of phase-separated TDP-43 controls the activation states of microglia after TBI and promotes CNS regeneration	209
Bibliography	216
Curriculum Vitae	233
Publications	236
Eidesstattliche Versicherung/Affidavit	237
Declaration of author contributions	238
Acknowledgements	242

Abstract

Reduced neuronal functionality and poor neuronal recovery are among the most detrimental outcomes in aging individuals and patients with neurodegenerative diseases and/or traumatic brain injuries.

Therapeutic interventions face the major problems of effectively enhancing the generation of new neurons and limiting the secondary tissue damage in the CNS. The presence of long-lasting glial scar and chronic neuroinflammation hinders the survival and proper integration of the limited pool of new neurons in the pre-existing circuitry of the mammalian CNS.

In contrast to mammals, zebrafish possess numerous active stem cell niches during adulthood as constant source of neurogenesis and display extensive regenerative capacity in the CNS. The high regenerative potential correlate with the ability to inactivate the immune response in a timely manner, thus avoiding the long-lasting neuroinflammation observed in mammals. For these reasons, understanding the cellular and molecular mechanisms underlying the neurogenic potential and the regenerative capacity in the injured CNS of zebrafish may play a pivotal role in the development of new therapeutic approaches aimed to ameliorate the quality of life of aging individuals and patients with neurodegenerative diseases and/or with CNS injuries.

To this goal, I first validated the relevance of zebrafish as model to study the development and progression of established age-associated hallmarks, including reduced neurogenesis, exacerbated neuroinflammation and telomere shortening. Furthermore, I demonstrated the role of granulins in regulating the aging kinetics of the adult zebrafish CNS. Granulin-deficient zebrafish showed premature aging in the brain, displaying typical age-related hallmarks already during young adulthood.

Moreover, I extensively studied the regenerative response to a mild model of traumatic brain injury and characterized the activation and de-activation of microglial cells during the regenerative time course. I identified an injury-

induced pro-regenerative microglial population that is initially beneficial for regeneration but needs to be inactivated in a timely manner to prevent long-lasting neuroinflammation and tissue scarring. The pro-regenerative microglial population was characterized by accumulation of lipid droplets and phase-separated TDP-43 that were promptly cleared to complete regeneration. Furthermore, I demonstrated that granulins play a pivotal role in the regulation of microglial de-activation, promoting the clearance of lipid droplets and phase separated TDP-43 in microglial cells, subsequently stimulating their transition back to homeostasis. The translational value of my research is strengthened by the presence of enhanced microglial reactivity associated with lipid droplets and TDP-43 condensates in human patients with stroke.

Altogether, the core data I present in this thesis identified granulins as key regulators of aging kinetics and regeneration in the adult zebrafish CNS, making them valuable targets for the development of new therapeutic applications aimed to ameliorate age-associated hallmarks and pathological outcomes caused by traumatic brain injuries in human patients.

Introduction

The human brain is one of the most complex organs in our body. Billions of different cells are perfectly interconnected, working as an orchestra sustaining a complex network that shapes our daily life. The Central Nervous System (CNS) receives and integrates information of the reality around us through our senses and coordinates the function of several organs in our body. Because of its delicacy, the CNS requires maximum protection, offered by the hard bone of the skull, three additional membranes, called meninges, and the blood-brain barrier (BBB), a barrier that safely prevents the entrance in the brain of harmful pathogens and substances.

Unfortunately, several disturbances can perturb the tightly regulated CNS, thus leading to the onset of neuropathologies that affect the quality of life of numerous patients worldwide. The impact of aging, traumatic brain injuries (TBI), and neurodegenerative diseases, such as Alzheimer's disease (AD), Parkinson's disease (PD), amyotrophic lateral sclerosis (ALS), multiple sclerosis (MS) and frontotemporal dementia (FTD), increases considerably in our society, leading to numerous deaths and disabilities, including cognitive and physical impairments (Stocchetti and Zanier, 2016; Winblad et al., 2016). For this reason, it is fundamental that the causes and mechanisms underlying the abovementioned pathologies are characterized in order to develop new therapies to ameliorate the quality of life of more than 50 million patients affected worldwide (Stocchetti and Zanier, 2016; Winblad et al., 2016).

To tackle these topics, I will first describe the hallmarks of aging and their consequences on CNS functions. I will then introduce and compare the cellular and molecular responses to TBI in mammals and zebrafish, specifically focusing on similarities and differences underlying microglial cell activation and de-activation. I will describe and highlight the importance of liquid-liquid phase separation (LLPS) as growing evidence supports its relevance in the context of brain injuries and neurodegenerative diseases. Finally, I will introduce granulins as targets of my research project, describing their known roles in the intact and injured CNS.

Hallmarks of brain aging

Aging can be defined as a series of alterations that affects living organisms, progressively reducing the functional capabilities of different organs (López-Otín et al., 2013; Mattson and Arumugam, 2018). The CNS, as well as other organ systems, is not spared by aging progression that can eventually result in dramatic motor and cognitive deficits (Alexander et al., 2012; Levin et al., 2014). In addition to such disabilities, brain aging is the main risk factor for the development of most neurodegenerative diseases, including AD and PD (Hou et al., 2019).

Aging research has advanced rapidly over the last years to identify genetic and biochemical mechanisms regulating brain aging. This research has led to the identification and categorization of several cellular and molecular hallmarks of brain aging that include: (1) mitochondrial dysfunction and dysregulated energy metabolism; (2) intracellular accumulation of radical oxygen species (ROS) and lipids; (3) impaired autophagosome and proteasome functions; (4) dysregulated neuronal calcium ion (Ca^{2+}) influx and efflux; (5) telomere attrition; (6) exhaustion of stem cell pool; (7) exacerbated inflammation (Figure 1) (Mattson and Arumugam, 2018). It is worth mentioning that the majority of aging hallmarks just defined have also been identified in the aging CNS of zebrafish, strengthening the validity of this model to study and compare cellular and molecular mechanisms of brain aging (Van houcke et al., 2015).

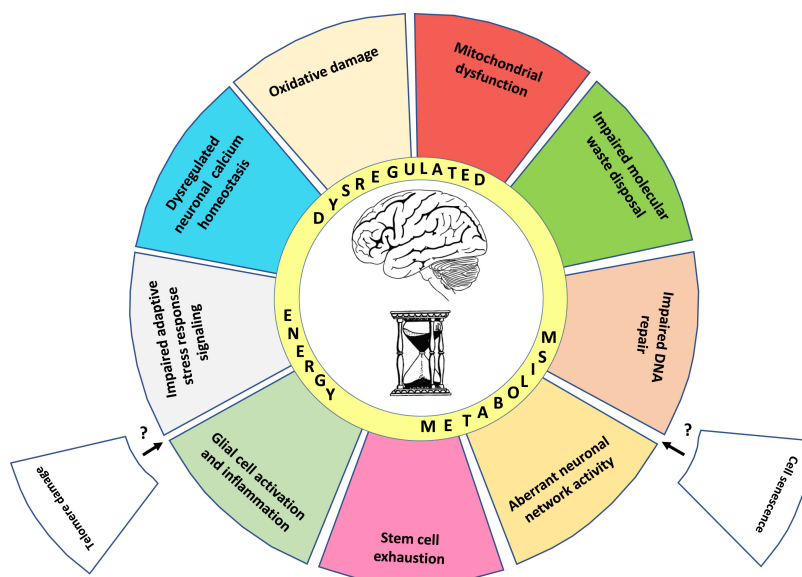


Figure 1. Age-related hallmarks in the brain (Mattson and Arumugam, 2018. License Number: 5081820121589).

The brain is an energy-demanding organ that requires 20% of body oxygen to properly function. A high percentage of cellular energy is produced as adenosine triphosphate (ATP) via oxidative phosphorylation (OXPHOS) within mitochondria (Mattson et al., 2008). However, while performing their physiological functions, mitochondria induce the formation of reactive oxygen species (ROS), which can become harmful if not properly disposed and buffered (Mattson and Arumugam, 2018; Mattson et al., 2008). Numerous studies have demonstrated the aging impact on mitochondria within cells in the CNS and revealed a number of age-related mitochondrial changes, including mitochondrial enlargement and fragmentation (Stahon et al., 2016), increased oxidative damage to mitochondrial DNA localized in proximity to the free radical production sites (Keil et al., 2004), impaired Ca²⁺ signaling (Calvo-Rodriguez et al., 2020) and dysfunctional electron transport chain (ETC) (Adav et al., 2019).

Age-related changes in mitochondria have a strong impact on several cells in the brain, and particularly on neurons. In fact, neurons are post-mitotic cells that are rarely replaced during life. With aging, neurons accumulate pathological proteins and aggregates that need to be degraded by proteasomes and lysosomes to avoid neurodegeneration. Furthermore, dysfunctional mitochondria produce excessive amounts of ROS that need to be buffered by antioxidant defenses to maintain neuronal integrity and survival. Failure to do so may result in the appearance of age-related diseases and neuronal degeneration (Paul et al., 2007).

Lipids have also been found to accumulate within cells in the aging CNS and their aberrant accumulation in lipid droplets (LDs) has been identified as a factor contributing to immune cell dysfunction and exacerbated inflammation in the aging brain (Farmer et al., 2020; Marschallinger et al., 2020).

LDs are lipid storage organelles, mainly containing neutral lipids such as glycerolipids and cholesterol, which can act as first-line intracellular defense, promoting the activation of innate immunity (Bosch et al., 2020). As pathogens often target host lipids in order to support their life and propagation (Libbing et al., 2019), LDs can act as hubs to organize the host defense. Specifically, clusters of immunity-related proteins are found within

LDs in response to infection, and are able to efficiently direct immune cells to target intracellular pathogens (Bosch et al., 2020).

Another mechanism of defense is represented by the physical separation of LDs and mitochondria in response to infection. This separation represents a mechanism to reduce mitochondrial damage and to increase the amount of LDs interacting with pathogens (Bosch et al., 2020).

Nonetheless, lipid metabolism needs to be tightly regulated to avoid marked progression of numerous pathologies, including atherosclerosis, ALS, AD and PD (Farmer et al., 2020; Hamilton et al., 2015; Pennetta and Welte, 2018). As an example, excessive accumulation of LDs in macrophages that display senescence markers has been found to be detrimental in atherosclerotic lesions as it accelerates pathology progression by enhanced expression of inflammatory cytokines and chemokines (Childs et al., 2016).

During aging, microglial cells, resident immune cells of the CNS, lose their homeostatic signature, increase the expression of pro-inflammatory cytokines and chemokines, display elevated levels of ROS and accumulate dysfunctional lysosomes (Mosher and Wyss-Coray, 2014). Interestingly, it has been demonstrated that microglia within aging brain also accumulate LDs and exhibit a unique phenotype, characterized by elevated expression of cytokines, defects in phagocytosis and high levels of ROS. These results have been confirmed by validation in *Grn*-deficient mice (Marschallinger et al., 2020), a model for FTD (Snowden et al., 2006; Wils et al., 2012), indicating that LDs can actively contribute to the development of age-related pathologies and neurodegenerative diseases.

As previously mentioned, the removal of pathological aggregates and dysfunctional organelles is a key defense in the CNS and is particularly important in neurons. Damaged cellular components are identified, targeted and degraded by specific cellular components, including lysosomes via autophagy and proteasomes. In the case of autophagy, damaged molecules, aggregates or dysfunctional organelles are enclosed in the phagosome which then fuses with lysosomes. The formation of the phago-lysosome is followed by release of hydrolases which degrade the targeted species (Galluzzi et al., 2017). Proteins that undergo proteasomal degradation are targeted by

ubiquitination, performed by a complex of four enzymes (E1, E2, E3, E4) that produce complex ubiquitylation patterns, recognized by the proteasome and subsequently degraded (Tai and Schuman, 2008). With aging, neuronal autophagy is impaired and results in the accumulation of autophagosomes with undegraded aggregates and lipids, and dysfunctional mitochondria. Proteasomal degradation is also affected as elevated numbers of polyubiquitinated proteins are detected in neurons within aging brain (Mattson and Arumugam, 2018).

Ca²⁺ is a key regulator of neuronal circuitry. Upon release of excitatory neurotransmitter glutamate, sodium ion (Na⁺)-AMPA receptors are activated in postsynaptic dendrites. The activation of AMPA receptors results in the depolarization of the membrane and Ca²⁺ influx through N-methyl-D-aspartate (NMDA) glutamate receptors and voltage-gated Ca²⁺ channels. The transient increase of cytosolic Ca²⁺ modulates the expression of kinases and phosphatases, regulating the phosphorylation of proteins in dendrites, promoting cytoskeletal remodeling, local protein synthesis and neuronal plasticity (Cohen et al., 2015; Kindler and Kreienkamp, 2012; Mattson, 2012). During aging, neuronal regulation of Ca²⁺ dynamics is compromised, leading to increased concentration of cytoplasmic Ca²⁺, which subsequently leads to dysregulation of protein phosphorylation and gene expression (Gant et al., 2006). Furthermore, abnormal concentration of intracellular Ca²⁺ can directly promote the activation of calpains and trigger caspase-mediated apoptosis and PARP1-mediated cell death, thus leading to neuronal damage and death (Mattson, 2000).

Ca²⁺ regulatory functions are not limited to neurons. Other non-excitable cells, including microglia, are affected by changes in Ca²⁺ concentration (Brawek et al., 2021; Mizoguchi and Monji, 2017; Del Moral et al., 2019; Wang et al., 2019). In physiological conditions, Ca²⁺ signaling has low incidence on microglial functions. However, in response to disturbance of tissue homeostasis, Ca²⁺ signaling become important for several processes in microglial cells, including proliferation, migration and secretion of pro-inflammatory molecules (Brawek et al., 2021; Mizoguchi and Monji, 2017; Del Moral et al., 2019; Wang et al., 2019). Notably, during aging microglial cells

respond to smaller changes in Ca^{2+} and, as Ca^{2+} signaling is also involved in regulation of phagocytosis, this observation correlates with microglial reduced phagocytic activity and dysfunctionality (Brawek et al., 2021; Del Moral et al., 2019). These results indicate that Ca^{2+} signaling is not only involved in the regulation of excitable cells (neurons) but also non-excitable cells (microglia), making it an important process to be studied to further characterize the development of a dysfunctional phenotype in microglial cells during aging.

The terminal part of eukaryotic chromosomes are capped by telomeres, arrays composed by TTAGGG repeats (Moyzis et al., 1988). Telomere-specific proteins, including TRF1, TRF2, POT1, TIN2, TPP1 and Rap1, form a complex known as shelterin and protect chromosome ends. This mechanism is required to distinguish telomeres from site of DNA damage, inhibiting the activation of the canonical DNA damage response that would target and process chromosome ends by DNA repair (De Lange, 2005). Lack of shelterin protective activity leads to telomere dysfunction, which can subsequently result in apoptosis or senescence (Karlseder et al., 1999).

In addition to possible damages caused by shelterin dysfunction, telomeres can be particularly susceptible to telomere shortening with each round of cell division in cells lacking telomerase activity (López-Otín et al., 2013; Mattson and Arumugam, 2018). In the majority of differentiated somatic cells that do not display sufficient expression of telomerase (Kim et al., 1994) - a specialized DNA polymerase that has the capacity to replicate the terminal ends of linear DNA molecules - telomeres are shortened to critical length and can trigger specific DNA-damage responses (DDR). These responses can subsequently lead to cell-cycle arrest, also known as “replicative senescence” (D’Adda Di Fagagna et al., 2003).

The direct link between aging and telomeres has been shown by studies demonstrating that mutations in telomere-protective genes are sufficient to cause the premature onset of age-related pathologies (Armanios et al., 2009). Notably, the premature aging phenotype developed by telomerase-deficient mice can be rescued by genetic re-activation of telomerase activity in aging mice (Jaskelioff et al., 2011). Furthermore, aging kinetics can be delayed

without increasing the incidence of cancer in adult mice by targeted activation of telomerase (Bernardes de Jesus et al., 2012).

Lastly, it is important to mention that age-associated telomere shortening is evolutionary conserved across different species and it has been described, among others, in humans, mice and zebrafish (Blasco, 2007; Carneiro et al., 2016).

It has been previously demonstrated that reduced telomerase activity is sufficient to negatively regulate adult neural stem cells (aNSCs) within the aging brain, reducing their neurogenic potential (Blasco, 2007; Ferrón et al., 2004).

The decline in stem cell potential and neurogenesis is an established aging hallmark affecting all stem cell compartments, including those in the brain (Kalamakis et al., 2019; Molofsky et al., 2006; Villeda et al., 2011). Studies focused on age-related changes within the neurogenic niche in the dentate gyrus (DG) of the hippocampus have revealed decreased neurogenesis and increased neuroinflammation, deficits in synaptic plasticity and additional behavioral deficits connected to decreased cognitive functions (Lazarov et al., 2010; Villeda et al., 2011). Interestingly, the reduced functions of NSC/progenitor cells may result from the complementary effect of both age-related cell intrinsic (i.e. changes in $p16^{INK4A}$ expression and mitochondrial dysfunction) and systemic changes (neuroinflammation).

The tumor suppressor $p16^{INK4A}$, which encodes a cyclin-dependent kinase inhibitor playing a key role in senescence and increasing during aging, has been shown to reduce cancer incidence, limiting stem cell proliferation and neurogenesis in the mouse forebrain (Molofsky et al., 2006).

Mitochondrial dysfunction and lower ATP levels have also been detected together with diminished hippocampal neurogenesis during aging, in line with previous reports of age-associated impairment of oxidative metabolism in aNSCs isolated from the mouse forebrain (Beckervordersandforth et al., 2017).

In the subependymal zone (SEZ), the pool of NSCs is depleted during aging and a higher fraction of NSCs are quiescent, as compensatory mechanism to avoid the full depletion of stem cell pool (Bast et al., 2018; Kalamakis et al.,

2019; Piccin et al., 2014). Nonetheless, once activated, young and old NSCs display similar behaviors in regard of proliferation and differentiation capacity. Furthermore, single-cell RNA sequencing analyses have demonstrated that aging causes only limited changes in the transcriptome of NSCs (Kalamakis et al., 2019), suggesting that systemic age-related changes affecting the neurogenic niches may be the main determinants of limited stem cell activation within the aging brain.

Notably, the age-dependent increased expression of inflammatory genes have been detected in the neurogenic niche of old mice, supporting the abovementioned hypothesis (Kalamakis et al., 2019). More specifically, higher systemic expression of blood-related pro-inflammatory chemokines, including CCL11, was detected in old animals and has been shown to directly affect NSC activation and neurogenesis (Kalamakis et al., 2019; Villeda et al., 2011). Interestingly, increasing the expression of CCL11 in adult mice was sufficient to recapitulate the phenotype observed in aging mice (Villeda et al., 2011), establishing a causal link between inflammation and NSC quiescence.

Microglia are myeloid-derived glial cells surveying the CNS environment to identify and eliminate detrimental aggregates and pathogens (Nimmerjahn et al., 2005). Microglial functions in the healthy brain also include the regulation of neuronal circuit maturation, particularly during early development, and the remodeling of neuronal network by synaptic pruning, resulting in synaptic plasticity during adulthood (Szepesi et al., 2018; Wu et al., 2015). For this reason, it is important that aberrant microglial activation is prevented to avoid uncontrolled synaptic pruning due to over-production of cytokines and complement factors that could subsequently lead to neurodegeneration and behavioral deficits (Lui et al., 2016).

Different stimuli, including neuronal damage or death, can lead to microglial activation via release of ATP or cytokines, changes in ion concentration, or loss of inhibitory molecules secreted by healthy neurons (Hanisch and Kettenmann, 2007). The proper execution of microglial functions, fundamental to protect the CNS, deteriorates with age, leading to dysfunctionality and hyper-reactivity.

CNS inflammaging, a term used to define the alteration of a wide range of inflammatory processes during aging (Franceschi et al., 2000), is characterized by a significant increase of complement factors, inflammatory cytokines and chemokines, and glial cell activation (Lucin and Wyss-Coray, 2009). Microglial activation during aging can be identified by numerous hallmarks that include the acquisition of amoeboid morphology, the secretion of inflammatory cytokines, such as interleukins and tumor necrosis factor α (TNF- α) (Cribbs et al., 2012), the enhanced activation of the NF- κ B signaling pathway resulting in the exacerbated activation of the NLRP3 inflammasome, and the secretion of complement factors involved in synaptic pruning (Lui et al., 2016; Stephan et al., 2013).

In addition to these features, age-related microglia display elevated levels of ROS (e.g. nitric oxide (NO)) and impaired phagocytosis (Mosher and Wyss-Coray, 2014).

As previously mentioned, the excessive production of ROS and the presence of unbuffered oxidative stress is detrimental for neuronal survival. Activation of microglial NADPH oxidase is among the primary sources of ROS production and the expression levels of NADPH oxidase enzyme NOX2 is elevated in aging brains, contributing to the elevated levels of oxidative stress (Qin et al., 2013). Furthermore, it has been demonstrated that increased production of ROS can directly stimulate the activation of the NLRP3 inflammasome, creating a positive feedback loop between immune cell activation, production of pro-inflammatory cytokines and oxidative stress (Zhou et al., 2011). The dysregulation of the abovementioned inflammatory processes during aging significantly impairs the mechanisms necessary for clearing misfolded or damaged neuronal proteins. This results in tau-associated pathologies, formation and accumulation of amyloid precursor protein (APP) and synaptic deficits, events that precede and/or accelerate neurodegeneration and cognitive decline (Sochocka et al., 2017).

CNS responses to TBI

Poor recovery and limited neuronal functions are the common denominators of aging, neurodegenerative diseases and TBI affecting the CNS. However,

the CNS responses to aging and neurodegenerative diseases, considered as chronic injuries, significantly differ from those triggered in response to TBI, considered as acute or focal injuries.

Furthermore, TBI can be extremely heterogeneous, inducing distinct pathological changes, making it difficult to develop effective therapeutic interventions.

In addition to the immediate neuronal loss and increased neuroinflammation (acute and subacute phases), TBI can cause chronic changes resulting in secondary pathological outcomes, such as seizures, neurodegenerative diseases and psychiatric disorders (Bramlett and Dietrich, 2015; Stocchetti and Zanier, 2016).

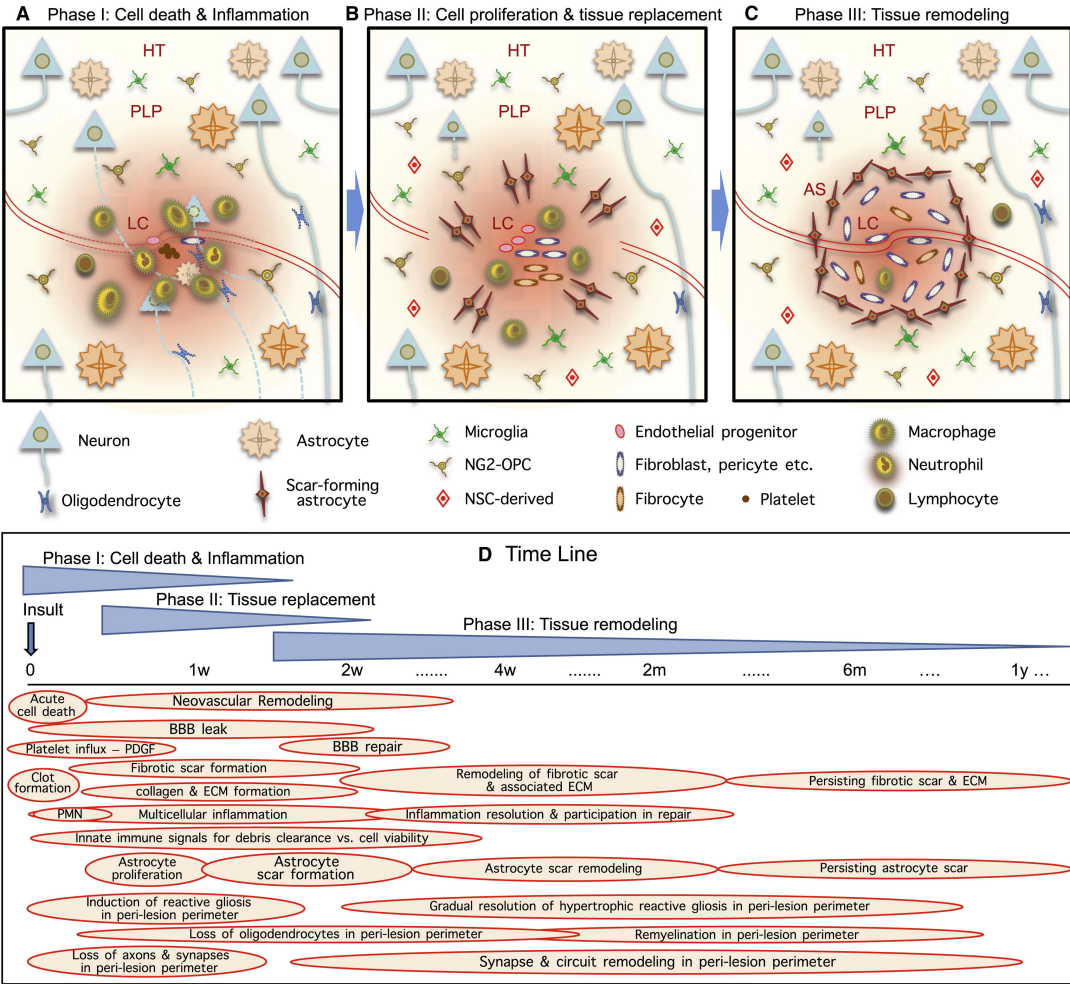


Figure 2. Phases and time course of cellular responses and processes activated in response to acute damage in the CNS (Burda and Sofroniew, 2014. License Number: 5100660178497).

During the first phase, TBI causes acute local cell death, axonal damage and blood vessel disruption, followed by influx of platelets that promptly form aggregates necessary for hemostasis (Figure 2) (Moore et al., 2021). The

secondary damage, developing minutes to month after the injury, includes excitotoxicity by excess of glutamate and elevated concentration of intracellular Ca^{2+} (Luo et al., 2019). Shortly after the injury, the concentration of glutamate increases at synapses, activating glutamate receptors, including NMDA receptors, which lead to Ca^{2+} -mediated excitotoxicity (Luo et al., 2019).

Damage associated molecular patterns (DAMPs), including ATP, are generated and released into the extracellular space and interact with different species of receptors, including Toll-like receptors (TLRs), nucleotide-binding oligomerization domain (NOD) like receptors (NLRs) and purinergic receptors to further enhance the inflammatory cascade and limit the damage in the CNS (Bramlett and Dietrich, 2015; Burda and Sofroniew, 2014; Jassam et al., 2017).

As an example, ATP resulting from TBI can elicit the response of purinergic receptors P2RY12 that play an active role in microglia migration at injury sites and microglia activation accompanied by morphological changes (Davalos et al., 2005; Haynes et al., 2006).

The release of DAMPs prompts CNS-resident cells, including astrocytes and microglia, to enhance the production and secretion of pro-inflammatory cytokines, such as IL-1 β , IL-6 and TNF, and ROS, thus fueling neuroinflammation. The existence of this type of inflammatory positive feedback loop further stimulates the recruitment at injury sites of additional immune cells, including neutrophils and macrophages, in order to clear debris and dead cells to promote wound healing (Alam et al., 2020).

Additional responses to TBI include the disruption of the BBB (Johnson et al., 2018). BBB leakage is a common feature of focal injuries in the brain facilitating the recruitment of neutrophils, macrophages and lymphocytes at injury sites (Alam et al., 2020).

The second response phase to acute injuries in the CNS is defined by increased proliferation and migration of cells involved in tissue repair (Figure 2). Fibroblast, pericytes, immune cells, scar-forming astrocytes and neuron-glia antigen 2-positive (NG2⁺) glia generate two structures defining the mature lesion, the fibrotic scar at the core of the injury (Dorrier et al., 2021) and the glial scar surrounding the lesion core (Adams and Gallo, 2018).

The glial scar in the CNS is primarily formed by three cell types: reactive astrocytes, NG2⁺ glia and microglial cells (Bellver-Landete et al., 2019; Buffo et al., 2005; Burda et al., 2016; Dimou and Gotz, 2014). Although it is typically considered a barrier preventing CNS regeneration, the formation of the glial scar is also beneficial to limit and separate the non-functional tissue from the healthy area, avoiding excessive spreading of inflammation in the surrounding areas of the CNS (Adams and Gallo, 2018; Burda and Sofroniew, 2014; Frik et al., 2018).

The third response phase to acute injuries in the CNS includes tissue remodeling, with BBB repair and re-organization of both fibrotic and glial scars, and long-lasting events that include chronic neuroinflammation (Figure 2). New blood vessels are generated in the vicinity of the damaged area and both astrocytes and pericytes are necessary for this process (Bhowmick et al., 2019; Michinaga and Koyama, 2019).

Lastly, it is important to mention that the lesion core, the glial scar and the peri-lesion areas undergo chronic remodeling, with significant changes in the extracellular matrix (ECM) composition and in the neuronal circuitry (Burda and Sofroniew, 2014). Notably, these events have the impact to define the functional outcomes of regeneration in the mammalian CNS.

In addition to the direct consequences of TBI explained above, growing evidence supports the concept that TBI may act as major risk factors for the onset of neurodegenerative diseases, including AD, ALS and chronic traumatic encephalopathy (CTE) (Jassam et al., 2017). Long-lasting neuroinflammation induced by TBI is proposed to be the major determinant of this phenomenon. For this reason, a better characterization of the inflammatory response to TBI and the window of intervention to modulate its progression and development are necessary to tailor regenerative therapies based on the type and stage of the injury in the CNS.

Cellular stress and liquid-liquid phase separation as sources of chronic neuroinflammation in the CNS

The activation of microglial cells in the mammalian CNS is tightly regulated by the balance between activating “ON” and inactivating “OFF” signals.

Notably, partial or complete loss of “OFF” signals, such as triggering receptor expressed on myeloid cells 2 (TREM2) or progranulin (PGRN), is sufficient to induce dysfunctional disease-associated microglia (DAM), contributing to the onset and progression of neurodegenerative diseases (Deczkowska et al., 2018; Götzl et al., 2019).

As previously mentioned, in response to TBI in the mammalian CNS, the inflammatory response is not promptly terminated, thus leading to chronic neuroinflammation and inadequate regenerative outcomes.

Among others, injury-induced cellular stress is now considered as a key factor sustaining long-lasting neuroinflammation, enhancing the production and secretion of inflammatory mediators and contributing to overruling the activation of “OFF” signals necessary to promote microglial de-activation in response to TBI (Anderson et al., 2018; Wiesner et al., 2018).

Multiple acute stress signals, including biotic stress (e.g. infections) or environmental stress (e.g. TBI, heat, oxidation) (Panas et al., 2016), can induce the formation of stress granules (SGs) (Anderson et al., 2018; Wiesner et al., 2018). SGs are cytoplasmic membrane-less organelles belonging to the RNA granule family, composed of RNA-binding proteins (RBPs) and untranslated mRNAs (Molliex et al., 2015; Protter and Parker, 2016; Roden and Gladfelter, 2021). SGs are transiently formed in the cytoplasm of stressed cells via liquid-liquid phase separation (LLPS), a reversible unmixing of molecules into two separate phases, one dilute and one condensed phase, in constant exchange with each other (Alberti et al., 2019; Shin and Brangwynne, 2017). In response to stress, cells inhibit global protein translation, mRNAs are released from polysomes and form condensates with scaffold RBPs, such as Ras GTPase-activating protein-binding protein 1 (G3BP1), undergoing LLPS with proteins and unfolded mRNAs and forming SGs (Alberti and Hyman, 2021; Shin and Brangwynne, 2017). If the damage is repaired and the source of stress is removed before a critical no-return point, SGs are disassembled and translation starts again (Anderson and Kedersha, 2002).

However, several factors can contribute to the permanent formation of SGs in the cytoplasm, thus causing the onset of pathologies in the CNS (Yu et al., 2020). Dysregulated accumulation of RBPs, such as fused in sarcoma (FUS)

and TAR DNA-binding protein 43 (TDP-43), into persistent SGs play an important role in the pathophysiology of numerous neurodegenerative diseases (including AD, FTD and ALS), leading to pathological aggregates of disease-associated proteins (Bentmann et al., 2012, 2013; Hofweber et al., 2018; Wolozin and Ivanov, 2019).

Interestingly, it has been demonstrated that failure to resolve SGs is also detrimental for microglial functions, limiting their phagocytic activity, and that excessive inflammation can enhance the formation of SGs (Ghosh and Geahlen, 2015; Herman et al., 2019), suggesting the existence of a positive feed-forward loop between inflammation and cellular stress detrimental for cell survival.

SGs also constitute signaling hubs, contributing to the modulation of pathways by sequestering signaling factors (Kedersha et al., 2013; Protter and Parker, 2016). Proteins and enzymes recruited to SGs include adaptors, lipid kinases, phosphatases and ubiquitin modifying enzymes. As an example, TNF receptor associated factor (TRAF) 2, an adaptor protein linking the TNF receptor to the signaling pathway activating NF- κ B, is recruited to SGs, thus blocking the activation of downstream NF- κ B signaling (Kedersha et al., 2013).

For these reasons, a better understanding of the link between TBI and SG formation via LLPS would be important to break an additional barrier preventing the resolution of chronic neuroinflammation and persistent glial scar in the mammalian CNS, thus hindering its regeneration.

Zebrafish as model to study aging kinetics in the CNS

Although our knowledge of the aging mechanisms has significantly improved in the last years, we still have much to explore and understand. To this goal, numerous models with different lifespan and evolutionary distance from mammals, including *Caenorhabditis elegans*, *Nothobranchius furzeri* and *Danio rerio* (zebrafish), have been used and characterized in the context of aging. Zebrafish are currently recognized as aging model as their life span is short, but they still display gradual aging progression as humans.

Furthermore, numerous age-related hallmarks in the human CNS have also been identified in zebrafish (Van houcke et al., 2015). Comparably to other vertebrates, zebrafish display age-related increase of DNA fragmentation, and elevated rate of apoptosis and hypomethylation (Shimoda et al., 2014), typical features of genomic instability in the aging CNS. Furthermore, zebrafish possess human-like telomeres that progressively shorten with aging, together with reduced telomerase expression (Carneiro et al., 2016). As previously described, the aging mammalian CNS is characterized by elevated ROS levels and mitochondrial dysfunction, aggravated by reduced mitochondrial turnover. Although not extensively studied, it has been demonstrated that protein oxidation in zebrafish increases with age (Ruhl et al., 2015), while antioxidant activity is reduced (Almaida-Pagán et al., 2014). These results suggest that in the aging zebrafish CNS, oxidative stress responses are comparable to those observed during aging in the mammalian CNS. Furthermore, it has been determined that the lipid composition of mitochondrial membrane in zebrafish is affected by aging, with decreased levels of phosphatidylinositol and cardiolipin, a feature that has also been associated to mitochondrial dysfunction in the aging brain of mammals (Almaida-Pagán et al., 2014; Chicco and Sparagna, 2007).

In contrast to mammals, zebrafish possess numerous niches actively contributing to neurogenesis during adulthood (Chapouton et al., 2007; Diotel et al., 2020; Grandel et al., 2006; Kaslin et al., 2009). Nonetheless, similarly to mammals, the stem cell pool progressively exhaust with aging (Edelmann et al., 2013). As consequence of the increased quiescence of NSCs, the neurogenic potential in the zebrafish CNS declines progressively with aging (Edelmann et al., 2013). Oligodendrogenesis within the zebrafish telencephalon is also reduced with aging, with fewer oligodendrocyte-precursor cells (OPCs) detected in old animals (Edelmann et al., 2013). The age-dependent reduction of both neurogenesis and oligodendrogenesis could significantly contribute to the limited regenerative capacity observed in the aging zebrafish CNS (Edelmann et al., 2013), characterized by the impossibility to replace lost neurons and by low remyelination rate (Graciarena et al., 2014).

To conclude, although mostly studied for their value as models for development and regeneration, zebrafish can be considered a valuable alternative for gerontology research aimed to further characterize the mechanisms of aging in the CNS. Comparably to mammals, zebrafish display numerous age-related hallmarks that progressively lead to CNS dysfunction. This concept, together with the short zebrafish lifespan, further corroborates the validity of using zebrafish as model to investigate both the aging kinetics and the causes underlying age-associated neurodegenerative diseases.

Zebrafish as model to study CNS regeneration

Oppositely to mammals, zebrafish have the capacity to regenerate and recover the lost functions of numerous vital organs, including the CNS. As previously mentioned, TBI represent a great burden to patients and society, calling for the development of new therapies. To tackle this problem, several approaches are possible, including the comparison between non-regenerative (mammals) and regenerative (zebrafish) models to identify similarities and differences that could be exploited to improve the regenerative outcome in the human CNS.

For long time, it has been speculated that the driving force promoting regeneration in the zebrafish CNS was the presence of numerous active neurogenic niches even during adulthood (Chapouton et al., 2007; Diotel et al., 2020; Kaslin et al., 2008).

However, it should not be forgotten that, although limited, neurogenic niches are also present in the mammalian brain (Boldrini et al., 2018), supporting the idea that additional mechanisms may differentiate the regenerative progression in the CNS of mammals and zebrafish.

An additional factor that significantly contributes to CNS regeneration in zebrafish is the transient activation of neuroinflammation, which, differently from mammals, is terminated in a timely manner to achieve complete resolution of glial scar, and promote neuronal integration and survival (Di Giaimo et al., 2018; Kyritsis et al., 2012).

Numerous regenerative programs have been identified in zebrafish and can be divided in three specific classes: 1) development-associated programs re-

activated in response to TBI; 2) injury-associated programs exclusively activated in response to TBI; 3) development-associated or constitutive programs with distinct functions in response to TBI (Figure 3) (Zambusi and Ninkovic, 2020).

Before describing them in a comprehensive manner, I will provide some introductory notions on the cellular composition of the neurogenic niches and the parenchyma of the adult zebrafish telencephalon, one of the most well studied areas of the zebrafish CNS in the context of neurogenesis and regeneration.

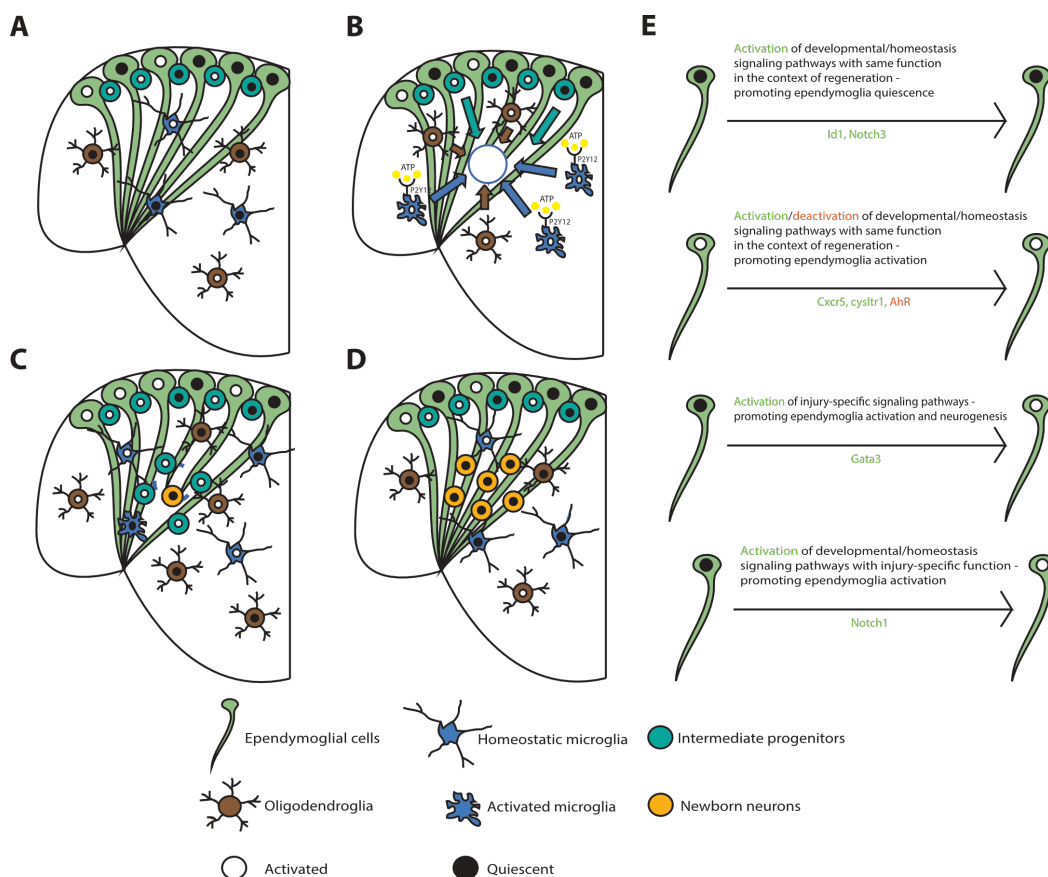


Figure 3. Cellular and molecular responses activated in response to TBI in the adult zebrafish telencephalon (Adapted from Zambusi and Ninkovic, 2020. This is an open access article distributed under the terms of the Creative Commons Attribution-Noncommercial (CC-BY-NC 4.0) License, which permits use, distribution and reproduction in any medium, provided the original work is properly cited).

Neurogenic niches and neural stem cells in the adult zebrafish telencephalon

Due to the everted nature of the zebrafish telencephalon, the ventricular zone (VZ) is located at the outer surface of the adult zebrafish telencephalon (Folgueira et al., 2012). Ependymoglia cells, also referred to as radial glia

cells (RGCs), are located at the neurogenic niches in the dorsal and medio-ventral part of the zebrafish telencephalon. During adulthood, newborn neurons are constitutively generated and deposited in the periventricular zone (Adolf et al., 2006). Ependymogial cells possess radial morphology, comparable to that observed in mammalian aNSCs, express specific markers, including glial fibrillary acidic protein (Gfap), brain lipid-binding protein (Blbp), SRY-box 2 (Sox2) and S100 calcium-binding protein B (S100 β), and are considered as functional orthologs of mammalian ependymal cells (Jurisch-Yaksi et al., 2020). As previously mentioned, ependymogial cells are located at distinct neurogenic niches, the dorsal and medio-ventral niches, and are characterized by different proliferation rates and type of neurons generated (März et al., 2010). Under physiological conditions a high number of ependymoglia remain quiescent, while the majority of active ependymoglia divide asymmetrically, preventing the stem cell pool exhaustion and generating neuronal progeny (Barbosa et al., 2015; Dray et al., 2015). Furthermore, a proportion of ependymoglia can directly convert into neurons, losing their NSC features and at the same time upregulating neuronal markers, such as HuC/D (Barbosa et al., 2015).

In addition to ependymogial cells, a distinct population of Nestin-positive progenitors have been identified in the ventral nucleus of the ventral part of the adult zebrafish telencephalon, weakly expressing typical RGC markers and displaying neuroepithelial-like morphology (März et al., 2010).

Lastly, progenitor cells displaying radial glia-like morphology, positive for oligodendrocyte transcription factor 2 (Olig2) and S100 β but negative for other oligodendroglial markers, such as Sox10 and myelin basic protein (Mbp), have been detected in the rostral migratory stream of the adult zebrafish telencephalon but their functions and properties remain to be determined (Marz et al., 2010).

Glial cells in the adult zebrafish telencephalon

Astrocytes, oligodendrocyte precursor cells (OPCs) and microglia are the main glial cells involved in the wound healing reaction to TBI in the mammalian CNS, contributing to the formation of the glial scar.

Interestingly, proliferating Olig2⁺ cells belonging to the oligodendroglial lineage have been identified in the parenchyma of the adult zebrafish telencephalon as well, together with differentiated Olig2⁺/Mbp⁺ mature oligodendrocytes (Marz et al., 2010). These observations support the hypothesis that zebrafish oligodendrocytes may behave in a similar manner to their mammalian counterpart, possibly contributing to the regeneration process in the zebrafish CNS.

As in mammals, microglial cells are the resident immune cells colonizing the zebrafish CNS. Under physiological conditions, they display ramified morphology with elongated processes to scan the CNS environment (Oosterhof et al., 2015). In response to infection or injury, zebrafish microglia are capable of migrating to the site of interest and phagocytizing pathogens and debris (Peri and Nüsslein-Volhard, 2008). Furthermore, zebrafish microglia share a high conserved gene signature with mammalian microglia, and are able to regulate neuronal activity and synapse pruning (Li et al., 2012).

Differently from the mammalian cerebral cortex, however, the zebrafish telencephalon lacks the characteristic parenchymal astrocytes (Alunni and Bally-Cuif, 2016; Jurisch-Yaksi et al., 2020). Nonetheless, zebrafish ependymoglia cells, as described in the section above, express typical astrocytic markers, including Gfap and S100 β , and the orthologs of the glutamate transporter EAAT2 detected in mammalian astrocytes (Jurisch-Yaksi et al., 2020). Moreover, it has been shown that TBI in the zebrafish CNS trigger upregulation of Gfap in ependymoglia cells (Kishimoto et al., 2012; Marz et al., 2011), suggesting that ependymoglia cells in the zebrafish telencephalon may take over the mammalian astrocytic functions, embodying the functional role of multiple cell types of the mammalian CNS, including RGCs, astrocytes and ependymal cells.

In addition to ependymoglia cells, a previously underscribed population, referred to as radial astrocytes, has been identified in the zebrafish brain (Chen et al., 2020). Zebrafish radial astrocytes derive from RGCs and exhibit typical features of mammalian astrocytes, such as expression of glutamine synthetase (GS), association with synapses and tiling behavior. Furthermore,

zebrafish radial astrocytes exhibit Ca^{2+} transients and respond to norepinephrine (NE), similarly to mammalian astrocytes (Chen et al., 2020). The identification of this new population in zebrafish raises new questions that needs to be addressed to better characterize the functional roles and the contribution of radial astrocytes to regeneration of the adult zebrafish CNS.

Cellular and molecular responses to TBI in the adult zebrafish telencephalon

Various injury paradigms have been established to acutely damage the adult zebrafish telencephalon, differing in the telencephalic structures affected by the TBI.

Two main types of TBI have been characterized in the adult zebrafish telencephalon and I will refer to them with the term “skull” and “nostril”. In the case of the “skull” injury, the TBI is performed from the dorsal part of the telencephalon, penetrating the skull and damaging both the VZ, containing the somata of ependymogial cells, and the telencephalic parenchyma, largely containing post-mitotic neurons and glial progenitors (Kishimoto et al., 2012; Lim et al., 2016; Marz et al., 2011). In the case of the “nostril” injury, the TBI is performed through the zebrafish nostrils, exclusively damaging the telencephalic parenchyma and the RGC processes spanning throughout the parenchyma, without directly affecting the neurogenic niches in the VZ (Ayari et al., 2010; Barbosa et al., 2015; Baumgart et al., 2012; Di Giaimo et al., 2018; Kroehne et al., 2011; Kyritsis et al., 2012). The common responses shared by these two injury paradigms include the transient activation and accumulation of immune cells and oligodendroglial cells at injury sites, the activation of restorative programs in ependymogial cells, the generation of new neurons and the resolution of the glial scar, although with different kinetics.

More specifically, in response to TBI and subsequent cell death, microglia migrate towards injury sites and this mobilization is triggered by Ca^{2+} waves that activate the ATP-dependent chemotaxis through P2RY12 (Haynes et al., 2006; Sieger et al., 2012). As already mentioned, one of the main differences in the regenerating zebrafish CNS is the prompt termination of

neuroinflammation and resolution of the glial scar shortly after injury. Among other “OFF” signals contributing to de-activation of immune cells, sigma-1 (σ_1) receptor has been identified as key modulator to “switch-off” microglial cells and to promote their migration away from injury sites (Moritz et al., 2015).

Following immune cell activation and migration at injury sites, proliferation is increased both in the parenchyma, where most of the injury-induced proliferating cells belong to the oligodendrocyte and microglial lineages, and in the VZ, where most of the injury-induced proliferating cells are ependymogial cells (Barbosa et al., 2015; Kyritsis et al., 2012; Marz et al., 2011). In addition to the enhancement of their proliferation rate, TBI induce behavioral changes in ependymogial cells, specifically modifying their mode of division in response to injury. Interestingly, live imaging of ependymogial cells in the injured zebrafish telencephalon has allowed the characterization of a novel mode of division of ependymogial cells not observed in the zebrafish telencephalon under physiological conditions (Barbosa et al., 2015; Dray et al., 2015). This mode of division, referred to as symmetric non-gliogenic mode, leads to the production of two intermediate neuronal progenitors, which, together with the contribution of direct neuronal conversion, can significantly promote the enlargement of the neuronal population at the expenses of the stem cell pool (Barbosa et al., 2015; Dray et al., 2015).

Moreover, it has been demonstrated that prokineticin 2 (Prok2) and sprouty-related EVH1 domain containing 2 (Spred2), genes that are activated during development and physiologically relevant for neuronal differentiation, are directly linked to the migration and the survival of newborn neurons and neuronal progenitors at injury sites in the zebrafish telencephalon (Ayari et al., 2010; Kishimoto et al., 2012; Lim et al., 2016). Newly formed HuC/D⁺ neurons make use of ependymogial processes as structures to migrate to the damaged area (Lim et al., 2016), mimicking their behavior during development (Cooper, 2013). Altogether, these observations strengthen the concept that zebrafish CNS regeneration relies on the combination of programs active under physiological conditions and programs exclusively induced in response to injury, including acute neuroinflammation (Kizil et al., 2012a; Kyritsis et al., 2012).

A recent study has confirmed that proper coordination of the regenerative responses is a key determinant of the successful regeneration of the adult zebrafish telencephalon. Specifically, it has been shown that the aryl hydrocarbon receptor (AhR) is a key synchronizer of the direct neuronal conversion of ependymoglia in response to injury and the inflammatory state in the brain (Di Giaimo et al., 2018). Shortly after injury, coinciding with the phase of elevated microglial cell activation and migration at injury sites, AhR signaling is deactivated, stimulating ependymoglia cell proliferation. Neuronal differentiation of ependymoglia through direct conversion is observed when AhR signaling returns to normal levels at 7 days post injury (dpi), coinciding with the phase of microglial cell de-activation and resolution of the glial scar (Di Giaimo et al., 2018). These results have been confirmed by temporally interfering with the AhR signaling in response to TBI, leading to aberrant neurogenesis with newly formed neurons failing to survive (Di Giaimo et al., 2018).

One additional class of molecular mechanisms promoting regeneration in the adult zebrafish telencephalon includes those programs constitutively expressed in the zebrafish telencephalon, which acquire a different function in response to TBI. As an example, Notch signaling is active in the intact zebrafish brain, where it promotes ependymoglia quiescence (Alunni et al., 2013; Chapouton et al., 2010). Interestingly, in response to TBI, Notch1, Notch3 and inhibitor of DNA binding 1 (Id1) are upregulated, although displaying opposite effect on NSCs (Diotel et al., 2015; Kishimoto et al., 2012; Viales et al., 2015). Id1 and Notch3 maintain their function, promoting quiescence in neuronal progenitors (Alunni et al., 2013; Chapouton et al., 2010; Viales et al., 2015). However, Notch1 acquires an injury-specific function, promoting ependymoglia activation (Kishimoto et al., 2012), oppositely to what has been observed in the zebrafish brain under physiological conditions. These results highlight the importance of tightly regulating NSC activation and quiescence for the long-term maintenance of the restorative capacity of the adult zebrafish telencephalon, avoiding stem cell pool depletion. In the zebrafish brain, this regulation is achieved by the synergistic effect of development-associated programs re-activated in response to TBI, injury-associated programs exclusively activated in response

to TBI and development-associated or constitutive programs with distinct functions in response to TBI (Figure 3) (Zambusi and Ninkovic, 2020).

Inflammation as positive contributor to restorative neurogenesis in the adult zebrafish telencephalon

For long time, the activation of neuroinflammation in response to TBI has been considered a hindrance for neurogenesis and regeneration in the mammalian CNS (Ekdahl et al., 2003). However, this dogma has been challenged and modified into a model in which neuroinflammation can have both beneficial and detrimental effects to the CNS, depending on the nature and the scale of the inflammatory response (Kyritsis et al., 2014; Sochocka et al., 2017).

In zebrafish, inflammation have been shown to be important for the regenerative outcome in different organs, including fin, heart, spinal cord and brain (Caldwell et al., 2019; Carrillo et al., 2016; Kyritsis et al., 2012; LeBert and Huttenlocher, 2014; Petrie et al., 2014; De Preux Charles et al., 2016).

Indeed, immunosuppression and subsequent reduced levels of neuroinflammation have been found to negatively affect the activation of programs associated with restorative neurogenesis in the adult zebrafish telencephalon, limiting the activation of NSCs and the generation of new neurons (Kyritsis et al., 2012).

Numerous neuroinflammatory programs are upregulated in response to TBI in the adult zebrafish telencephalon and positively regulate the activation of NSCs. Among these, the C-X-C chemokine receptor type 5 (Cxcr5) and cysteinyl leukotriene receptor 1 (Cysltr1) display higher expression levels in response to TBI (Kizil et al., 2012b; Kyritsis et al., 2012). The activation of Cxcr5 and Cysltr1 significantly enhances the proliferation of ependymogial cells and the number of newborn neurons generated, thus contributing to CNS regeneration (Kizil et al., 2012b; Kyritsis et al., 2012). Furthermore, neuroinflammation is required to induce the activation of injury-specific programs, including GATA binding protein 3 (Gata3), which is not expressed in the zebrafish telencephalon under physiological conditions (Kizil et al., 2012a; Kyritsis et al., 2012). Gata3 activation in response to TBI is required

for ependymogial cell activation, neurogenesis and migration of newly generated neurons at injury sites (Kizil et al., 2012a). Interestingly, Gata3 neurogenic potential is strictly limited to the injured CNS, as overexpression of Gata3 under physiological conditions does not enhance neurogenesis (Kizil et al., 2012a). The direct link between neuroinflammation and Gata3 activation has been established by injecting inflammatory molecules such as zymosan A and leukotriene C4, a ligand of the Cysltr1, in the intact zebrafish ventricles. Intraventricular injection of these molecules is sufficient to induce Gata3 expression, in a similar manner to the response observed after TBI (Kyritsis et al., 2012). Furthermore, immunosuppression via administration of dexamethasone significantly reduces Gata3 induction after zymosan A injection, corroborating the association between neuroinflammation and restorative neurogenesis in the adult zebrafish telencephalon (Kyritsis et al., 2012).

The relevance of neuroinflammation for the activation of restorative programs is not limited to TBI. In a zebrafish model for AD, based on cerebroventricular microinjections of amyloid- β 42 (A β -42) derivatives, A β -42-accumulating neurons stimulate the activation of microglial cells and interleukin-4 (IL-4) is upregulated both in neurons and microglial cells (Bhattarai et al., 2016, 2017). Binding of IL-4 to its respective receptor found in NSCs is sufficient to trigger a cascade via Stat6 phosphorylation that leads to increased NSC proliferation and neurogenesis (Bhattarai et al., 2016, 2017).

Altogether, these results demonstrate that neuroinflammation, when properly tuned, significantly contribute to CNS regeneration in different contexts, positively affecting NSC proliferation and restorative neurogenesis. For this reason, a better understanding and characterization of neuroinflammation-driven programs activated in response to TBI in the adult zebrafish telencephalon would facilitate the development of new therapies to ameliorate the outcome of human patients with TBI and neurodegenerative diseases.

Progranulin structure and expression in the CNS

Progranulin (PGRN), also known as proepithelin and PC cell-derived growth factor (Shoyab et al., 1990; Xia and Serrero, 1998), is a glycoprotein composed of 593 amino acid (~75–90 kDa). The full length protein (PGRN) contains seven and half cysteine-rich domains called granulins, and it can be cleaved in the linker regions between granulin domains, producing granulin peptides (Cenik et al., 2012). PGRN is proteolytically cleaved by neutrophil elastase, proteinase 3, matrix metalloproteinase 12 (MMP-12), MMP-14 and a disintegrin and metalloproteinase with thrombospondin motifs 7 (ADAMTS-7) (Zhu et al., 2002). Conversely, the secretory leucocyte protease inhibitor (SLPI) binds to PGRN, thus limiting its proteolytic cleavage and regulating the balance between full-length PGRN and proteolytically-derived granulin peptides. Both the full-length PGRN and the granulin peptides are biologically active and, in some cases, they are characterized by opposite functions, as in their regulation of inflammatory processes (Zhu et al., 2002). PGRN is expressed by different cell types and, within the CNS, mainly by neurons and microglia (Petkau et al., 2010). Interestingly, in microglial cells PGRN expression varies according to their activation state as it has been reported that PGRN is significantly upregulated in response to injury (He et al., 2003; Menzel et al., 2017). Furthermore, as PGRN can be secreted, it is important to distinguish between its roles as autocrine and endocrine factor in the CNS.

Although PGRN has been associated to neurodegenerative diseases, cancer and inflammation, its precise roles under physiological conditions and in the damaged CNS are still not completely understood.

PGRN as risk factor for aging and brain pathologies

In 2006, two studies have revealed that heterozygous mutations in the human *PGRN* gene are associated to frontotemporal lobar degeneration (FTLD) (Baker et al., 2006; Cruts et al., 2006), with ubiquitin-positive protein aggregates enriched in TDP-43 (Neumann et al., 2006).

Moreover, homozygous mutations in the human *PGRN* gene cause the onset of neuronal ceroid lipofuscinosis (NCL), a lysosomal storage disorder

characterized by the formation of persistent deposit of autofluorescent storage material lipofuscin (Smith et al., 2012).

Notably, it has been reported that some phenotypes associated with NCL are also found in FTLD patients with *PGRN* mutations (Götzl et al., 2014; Valdez et al., 2017), suggesting that lysosomal dysfunction may act as shared mechanisms for both diseases.

Lastly, *PGRN* has been identified as key determinant of aging in the mammalian CNS, increasing the rate of biological aging of the human cerebral cortex and influencing numerous age-related hallmarks in the brain, including lipid metabolism and neuroinflammation (Farr et al., 2020; Lui et al., 2016; Marschallinger et al., 2020; Rhinn and Abeliovich, 2017).

As aging is the primary risk factor for neurodegenerative diseases, a better understanding of the link between *PGRN* and aging needs to be achieved to slow the progression of neurodegenerative disorders.

***PGRN* as regulator of neuroinflammation and immune cell functions in the CNS**

PGRN regulate numerous processes, including tumorigenesis, cell proliferation, wound healing and neuronal cell survival (Bateman and Bennett, 2009; Chitramuthu et al., 2017; He et al., 2003; Kao et al., 2017). Importantly, *PGRN* is also a key factor modulating the immune system and inflammatory state in the CNS under physiological conditions, during aging and in response to TBI (Götzl et al., 2018, 2019; Lui et al., 2016; Marschallinger et al., 2020; Martens et al., 2012; Rhinn and Abeliovich, 2017; Tanaka et al., 2013a; Yin et al., 2010; Zhang et al., 2020).

For instance, it has been demonstrated that *PGRN* binds to the toll-like receptor 9 (TLR9), a receptor which belongs to a family of proteins involved in innate immunity, supporting antigen presentation in macrophages (Park et al., 2011). Furthermore, *PGRN* is highly expressed in T-suppressor cells, a class of T cells inhibiting autoimmune diseases, and protects T-regulatory cells from the negative effects of pro-inflammatory TNF- α (Tang et al., 2011). *PGRN* also affects the production and secretion of cytokines, and promote microglial cell chemotaxis and endocytosis of extracellular peptides (Pickford

et al., 2011). PGRN overexpression is sufficient to stimulate the secretion of several anti-inflammatory cytokines, including IL-4, IL-5 and IL-10, which induce de-activation of microglial cells, and fractalkine (CX3CL1), which reduces the secretion of NO synthase, TNF- α and IL-6 from activated microglia (Jian et al., 2013). Conversely, PGRN-deficient microglial cells activated in response to LPS injection secrete higher levels of pro-inflammatory IL-6 and TNF- α (Yin et al., 2010).

In addition to the abovementioned functional roles, PGRN is shuttled to lysosomes, regulating the expression, maturation and activity of lysosomal proteins. PGRN deficiency has been found to impair the lysosomal function and maturation of lysosomal cathepsins already during adulthood in microglial cells (Götzl et al., 2018). These results suggest that the lysosomal impairment of PGRN-deficient microglial cells of young adult animals could be responsible for the impaired protein degradation and accumulation of cytotoxic aggregates observed during aging (Götzl et al., 2018).

As previously mentioned, PGRN contribute to regulate the aging kinetics of the mammalian CNS (Farr et al., 2020; Rhinn and Abeliovich, 2017). Numerous age-related impairments have been detected in PGRN-deficient immune cells. Indeed, in addition to the altered production and secretion of cytokines, PGRN-deficient microglial cells display age-related upregulation of complement proteins, such as C3 and C1qa, which subsequently accumulate in synaptosomes of aging PGRN-deficient brain (Lui et al., 2016). As a result, a significant increase in synaptic pruning has been detected in PGRN-deficient brain during aging, suggesting that PGRN acts as regulator of neuroinflammation, suppressing aberrant microglial activation and protecting neurons from excessive pruning (Lui et al., 2016). Indeed, higher levels of complement proteins have been associated to the transition of microglial cells from a homeostatic to disease-associated state in the aging brain of PGRN-deficient mice (Zhang et al., 2020). Moreover, DAMs promote the accumulation of cytoplasmic TDP-43, contributing to neuronal proteinopathy and neuronal cell death. Blocking of complement activation is sufficient to reduce the neurotoxic properties of DAMs in PGRN-deficient brain (Zhang et al., 2020).

Lastly, in a recent study, a novel microglial state has been identified in the aging brain, characterized by a transcriptomic signature similar to the one identified in DAMs, defects in phagocytosis, increased ROS levels and high levels of pro-inflammatory cytokines (Marschallinger et al., 2020). Interestingly, microglial cells belonging to this dysfunctional cluster exhibit aberrant accumulation of lipid droplets (LDs) (Marschallinger et al., 2020). A similar phenotype has been identified in PGRN-deficient brain, where microglial cells display numerous LDs, deficits in phagocytosis and pro-inflammatory signature (Marschallinger et al., 2020), confirming a previous study where numerous genes associated to lipid metabolism were altered in the brain of PGRN-deficient mice (Evers et al., 2017).

PGRN is also important to regulate immune cell reactivity in response to injuries in the CNS. In a model of induced toxicity in the CNS via administration of 1-methyl-4-(2'-methylphenyl)-1,2,3,6-tetrahydrophine (MPTP), PGRN deficiency leads to exacerbated neuroinflammation and neuronal death, although the molecular mechanisms behind this phenotype have not yet been fully understood (Martens et al., 2012).

Similarly, PGRN regulate microglial cell activation and glial scar formation in response to TBI (Menzel et al., 2017; Tanaka et al., 2013a, 2013b). TGF β 1–Smad3 signaling pathway is increased in response to injury in PGRN-deficient brain, together with excessive microglial activation and altered lysosomal functions (Tanaka et al., 2013a, 2013b). Importantly, the TGF β 1–Smad3 signaling pathway is also a mediator promoting the formation of the glial scar, representing a barrier for neuronal regeneration and survival (Wang et al., 2007).

Lastly, it is worth to mention that PGRN deficiency results in elevated axonal damage and astrogliosis in response to TBI, supporting the concept that PGRN is a key regulator of both microglial cells and astrocytes, two major cell populations contributing to the formation of the glial scar in the mammalian CNS (Menzel et al., 2017). *In vitro* experiments have demonstrated that injection of recombinant PGRN is sufficient to attenuate the expression of TNF- α and iNOS in activated astrocytes, limiting the secretion of pro-inflammatory molecules detrimental for regeneration.

Four granulins (Grns) in the zebrafish brain

Differently from mammalian species, zebrafish possess four distinct granulin genes: two orthologs of the human *PGRN* gene, granulin a (*grna*) and granulin b (*grnb*), in addition to granulin 1 (*grn1*) and granulin 2 (*grn2*), paralogs encoding for shorter proteins (Figure 4) (Cadieux et al., 2005; Solchenberger et al., 2015).

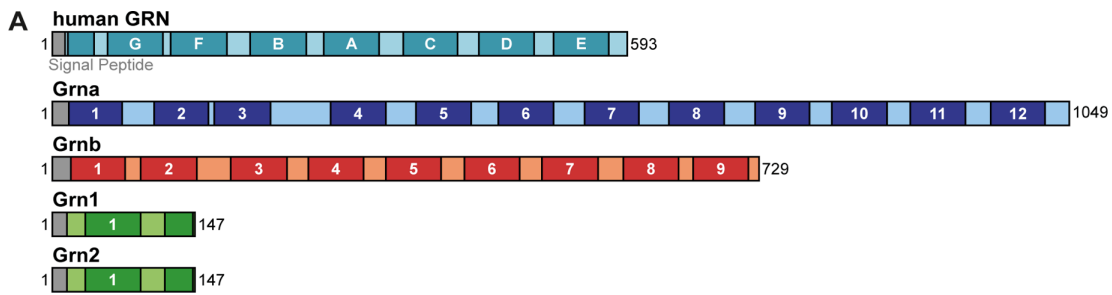


Figure 4. Schematic of human *PGRN* and zebrafish granulins (Adapted from Solchenberger et al., 2015. This is an open access article distributed under the terms of the Creative Commons Attribution License, which permits use, distribution and reproduction in any medium, provided the original work is properly cited).

Interestingly, *Grna*-deficient zebrafish larvae are unable to produce mature neutrophils and macrophages and display abnormal healing in response to tail fin resection, failing to recruit macrophages at injury sites (Campbell et al., 2021). These results suggest the existence of functional conservation between *Grna* and mammalian *PGRN* (Campbell et al., 2021). Moreover, it has been demonstrated that *Grn1*-deficient zebrafish are characterized by limited regenerative capacity in response to retinal injury, with reduced number of de-differentiating Müller cells and proliferating progenitor cells (Tsuruma et al., 2018).

Altogether, these results strengthen the hypothesis that, similarly to *PGRN* in mammalian species, zebrafish granulins are important factors in the context of regeneration in numerous organs, including the CNS.

Furthermore, it appears that in zebrafish distinct granulins may be relevant for regeneration in specific organs and injury paradigms, offering a new system to better characterize the mechanisms of action of *PGRN* and granulin peptides in the mammalian CNS.

Results

Aim of the study I

The aim of the study is to investigate:

The age-related hallmarks and the role of granulins in regulating aging kinetics in the adult zebrafish telencephalon.

Granulins Regulate Aging Kinetics in the Adult Zebrafish Telencephalon

Alessandro Zambusi, Özge Pelin Burhan, Rossella Di Giaimo, Bettina Schmid, Jovica Ninkovic.

For this paper I was involved in performing and analyzing all the experiments, except for the measurement of telomere length (Figure 9, Panel B), performed by Özge Pelin Burhan.

I was also involved in writing, editing and reviewing the paper, together with Prof. Dr. Jovica Ninkovic.

The paper is published on Cells (2020), 9(2):350.

<https://doi.org/10.3390/cells9020350>

As an open access article distributed under the Creative Commons Attribution License and as author of this publication, I have the right to include it in a thesis or dissertation, provided the work is properly attributed.

Article

Granulins Regulate Aging Kinetics in the Adult Zebrafish Telencephalon

Alessandro Zambusi ^{1,2,*}, Özge Pelin Burhan ³, Rossella Di Giaimo ⁴ , Bettina Schmid ³ and Jovica Ninkovic ^{1,2,*}

¹ Institute of Stem Cell Research, Helmholtz Center Munich, 85764 Neuherberg, Germany

² Graduate School of Systemic Neuroscience; Biomedical Center, Faculty of Medicine, LMU Munich, 82152 Planegg, Germany

³ German Center for Neurodegenerative Diseases (DZNE), 81377 München, Germany; oezge-pelin.burhan@dzne.de (Ö.P.B.); bettina.schmid@dzne.de (B.S.)

⁴ Department of Biology, University of Naples Federico II, 80134 Naples, Italy; digiaimo@unina.it

* Correspondence: alessandro.zambusi@helmholtz-muenchen.de (A.Z.); ninkovic@helmholtz-muenchen.de (J.N.)

Received: 19 December 2019; Accepted: 31 January 2020; Published: 3 February 2020



Abstract: Granulins (GRN) are secreted factors that promote neuronal survival and regulate inflammation in various pathological conditions. However, their roles in physiological conditions in the brain remain poorly understood. To address this knowledge gap, we analysed the telencephalon in Grn-deficient zebrafish and identified morphological and transcriptional changes in microglial cells, indicative of a pro-inflammatory phenotype in the absence of any insult. Unexpectedly, activated mutant microglia shared part of their transcriptional signature with aged human microglia. Furthermore, transcriptome profiles of the entire telencephali isolated from young Grn-deficient animals showed remarkable similarities with the profiles of the telencephali isolated from aged wildtype animals. Additionally, 50% of differentially regulated genes during aging were regulated in the telencephalon of young Grn-deficient animals compared to their wildtype littermates. Importantly, the telencephalon transcriptome in young Grn-deficient animals changed only mildly with aging, further suggesting premature aging of Grn-deficient brain. Indeed, Grn loss led to decreased neurogenesis and oligodendrogenesis, and to shortening of telomeres at young ages, to an extent comparable to that observed during aging. Altogether, our data demonstrate a role of Grn in regulating aging kinetics in the zebrafish telencephalon, thus providing a valuable tool for the development of new therapeutic approaches to treat age-associated pathologies.

Keywords: neurogenesis; microglia; granulin; aging

1. Introduction

Aging is associated with numerous changes in a wide range of processes, thus progressively leading to impaired organ function and increasing the risk of the onset of numerous pathologies. Accordingly, brain aging is one of the greatest risk factors for multifactorial diseases including Alzheimer's and Parkinson's diseases [1]. Typical aging hallmarks such as genomic instability, telomere shortening, metabolic dysregulation, cellular senescence, stem cell exhaustion, and decreased neurogenesis are observed in the brain and affect a broad range of cellular functions [2], thereby leading to impaired tissue homeostasis and regeneration. A primary reason for this impaired tissue homeostasis and regeneration is age-related exhaustion of tissue-specific stem cells, a process observed in various organs [3–5], including the mammalian brain [6–10]. Although prominent age-associated changes, including decreased neurogenesis and changes in the lateral ventricle choroid plexus [11–13], have

been detected in the aging mammalian brain, comparisons of neural stem cell transcriptomes have revealed a remarkably small set of differentially regulated transcripts, which are largely associated with cell cycle regulation, neuronal differentiation, and inflammation [10,14–16]. These analyses support the hypothesis that specific changes in a limited number of key regulators influenced by both intrinsic [16] and extrinsic [11,12,17,18] aging-associated pathways lead to the aging of the neural stem cell compartment. Interestingly, a prominent phenomenon associated with aging in the neural stem cell niche is the activation of resident microglial cells, which develop a pro-inflammatory phenotype [19–22]. This process results in the activation of NF- κ B signalling and enrichment in pro-inflammatory cytokines, with increased production of IL-1 β , TNF, and interferons- typical activators of pro-inflammatory responses [23]. Indeed, the activation of NF- κ B signalling in the hypothalamus decreases the production of gonadotropin-releasing hormone in neurons [24], thus causing various age-associated changes in stem cell compartments of the brain, but also modulates systemic aging, including muscle weakness and skin atrophy [24]. Furthermore, the mRNA decay factor AUF1 regulates both the aging-associated inflammatory response and maintenance of telomere length [25], thereby suggesting not only that the interactions among different cells in the stem cell compartment contributes to tissue aging but also that the same factor might be involved in both cell-intrinsic and -extrinsic pathways involved in the aging process. Therefore, one major challenge is to better understand the relationship among these processes in different cell types and to identify novel pathways and regulators contributing to aging regulation. These pathways would be suitable targets for the development of new therapeutic approaches aiming to limit or block the detrimental phenotypes acquired with aging, thus decreasing the risk of associated pathologies.

Progranulin (GRN) is a secreted factor that is mainly expressed in microglia and neurons, and can be proteolytically processed into granulin peptides [26–28]. Both GRN and granulin peptides are biologically active [29,30]. Granulin deficiency shortens lifespan in mice [31] and African turquoise killifish [32], in line with the association of genetic variants in the *GRN* gene with age-associated phenotypes in the human cerebral cortex [33]. Moreover, mutations in the human *GRN* gene are associated with early onset of age-related neurodegenerative diseases, such as frontotemporal lobar degeneration (FTLD) [34,35] and neuronal ceroid lipofuscinosis (NCL) [36,37]. Additionally, GRN regulates aging-related processes such as inflammation [38–43] and neuronal survival [44–46], thus supporting a possible role of GRN in the regulation of brain aging.

Although GRN is associated with aging in the human cerebral cortex, the specific molecular mechanisms and cellular basis leading to the accelerated aging phenotypes remain poorly understood, possibly because of the opposing roles of GRN and granulin peptides, generated by GRN proteolysis in mammals [29,30]. Whereas GRN, for example, has an anti-inflammatory function, some granulin peptides enhance the inflammatory response [29,30]. In contrast to mammals, zebrafish have two orthologs of *Grn*, *granulin a* (*grna*) and *granulin b* (*grnb*), in addition to two paralogs, *granulin 1* (*grn1*) and *granulin 2* (*grn2*), which encode shorter proteins similar to the products of mammalian GRN proteolytic cleavage [47]. Therefore, the zebrafish model of aging [48–50], combined with a recently generated double mutant for *Grna* and *Grnb*, offers the possibility of determining the specific functions of GRN and granulin peptides in brain aging [51].

2. Materials and Methods

2.1. Animal Experiments

Adult (3–5-month-old) and aged (15–24-month-old) *grna*^{+/+};*grnb*^{+/+} and *grna*^{-/-};*grnb*^{-/-} zebrafish siblings [51], and zebrafish from the AB/EK strain and from the transgenic lines *Tg* (*olig2:DsRed*) [52], *Tg* (*mpeg1:mCherry*) [53], *Tg* (*olig2:DsRed;grna*^{-/-};*grnb*^{-/-}) and *Tg* (*mpeg1:mCherry;grna*^{-/-};*grnb*^{-/-}) were used in all experiments. The fish were reared under standard husbandry conditions [54], and experiments were performed according to the handling guidelines and regulation of EU and the Government of Upper Bavaria (AZ 55.2-1-54-2532-09-16).

2.2. DNA Extraction and Genotyping

Genotyping of *grna* and *grnb* was performed by cutting a small part of the zebrafish tail fin. REDExtract-N-Amp Tissue Kit (Sigma-Aldrich[®], Merck, Darmstadt, Germany) was used to rapidly extract the genomic DNA from animal tissues according to the manufacturer's instructions. Isolated genomic DNA was amplified by PCR with the following primers: *grna* forward (TTCAGTCATTGTTTCAGAGGTCA), *grna* reverse (TTCCTCTGATCCACTTTCTACCA), *grnb* forward (AATGACACAAGACGTCCTCATAAA) and *grnb* reverse (AAAAATAATAACCACAGCGCAACT). Sanger sequencing was then performed to obtain and compare the nucleotide sequences of different samples and identify the selected mutations for *grna* and *grnb*. The *grna* selected mutation was identified by a deletion of 11 nucleotides, which caused a frameshift of the open reading frame and resulted in a premature STOP codon. The *grnb* selected mutation was identified by a deletion of 13 nucleotides and insertion of 9 nucleotides, which caused a frameshift of the open reading frame and resulted in a premature STOP codon.

2.3. Tissue Preparation and Immunohistochemistry

Animals were sacrificed through overdose of tricaine methane sulfonate (MS222, 0.2%) via prolonged immersion. Tissue processing was performed as previously described [55]. For cell immunolabelling, we used rat anti-BrdU (1:200, ab6326, Abcam, Berlin, Germany), mouse anti-fish leukocytes 4C4 antigen (1:500, 92092321, 7.4.C4, Health Protection Agency Culture Collections, Salisbury, England), rabbit anti-HuC/HuD (1:500, 210554, Abcam, Berlin, Germany) and rabbit anti-Sox10 (1:2000, GTX128374, Biozol, Eching, Germany). The primary antibodies were detected with specific secondary antibodies labelled with Alexa 488, Alexa 546, and Alexa 633 (1:1000, Invitrogen, Thermo Fisher, Dreieich, Germany). Sections were embedded in Aqua Polymount (Polyscience, Hirschberg an der Bergstraße, Germany).

Immunodetection of BrdU required a pretreatment with 4 N HCl followed by washes with borate buffer and PBS before the sections were immersed in the anti-BrdU antibody. All antibodies were dissolved in 0.5% Triton X-100 and 10% normal goat serum.

2.4. Bromodeoxyuridine (BrdU) Labelling Experiments

To analyse the proliferative capacity of glial cells, we performed long-term bromodeoxyuridine (BrdU) (Sigma Aldrich) incorporation. Fish were kept in BrdU-containing aerated water (10 mM) for 16 h/day during 5 consecutive days for long-term analysis. This time frame was determined to label a substantial proportion of activated neural stem cells that would generate neurons, based on the basis of the observations that adult neural stem cells (aNSCs) are largely quiescent in the intact adult zebrafish telencephalon [56]. During the 8 h outside BrdU-containing water, fish were kept in fresh water and fed. Animals were sacrificed 14 days after BrdU treatment (5 days BrdU water + 14 day chase), because this time point was previously described to have the greatest number of newly generated neurons incorporating BrdU in the adult zebrafish telencephalon [57].

2.5. Image Acquisition and Processing

All images were acquired with an Olympus FV1000 cLSM system (Olympus, Tokyo, Japan), using the FW10-ASW 4.0 software (Olympus, Tokyo, Japan). Quantifications and co-localisation analysis were performed in Imaris software version 8.4 (Bitplane, Zurich, Switzerland) and ImageJ software (National Institutes of Health, Bethesda, MD, USA).

2.6. Quantitative Analysis and Statistical Tests

For all analyses, the group size was previously determined to have a statistical power ≥ 0.95 , identifying a group size of at least four independent telencephali. The number of telencephali analysed

is specified in the figure legends and in the graphs, where each data point represents a distinct biological replicate.

All the sections belonging to the telencephalon were quantified (sections containing the olfactory bulb or optic tectum were excluded). All quantifications are displayed as cell density, defined as the total number of cells occupying a specific area (ventricular or parenchymal zone). The volumes (mm^3) of either ventricular (Figure 6c) or parenchymal (Figure 7b) zones were calculated in Imaris software version 8.4 (Bitplane, Zurich, Switzerland). For normalisation, the total numbers of cells occupying a specific zone were divided by the calculated volumes of the corresponding zones.

Data are presented as the mean with SEM, and each data point represents a distinct biological replicate. Statistical analysis was performed with one-way ANOVA test for the oligodendrogenesis experiment (Figure 7) and two-way ANOVA test for the microglial morphology experiment (Figure 2), the constitutive neurogenesis experiment (Figure 6) and the comparison of relative telomere length (Figure 9b). GraphPad Prism Version 8.2.0 was used for the statistical tests. Statistical analysis for data associated with Figure 4a, Figure 9a, and Figure S3b,c was automatically performed with the DESeq2 pipeline (release 3.9) for differential expression analysis.

2.7. Morphological Analysis of Microglial Cells

To assess and compare the morphology of microglial cells between different groups in Figure 2, we quantified the average process length (μm), number of main processes and area of microglial somata (μm^2) in ImageJ (Fiji) software. a total of 80 cells from four different telencephali per group were analysed.

2.8. Fluorescence-Activated Cell Sorting (FACS) Isolation Method

Animals from the *Tg (olig2:DsRed)*, *Tg (mpeg1:mCherry)*, *Tg (olig2:DsRed; grna^{-/-};grnb^{-/-})*, and *Tg (mpeg1:mCherry; grna^{-/-};grnb^{-/-})* transgenic lines were sacrificed through MS222 overdoses, the telencephalon was dissected from each single animal, and three telencephali were pooled for each replicate. a single-cell suspension was prepared as previously described [58], and cells were analysed with a BD FACS Aria III instrument in BD FACS Flow TM medium. Debris and aggregated cells were gated by forward scatter-sideward scatter; single cells were gated in by FSC-W/FSC-A. Gating for fluorophores was performed using AB/EK animals as a baseline (Figure S1). Cells were directly sorted into extraction buffer from PicoPure RNA isolation kit (Thermo Fisher, Dreieich, Germany).

2.9. Libraries for Deep Sequencing of Whole Telencephali and FACS Sorted Cells

Total RNA from the entire telencephalon was isolated with Qiagen RNeasy kit, whereas total RNA from sorted cells was isolated with PicoPure RNA isolation kit from Thermo Scientific, according to manufacturer's instructions.

The quality and concentration of RNA were assessed on an Agilent 2100 Bioanalyzer. Only RNA with a RIN value ≥ 8 were used for library preparation. cDNA was synthesised from 10 ng of total RNA (whole telencephalon) or 500–1000 pg of total RNA (fluorescence activated cell sorting (FACS) isolated cells) with a SMART-Seq v4 Ultra Low Input RNA kit for Sequencing (Takara, Mountain View, CA, USA), according to the manufacturer's instructions. cDNA quality and concentration were assessed on an Agilent 2100 Bioanalyzer before library preparation with MicroPlex Library Preparation kit v2 (Diagenode, Liège, Belgium). All libraries (five replicates per condition in the case of samples from the whole telencephalon and three or four replicates per condition in the case of samples from FACS isolated cells) were processed together to minimise batch effects. Final libraries were evaluated and quantified with an Agilent 2100 Bioanalyzer, and the concentration was measured additionally with a Qubit 4 instrument and the Qubit dsDNA HS assay (Thermo Fisher, Dreieich, Germany) before sequencing. The uniquely barcoded libraries were multiplexed onto one lane, and 100-bp paired-end deep sequencing was carried out on a HiSeq 4000 instrument (Illumina, San Diego, CA, USA), generating approximately 20 million reads per sample. FASTQ files are available at GEO



Figure 1. Grna and Grnb deficiency leads to transcriptional changes associated with an activated microglial state. (a) Schematic of a typical section from the adult zebrafish telencephalon. (b–c’) Micrographs depicting microglial cells in the telencephalon in *Tg(mpeg1:mCherry)* animals. (c,c’) Magnifications of areas boxed in (b) and (b’), respectively. Scale bars: 100 μm (b,b’) and 20 μm (c,c’). (d) Scheme depicting the isolation procedure of *Mpeg1*⁺ cells for transcriptome analysis. (e) Volcano plot of differentially expressed genes (DEGs) in mutant *Mpeg1*⁺ cells (*padj* ≤ 0.05; 1 ≤ log₂FC ≤ -1). (f,g) Histograms depicting gene ontology (GO) terms enriched in the set of upregulated (f) and downregulated (g) genes in mutant *Mpeg1*⁺ cells.

To determine the purity of isolated cells, we analysed the expression of typical microglial, neuronal, and oligodendroglial genes [65] in the sorted mCherry⁺ population (Figure S2a). Significant enrichment in microglial genes was detected in Mpeg1⁺ isolated cells, thus confirming the purity of our enrichment (Figure S2a). Importantly, *grna* was strongly enriched in Mpeg1⁺ cells, in line with high *Grn* expression in mammalian microglia [27], whereas *grnb* was expressed at lower levels (Figure S2c).

The comparison of the transcriptomes of wildtype and mutant Mpeg1⁺ cells and differential expression analysis (DESeq2) revealed 1567 significantly upregulated and 2018 significantly downregulated genes in mutant Mpeg1⁺ cells ($padj \leq 0.05$; $1 \leq \log_2FC \leq -1$) (Figure 1e; Table S1). GO analysis (based on DAVID 6.8) revealed an enrichment in genes associated with inflammation, apoptosis, cell proliferation and extracellular matrix composition (Figure 1f,g; Table S1). Notably, many upregulated genes in mutant Mpeg1⁺ cells were associated with the tumor necrosis factor receptor, the MAPK and the JAK/STAT signalling pathways, which are involved in the induction of pro-inflammatory cytokine expression [66,67] (Figure 1f and Figure S3a). Furthermore, we identified numerous downregulated genes belonging to the PPAR signalling pathway, which has a role in counteracting the expression of pro-inflammatory cytokines [68] (Figure 1g and Figure S3a). These results indicate a switch toward a pro-inflammatory state of microglial cells in the adult telencephalon in *Grna*; *Grnb*-deficient animals. To confirm this hypothesis, we analysed the expression levels of several cytokines associated with pro-inflammatory and anti-inflammatory microglial phenotypes and detected higher mRNA levels of pro-inflammatory cytokines including *il6*, *tnfa*, *il12bb*, and *Cxcl8a (il8)* in mutant Mpeg1⁺ cells (Figure S3b; Table S1). In contrast, the mRNA levels of anti-inflammatory cytokines including *tgfb3*, *igf1*, and *il10* were significantly lower in mutant Mpeg1⁺ cells than wildtype Mpeg1⁺ cells (Figure S3c; Table S1), thus demonstrating their activated state. The numerous transcriptional changes observed in mutant Mpeg1⁺ cells contrast with the results obtained from GRN-deficient microglia in the mouse brain [38]. In contrast to our observations, GRN-deficient microglia in the mouse brain display different transcriptional profiles only during advanced aging [38], thereby suggesting that granulins might regulate microglia activation with different kinetics in the mouse and zebrafish brains. We compared the differentially expressed genes (DEGs) in our dataset with age-dependent upregulated genes in the cerebral cortex in GRN-deficient mice enriched in two major categories (immune response and lysosomal pathway) that showed exclusive association with the microglial population in mice (Table S1) [38]. Interestingly, some of the genes that displayed age-dependent upregulation in the cerebral cortex in GRN-deficient mice were also upregulated in young mutant Mpeg1⁺ cells (Table S1), thus indeed suggesting that granulin age-dependent role in suppressing aberrant microglial activation might be fundamental already during young adulthood in the adult zebrafish brain.

Because the transcriptome analysis suggested *Grna*; *Grnb*-dependent changes in the activation state of microglial cells, we further examined their morphology as an activation hallmark. We labelled microglial cells in the intact adult zebrafish telencephalon through immunohistochemistry against 4C4 [69] and compared 4C4⁺ cells in the telencephalon in young wildtype (3–5-month-old) and mutant (3–5-month-old) animals (Figure 2a–b'',e–g). Wildtype 4C4⁺ cells displayed a typical elongated morphology, characteristic of resident non-activated microglia (Figure 2a–a'',e–g). In contrast, most mutant 4C4⁺ cells displayed larger somata, and hyper-ramified and shorter processes-morphological characteristics typical of the activated state (Figure 2b–b'',e–g).

Together, our transcriptome and morphological analyses demonstrate the roles of *Grna* and *Grnb* in tuning the activation state of microglial cells in the zebrafish telencephalon. *Grna* and *Grnb* deficiency promotes the switch toward a pro-inflammatory and possibly detrimental microglial phenotype.

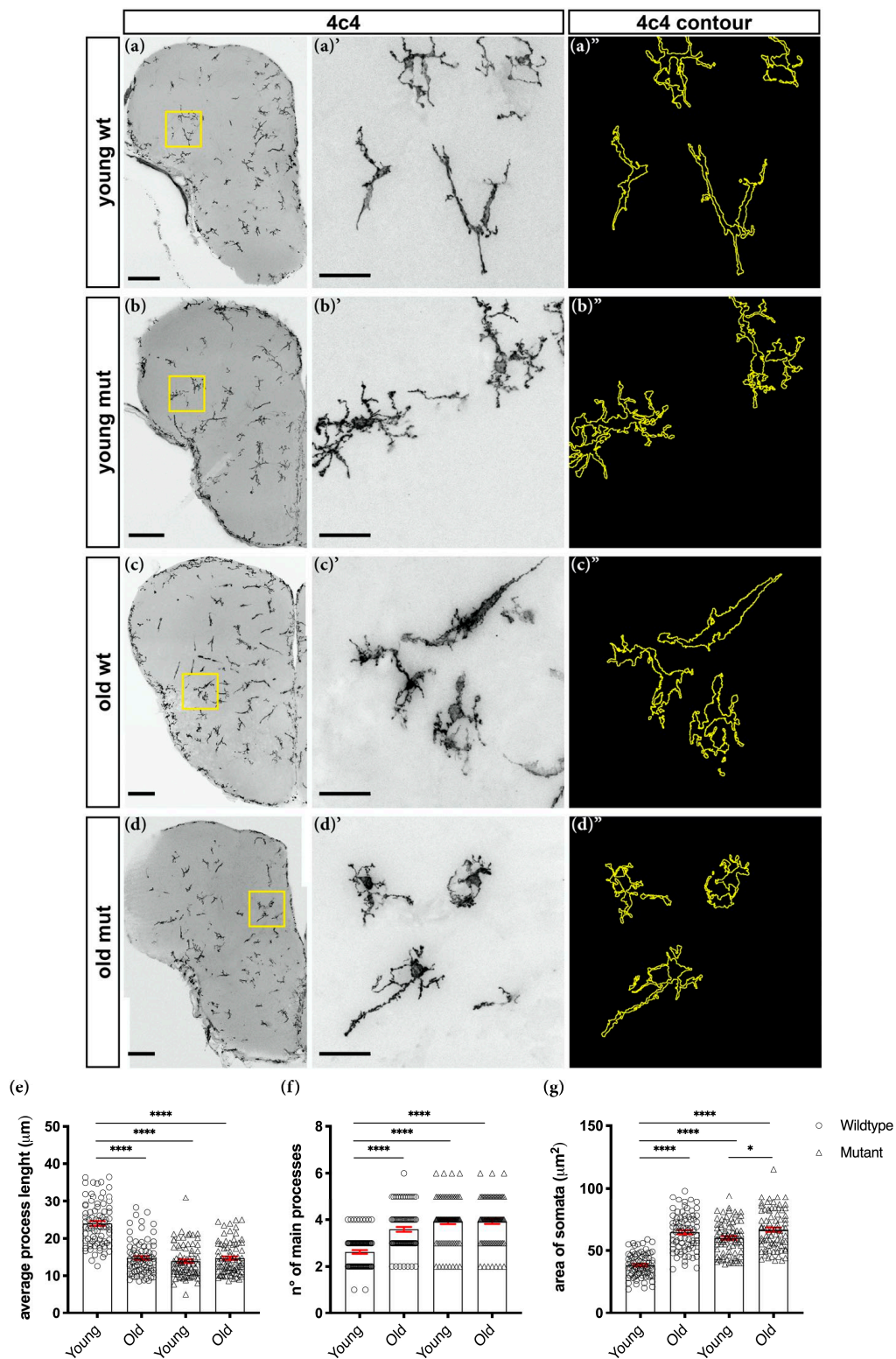


Figure 2. Grna; Grnb-deficient microglial cells display morphological changes associated with aging. (a–d) Micrographs depicting 4C4⁺ microglial cells. (a’–d’) Magnifications of boxed areas in (a–d), respectively. (a’’–d’’) Morphological tracing of 4C4⁺ microglial cells. Scale bars: 100 μm (a–d magnification) and 20 μm (a’–d’). (e–g) Morphological analysis depicting the average process length (e), number of main processes (f) and area of somata (g) of 4C4⁺ microglial cells. n.s., not significant, * $p \leq 0.05$, **** $p \leq 0.0001$, each data point represents a single cell (a total of 80 cells from four telencephali were analysed in each group).

3.2. Loss of *Grna*; *Grnb* Function Induces Premature Microglial Aging

The pro-inflammatory phenotype of microglial cells, including both morphological and characteristic transcriptomic changes, has been associated with aging [70,71]. Indeed, most 4C4⁺ cells in old (15–24-month-old) wildtype animals displayed larger somata and shorter processes (Figure 2c–c'',e–g), in agreement with findings from previous reports [70,71]. For these reasons, we speculated that *Grna*; *Grnb* deficiency might cause a premature aging phenotype in microglial cells in the telencephalon in young animals. Therefore, we analysed and compared the morphology of 4C4⁺ cells in young (3–5-month-old) mutant and old (15–24-month-old) wildtype animals (Figure 2b–c'',e–g). Notably, we observed similar 4C4⁺ cell morphology in the telencephali of young mutant and old wildtype animals (Figure 2b–c'',e–g). Unexpectedly, we detected no additional morphological changes in 4C4⁺ cells of old (15–24-month-old) mutant animals (Figure 2d–d'',e–g). Together, our results indicate a premature aging phenotype in *Grna*; *Grnb*-deficient microglia.

To substantiate this hypothesis, we compared the DEGs in young *Grna*; *Grnb*-deficient *Mpeg1*⁺ cells with the dataset of DEGs of aged (~95-years-old) human microglial cells [70] (Figure 3). Interestingly, 271 DEGs identified in young *Grna*; *Grnb*-deficient *Mpeg1*⁺ cells showed the same regulation pattern seen in aging human microglia (~10% of all human DEGs with existing zebrafish orthologs) (Figure 3a). Notably, GO analysis of overlapping genes revealed an enrichment in genes associated with cholesterol biosynthesis, aging, cell cycle, multiple sclerosis, and Alzheimer's disease (Figure 3b and Figure S4).

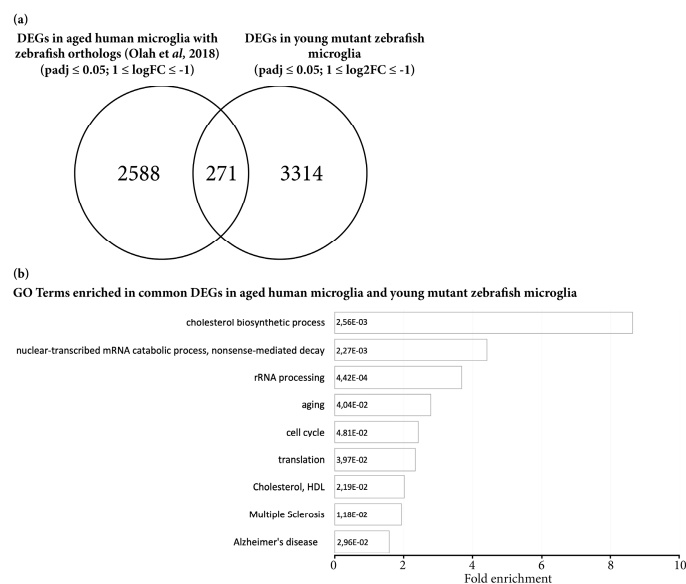


Figure 3. Microglial cells isolated from young mutant zebrafish share a proportion of DEGs with aging human microglial cells. (a) Venn diagram depicting common DEGs in aging human microglial cells with existing zebrafish orthologs and in young mutant zebrafish *Mpeg1*⁺ cells. (b) Histograms depicting gene ontology (GO) terms enriched in the set of 271 common DEGs in aging human and young mutant zebrafish microglial cells.

In summary, our results support roles of *Grna* and *Grnb* in regulating the aging kinetics of microglial cells. Furthermore, these results are in agreement with the described role of GRN in suppressing excessive microglial activation [38] and with previous studies identifying the GRN gene locus as a determinant of accelerated aging in the human cerebral cortex and short lifespan in the African turquoise killifish [32,33].

3.3. Transcriptome Analysis Reveals Premature Aging of *Grna*; *Grnb*-Deficient Brains

To assess whether *Grna* and *Grnb* deficiency might cause a premature aging phenotype exclusively in microglial cells, or affected other cell types and processes in the zebrafish telencephalon,

we compared the total mRNA from whole telencephali of young wildtype (3–5-month-old), old wildtype (15–24-month-old), young mutant (3–5-month-old), and old mutant (15–24-month-old) animals (Figure 4; Figure 5).

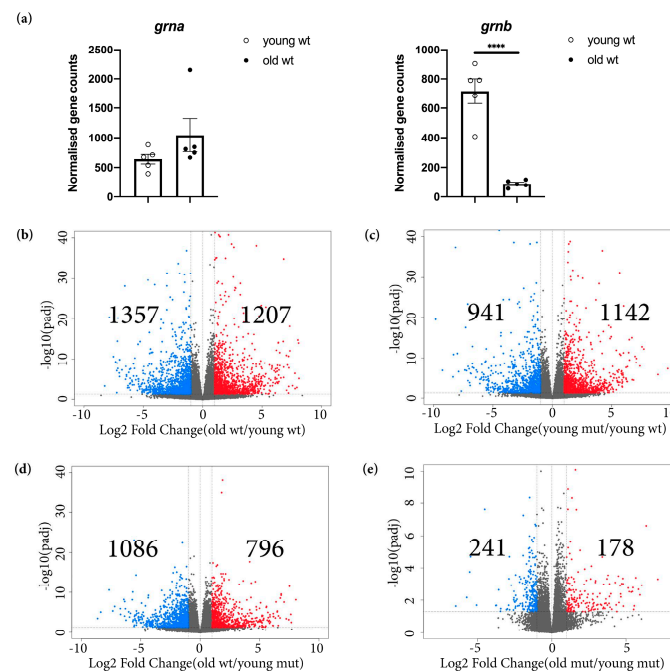


Figure 4. Transcriptomic changes detected in old wildtype, young mutant, and old mutant telencephali. (a) Normalised gene counts of *grna* and *grnb* in young and old wildtype animals. **** $p_{adj} \leq 0.0001$, each data point represents a distinct biological replicate (five telencephali per group were analysed). (b) Volcano plot of DEGs in old wildtype animals (young wildtype animals were used as a reference) ($p_{adj} \leq 0.05$; $1 \leq \log_2FC \leq -1$). (c) Volcano plot of DEGs in young mutant animals (young wildtype animals were used as a reference) ($p_{adj} \leq 0.05$; $1 \leq \log_2FC \leq -1$). (d) Volcano plot of DEGs in old wildtype animals (young mutant animals were used as a reference) ($p_{adj} \leq 0.05$; $1 \leq \log_2FC \leq -1$). (e) Volcano plot of DEGs in old mutant animals (young mutant animals were used as a reference) ($p_{adj} \leq 0.05$; $1 \leq \log_2FC \leq -1$).

First, we analysed *Grna* and *Grnb* mRNA levels in young and old wildtype animals. In contrast to the unchanged *Grna* mRNA levels, the *Grnb* mRNA levels were significantly lower in old wildtype animals (Figure 4a). For this reason, we speculate that *Grnb* deficiency at the stage of young adulthood (3–5-month-old) might mimic the physiological decrease observed in old animals, thus accelerating aging kinetics in the brain.

The differential expression analysis between young and old wildtype telencephali revealed numerous transcriptional changes associated with aging in old wildtype animals, in which we identified 1207 significantly upregulated and 1357 significantly downregulated genes ($p_{adj} \leq 0.05$; $1 \leq \log_2FC \leq -1$) (Figure 4b; Table S2). Similarly, when we compared the transcriptomes of young mutant and young wildtype animals, we identified 1142 significantly upregulated and 941 significantly downregulated genes ($p_{adj} \leq 0.05$; $1 \leq \log_2FC \leq -1$) (Figure 4c; Table S2). Additionally, in a direct comparison of the transcriptomes of old wildtype and young mutant animals, we detected fewer DEGs (Figure 4d; Table S2). Notably, the comparison of the transcriptomes of young mutant and old mutant animals indicated only 178 significantly upregulated and 241 significantly downregulated genes (Figure 4e; Table S2), thus supporting the shift in the brain-wide transcriptome in young mutant animals toward that of aged brains.

We further selected the top 100 significantly upregulated and top 100 significantly downregulated genes in old wildtype animals (using young wildtype animals as a reference) and compared the

rlog-transformed values representing the expression levels of these genes in different ages and genotypes (Figure 5a,b). Unexpectedly, most selected genes had comparable rlog-transformed values in old wildtype, young mutant, and old mutant telencephali (Figure 5a,b). These data provide additional evidence of premature aging in the brain in young *Grna*; *Grnb*-deficient animals.

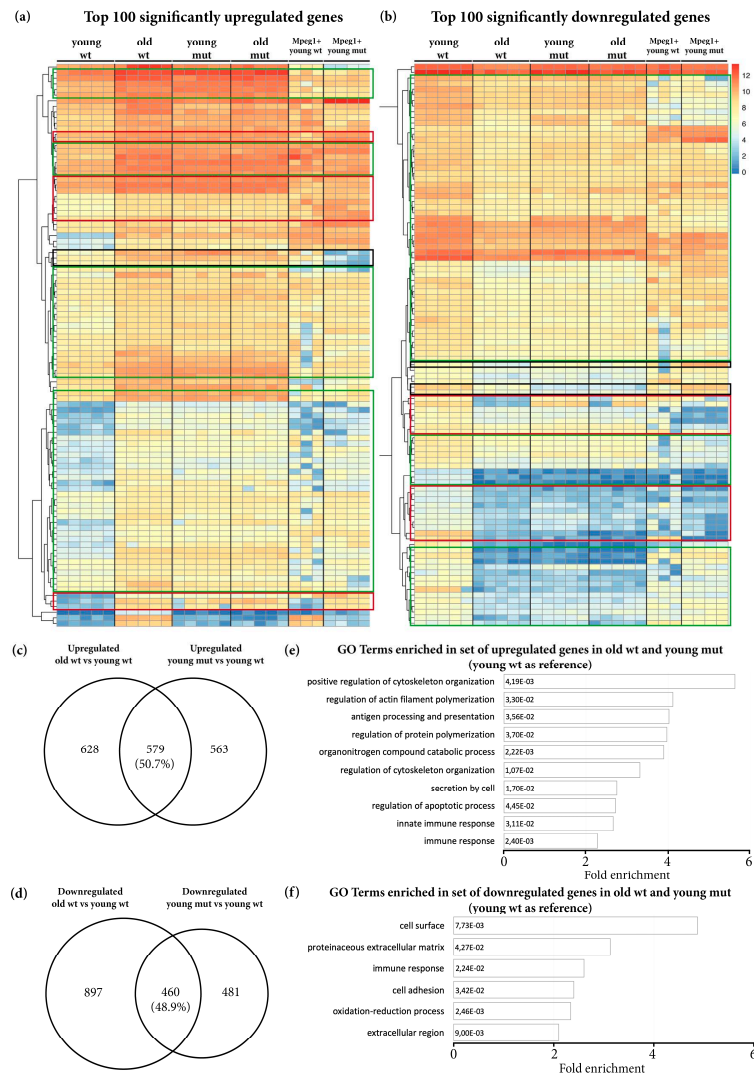


Figure 5. The phenotype of age-related transcriptional changes detected in old wildtype animals is partially mimicked by *Grna* and *Grnb* deficiency in young mutant animals. **(a,b)** Heat maps depicting rlog-transformed values of the top 100 significantly upregulated and downregulated genes in old wildtype telencephali (young wildtype were used as a reference) in young wildtype animals, old wildtype animals, young mutant animals, old mutant animals, young wildtype *Mpeg1*⁺ cells, and young mutant *Mpeg1*⁺ cells. Green boxes: DEGs in old wildtype animals with the same direction of regulation in young mutant and old mutant animals, but not regulated in mutant microglial *Mpeg1*⁺ cells. Red boxes: DEGs in old wildtype animals with comparable levels in young mutant and old mutant animals, regulated in the same direction in mutant microglial *Mpeg1*⁺ cells. Black boxes: DEGs in old wildtype animals with comparable values in young mutant and old mutant animals, regulated in the opposite direction in mutant microglial *Mpeg1*⁺ cells. **(c,d)** Venn diagrams depicting common DEGs in old wildtype and young mutant telencephali (young wildtype were used as a reference). **(e,f)** Histograms depicting gene ontology (GO) terms enriched in the set of common upregulated and downregulated genes in old wildtype and young mutant telencephali (young wildtype were used as a reference).

Our transcriptome analysis of microglia, however, highlighted numerous transcriptomic changes in mutant microglial cells, thus indicating a possibility that the transcriptional changes in mutant microglia might largely contribute to the transcriptional changes observed in the entire telencephalon. To address this possibility, we analysed the expression of the top 100 upregulated and top 100 downregulated genes, as described above, in wildtype Mpeg1⁺ and mutant Mpeg1⁺ cells. Indeed, only a small proportion of selected genes were also regulated with the same pattern in mutant microglial cells (Figure 5a,b). To further address the total contribution of microglia-specific transcriptomic changes to the overall changes in the whole telencephalon in young mutant animals, we compared the DEGs in mutant Mpeg1⁺ cells and in the whole telencephalon in young mutant animals and we detected an overlap of 10.9%. Together, our data demonstrate that Grna and Grnb deficiency promote additional transcriptional changes beyond those specifically detected in microglial cells.

To specifically identify the size and nature of commonly DEGs in old wildtype and young mutant telencephali, we selected and compared the common upregulated and downregulated genes in old wildtype and young mutant animals (using young wildtype animals as a reference) (Figure 5c,d). Notably, 50.7% of upregulated genes and 48.8% downregulated genes were shared between old wildtype and young mutant animals (Figure 5c,d). GO analysis revealed common enrichment in genes associated with programs previously identified in the transcriptome of *Notobranchius furzeri*, a well-established model of aging, including regulation of apoptosis, immune response, extracellular matrix composition and cell adhesion [72] (Figure 5e,f and Figure S5a).

Because GRN has been found to be involved in lysosomal homeostasis and GRN-deficient mice displayed lysosomal dysfunction, we analysed mRNA expression levels of genes associated with lysosomal regulation differentially regulated in GRN-deficient mice [73,74]. In contrast to the results in GRN-deficient mice, expression of lysosomal genes was only slightly changed in the adult telencephalon in young Grna; Grnb-deficient zebrafish, as previously described [51], and was not further changed in old mutant brains, thereby suggesting a discrepancy between the lysosomal regulatory function of granulins in mouse and zebrafish brains (Figure S5b). The observed discrepancy may be explained by the possible involvement of *grn1* and *grn2* in regulating the lysosomal homeostasis in the adult zebrafish brain, thus compensating for the loss of Grna and Grnb.

Collectively, our data indicate that aging causes numerous transcriptional changes in the brain in old wildtype animals. A significant proportion of these changes was mimicked by Grna; Grnb deficiency in the brain in young animals and was not limited to microglial cells. Furthermore, in Grna; Grnb-deficient animals, these changes are significantly reduced between young and old animals, thus strengthening our hypothesis that Grna and Grnb deficiency causes a premature aging phenotype in the brain in young animals.

3.4. Grna and Grnb Deficiency Causes a Reduction in Neurogenesis in the Ventricular Zone of the Zebrafish Telencephalon, thus Mimicking the Phenotype of Reduction Observed during Aging

To understand the aging-related biological processes affected by Grna; Grnb-deficiency, we further analysed shared DEGs in old wildtype and young mutant animals. We identified a significant downregulation of *il4* and *stat6* (Figure 6a). These genes have been implicated in the regulation of age-related inflammatory changes in the rat hippocampus and have a pivotal role in the activation of restorative neurogenesis in a zebrafish model for Alzheimer's disease [75,76].

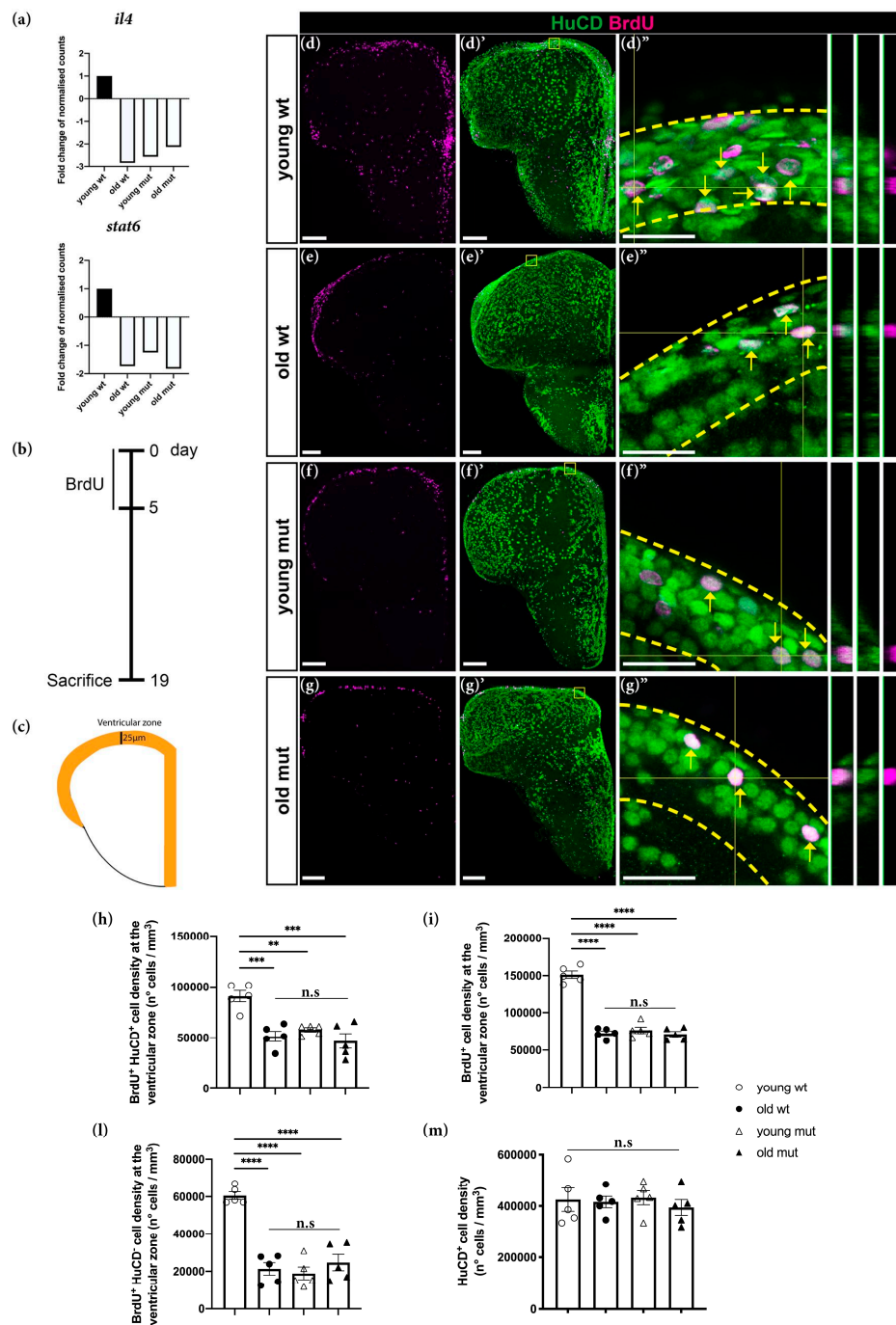


Figure 6. Grna and Grnb deficiency mimics the phenotype of the decrease in neurogenesis observed during aging in the adult zebrafish telencephalon. (a) Histograms depicting relative expression (normalised to that in young wildtype animals) of *il4* and *stat6*. (b) Experimental scheme to assess neurogenesis. (c) Schematic of a typical section from the adult zebrafish telencephalon. Orange area: ventricular area analysed in the experiment. (d–g'') Micrographs depicting newly generated neurons (arrow). (d'–g'') Magnifications with orthogonal projections of boxed areas in (d'–g'), respectively. Scale bars: 100 µm (d–g') and 20 µm (d'–g''). (h–l) Histograms depicting the density of newly generated neurons (h), BrdU⁺ cells (i), and density of non-neuronal BrdU-label retaining cells (l) in the ventricular zone of the adult zebrafish telencephalon. (m) Histogram depicting the density of total HuCD⁺ neurons. n.s, not significant, ** $p \leq 0.01$, *** $p \leq 0.001$, **** $p \leq 0.0001$, each data point represents a distinct biological replicate (five telencephali per group were analysed).

Specifically, in response to the injection of A β 42 derivatives, Il4 is activated and promotes stem cell proliferation and neurogenesis via Stat6 phosphorylation [75]. Furthermore, neurogenesis has been demonstrated to decline with aging: ependymogial cells (neural stem cells in the adult zebrafish telencephalon) enter the cell cycle less frequently, thus producing fewer neuroblasts and consequently fewer neurons [77]. For these reasons, we hypothesised that Grna and Grnb deficiency in young mutant animals might affect neurogenesis as a hallmark of aging, and the downregulation of *il4* and *stat6* might be a possible underlying mechanism. To verify this hypothesis, we assessed the proliferative capacity and the neurogenic potential of young wildtype, old wildtype, young mutant, and old mutant animals in the ventricular zone (VZ) of the zebrafish telencephalon (Figure 6b–l). The VZ is a neurogenic niche that hosts somata of ependymogial cells, which produce new neurons throughout the lifetime [56,57], but show an age-dependent decline [77]. Newborn neurons are generated and deposited in the area immediately below the VZ, the subventricular zone (SVZ) [78]. In this analysis, animals were kept in BrdU water for 5 consecutive days to label all stem cells and neuronal progenitors going through S-phase during the labelling phase (Figure 6b). After the labelling period, we kept animals in normal water for 2 weeks to allow neuronal differentiation of cells that exited the cell cycle and dilution of the label in the still-cycling progenitor population. Therefore, the BrdU⁺ HuCD⁻ cells were classical label-retaining neural stem cells [13]. The number of newborn neurons was assessed by quantification of BrdU⁺ HuCD⁺ (marker for post-mitotic neurons) cells in the VZ and SVZ (25 μ m from the outer layer of the ventricle, as indicated in Figure 6c) (Figure 6d–g'',h). In agreement with previously published data, we detected a significant decrease in the number of BrdU⁺ HuCD⁺ cells (newborn neurons) in the VZ in old wildtype animals (Figure 6d–e'',h). To assess whether Grna and Grnb deficiency might affect the constitutive neurogenic potential to the same extent as that observed in old wildtype animals, we quantified the number of BrdU⁺ HuCD⁺ in young mutant animals (Figure 6d–f'',h) and we detected significantly fewer newborn neurons (BrdU⁺ HuCD⁺) in the VZ in young mutant animals (Figure 6f–f'',h). Interestingly, the numbers were comparable to those observed in old wildtype animals and did not further decrease in old mutant animals, in agreement with the absence of further transcriptional changes between young and old mutant animals (Figure 6g–g'',h). Together, our results demonstrate that aging causes a significant decline in constitutive neurogenesis in the zebrafish telencephalon, and that the phenotype of this decrease is mimicked by Grna and Grnb deficiency in the telencephalon in young animals. This analysis further supports Grna and Grnb being key regulators of aging kinetics in the zebrafish brain. Moreover, we detected a ~50% reduction in the number of BrdU⁺ (label retaining) cells in the VZ in young mutant animals (Figure 6d,f,i). Interestingly, the number of BrdU⁺ cells in the VZ in young mutant animals was comparable to the number of BrdU⁺ cells observed in the VZ in old wildtype animals (Figure 6d–f,i). Notably, no further decrease in the number of BrdU⁺ cells was observed in the VZ in old mutant animals (Figure 6d–g,i).

Because ependymogial cells enter the cell cycle less frequently during aging [77], we speculated that the decreased constitutive neurogenesis in old wildtype and both young and old mutant animals might be explained by an increased number of quiescent ependymogial cells that do not enter the cell cycle and therefore do not incorporate BrdU. Therefore, we analysed the number of BrdU⁺ HuCD⁻ cells in the neurogenic niche (Figure 6l). Notably, we detected a significant decrease in the number of BrdU⁺ HuCD⁻ cells in old wildtype animals, to a level comparable to the number of BrdU⁺ HuCD⁻ cells in young and old mutant animals (Figure 6l). Therefore, these data suggest the premature entry to quiescence of neural stem cells in Grna; Grnb-deficient animals and demonstrate a clear decline in adult neurogenesis, as hallmark of aging. Finally, we quantified the cell density of total HuCD⁺ neurons in the parenchymal area among different groups and observed no significant differences (Figure 6m), a finding in line with different regulatory mechanisms underlying embryonic and adult neurogenesis.

3.5. Grna and Grnb Deficiency Leads to Impaired Oligodendrocyte Precursor Cells Differentiation

Along with a decline in neurogenesis, aging causes a decline in oligodendrogenesis, thus decreasing the abundance of oligodendrocyte precursor cells (OPCs) in the parenchymal area of the adult zebrafish

telencephalon [77]. To verify this concept, we kept animals in BrdU water for 5 consecutive days to label OPCs and performed a 14-day chase (Figure 7a). Oligodendrocyte lineage cells that proliferated during the labelling time were identified by double labelling for BrdU and Sox10 (an oligodendrocyte lineage marker) in the parenchymal area (Figure 7b). In old wildtype animals, we detected a threefold decrease in the number of BrdU⁺ Sox10⁺ cells (Figure 7c–d'',f) in line with findings from previous reports [77]. Unexpectedly, young mutant animals showed a similar decrease (Figure 7e–e'',f). Together, our data indicate that both aging and *Grna*; *Grnb* deficiency induce a decrease in oligodendrogenesis in the zebrafish brain parenchyma.

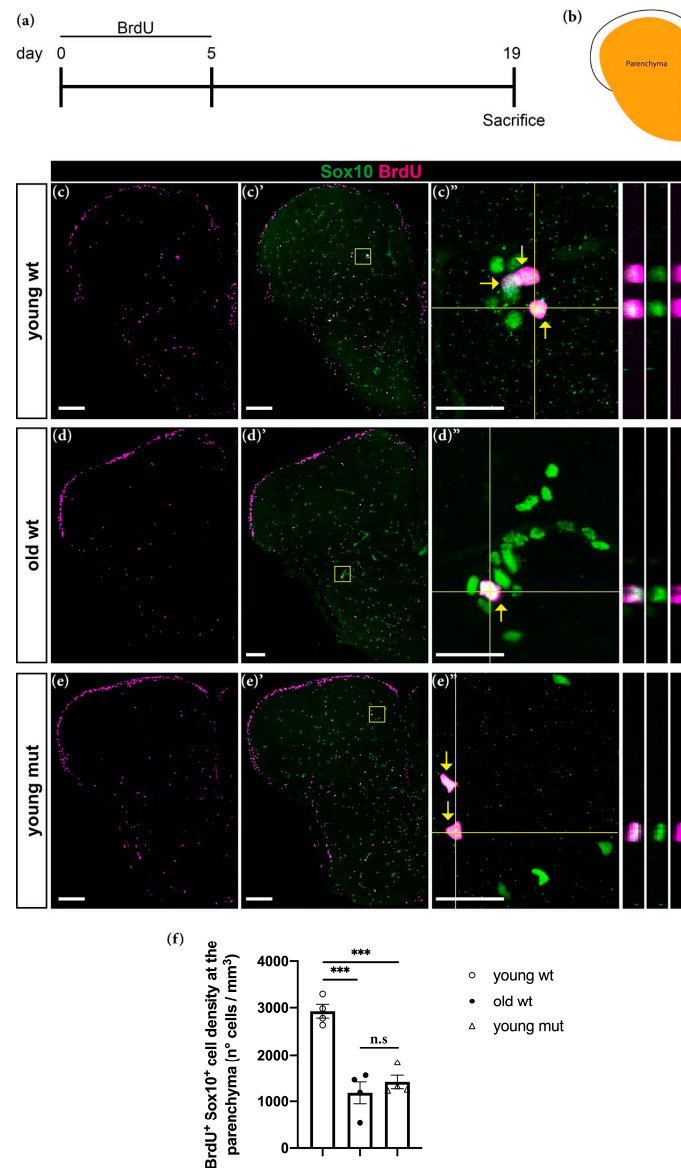


Figure 7. *Grna*; *Grnb* deficiency mimics the phenotype of the decrease in oligodendrogenesis observed during aging in the adult zebrafish telencephalon. (a) Experimental scheme. (b) Schematic of a typical section from the adult zebrafish telencephalon. Orange area: parenchymal area analysed in the experiment. (c–e'') Micrographs depicting BrdU positive oligodendroglial cells stained with Sox10 (green). (c'–e') Magnifications with orthogonal projections of boxed areas in (c'–e'), respectively. Yellow arrows depict cells positive for Sox10 and BrdU. Scale bars: 100 μm in (c–e') and 20 μm in (c''–e''). (f) Histogram depicting the density of BrdU⁺ Sox10⁺ cells in the parenchyma. n.s, not significant, *** $p \leq 0.001$, each data point represents a distinct biological replicate (four telencephali per group were analysed).

The observed phenotype could potentially be explained by lower proliferation of OPCs or impaired oligodendrogenesis. To distinguish between these two possibilities, we assessed the transcriptomic changes in oligodendroglial cells from *Grna*; *Grnb*-deficient animals. By using FACS, we isolated oligodendroglial cells from the *Tg (olig2:DsRed)* animals according to the DsRed expression in Olig2-positive oligodendroglial cells (Figure 8a–c and Figure S1b). Importantly, the identity of cells was validated by co-staining with previously reported oligodendroglial marker, such as Sox10 (Figure 8a–b') [79].

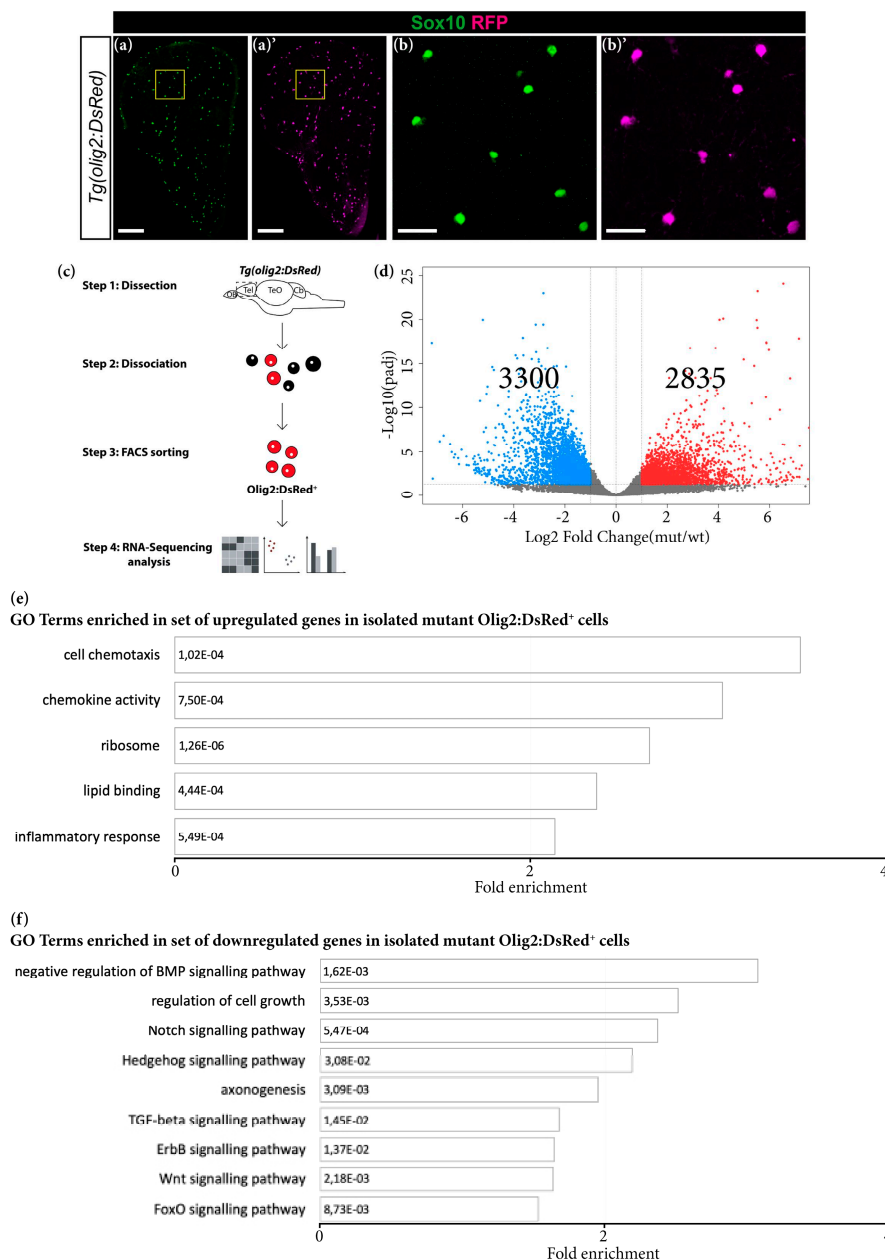


Figure 8. Transcriptomic changes in FACS-isolated mutant oligodendroglial cells. (a–b') Micrographs showing perfect co-localisation of DsRed in the *Tg (olig2:DsRed)* line with the oligodendrocyte lineage marker Sox10. (b,b') Magnifications of the boxed areas in (a) and (a'), respectively. Scale bars: 100 μm in (a,a') and 20 μm in (b,b'). (c) Scheme depicting isolation procedure of *Olig2⁺* cells for transcriptome analysis. (d) Volcano plot of differentially regulated genes in mutant *Olig2⁺* cells ($\text{padj} \leq 0.05$; $1 \leq \log_2\text{FC} \leq -1$). (e,f) Histograms depicting gene ontology (GO) terms enriched in the set of upregulated (e) and downregulated (f) genes in mutant *Olig2⁺* cells.

To determine the purity of isolated cells, we analysed the expression of typical oligodendroglial, neuronal and microglial genes [65] in the sorted DsRed⁺ population (Figure S2b). Significant enrichment in oligodendroglial genes was detected in Olig2⁺ isolated cells together with expression of neuronal genes, in line with the expression of Olig2 in a small subset of neuronal progenitors in the ventral telencephalon (Figure S2b) [79]. Interestingly, we observed comparable expression levels of *grnb* in Mpeg1⁺ and Olig2⁺ cells (Figure S2c), thus suggesting a possible previously undescribed direct role of granulins in oligodendrocyte cells.

By comparing the transcriptomes of young wildtype and mutant Olig2⁺ cells, we detected 2835 significantly upregulated and 3300 significantly downregulated genes in mutant Olig2⁺ cells ($p_{adj} \leq 0.05$; $1 \leq \log_2FC \leq -1$) (Figure 8d; Table S1). GO analysis of significantly upregulated genes in mutant Olig2⁺ cells revealed overrepresentation of terms associated with the immune response, chemokine activity and cell chemotaxis (Figure 8e). Notably, GO analysis of significantly downregulated genes in mutant Olig2⁺ cells revealed enrichment in several terms associated with pathways involved in oligodendroglial cell differentiation and myelination, including negative regulation of BMP, Hedgehog, Notch, TGF- β and ErbB signalling pathways [80–84] (Figure 8f; Figure S6). These results, together with the observed decrease in number of BrdU⁺ Sox10⁺ cells in the telencephalon in young mutant animals, strongly suggest that *Grna* and *Grnb* deficiency affects the normal differentiation process of OPCs. Furthermore, these data suggest that the decreased oligodendrogenesis observed during aging might be partially explained by the decreased granulins levels.

3.6. *Grna* and *Grnb* Deficiency Decreases of Telomere Length

Grna; *Grnb* deficiency leads to numerous aging-associated changes in the adult zebrafish brain. Therefore, we investigated telomere length, an established cell-intrinsic feature of aging cells. Telomeres are known to shorten with aging [2,48,85]. First, we addressed the expression levels of genes involved in telomere protection (Figure 9a). Indeed, we detected a significant downregulation of genes preventing telomere shortening (*tert*, *tp53*, and *tpp1*) in old wildtype, young mutant, and old mutant animals (Figure 9a). To examine the relevance of these genes to telomere length regulation, we quantified the relative telomere length in the brain in young wildtype, old wildtype, young mutant, and old mutant animals, as previously described [64]. Our analysis revealed a significant decrease in the relative telomere length in old wildtype, young mutant, and old mutant animals (Figure 9b), thereby supporting the roles of *Grna* and *Grnb* in regulating physiological aging kinetics in the adult zebrafish brain.

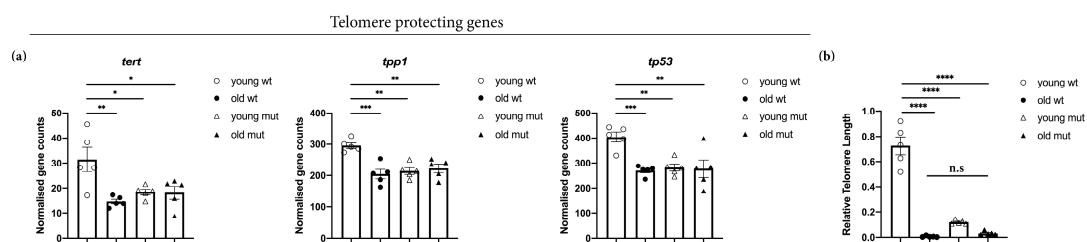


Figure 9. *Grna* and *Grnb* deficiency causes downregulation of telomere-protective genes and telomere shortening in the telencephalon in young zebrafish, as observed in old animals. (a) Histogram depicting normalised gene counts of *tert*, *tp53*, and *tpp1*. (b) Histogram depicting relative telomere length in the young wildtype, old wildtype, young mutant, and old mutant zebrafish telencephalon. *n.s.* not significant, * $p_{adj} \leq 0.05$, ** $p_{adj} \leq 0.01$, *** $p_{adj} \leq 0.001$, **** $p_{adj} \leq 0.0001$, each data point represents a distinct biological replicate (five telencephali per group were analysed).

4. Discussion

Despite numerous studies performed in the context of neurodegeneration and wound healing that have revealed the association of GRN with various processes including wound healing, inflammation, lysosome regulation, neuronal survival, and neurodegeneration [86,87], the physiological roles of GRN in the central nervous system (CNS) remain elusive. Here, we identified *Grna* and *Grnb* as

key regulators of the aging kinetics in the adult zebrafish telencephalon. Specifically, *Grna* and *Grnb* deficiency in microglial cells led to a pro-inflammatory phenotype, which has been previously associated with aging [88]. Moreover, we observed additional aging-associated changes including a decrease in constitutive neurogenesis and oligodendrogenesis, and telomere shortening. The phenotype of changes observed in *Grna*; *Grnb*-deficient animals was also observed in wildtype animals during aging, thus supporting the role of *Grna* and *Grnb* in regulating aging kinetics in the zebrafish telencephalon. Our data are in line with the association of the *GRN* gene locus with aging in the human cerebral cortex [33] as well as with evidences that *GRN* suppresses inflammation in the mouse brain during aging [38]. Interestingly, the levels of *Grnb* physiologically decreased during aging in the adult zebrafish telencephalon, thus partially mimicking the levels observed in mutant animals. These results suggest that progressive loss of *Grnb* may be a key determinant of physiological aging in the adult zebrafish telencephalon.

Our data show that *Grna* and *Grnb* deficiency induces a pro-inflammatory phenotype in microglial cells, which display larger cell bodies, hyper-ramifications and shorter processes—morphological characteristics described in microglial cells during aging in the mouse brain [89]. The altered morphology of mutant microglial cells was accompanied by an increase in the levels of numerous pro-inflammatory cytokines and complement factors as well as a decrease in the levels of anti-inflammatory cytokines. Indeed, one of the most prominent features of brain aging is the activated state of immune cells, thus leading to the secretion of pro-inflammatory cytokines that might not only affect neurons and glia in the central nervous system, but also induce systemic aging-related phenotypes [90]. However, how microglial cells are activated in the brain in *Grna*; *Grnb*-deficient animals remains elusive. Comparing the transcriptomes of wildtype and mutant microglial cells, we detected significant upregulation of numerous genes associated with MAPK and JAK/STAT signalling pathways, which are known to be involved in the regulation of pro-inflammatory cytokine production and microglial activation [66,67]. Similar results have been observed in the mouse brain, where *GRN* has been identified as a key regulator of inflammation, by tuning the expression of pro-inflammatory cytokines and complement factors during aging [38], thus suggesting that granulin directly adjust the levels of inflammatory cytokines to the corresponding aging state in both zebrafish and mammalian brains.

Because we hypothesised that *Grna* and *Grnb* directly regulate the kinetics of aging in the adult zebrafish telencephalon and speculated that *Grna*; *Grnb* deficiency cause a premature aging phenotype in the telencephalon in young animals, we examined the transcriptional signature in the entire telencephalon in wildtype and mutant animals at two different ages (young and old animals). Indeed, aging caused significant changes in the transcription levels of numerous genes in the telencephalon in old wildtype animals. Unexpectedly, a high proportion (~50%) of DEGs in old wildtype animals were also altered in same trend as that in young mutant animals, thereby indicating a similar transcriptome signature. The set of common DEGs was enriched in programs associated with innate immunity, regulation of apoptotic process, extracellular matrix composition, and p53 signalling; similar enrichment has also been identified in the transcriptome of *Notobranchius furzeri*, a well-established model of brain aging [72], thus supporting the concept of a premature aging phenotype in the telencephalon in young mutant animals. Importantly, a large proportion of common DEGs included genes that were not regulated in mutant microglial cells, thus suggesting that granulin deficiency not only affects microglia but also induces additional aging-related changes in other cell populations. However, whether these effects are due to a direct function of *Grna* and *Grnb* in these cell types or whether the observed changes are indirect and induced by altered mutant microglial cells remains unclear.

Interestingly, we identified diminished mRNA levels of *il4* and *stat6* in the telencephalon in old wildtype, young mutant, and old mutant animals. *Il4* and *Stat6* have been implicated in the regulation of neuronal progenitor proliferation and neurogenesis [75], whose rates are directly controlled by microglial activity [91–93]. Therefore, our data, at least in part, support the hypothesis that the

proinflammatory phenotype of *Grna*; *Grnb*-deficient microglial cells contributes to the aging of the zebrafish neural stem cell compartment. Moreover, the ependymoglia population (the neural stem cells in the adult zebrafish telencephalon) displays an age-related increased proportion of quiescent cells, thereby decreasing the number of newly generated neurons [77]. Indeed, we demonstrated that both aging and *Grna*; *Grnb* deficiency in young animals caused a similar reduction in the number of proliferating cells (mostly neuronal progenitors in the neural stem cell niche) and newly generated neurons, thus strengthening the association between granulins and regulation of brain aging. Moreover, both aging and *Grna*; *Grnb* deficiency in young animals led to a decrease in oligodendrogenesis, a process severely affected in the aging CNS in both mice and zebrafish [77,94,95]. Furthermore, the decreased oligodendrogenesis could be explained by dramatic changes in the transcriptome of mutant oligodendroglial cells. In fact, GO term analysis revealed downregulation of several genes associated with Hedgehog, canonical Wnt, Notch, TGF- β , ErbB signalling, and with negative regulation of BMP signalling pathways. Notably, all these pathways have been associated with oligodendroglial cell maturation, differentiation and myelination [80–84], and they depend on niche-provided signals amenable to changes by microglial cells [96]. These findings further support the idea that initial changes in microglial cells trigger age-related changes in neurogenesis and oligodendrogenesis in a cell non-autonomous manner.

Finally, we also observed significant telomere shortening in the brain in young mutant animals, to levels comparable to those detected in aging brains. Moreover, we detected diminished mRNA levels of genes encoding for enzymes involved in telomere length maintenance. Because telomere shortening is a typical cell-intrinsic feature associated with aging [97], *Grna* and *Grnb* might coordinate the acquisition of both cell-extrinsic and -intrinsic aging features in the adult zebrafish brain.

In this study, we identified the roles of *Grna* and *Grnb* in regulating the inflammatory state under physiological conditions and during aging in the zebrafish brain, in line with observations in the mouse CNS [38,98]. Furthermore, we provide new evidence that *Grna* and *Grnb* directly regulate aging and that their loss causes a premature aging phenotype in the telencephalon in young zebrafish, thus providing new insights into the physiological roles of granulins that could potentially be used for the development of new therapeutic interventions in the mammalian CNS.

Supplementary Materials: The following are available online at <http://www.mdpi.com/2073-4409/9/2/350/s1>, Figure S1: FACS plots illustrating sorting gates for FACS isolation. (a) Gates are defined with the wildtype AB/EK strain to sort mCherry⁺ cells from the *Tg (mpeg1:mCherry)* line. (b) Gates are defined with the wildtype AB/EK strain to sort DsRed⁺ cells from the *Tg (olig2:DsRed)* line. Abbreviations: FSC-A: forward scatter-area; SSC-A: side scatter- area; FSC-W: forward scatter-width, Figure S2: Gene enrichment in FACS isolated Mpeg1⁺ and Olig2⁺ cells. (a,b) Histograms depicting normalised gene counts for typical microglial, neuronal and oligodendroglial genes detected in Mpeg1⁺ (a) and Olig2⁺ (b) cells. (c) Histogram depicting normalised gene counts for *grna* and *grnb* in Mpeg1⁺ and Olig2⁺ cells. Each data point represents a distinct biological replicate, Figure S3: *Grna*; *Grnb* deficiency causes numerous transcriptional changes in microglial cells. (a) Heat maps depicting rlog-transformed values of DEGs in mutant Mpeg1⁺ cells associated with main GO terms analysed. (b,c) Histograms showing normalised gene counts for pro-inflammatory (b) and anti-inflammatory (c) cytokines. ** $p \leq 0.01$, *** $p \leq 0.001$, **** $p \leq 0.0001$, each data point represents a distinct biological replicate, Figure S4: Heat maps depicting rlog-transformed values of common DEGs in mutant Mpeg1⁺ cells and aging human microglia associated with main GO terms analysed, Figure S5: a high proportion of transcriptional changes observed in old wildtype telencephali is mimicked by *Grna* and *Grnb* deficiency. (a) Heat maps depicting rlog-transformed values of common DEGs in whole telencephalon in young mutant and old wildtype animals associated with main GO terms analysed. (b) Histograms depicting normalised gene counts for lysosomal genes in the entire telencephalon in young wildtype, old wildtype, young mutant and old mutant animals, Figure S6: Heat maps depicting rlog-transformed values of DEGs in mutant Olig2⁺ cells associated with main GO terms analysed, Table S1: List of DEGs in mutant Mpeg1:mCherry⁺ and mutant Olig2:DsRed⁺ cells. The following filtering was applied ($padj \leq 0.05$; $1 \leq \log_2FC \leq -1$). Comparison with upregulated genes enriched in major categories from Lui et al., 2016. Genes that are upregulated in our analysis and in the dataset from Lui et al., 2016 are highlighted in green, Table S2: List of DEGs in old wildtype vs young wildtype telencephali; in young mutant vs young wildtype telencephali; in old wildtype vs young mutant telencephali; in old mutant vs young mutant telencephali. The following filtering was applied ($padj \leq 0.05$; $1 \leq \log_2FC \leq -1$).

Author Contributions: Conceptualization, A.Z., R.D.G., J.N.; methodology, A.Z., Ö.P.B.; software, A.Z.; validation, A.Z., J.N.; visualization, A.Z., J.N.; formal analysis, A.Z., J.N.; investigation, A.Z., Ö.P.B., B.S., J.N.; data curation,

A.Z., Ö.P.B., J.N.; writing—original draft preparation, A.Z., J.N.; supervision, B.S., J.N.; funding acquisition, B.S., J.N. All authors have read and agreed to the published version of the manuscript.

Funding: This research was funded by the German research foundation (DFG) by the SFB 870; TRR274; SPP 1738 “Emerging roles of non-coding RNAs in nervous system development, plasticity & disease”, SPP1757 “Glial heterogeneity”; and Excellence Strategy within the framework of the Munich Cluster for Systems Neurology (EXC 2145/1010 SyNergy – ID 390857198) and Ampro Helmholtz Alliance.

Acknowledgments: We thank Sabine Schlink, Roberto Rojas, and Michael Lange for fish care. We are also very grateful to Sabrina Bortoluzzi, Tjasa Lepko, Christina Koupourtidou, and Tobias Straub for help with figure design and transcriptome analysis.

Conflicts of Interest: The authors declare no conflicts of interest.

Abbreviations

NF-κB	Nuclear factor kappa B
wt	Wildtype
mut	Mutant
<i>grna</i>	Granulin a
<i>grnb</i>	Granulin b
<i>mpeg1</i>	Macrophage expressed 1
MAPK	Mitogen-activated protein kinase
JAK/STAT	Janus kinase/signal transducer and activator of transcription
PPAR	Peroxisome proliferator-activated receptor
<i>il1b</i>	Interleukin 1 beta
<i>il6</i>	Interleukin 6
<i>tnfa</i>	Tumor necrosis factor alpha
<i>il12bβ</i>	Interleukin 12b beta
<i>Cxcl8a</i>	Chemokine (C-X-C motif) ligand 8a
<i>tgfb3</i>	Transforming growth factor beta 3
<i>igf1</i>	Insulin-like growth factor 1
<i>il10</i>	Interleukin 10
<i>il4</i>	Interleukin 4
<i>stat6</i>	Signal transducer and activator of transcription 6
VZ	Ventricular zone
SVZ	Subventricular zone
<i>sox10</i>	SRY-box transcription Factor 10
<i>olig2</i>	Oligodendrocyte lineage transcription factor 2
BMP	Bone morphogenetic protein
TGF-β	Transforming growth factor-beta
ErbB	EGFR family signalling pathway
<i>tert</i>	Telomerase reverse transcriptase
<i>tp53</i>	Tumor protein p53
<i>tpp1</i>	Tripeptidyl peptidase 1

References

1. Mattson, M.P.; Arumugam, T.V. Hallmarks of Brain Aging: Adaptive and Pathological Modification by Metabolic States. *Cell Metab.* **2018**, *27*, 1176–1199. [[CrossRef](#)] [[PubMed](#)]
2. Lopez-Otin, C.; Blasco, M.A.; Partridge, L.; Serrano, M.; Kroemer, G. The hallmarks of aging. *Cell* **2013**, *153*, 1194–1217. [[CrossRef](#)] [[PubMed](#)]
3. Gruber, R.; Koch, H.; Doll, B.A.; Tegtmeier, F.; Einhorn, T.A.; Hollinger, J.O. Fracture healing in the elderly patient. *Exp. Gerontol.* **2006**, *41*, 1080–1093. [[CrossRef](#)] [[PubMed](#)]
4. Shaw, R.L.; Kohlmaier, A.; Polesello, C.; Veelken, C.; Edgar, B.A.; Tapon, N. The Hippo pathway regulates intestinal stem cell proliferation during *Drosophila* adult midgut regeneration. *Development* **2010**, *137*, 4147–4158. [[CrossRef](#)] [[PubMed](#)]

5. Conboy, I.M.; Rando, T.A. Heterochronic parabiosis for the study of the effects of aging on stem cells and their niches. *Cell Cycle* **2012**, *11*, 2260–2267. [[CrossRef](#)] [[PubMed](#)]
6. Molofsky, A.V.; Slutsky, S.G.; Joseph, N.M.; He, S.; Pardal, R.; Krishnamurthy, J.; Sharpless, N.E.; Morrison, S.J. Increasing p16INK4a expression decreases forebrain progenitors and neurogenesis during ageing. *Nature* **2006**, *443*, 448–452. [[CrossRef](#)]
7. Bast, L.; Calzolari, F.; Strasser, M.K.; Hasenauer, J.; Theis, F.J.; Ninkovic, J.; Marr, C. Increasing Neural Stem Cell Division Asymmetry and Quiescence Are Predicted to Contribute to the Age-Related Decline in Neurogenesis. *Cell Rep.* **2018**, *25*, 3231–3240.e8. [[CrossRef](#)]
8. Lupo, G.; Gioia, R.; Nisi, P.S.; Biagioni, S.; Cacci, E. Molecular Mechanisms of Neurogenic Aging in the Adult Mouse Subventricular Zone. *J. Exp. Neurosci.* **2019**, *13*, 1179069519829040. [[CrossRef](#)]
9. Enwere, E.; Shingo, T.; Gregg, C.; Fujikawa, H.; Ohta, S.; Weiss, S. Aging results in reduced epidermal growth factor receptor signaling, diminished olfactory neurogenesis, and deficits in fine olfactory discrimination. *J. Neurosci.* **2004**, *24*, 8354–8365. [[CrossRef](#)]
10. Daynac, M.; Morizur, L.; Chicheportiche, A.; Mouthon, M.A.; Boussin, F.D. Age-related neurogenesis decline in the subventricular zone is associated with specific cell cycle regulation changes in activated neural stem cells. *Sci. Rep.* **2016**, *6*, 21505. [[CrossRef](#)]
11. Silva-Vargas, V.; Maldonado-Soto, A.R.; Mizrak, D.; Codega, P.; Doetsch, F. Age-Dependent Niche Signals from the Choroid Plexus Regulate Adult Neural Stem Cells. *Cell Stem Cell* **2016**, *19*, 643–652. [[CrossRef](#)] [[PubMed](#)]
12. Baruch, K.; Deczkowska, A.; David, E.; Castellano, J.M.; Miller, O.; Kertser, A.; Berkutzki, T.; Barnett-Itzhaki, Z.; Bezalel, D.; Wyss-Coray, T.; et al. Aging. Aging-induced type I interferon response at the choroid plexus negatively affects brain function. *Science* **2014**, *346*, 89–93. [[CrossRef](#)] [[PubMed](#)]
13. Lepko, T.; Pusch, M.; Muller, T.; Schulte, D.; Ehses, J.; Kiebler, M.; Hasler, J.; Huttner, H.B.; Vandenbroucke, R.E.; Vandendriessche, C.; et al. Choroid plexus-derived miR-204 regulates the number of quiescent neural stem cells in the adult brain. *EMBO J.* **2019**, *38*, e100481. [[CrossRef](#)] [[PubMed](#)]
14. Lupo, G.; Nisi, P.S.; Esteve, P.; Paul, Y.L.; Novo, C.L.; Sidders, B.; Khan, M.A.; Biagioni, S.; Liu, H.K.; Bovolenta, P.; et al. Molecular profiling of aged neural progenitors identifies Dbx2 as a candidate regulator of age-associated neurogenic decline. *Aging Cell* **2018**, *17*, e12745. [[CrossRef](#)]
15. Apostolopoulou, M.; Kiehl, T.R.; Winter, M.; Cardenas De La Hoz, E.; Boles, N.C.; Bjornsson, C.S.; Zuloaga, K.L.; Goderie, S.K.; Wang, Y.; Cohen, A.R.; et al. Non-monotonic Changes in Progenitor Cell Behavior and Gene Expression during Aging of the Adult V-SVZ Neural Stem Cell Niche. *Stem Cell Rep.* **2017**, *9*, 1931–1947. [[CrossRef](#)]
16. Leeman, D.S.; Hebestreit, K.; Ruetz, T.; Webb, A.E.; McKay, A.; Pollina, E.A.; Dulken, B.W.; Zhao, X.; Yeo, R.W.; Ho, T.T.; et al. Lysosome activation clears aggregates and enhances quiescent neural stem cell activation during aging. *Science* **2018**, *359*, 1277–1283. [[CrossRef](#)]
17. Piccin, D.; Tufford, A.; Morshead, C.M. Neural stem and progenitor cells in the aged subependyma are activated by the young niche. *Neurobiol. Aging* **2014**, *35*, 1669–1679. [[CrossRef](#)]
18. Villeda, S.A.; Luo, J.; Mosher, K.I.; Zou, B.; Britschgi, M.; Bieri, G.; Stan, T.M.; Fainberg, N.; Ding, Z.; Eggel, A.; et al. The ageing systemic milieu negatively regulates neurogenesis and cognitive function. *Nature* **2011**, *477*, 90–94. [[CrossRef](#)]
19. Butovsky, O.; Ziv, Y.; Schwartz, A.; Landa, G.; Talpalar, A.E.; Pluchino, S.; Martino, G.; Schwartz, M. Microglia activated by IL-4 or IFN-gamma differentially induce neurogenesis and oligodendrogenesis from adult stem/progenitor cells. *Mol. Cell. Neurosci.* **2006**, *31*, 149–160. [[CrossRef](#)]
20. Wong, W.T. Microglial aging in the healthy CNS: Phenotypes, drivers, and rejuvenation. *Front. Cell. Neurosci.* **2013**, *7*, 22. [[CrossRef](#)] [[PubMed](#)]
21. Ziv, Y.; Ron, N.; Butovsky, O.; Landa, G.; Sudai, E.; Greenberg, N.; Cohen, H.; Kipnis, J.; Schwartz, M. Immune cells contribute to the maintenance of neurogenesis and spatial learning abilities in adulthood. *Nat. Neurosci.* **2006**, *9*, 268–275. [[CrossRef](#)] [[PubMed](#)]
22. Ekdahl, C.T.; Kokaia, Z.; Lindvall, O. Brain inflammation and adult neurogenesis: The dual role of microglia. *Neuroscience* **2009**, *158*, 1021–1029. [[CrossRef](#)] [[PubMed](#)]
23. Salminen, A.; Kaarniranta, K.; Kauppinen, A. Inflammaging: Disturbed interplay between autophagy and inflammasomes. *Aging* **2012**, *4*, 166–175. [[CrossRef](#)] [[PubMed](#)]

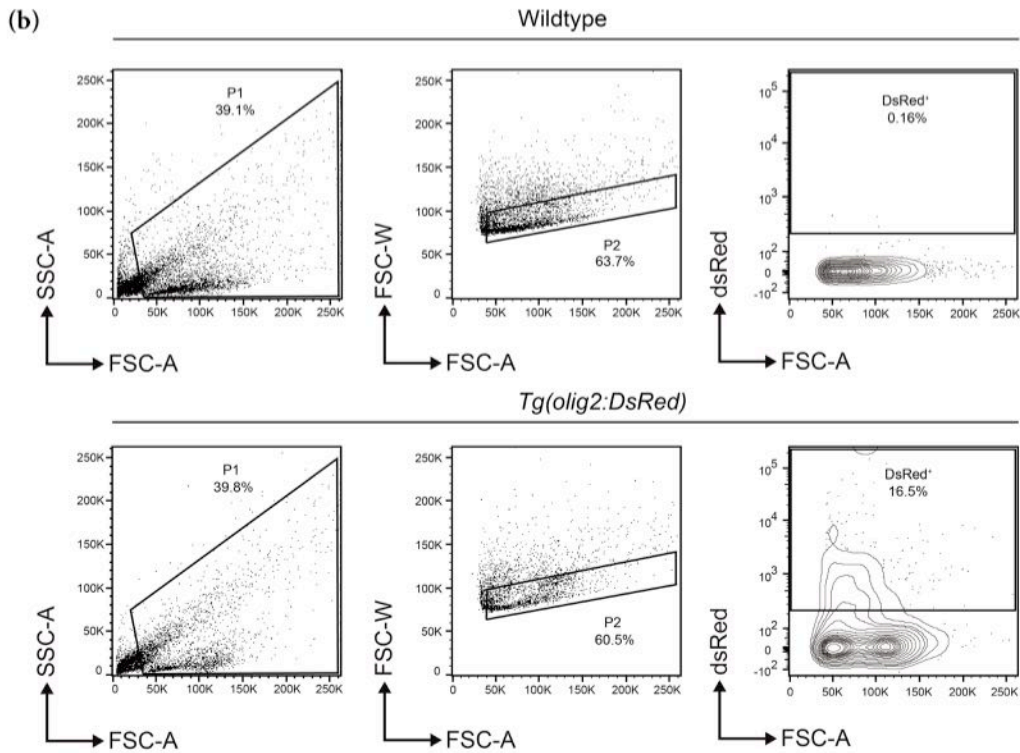
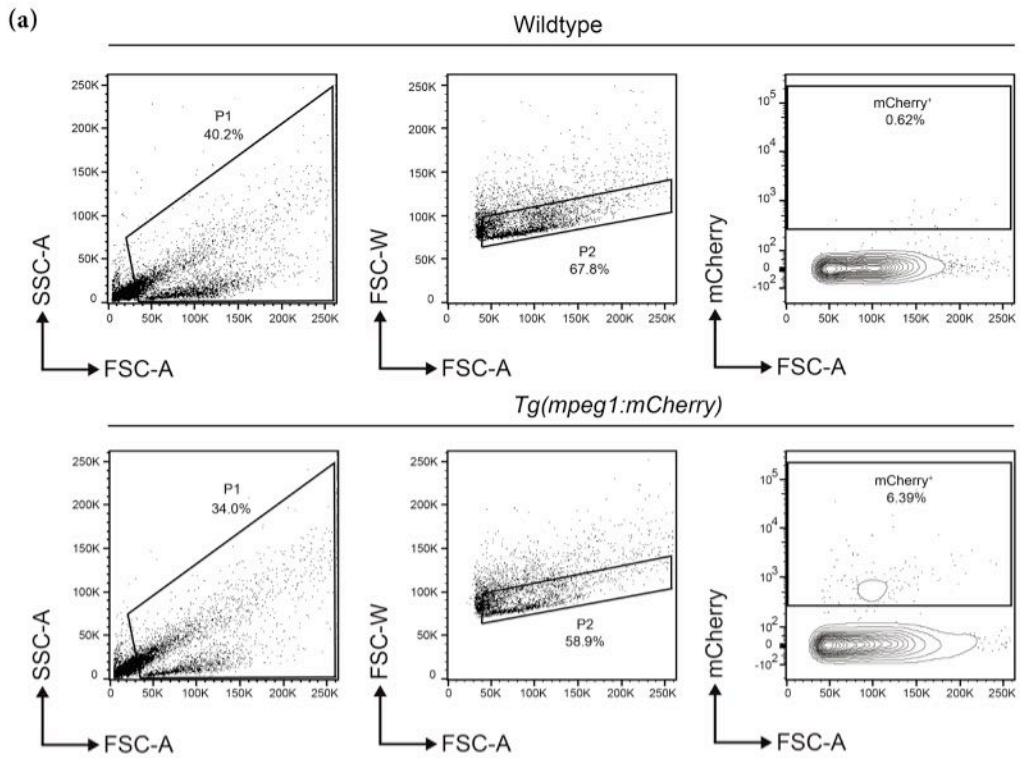
24. Zhang, G.; Li, J.; Purkayastha, S.; Tang, Y.; Zhang, H.; Yin, Y.; Li, B.; Liu, G.; Cai, D. Hypothalamic programming of systemic ageing involving IKK-beta, NF-kappaB and GnRH. *Nature* **2013**, *497*, 211–216. [[CrossRef](#)] [[PubMed](#)]
25. Pont, A.R.; Sadri, N.; Hsiao, S.J.; Smith, S.; Schneider, R.J. mRNA decay factor AUF1 maintains normal aging, telomere maintenance, and suppression of senescence by activation of telomerase transcription. *Mol. Cell* **2012**, *47*, 5–15. [[CrossRef](#)]
26. He, Z.; Bateman, A. Progranulin (granulin-epithelin precursor, PC-cell-derived growth factor, acrogranin) mediates tissue repair and tumorigenesis. *J. Mol. Med. (Berl.)* **2003**, *81*, 600–612. [[CrossRef](#)]
27. Petkau, T.L.; Neal, S.J.; Orban, P.C.; MacDonald, J.L.; Hill, A.M.; Lu, G.; Feldman, H.H.; Mackenzie, I.R.; Leavitt, B.R. Progranulin expression in the developing and adult murine brain. *J. Comp. Neurol.* **2010**, *518*, 3931–3947. [[CrossRef](#)]
28. Cenik, B.; Sephton, C.F.; Kutluk Cenik, B.; Herz, J.; Yu, G. Progranulin: a proteolytically processed protein at the crossroads of inflammation and neurodegeneration. *J. Biol. Chem.* **2012**, *287*, 32298–32306. [[CrossRef](#)]
29. Zhu, J.; Nathan, C.; Jin, W.; Sim, D.; Ashcroft, G.S.; Wahl, S.M.; Lacomis, L.; Erdjument-Bromage, H.; Tempst, P.; Wright, C.D.; et al. Conversion of proepithelin to epithelins: Roles of SLPI and elastase in host defense and wound repair. *Cell* **2002**, *111*, 867–878. [[CrossRef](#)]
30. Jian, J.; Konopka, J.; Liu, C. Insights into the role of progranulin in immunity, infection, and inflammation. *J. Leukoc. Biol.* **2013**, *93*, 199–208. [[CrossRef](#)]
31. Wils, H.; Kleinberger, G.; Pereson, S.; Janssens, J.; Capell, A.; Van Dam, D.; Cuijt, I.; Joris, G.; De Deyn, P.P.; Haass, C.; et al. Cellular ageing, increased mortality and FTLT-DTP-associated neuropathology in progranulin knockout mice. *J. Pathol.* **2012**, *228*, 67–76. [[CrossRef](#)] [[PubMed](#)]
32. Valenzano, D.R.; Benayoun, B.A.; Singh, P.P.; Zhang, E.; Etter, P.D.; Hu, C.K.; Clément-Ziza, M.; Willemsen, D.; Cui, R.; Harel, I.; et al. The African Turquoise Killifish Genome Provides Insights into Evolution and Genetic Architecture of Lifespan. *Cell* **2015**, *163*, 1539–1554. [[CrossRef](#)] [[PubMed](#)]
33. Rhinn, H.; Abeliovich, A. Differential Aging Analysis in Human Cerebral Cortex Identifies Variants in TMEM106B and GRN that Regulate Aging Phenotypes. *Cell Syst.* **2017**, *4*, 404.e5–415.e5. [[CrossRef](#)] [[PubMed](#)]
34. Baker, M.; Mackenzie, I.R.; Pickering-Brown, S.M.; Gass, J.; Rademakers, R.; Lindholm, C.; Snowden, J.; Adamson, J.; Sadvnick, A.D.; Rollinson, S.; et al. Mutations in progranulin cause tau-negative frontotemporal dementia linked to chromosome 17. *Nature* **2006**, *442*, 916–919. [[CrossRef](#)]
35. Cruets, M.; Gijssels, I.; van der Zee, J.; Engelborghs, S.; Wils, H.; Pirici, D.; Rademakers, R.; Vandenberghe, R.; Dermaut, B.; Martin, J.-J.; et al. Null mutations in progranulin cause ubiquitin-positive frontotemporal dementia linked to chromosome 17q21. *Nature* **2006**, *442*, 920–924. [[CrossRef](#)] [[PubMed](#)]
36. Smith, K.R.; Damiano, J.; Franceschetti, S.; Carpenter, S.; Canafoglia, L.; Morbin, M.; Rossi, G.; Pareyson, D.; Mole, S.E.; Staropoli, J.F.; et al. Strikingly different clinicopathological phenotypes determined by progranulin-mutation dosage. *Am. J. Hum. Genet.* **2012**, *90*, 1102–1107. [[CrossRef](#)]
37. Almeida, M.R.; Macario, M.C.; Ramos, L.; Baldeiras, I.; Ribeiro, M.H.; Santana, I. Portuguese family with the co-occurrence of frontotemporal lobar degeneration and neuronal ceroid lipofuscinosis phenotypes due to progranulin gene mutation. *Neurobiol. Aging* **2016**, *41*, 200.e1–200.e5. [[CrossRef](#)]
38. Lui, H.; Zhang, J.; Makinson, S.R.; Cahill, M.K.; Kelley, K.W.; Huang, H.Y.; Shang, Y.; Oldham, M.C.; Martens, L.H.; Gao, F.; et al. Progranulin Deficiency Promotes Circuit-Specific Synaptic Pruning by Microglia via Complement Activation. *Cell* **2016**, *165*, 921–935. [[CrossRef](#)]
39. Götzl, J.K.; Brendel, M.; Werner, G.; Parhizkar, S.; Sebastian Monasor, L.; Kleinberger, G.; Colombo, A.V.; Deussing, M.; Wagner, M.; Winkelmann, J.; et al. Opposite microglial activation stages upon loss of PGRN or TREM2 result in reduced cerebral glucose metabolism. *EMBO Mol. Med.* **2019**, *11*. [[CrossRef](#)]
40. Yin, F.; Banerjee, R.; Thomas, B.; Zhou, P.; Qian, L.; Jia, T.; Ma, X.; Ma, Y.; Iadecola, C.; Beal, M.F.; et al. Exaggerated inflammation, impaired host defense, and neuropathology in progranulin-deficient mice. *J. Exp. Med.* **2010**, *207*, 117–128. [[CrossRef](#)]
41. Martens, L.H.; Zhang, J.; Barmada, S.J.; Zhou, P.; Kamiya, S.; Sun, B.; Min, S.W.; Gan, L.; Finkbeiner, S.; Huang, E.J.; et al. Progranulin deficiency promotes neuroinflammation and neuron loss following toxin-induced injury. *J. Clin. Investig.* **2012**, *122*, 3955–3959. [[CrossRef](#)] [[PubMed](#)]
42. Tanaka, Y.; Matsuwaki, T.; Yamanouchi, K.; Nishihara, M. Exacerbated inflammatory responses related to activated microglia after traumatic brain injury in progranulin-deficient mice. *Neuroscience* **2013**, *231*, 49–60. [[CrossRef](#)]

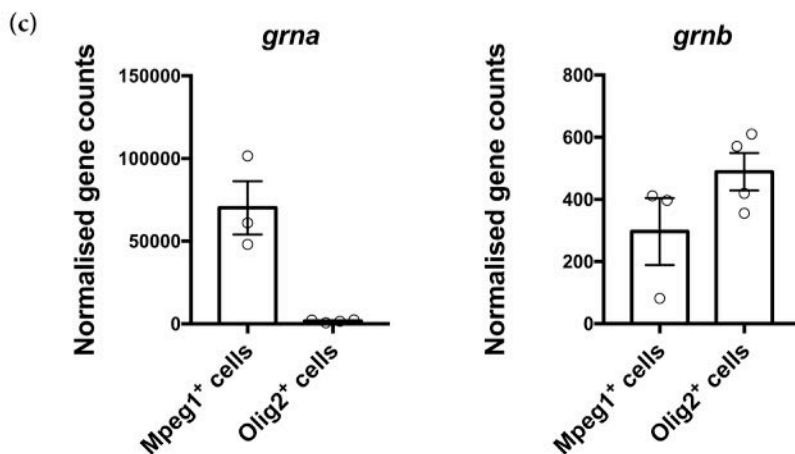
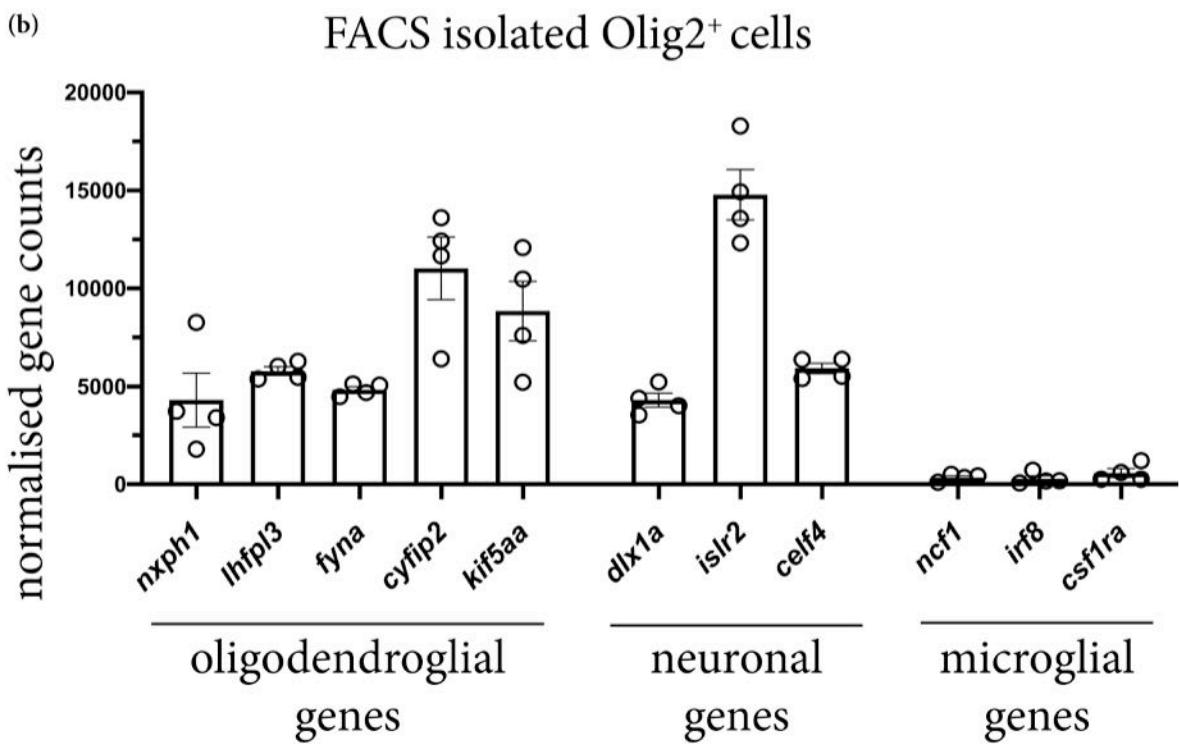
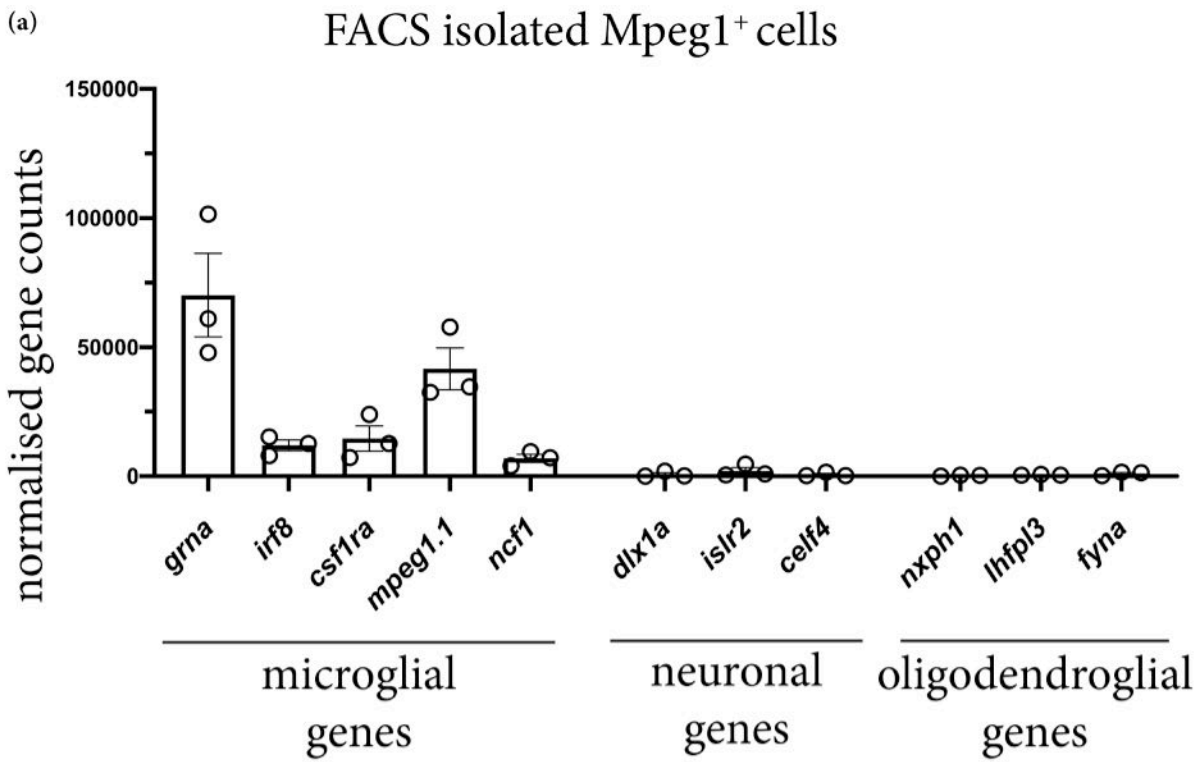
43. Altmann, C.; Vasic, V.; Hardt, S.; Heidler, J.; Häussler, A.; Wittig, I.; Schmidt, M.H.H.; Tegeder, I. Progranulin promotes peripheral nerve regeneration and reinnervation: Role of notch signaling. *Mol. Neurodegener.* **2016**, *11*, 69. [[CrossRef](#)] [[PubMed](#)]
44. Toh, H.; Chitramuthu, B.P.; Bennett, H.P.J.; Bateman, A. Structure, function, and mechanism of progranulin; the brain and beyond. *J. Mol. Neurosci.* **2011**, *45*, 538–548. [[CrossRef](#)]
45. Ryan, C.L.; Baranowski, D.C.; Chitramuthu, B.P.; Malik, S.; Li, Z.; Cao, M.; Minotti, S.; Durham, H.D.; Kay, D.G.; Shaw, C.A.; et al. Progranulin is expressed within motor neurons and promotes neuronal cell survival. *BMC Neurosci.* **2009**, *10*, 130. [[CrossRef](#)] [[PubMed](#)]
46. Van Damme, P.; Van Hoecke, A.; Lambrechts, D.; Vanacker, P.; Bogaert, E.; van Swieten, J.; Carmeliet, P.; Van Den Bosch, L.; Robberecht, W. Progranulin functions as a neurotrophic factor to regulate neurite outgrowth and enhance neuronal survival. *J. Cell Biol.* **2008**, *181*, 37–41. [[CrossRef](#)] [[PubMed](#)]
47. Cadieux, B.; Chitramuthu, B.P.; Baranowski, D.; Bennett, H.P.J. The zebrafish progranulin gene family and antisense transcripts. *BMC Genomics* **2005**, *6*, 156. [[CrossRef](#)]
48. Carneiro, M.C.; de Castro, I.P.; Ferreira, M.G. Telomeres in aging and disease: Lessons from zebrafish. *Dis. Model. Mech.* **2016**, *9*, 737–748. [[CrossRef](#)]
49. Van Houcke, J.; De Groef, L.; Dekeyster, E.; Moons, L. The zebrafish as a gerontology model in nervous system aging, disease, and repair. *Ageing Res. Rev.* **2015**, *24*, 358–368. [[CrossRef](#)]
50. Cayuela, M.L.; Claes, K.B.M.; Ferreira, M.G.; Henriques, C.M.; van Eeden, F.; Varga, M.; Vierstraete, J.; Mione, M.C. The Zebrafish as an Emerging Model to Study DNA Damage in Aging, Cancer and Other Diseases. *Front. Cell Dev. Biol.* **2018**, *6*, 178. [[CrossRef](#)]
51. Solchenberger, B.; Russell, C.; Kremmer, E.; Haass, C.; Schmid, B. Granulin knock out zebrafish lack frontotemporal lobar degeneration and neuronal ceroid lipofuscinosis pathology. *PLoS ONE* **2015**, *10*, e0118956. [[CrossRef](#)] [[PubMed](#)]
52. Shin, J.; Park, H.C.; Topczewska, J.M.; Mawdsley, D.J.; Appel, B. Neural cell fate analysis in zebrafish using olig2 BAC transgenics. *Methods Cell Sci.* **2003**, *25*, 7–14. [[CrossRef](#)] [[PubMed](#)]
53. Bernut, A.; Herrmann, J.L.; Kissa, K.; Dubremetz, J.F.; Gaillard, J.L.; Lutfalla, G.; Kremer, L. Mycobacterium abscessus cording prevents phagocytosis and promotes abscess formation. *Proc. Natl. Acad. Sci. USA* **2014**, *111*, E943–E952. [[CrossRef](#)] [[PubMed](#)]
54. Westerfield, M. *The Zebrafish Book. a Guide for the Laboratory Use of Zebrafish (Danio rerio)*, 4th ed.; University of Oregon Press: Eugene, OR, USA, 2000.
55. Baumgart, E.V.; Barbosa, J.S.; Bally-Cuif, L.; Götz, M.; Ninkovic, J. Stab wound injury of the zebrafish telencephalon: a model for comparative analysis of reactive gliosis. *Glia* **2012**, *60*, 343–357. [[CrossRef](#)] [[PubMed](#)]
56. Barbosa, J.; Gonzalez-Sanchez, R.; Di Giaimo, R.; Baumgardt Violette, E.; Theis, F.; Götz, M.; Ninkovic, J. Live imaging of adult neural stem cell behavior in the intact and injured zebrafish brain. *Science* **2015**, *348*, 789–793. [[CrossRef](#)] [[PubMed](#)]
57. Adolf, B.; Chapouton, P.; Lam, C.S.; Topp, S.; Tannhauser, B.; Strahle, U.; Gotz, M.; Bally-Cuif, L. Conserved and acquired features of adult neurogenesis in the zebrafish telencephalon. *Dev. Biol.* **2006**, *295*, 278–293. [[CrossRef](#)] [[PubMed](#)]
58. Fischer, J.; Beckervordersandforth, R.; Tripathi, P.; Steiner-Mezzadri, A.; Ninkovic, J.; Gotz, M. Prospective isolation of adult neural stem cells from the mouse subependymal zone. *Nat. Protoc.* **2011**, *6*, 1981–1989. [[CrossRef](#)]
59. Dobin, A.; Gingeras, T.R. Mapping RNA-seq Reads with STAR. *Curr. Protoc. Bioinform.* **2015**, *51*, 11.14.11–11.14.19. [[CrossRef](#)]
60. Love, M.I.; Huber, W.; Anders, S. Moderated estimation of fold change and dispersion for RNA-seq data with DESeq2. *Genome Biol.* **2014**, *15*, 550. [[CrossRef](#)]
61. Huang da, W.; Sherman, B.T.; Lempicki, R.A. Systematic and integrative analysis of large gene lists using DAVID bioinformatics resources. *Nat. Protoc.* **2009**, *4*, 44–57. [[CrossRef](#)]
62. Huang da, W.; Sherman, B.T.; Lempicki, R.A. Bioinformatics enrichment tools: Paths toward the comprehensive functional analysis of large gene lists. *Nucleic Acids Res.* **2009**, *37*, 1–13. [[CrossRef](#)] [[PubMed](#)]
63. Arslan-Ergul, A.; Erbab, B.; Karoglu, E.T.; Halim, D.O.; Adams, M.M. Short-term dietary restriction in old zebrafish changes cell senescence mechanisms. *Neuroscience* **2016**, *334*, 64–75. [[CrossRef](#)] [[PubMed](#)]

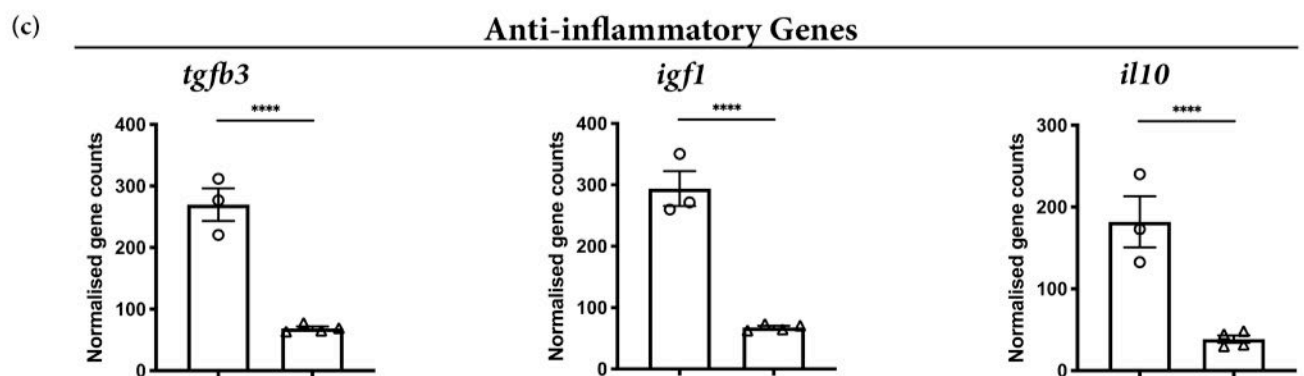
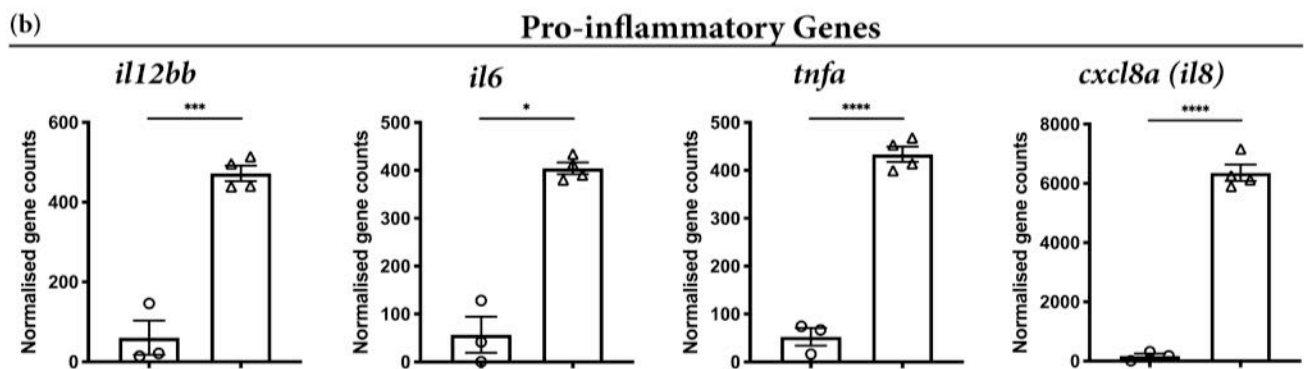
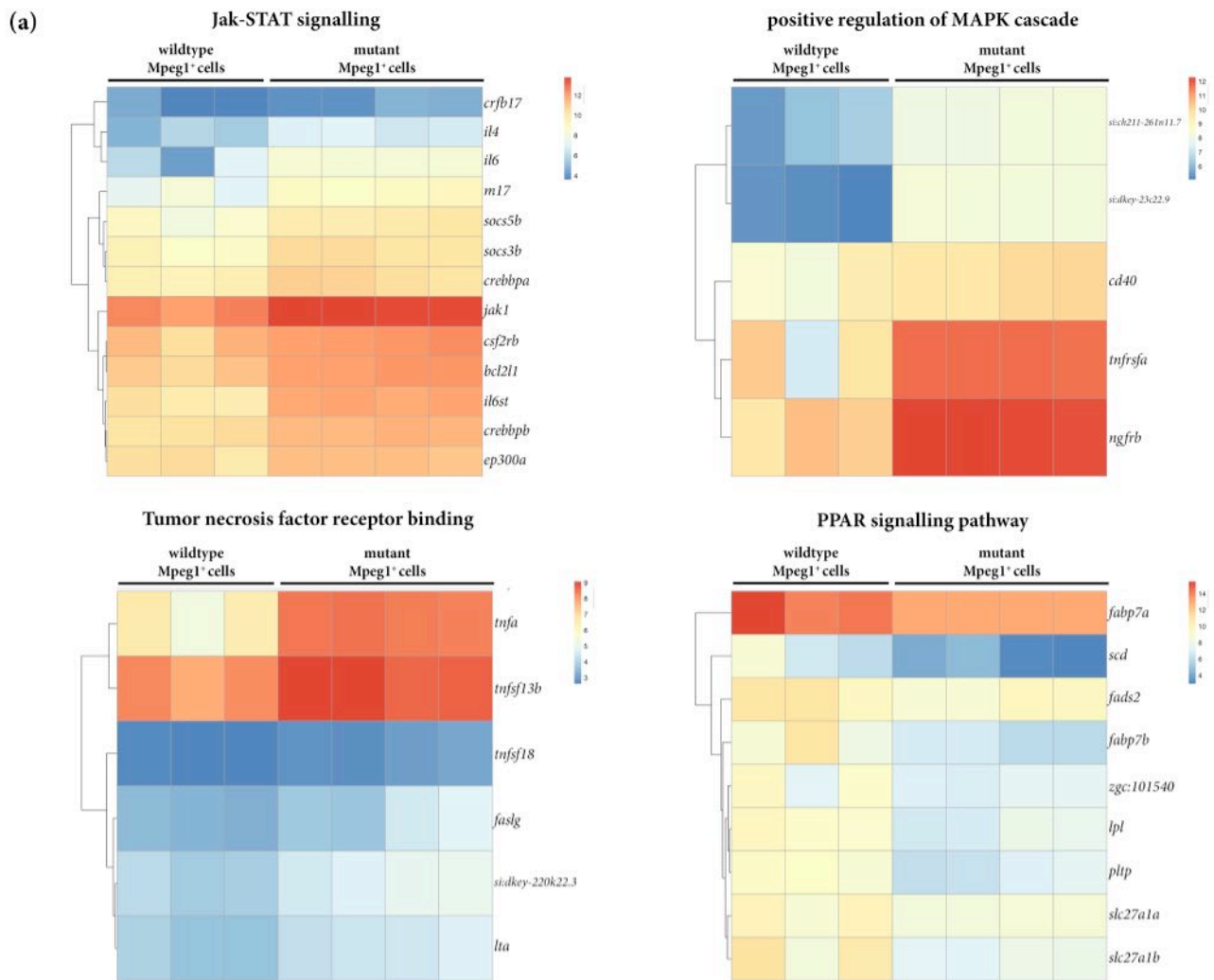
64. Cawthon, R.M. Telomere measurement by quantitative PCR. *Nucleic Acids Res.* **2002**, *30*, e47. [[CrossRef](#)]
65. Zhang, Y.; Chen, K.; Sloan, S.A.; Bennett, M.L.; Scholze, A.R.; O’Keeffe, S.; Phatnani, H.P.; Guarnieri, P.; Caneda, C.; Ruderisch, N.; et al. An RNA-sequencing transcriptome and splicing database of glia, neurons, and vascular cells of the cerebral cortex. *J. Neurosci.* **2014**, *34*, 11929–11947. [[CrossRef](#)]
66. Lim, M.X.; Png, C.W.; Tay, C.Y.; Teo, J.D.; Jiao, H.; Lehming, N.; Tan, K.S.; Zhang, Y. Differential regulation of proinflammatory cytokine expression by mitogen-activated protein kinases in macrophages in response to intestinal parasite infection. *Infect. Immun.* **2014**, *82*, 4789–4801. [[CrossRef](#)] [[PubMed](#)]
67. Perner, F.; Perner, C.; Ernst, T.; Heidel, F.H. Roles of JAK2 in Aging, Inflammation, Hematopoiesis and Malignant Transformation. *Cells* **2019**, *8*, 854. [[CrossRef](#)] [[PubMed](#)]
68. Heming, M.; Gran, S.; Jauch, S.L.; Fischer-Riepe, L.; Russo, A.; Klotz, L.; Hermann, S.; Schafers, M.; Roth, J.; Barczyk-Kahlert, K. Peroxisome Proliferator-Activated Receptor-gamma Modulates the Response of Macrophages to Lipopolysaccharide and Glucocorticoids. *Front. Immunol.* **2018**, *9*, 893. [[CrossRef](#)]
69. Becker, T.; Becker, C.G. Regenerating descending axons preferentially reroute to the gray matter in the presence of a general macrophage/microglial reaction caudal to a spinal transection in adult zebrafish. *J. Comp. Neurol.* **2001**, *433*, 131–147. [[CrossRef](#)]
70. Olah, M.; Patrick, E.; Villani, A.C.; Xu, J.; White, C.C.; Ryan, K.J.; Piehowski, P.; Kapasi, A.; Nejad, P.; Cimpean, M.; et al. a transcriptomic atlas of aged human microglia. *Nat. Commun.* **2018**, *9*, 539. [[CrossRef](#)]
71. Hart, A.D.; Wyttenbach, A.; Perry, V.H.; Teeling, J.L. Age related changes in microglial phenotype vary between CNS regions: Grey versus white matter differences. *Brain Behav. Immun.* **2012**, *26*, 754–765. [[CrossRef](#)]
72. Baumgart, M.; Groth, M.; Priebe, S.; Savino, A.; Testa, G.; Dix, A.; Ripa, R.; Spallotta, F.; Gaetano, C.; Ori, M.; et al. RNA-seq of the aging brain in the short-lived fish *N. furzeri* - conserved pathways and novel genes associated with neurogenesis. *Aging Cell* **2014**, *13*, 965–974. [[CrossRef](#)] [[PubMed](#)]
73. Evers, B.M.; Rodriguez-Navas, C.; Tesla, R.J.; Prange-Kiel, J.; Wasser, C.R.; Yoo, K.S.; McDonald, J.; Cenik, B.; Ravenscroft, T.A.; Plattner, F.; et al. Lipidomic and Transcriptomic Basis of Lysosomal Dysfunction in Progranulin Deficiency. *Cell Rep.* **2017**, *20*, 2565–2574. [[CrossRef](#)] [[PubMed](#)]
74. Gotzl, J.K.; Colombo, A.V.; Fellerer, K.; Reifschneider, A.; Werner, G.; Tahirovic, S.; Haass, C.; Capell, A. Early lysosomal maturation deficits in microglia triggers enhanced lysosomal activity in other brain cells of progranulin knockout mice. *Mol. Neurodegener.* **2018**, *13*, 48. [[CrossRef](#)] [[PubMed](#)]
75. Bhattarai, P.; Thomas, A.K.; Cosacak, M.I.; Papadimitriou, C.; Mashkaryan, V.; Froc, C.; Reinhardt, S.; Kurth, T.; Dahl, A.; Zhang, Y.; et al. IL4/STAT6 Signaling Activates Neural Stem Cell Proliferation and Neurogenesis upon Amyloid-beta42 Aggregation in Adult Zebrafish Brain. *Cell Rep.* **2016**, *17*, 941–948. [[CrossRef](#)]
76. Nolan, Y.; Maher, F.O.; Martin, D.S.; Clarke, R.M.; Brady, M.T.; Bolton, A.E.; Mills, K.H.; Lynch, M.A. Role of interleukin-4 in regulation of age-related inflammatory changes in the hippocampus. *J. Biol. Chem.* **2005**, *280*, 9354–9362. [[CrossRef](#)]
77. Edelmann, K.; Glashauser, L.; Sprungala, S.; Hesl, B.; Fritschle, M.; Ninkovic, J.; Godinho, L.; Chapouton, P. Increased radial glia quiescence, decreased reactivation upon injury and unaltered neuroblast behavior underlie decreased neurogenesis in the aging zebrafish telencephalon. *J. Comp. Neurol.* **2013**, *521*, 3099–3115. [[CrossRef](#)]
78. Barbosa, J.S.; Ninkovic, J. Adult neural stem cell behavior underlying constitutive and restorative neurogenesis in zebrafish. *Neurogenesis (Austin)* **2016**, *3*, e1148101. [[CrossRef](#)]
79. März, M.; Schmidt, R.; Rastegar, S.; Strähle, U. Expression of the transcription factor Olig2 in proliferating cells in the adult zebrafish telencephalon. *Dev. Dyn.* **2010**, *239*, 3336–3349. [[CrossRef](#)]
80. Wang, L.C.; Almazan, G. Role of Sonic Hedgehog Signaling in Oligodendrocyte Differentiation. *Neurochem. Res.* **2016**, *41*, 3289–3299. [[CrossRef](#)]
81. Bartus, K.; Burnside, E.R.; Galino, J.; James, N.D.; Bennett, D.L.H.; Bradbury, E.J. ErbB receptor signaling directly controls oligodendrocyte progenitor cell transformation and spontaneous remyelination after spinal cord injury. *Glia* **2019**, *67*, 1036–1046. [[CrossRef](#)]
82. Palazuelos, J.; Klingener, M.; Aguirre, A. TGF β signaling regulates the timing of CNS myelination by modulating oligodendrocyte progenitor cell cycle exit through SMAD3/4/FoxO1/Sp1. *J. Neurosci.* **2014**, *34*, 7917–7930. [[CrossRef](#)] [[PubMed](#)]

83. López-Juárez, A.; Titus, H.E.; Silbak, S.H.; Pressler, J.W.; Rizvi, T.A.; Bogard, M.; Bennett, M.R.; Ciraolo, G.; Williams, M.T.; Vorhees, C.V.; et al. Oligodendrocyte Nf1 Controls Aberrant Notch Activation and Regulates Myelin Structure and Behavior. *Cell Rep.* **2017**, *19*, 545–557. [[CrossRef](#)] [[PubMed](#)]
84. Grinspan, J.B. Bone Morphogenetic Proteins: Inhibitors of Myelination in Development and Disease. *Vitam. Horm.* **2015**, *99*, 195–222.
85. Whittmore, K.; Vera, E.; Martínez-Nevado, E.; Sanpera, C.; Blasco, M.A. Telomere shortening rate predicts species life span. *Proc. Natl. Acad. Sci. USA* **2019**, *116*, 15122–15127. [[CrossRef](#)]
86. Kao, A.W.; McKay, A.; Singh, P.P.; Brunet, A.; Huang, E.J. Progranulin, lysosomal regulation and neurodegenerative disease. *Nat. Rev. Neurosci.* **2017**, *18*, 325–333. [[CrossRef](#)]
87. Chitramuthu, B.P.; Bennett, H.P.J.; Bateman, A. Progranulin: a new avenue towards the understanding and treatment of neurodegenerative disease. *Brain* **2017**, *140*, 3081–3104. [[CrossRef](#)]
88. Spittau, B. Aging Microglia-Phenotypes, Functions and Implications for Age-Related Neurodegenerative Diseases. *Front. Aging Neurosci.* **2017**, *9*, 194. [[CrossRef](#)]
89. Von Bernhardi, R.; Eugenin-von Bernhardi, L.; Eugenin, J. Microglial cell dysregulation in brain aging and neurodegeneration. *Front. Aging Neurosci.* **2015**, *7*, 124. [[CrossRef](#)]
90. Gabuzda, D.; Yankner, B.A. Physiology: Inflammation links ageing to the brain. *Nature* **2013**, *497*, 197–198. [[CrossRef](#)]
91. Kizil, C.; Dudczig, S.; Kyritsis, N.; Machate, A.; Blaesche, J.; Kroehne, V.; Brand, M. The chemokine receptor cxcr5 regulates the regenerative neurogenesis response in the adult zebrafish brain. *Neural Dev.* **2012**, *7*, 27. [[CrossRef](#)]
92. Kizil, C.; Kyritsis, N.; Dudczig, S.; Kroehne, V.; Freudenreich, D.; Kaslin, J.; Brand, M. Regenerative neurogenesis from neural progenitor cells requires injury-induced expression of Gata3. *Dev. Cell* **2012**, *23*, 1230–1237. [[CrossRef](#)]
93. Kyritsis, N.; Kizil, C.; Zocher, S.; Kroehne, V.; Kaslin, J.; Freudenreich, D.; Iltzsche, A.; Brand, M. Acute inflammation initiates the regenerative response in the adult zebrafish brain. *Science* **2012**, *338*, 1353–1356. [[CrossRef](#)]
94. Miyamoto, N.; Pham, L.D.; Hayakawa, K.; Matsuzaki, T.; Seo, J.H.; Magnain, C.; Ayata, C.; Kim, K.W.; Boas, D.; Lo, E.H.; et al. Age-related decline in oligodendrogenesis retards white matter repair in mice. *Stroke* **2013**, *44*, 2573–2578. [[CrossRef](#)]
95. El Waly, B.; Macchi, M.; Cayre, M.; Durbec, P. Oligodendrogenesis in the normal and pathological central nervous system. *Front. Neurosci.* **2014**, *8*, 145. [[CrossRef](#)]
96. Petersen, M.A.; Ryu, J.K.; Chang, K.J.; Etxeberria, A.; Bardehle, S.; Mendiola, A.S.; Kamau-Devers, W.; Fancy, S.P.J.; Thor, A.; Bushong, E.A.; et al. Fibrinogen Activates BMP Signaling in Oligodendrocyte Progenitor Cells and Inhibits Remyelination after Vascular Damage. *Neuron* **2017**, *96*, 1003.e1007–1012.e1007. [[CrossRef](#)]
97. Ju, Z.; Lenhard Rudolph, K. Telomere dysfunction and stem cell ageing. *Biochimie* **2008**, *90*, 24–32. [[CrossRef](#)]
98. Ahmed, Z.; Sheng, H.; Xu, Y.F.; Lin, W.L.; Innes, A.E.; Gass, J.; Yu, X.; Wuertzer, C.A.; Hou, H.; Chiba, S.; et al. Accelerated lipofuscinosis and ubiquitination in granulin knockout mice suggest a role for progranulin in successful aging. *Am. J. Pathol.* **2010**, *177*, 311–324. [[CrossRef](#)]

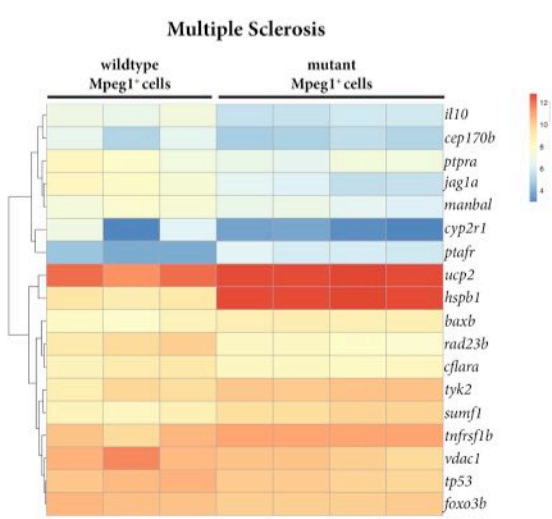
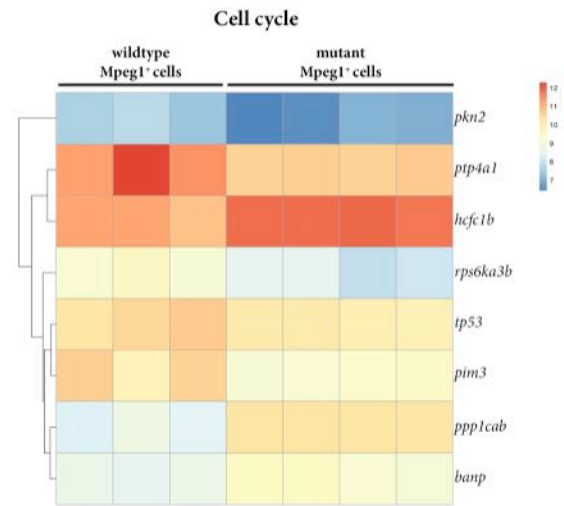
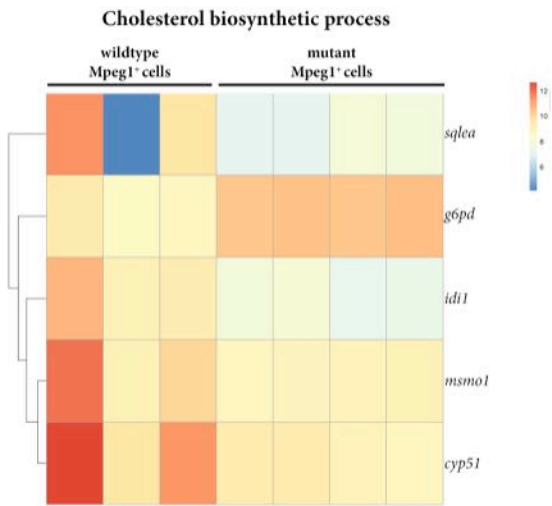
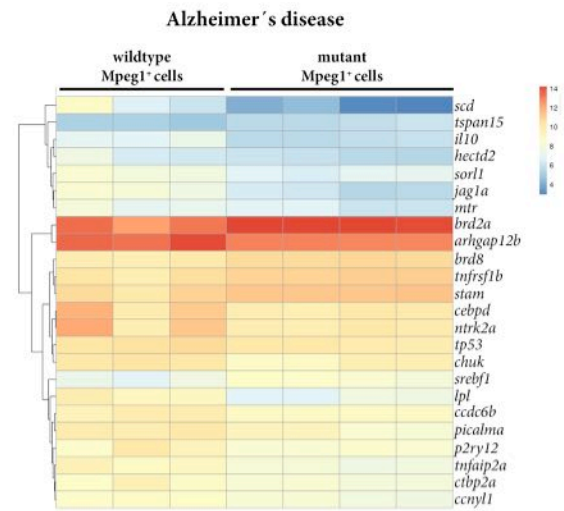
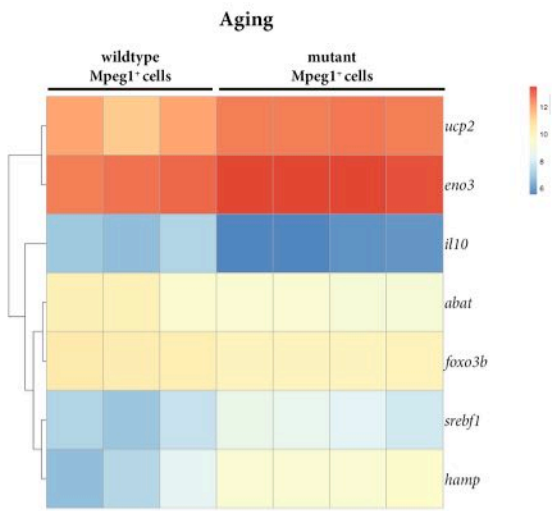




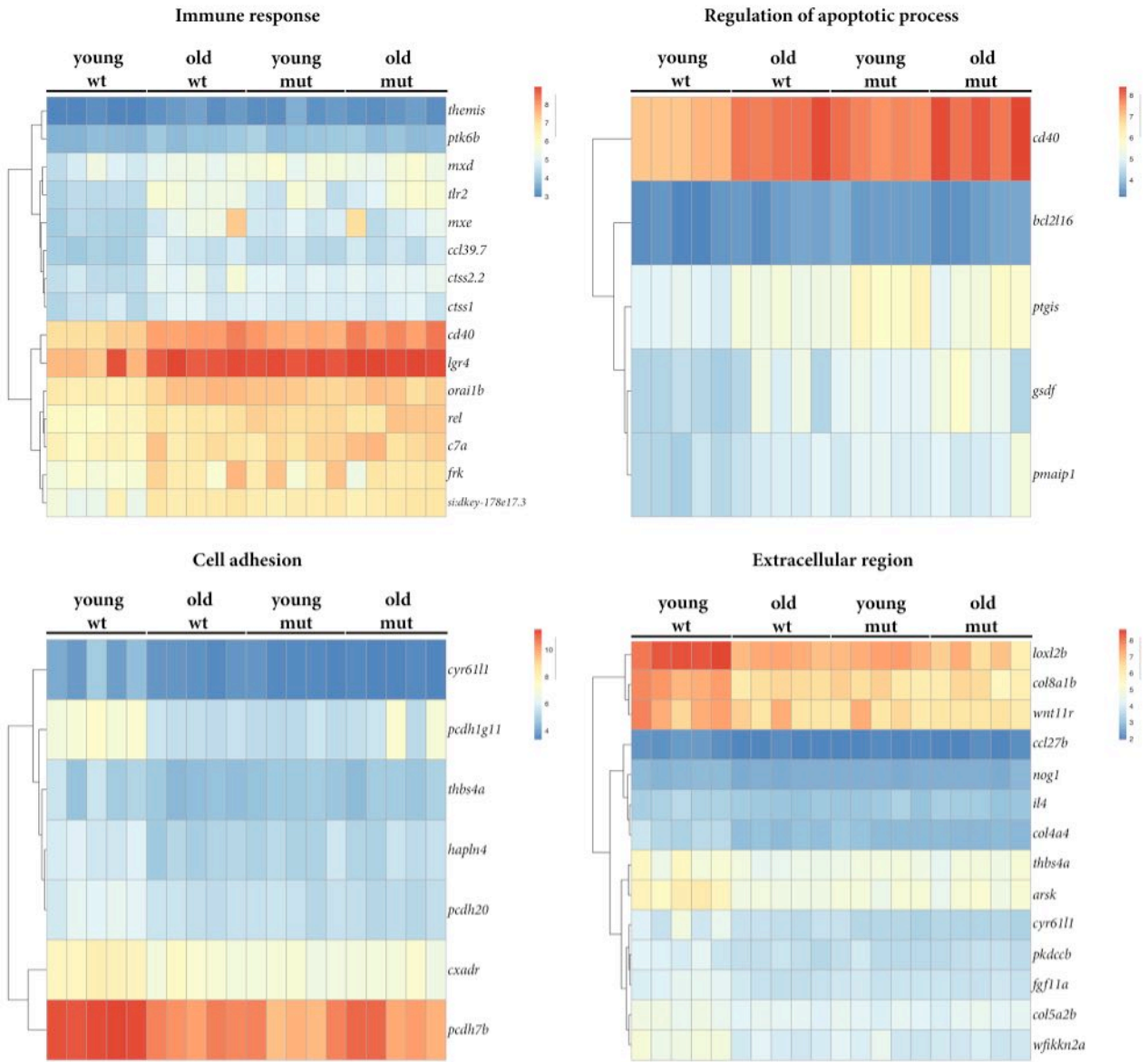




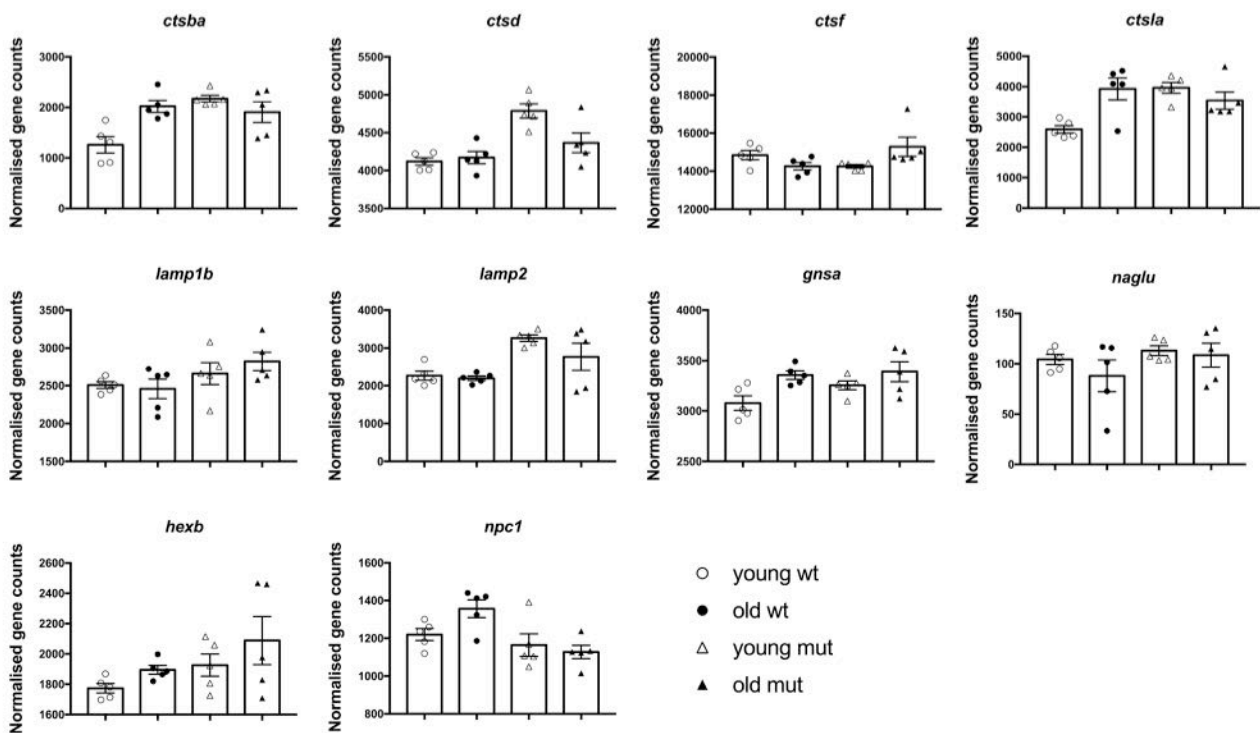
○ wt Mpeg1:mCherry⁺ cells
 △ mut Mpeg1:mCherry⁺ cells



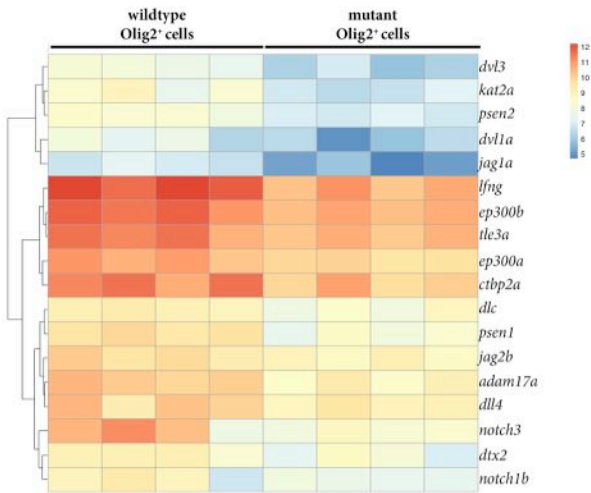
(a)



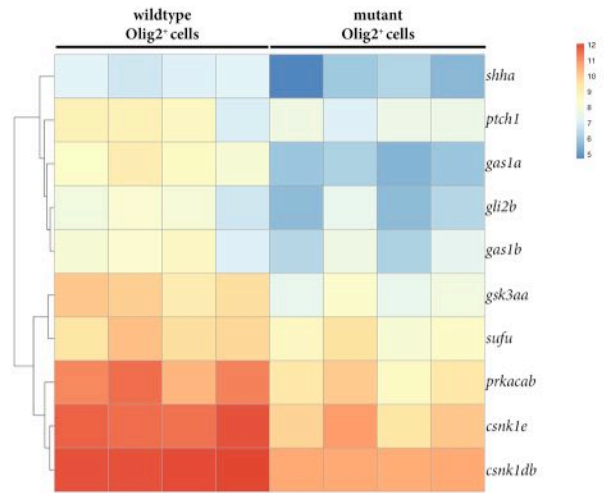
(b)



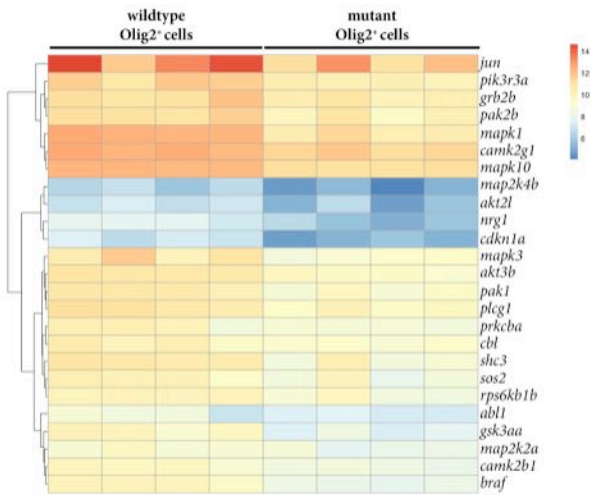
Notch signalling pathway



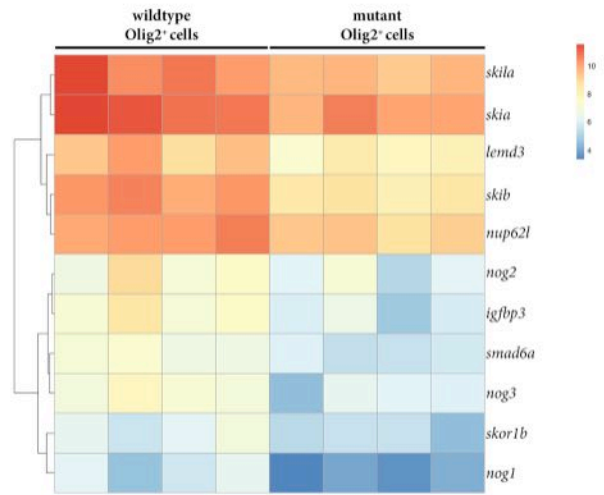
Hedgehog signalling pathway



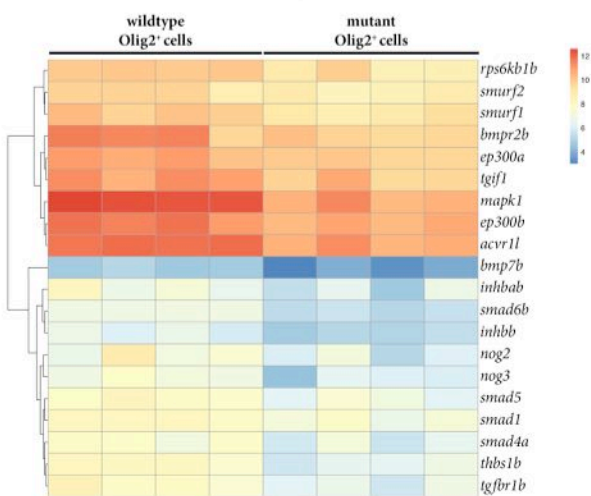
ErbB signalling pathway



Negative regulation of BMP signalling pathway



TGF-beta signalling pathway



Aim of the study II

The aim of the study is to investigate:

The age-related changes in the proteome of adult neural stem cells in the zebrafish telencephalon.

The Surface Proteome of Adult Neural Stem Cells in Zebrafish Unveils Long-Range Cell-Cell Connections and Age-Related Changes in Responsiveness to IGF

Jara Obermann, Felicia Wagner, Anita Kociaj, Alessandro Zambusi, Jovica Ninkovic, Stefanie Hauck, Prisca Chapouton.

For this paper I was involved in preparing RNA-Seq libraries from FACS isolated cells.

The paper is published on Stem Cell Reports (2019).

<https://doi.org/10.1016/j.stemcr.2018.12.005>.

As an open access article distributed under the Creative Commons Attribution License and as author of this publication, I have the right to include it in a thesis or dissertation, provided the work is properly attributed.

The Surface Proteome of Adult Neural Stem Cells in Zebrafish Unveils Long-Range Cell-Cell Connections and Age-Related Changes in Responsiveness to IGF

Jara Obermann,¹ Felicia Wagner,¹ Anita Kociaj,^{2,3,4} Alessandro Zambusi,^{2,4,5} Jovica Ninkovic,^{2,3,5} Stefanie M. Hauck,¹ and Prisca Chapouton^{6,*}

¹Research Unit Protein Science, Helmholtz Zentrum München, German Research Center for Environmental Health, Heidemannstrasse 1, 80939 Munich, Germany

²Institute of Stem Cell Research, Helmholtz Zentrum München, German Research Center for Environmental Health, Ingolstädter Landstrasse 1, 85764 Neuherberg, Germany

³Physiological Genomics, Biomedical Center, Ludwig Maximilian University Munich, Grosshaderner Strasse 9, 82152 Planegg-Martinsried, Germany

⁴Graduate School of Systemic Neurosciences, Ludwig Maximilian University Munich, Grosshaderner Strasse 2, 82152 Planegg-Martinsried, Germany

⁵Department of Cell Biology and Anatomy, BMC, Ludwig Maximilian University, Munich, Germany

⁶Research Unit Sensory Biology and Organogenesis, Helmholtz Zentrum München, German Research Center for Environmental Health, Ingolstädter Landstrasse 1, 85764 Neuherberg, Germany

*Correspondence: chapouton@helmholtz-muenchen.de
<https://doi.org/10.1016/j.stemcr.2018.12.005>

SUMMARY

In adult stem cell populations, recruitment into division is parsimonious and most cells maintain a quiescent state. How individual cells decide to enter the cell cycle and how they coordinate their activity remains an essential problem to be resolved. It is thus important to develop methods to elucidate the mechanisms of cell communication and recruitment into the cell cycle. We made use of the advantageous architecture of the adult zebrafish telencephalon to isolate the surface proteins of an intact neural stem cell (NSC) population. We identified the proteome of NSCs in young and old brains. The data revealed a group of proteins involved in filopodia, which we validated by a morphological analysis of single cells, showing apically located cellular extensions. We further identified an age-related decrease in insulin-like growth factor (IGF) receptors. Expressing IGF2b induced divisions in young brains but resulted in incomplete divisions in old brains, stressing the role of cell-intrinsic processes in stem cell behavior.

INTRODUCTION

In all organisms, developmental processes continue throughout life, overlapping with signs of aging. Many organs maintain stem cell niches after having reached maturation, in which mitotic activity allows for the generation of new differentiated cells. However, the frequency of mitotic activity slowly decreases. Levels of quiescence and cell-cycle entry change following mechanisms that are incompletely understood. This regulation of adult stem cells' quiescence or cell cycle, important both for the unwanted occurrence of cancers and for the desired repair of damaged tissues, remains a fundamental problem in biology.

In vertebrate brains, neural stem cells (NSCs) remain present in defined areas and give rise to new neuronal cells throughout life, albeit in a declining manner. In mammals, well-studied areas are the subependymal/subventricular zone (SVZ) lining the lateral ventricle, giving rise to neuronal cells populating the olfactory bulb as well as the prefrontal cortex in juvenile humans (Lim and Alvarez-Buylla, 2016), the subgranular zone (SGZ) of the hippocampal formation, generating new granule neurons in the dentate gyrus (Goncalves et al., 2016), as well as the hypothalamus (Recabal et al., 2017). The NSCs of

these areas display similar morphologies, being tanycytes in the hypothalamus, radial glia in the dentate gyrus of the hippocampus, and radial-shaped astrocytes in the SVZ (Chaker et al., 2016; Fuentealba et al., 2012; Maggi et al., 2014). A special feature of the SVZ is the mixture of radial astrocytes with ependymal cells (Mirzadeh et al., 2008), the latter being recruited only in case of injury (Carlen et al., 2009).

Several parameters influencing the recruitment into the cell cycle of NSCs have been defined: growth factors, cell-adhesion molecules and the extracellular matrix, contact with blood vessels, cerebrospinal fluid, and metabolism (Goncalves et al., 2016; Lim and Alvarez-Buylla, 2016; Rafalski and Brunet, 2011). As aging progresses, the fraction of mitotically active NSCs declines (Capilla-Gonzalez et al., 2014; Kuhn et al., 1996). Several mechanisms of cell-intrinsic and cell-extrinsic nature, leading to this overall reduction of activity of NSCs, have been revealed. Stem cells have been shown to divide only a limited number of times in the dentate gyrus (Encinas et al., 2011) and reveal signs of depletion in the SVZ too (Calzolari et al., 2015). Progressive lengthening of the G₁ phase of NSCs might be a factor for their less frequent recruitment (Daynac et al., 2014, 2016). The milieu has also been shown to play a role in parabiosis experiments, exchanging the



lymphatic system of young and old mice (Villeda et al., 2011). The levels of distinct growth factors progressively change with age: insulin-like growth factor 1 (IGF1), fibroblast growth factor (FGF), and vascular endothelial growth factor decline in the dentate gyrus (Kang and Hebert, 2015; Shetty et al., 2005). The immediate surrounding niche, made of the neighboring cells and the extracellular matrix, known to play a role in stem cell activity (Kazanis et al., 2010; Porlan et al., 2014), might also be subjected to age-related changes influencing mitotic activity (Yamada et al., 2017). A clear picture to explain the individual behaviors within stem cell populations is nevertheless missing.

In the adult zebrafish brain, transcription factors homologous to their mammalian counterparts are at play in the neurogenic process (Diotel et al., 2015), making it a valid comparative vertebrate model organism. Moreover, it presents the advantage of a broader neurogenic activity within all brain regions and a high regenerative potential (Alunni and Bally-Cuif, 2016; Baumgart et al., 2012; Grandel and Brand, 2013). The radial glia in zebrafish display similar features to those of the NSCs of the mammalian neurogenic areas. Their somata are in immediate contact with the ventricles, they express the intermediate filaments glial fibrillary acidic protein (GFAP), Nestin, and Vimentin, and generate new neurons and glial cells (Kroehne et al., 2011; Rothenaigner et al., 2011). Their transitions back and forth between quiescence and cell cycle have been shown by long-term bromodeoxyuridine tracing and by Notch blocking experiments (Chapouton et al., 2010; März et al., 2010). Whether every cell or only a subpopulation enter the cell cycle regularly remains uncertain (Dray et al., 2015). The radial glia might give rise to newly born neurons through a direct conversion process without an immediately preceding mitosis (Barbosa et al., 2015). Additionally, progenitors without GFAP expression are also present in close proximity to the somata of the radial glia and are considered intermediate progenitors, even if similar cells organized in pools function as stem cells in other regions of the brain (Galant et al., 2016; Kaslin et al., 2009, 2017; Than-Trong and Bally-Cuif, 2015).

In addition to the abundance of NSCs, a major advantage of the zebrafish brain is the architecture of its pallium (dorsal telencephalon), where the ventricular surface opens on the outside instead of enclosing a lumen, due to an eversion process during embryonic development (Wullmann and Mueller, 2004), thus becoming accessible to imaging or manipulations (Barbosa et al., 2015; Dray et al., 2015).

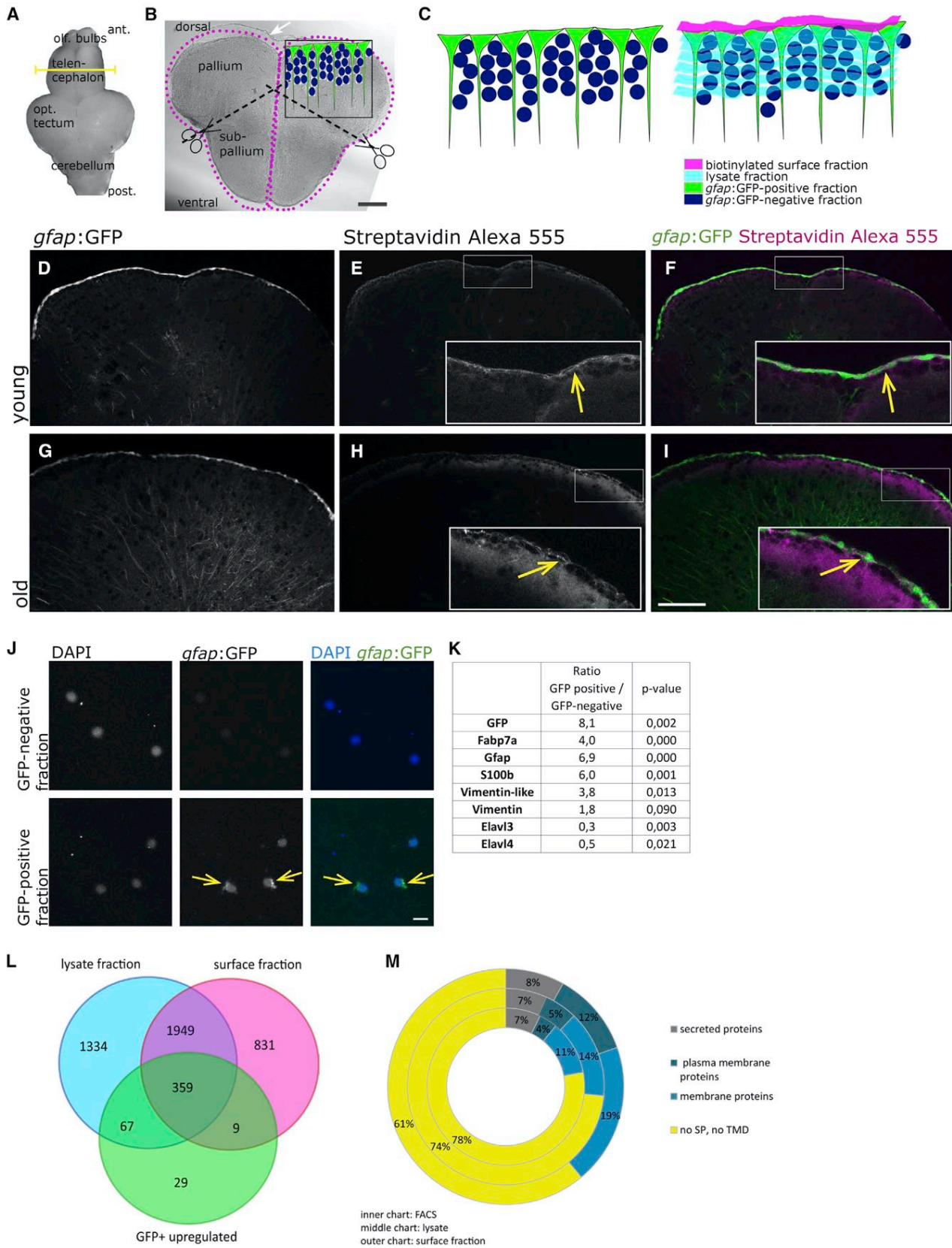
We made use of this architecture to isolate the proteins present in an intact population of NSCs. As this cell population reveals an age-related increase of quiescent cells (Edelmann et al., 2013), we identified the surface prote-

ome of the young and old ventricular zone to obtain sets of proteins likely implicated in the intercellular communication and in the regulation of cell cycle and quiescence. We focused on two aspects of the dataset. The significant over-representation of filopodial and lamellipodial protein components allowed us to discern new morphological features of NSCs. Furthermore, age-related changes revealed a decline in IGF1-receptor (IGF1R) expression, observed by both mass spectrometry and immunocytochemistry of the phosphorylated IGF receptor. This decrease was measurable by an altered response to the ligand IGF2b, able to induce complete cell divisions in young, but not in aged animals.

RESULTS

Identifying the Proteome of Neural Stem Cell Surfaces in Intact Brains

The closest contacts between the radial glia are at the level of their cell bodies, adjacent to the brain ventricle. With the aim of defining signaling pathways putatively implicated in their intercellular communication, we designed an approach to isolate all proteins present on the cell bodies in a native configuration of freshly isolated brains. The biotinylation protocol allowed the binding of biotin to the proteins expressed on the surface of the radial glia (Figures 1A–1C). We tested two different protocols of biotinylation, based on either covalent coupling to glycosyl side chains or covalent coupling to free amino groups of the proteins. We observed a systematic bias toward increased expression levels in old brains with the glycosylation-dependent biotinylation (Figure S1A), which might indicate age-dependent altered total glycosylation levels. While the majority of proteins identified by the glycosylation-dependent biotinylation was also identified by the direct amino acid binding biotinylation (Figure S1B), we obtained a higher number of proteins with the latter protocol, and concentrated our further analysis on those results. Three replicates of 6–7 brains (2-year-old and 4-month-old, respectively) were prepared in parallel. To verify the localization of biotin anchoring, we fixed two brains and incubated them with streptavidin-AlexaFluor 555. Both young and old brains revealed a specific surface anchorage of biotin with a minor penetration below the row of radial glia (Figures 1D–1I), indicating the validity of the method. After biotinylation, brains were dissected into pallium and subpallium (Figure 1B) in order to separate the apical part of the radial glia located on the dorsal surface, where we expect cell-to-cell communication to take place, from their basal endfeet located on the ventral pial surface. After tissue lysis, biotinylated proteins were bound to streptavidin beads, proteolyzed, and analyzed by mass spectrometry.



(legend on next page)



The non-biotinylated proteins, representing the remaining material of the telencephalon (Figure 1C, lysate fraction) were also analyzed by mass spectrometry. We compared the results obtained by this approach, with proteins from sorted radial glia of the telencephalon of *gfap*:GFP transgenic fish (fluorescence-activated cell sorting [FACS] scatterplots in are shown in Figures S2A–S2F and 1J). These experiments revealed consistent clustering of the GFP-positive and GFP-negative fractions by principal component analysis (Figure S2G), and an even distribution of proteins respectively up- and downregulated (Figure S2H). The set of proteins enriched in the GFP-positive fraction contained expected proteins known to be expressed by radial glia (GFP, GFAP, S100 β , FABP7a/BLBP, Vimentin) (Ganz et al., 2010; März et al., 2010) while the GFP-negative fraction was enriched in proteins present on differentiated neurons (Elavl3/HuC, Elavl4/HuD) (Adolf et al., 2006; Grandel et al., 2006) (Figure 1K). A high number of proteins in the biotinylated fraction was not present in the FACS-GFP-positive cells, which might be due to a loss of proteins during the enzymatic dissociation of the cells. Conversely, a large proportion (79.3%) of the proteins isolated from the FACS-GFP-positive cells were also identified in the biotinylated fraction (Figure 1L). According to our experimental design, this overlap is expected to be incomplete, as FACS-sorted cells contain in addition to plasma membrane the whole cytosolic fraction of radial glia (Figure 1C). GeneRanker analysis of the FACS-GFP-positive fraction revealed overrepresentation of the insulin pathway, cannabinoid receptor 1 pathway, glial cell line-derived neurotrophic factor (GDNF) and platelet-derived growth factor receptor β (PDGFR β) signaling pathways (Table S1A). While sorting cells by FACS allows for the analysis of the whole content

of proteins in a certain cellular type, the advantage of the biotinylation approach was to isolate proteins of intact, non-dissociated cells.

Phobius analysis was used to assess the proportion of proteins with transmembrane domains and signal peptides (Figure 1M). The surface biotinylation technique led to a protein set enriched in membrane proteins compared with the lysate fraction and the FACS-sorted cells fraction. Of the proteins listed in the Genomatix Pathway System, 645 belong to the plasma membrane, 51 are localized in the cell cortex, 145 are cytoskeletal binding proteins, and 43 are cell-adhesion molecule binding proteins.

Taken together, comparison of the datasets obtained from sorted radial glia, biotinylated surface fraction, and the non-biotinylated lysate of the telencephalon (for original dataset files see Table S6) indicate that the biotinylation approach specifically isolates proteins expressed on the surface of the stem cell compartment.

Identified Proteins Indicate an Epithelial Character and Display a Group Associated with Lamellipodia and Filopodia

The radial glia, as opposed to embryonic neuroepithelial cells, do not form a columnar epithelium, but their somata are cone-shaped and are connected laterally to each other only by a thin apical junctional region. Their highly branched radial processes extend far into the parenchyme. Considering this morphology, it is interesting to define to which extent these cells reveal an epithelial character. In the list of identified surface proteins, members with specific apicobasal localizations appeared (Table 1). For instance, proteins involved in formation of tight junctions (i.e., Discs large 1 and 3, Junctional Adhesion Molecule 3,

Figure 1. Proteome Identification

(A) The biotinylation reaction was performed on freshly isolated brains. The yellow line depicts the location of the cross-section shown in (B).

(B) Cross-section through the telencephalon of a zebrafish. Biotinylated surfaces are depicted as magenta dots. The upper surface of the pallium borders the ventricle, located below the tela choroidea (white arrow) and is composed of the cell somata of the radial glia (depicted in green in the inset). The midline between both hemispheres is also filled by a thin part of the ventricle. After the biotinylation reaction, telencephalons were separated into the dorsal part (pallium) and ventral part (subpallium).

(C) Drawing of the fractions isolated by FACS and by biotinylation, depicting in green the radial glia, in dark blue the remaining cells of the telencephalon, in magenta the biotinylated fraction containing the cell surfaces of the radial glia, and in light blue the lysate fraction containing the remainder of these cells as well as the rest of the telencephalon.

(D–I) Histochemistry on cross-sections with streptavidin coupled to AlexaFluor 555 after biotinylation of the brain, revealing the expected binding of biotin on the cell surfaces in young (D–F) and old (G–I) brains.

(J) Cells of the GFP-positive and -negative fraction plated directly after the sorting; nuclei are stained by DAPI.

(K) Known proteins isolated on FACS-sorted radial glia.

(L) The overlaps between the surface fraction, lysate fraction, and GFP-positive fraction are represented. The majority (79.3%) of proteins identified in the FACS-GFP-positive fraction were also found in the biotinylated fraction.

(M) Identified proteins were categorized according to the presence of signal peptides and transmembrane domains, revealing an enrichment of plasma membrane proteins in the biotinylated fraction compared with the lysate and to the FACS-retrieved proteins.

Scale bars, 100 μ m (B and I) and 10 μ m (J).



Table 1. Biotinylated Fraction: Proteins Indicating the Epithelial Character of the Radial Glia and Proteins Associated with Filopodia and Lamellipodia

Cell-Cell Adherens Junctions p value: 1.23×10^{-3} No. of genes (observed): 13 No. of genes (expected): 5.09 No. of genes (total): 54	CDH2, ACTN1, DSP, FLOT1, CTNNB1, DAG1, CADM4, NDRG1, FLOT2, CTNNA1, GJA1, CADM1, CTNNA2
Bicellular tight junctions p value: 7.60×10^{-3} No. of genes (observed): 19 No. of genes (expected): 10.5 No. of genes (total): 111	ANK3, DLG3, RAP2B, CTNNB1, CXADR, MAGI1, TBCD, AOC1, STRN, FZD5, MTDH, ADCYAP1R1, RAP2C, VAPA, RAPGEF2, LIN7A, JAM3, DLG1, LIN7C
Gap junctions	CX43; +FACS dataset: Cx28.8
Apical plasma membrane p value: 8.38×10^{-3} No. of genes (observed): 40 No. of genes (expected): 27.2 No. of genes (total): 288	AP2A1, CDH2, FLOT1, CD81, ANO1, CLCN3, BMPR2, TF, ATP2B1, PRKAA1, FLOT2, SHANK2, ATP1B1, MTDH, ATP6V1E1, PDGFRB, ATP6VOD1, CNTFR, TMEM30A, GJA1, GNAT3, RAB14, CD36, STXB3, ATP6V1A, RAB27B, RAPGEF2, NOD1, KCNA1, SORBS2, PTPRO, PTEN, ATP8B1, CSPG4, FZD3, PTK2, KCNN4, SEPT7, ITPK1, SLC7A5
Basolateral plasma membrane p value: 5.27×10^{-6} No. of genes (observed): 41 No. of genes (expected): 19.8 No. of genes (total): 210	ENPP1, SLC4A4, AP2A1, CDH2, ANK3, DLG3, DSP, FLOT1, SLC12A6, SLC38A3, CTNNB1, CXADR, NDRG4, DAG1, BMPR2, TF, ATP2B1, FLOT2, ATP1B1, CNM2, PALM, CADM1, ARRB1, STXB3, ERBB4, ANK1, NOD1, MPZ, LIN7A, CTNNA2, HEPH, DLG2, ARRB2, SLC1A3, DLG4, ANXA2, CASK, DLG1, KCNN4, LIN7C, EGFR
Filopodium formation (integrin signaling) p value: 2.01×10^{-2} No. of genes (observed): 27 No. of genes (expected): 18.3 No. of genes (total): 123	BCAN, SMC3, ITGAV, GPC1, LAMB3, GPC4, RAP1B, COL4A1, COL1A1, BRAF, CDC42, TLN1, MAPK1, DOCK3, ITGB5, AGRN, SHC3, TLN2, ITGB7, ITGB2, KRAS, MAP2K1, DOCK10, ITGB4, COL15A1, PTK2, GRB2 Y-branching of filopodia: ACTR2, NCKAP1, CDC42, ARPC3, ARPC2, PSMA7, RAC1
Lamellipodium p value: 1.74×10^{-7} No. of genes (observed): 39 No. of genes (expected): 16.2 No. of genes (total): 172	MYH10, RAC2, RUFY3, CDH2, FLOT1, ITGAV, CTNNB1, NCKAP1, SLC39A6, PPP1R9A, DAG1, FERMT2, FGD1, FLOT2, CTTN, ARPC3, GSN, CTNNA1, FSCN1, PPP1R9B, CDK5, APP, DPYSL3, SORBS2, CTNNA2, BRK1, CORO1A, ENAH, NRBP1, PTPRO, DBNL, CSPG4, PTK2, ITSN1, CARMIL2, SRCIN1, ABI2, DGK2, PTPRZ1

Metadherin, Striatin, Ankyrin3) and in cell-cell adherens junctions (i.e., Dystroglycan 1, N-Cadherin, Catenin- β 1, - α 1, and - α 2, Desmoplakin) were identified (Table 1). Therefore, even if this adult ventricular surface on the dorsal pallium is classically not considered as a neuroepithelium, these cells that pave the whole ventricular surface express epithelial marker proteins.

We observed a group of proteins involved in filopodia and lamellipodia formation (Table 1), such as CDC42, RAC1 and -2, DOCK 3 and 10, Integrin α 5 β 2 and β 7, RUFY3, BRK1, Formin-like 3, and Fascin 1a and 1b. The high ramification of radial glia in the parenchyme (inset in Figure 2C) might explain this finding. However, as the biotinylation was specifically targeting the apical surface and could not reach the deep processes, we wondered whether filopodia are present apically. Indeed, different expression levels occurred predominantly between the ventral and dorsal domains of the telencephalon (Figure 2A). We performed morphological analyses of single cells by lipofections *in vivo*, using either a combination of two plasmids (EF1 α : Gal4 and UAS: mtdTomato) or a single plasmid (pCS2-Lifeact-RFP) highlighting F-actin, to label the membrane of a few scattered cells. The infusion of the lipofection mix into the brain ventricle led in all cases to an exclusive expression in the radial glia (Figures 2B–2D, yellow arrows). We took serial confocal pictures to obtain z stacks of whole-mount brains with mtdTomato membrane staining. Lamellipodia were observed in some cells that overlapped with the apical surface of a neighboring cell (Figures 2E–2G). In the majority of analyzed cells, we identified at least one filopodium-like extension. The extension was either extending apically along borders between two cells (Figures 2H–2J), reaching the second next cell, or extending from the basolateral cell surface and reaching apical locations of neighboring cells, furthest to the fourth *gfap*:GFP-positive cell (Figures 2K–2P). We used a Lifeact construct and analyzed 23 cells from 3 sectioned brains. The cellular extensions contained Lifeact labeling, revealing the presence of F-actin (Figures 2Q–2S). Co-lipofections of Lyn-GFP and Lifeact-RFP plasmids showed that the cellular extensions could be distinct in their composition, as a few of them were not labeled by Lifeact (Figures 2T–2V').

Since the mass spectrometric analysis showed some differences with age in the expression levels of some filopodia-associated proteins, such as the downregulated Neuroigin 1 and FARP1, and the upregulated Flotillin 2, Gelsolin, Talin 2, and Src kinase signaling inhibitor 1 (Figure 2A), we compared morphologies and performed measurements of length and number of filopodia on 16 young (3-month-old) and 26 old (2-year-old) mtdTomato-labeled cells (Figure S3). Neither the mean size of these extensions, nor their numbers, varied significantly between young and old

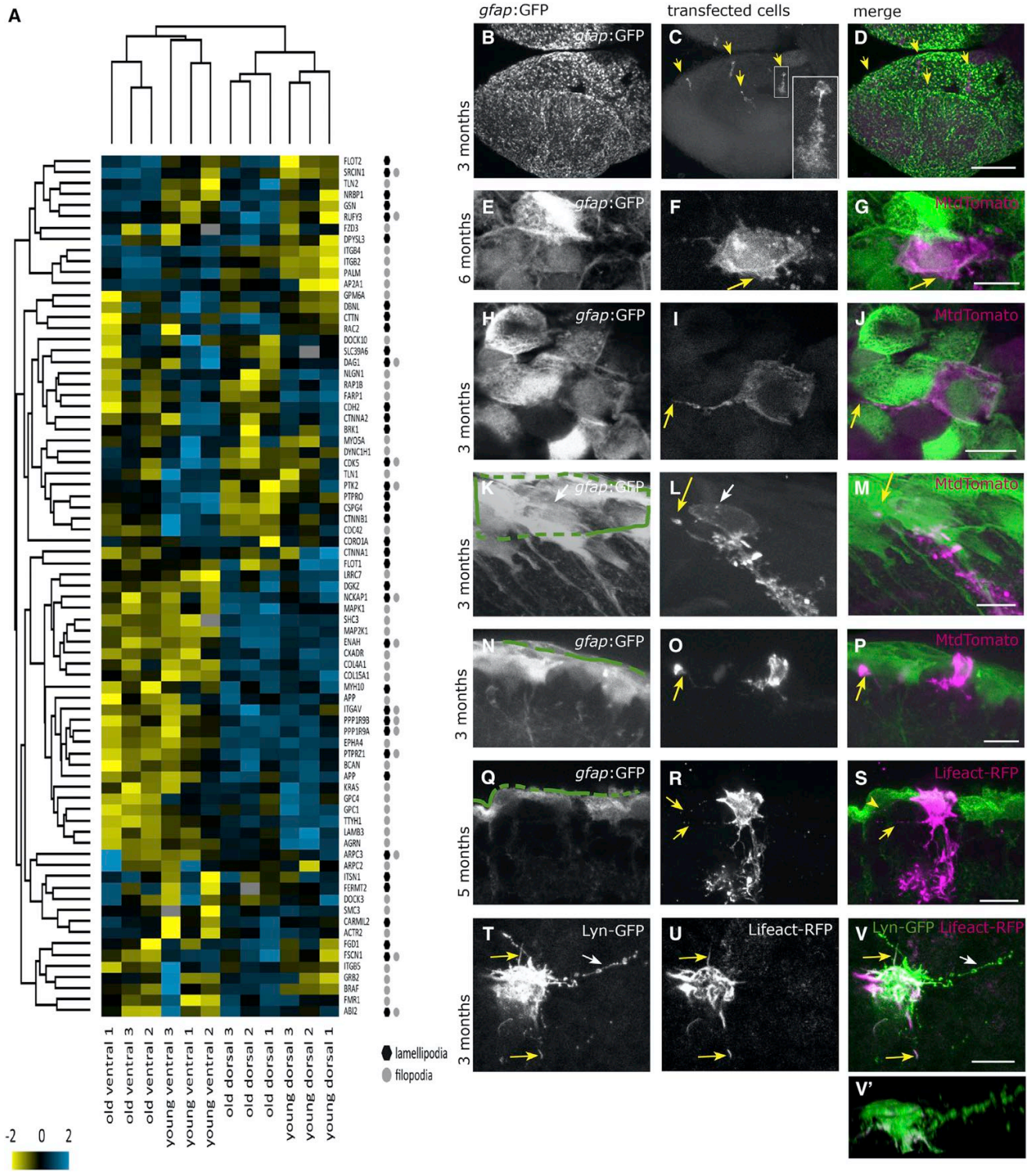


Figure 2. Proteins Associated with Lamellipodia and Filopodia, Detected in Apical and Basolateral Locations of the Radial Glia
 (A) Hierarchical clustering for proteins associated with lamellipodia and filopodia, revealing that some of them display age-related changes.
 (B–V') Lipofections *in vivo* were performed and imaged after fixation as whole-mount preparations or as sections (Q–S). (B–D) Overview of one telencephalic hemisphere visualized from the top onto the dorsal surface as a maximum-intensity projection. (B) Cell bodies of the
 (legend continued on next page)



brains (Figures S3J–S3K). Nevertheless, possible structural alterations might exist and will need to be examined in future studies.

Together, these results reveal cellular extensions between the cell bodies of NSCs, which might promote cell-to-cell communication ranging up to 4 cells apart.

Signaling Pathways Active in the Surface Fraction

Besides a possible communication via filopodial extensions, other candidates might relay intercellular signals, such as the gap-junction protein Cx 43, or Cx 28.8 identified in the GFP-positive FACS fraction. We further identified a high number of proteins (557) associated with extracellular exosomes that might convey signals.

We examined pathways significantly overrepresented on the dorsal versus ventral side of the telencephalon, hence likely involved in the communication at the apical location of the radial glia. GeneRanker analysis revealed among others the planar cell polarity, brain-derived growth factor, Semaphorin, and Eph receptor pathways (Table S2).

Cell-surface receptors and their differential expression are listed in Figure S4A. We identified, for instance, Notch3 as well as Dner, another Notch family member, and receptors for GDNF, ciliary neurotrophic factor (CNTF), PDGF, epidermal growth factor (EGF), bone morphogenetic protein (BMP), FGF, and WNT. Many of these receptors and ligands were missing in the proteins identified from cells isolated by FACS, possibly due the enzymatic dissociation. We nonetheless confirmed the expression of these signaling molecules in the radial glia by RNA sequencing (RNA-seq) analysis of FACS-sorted GFP-positive and -negative fractions (Figure S4B).

Following the intriguing finding of filopodia on the radial glia, we tested whether they would relay signals identified here in the biotinylated fraction, similarly to results obtained in other cells with filopodia (Prols et al., 2016). We investigated the co-localization of two signaling pathways in the cellular protrusions, Wnt and EGF.

The localization of Wnt signals was examined (Stanganello et al., 2015) in NSCs co-lipofected with Wnt8a-

mcherry and Lyn-GFP. Lipofected cells did reveal a dotted localization of Wnt8a-mCherry (Figures S5B, S5E, S5H, and S5K), also at the edges of the cell soma close to neighboring cells. However, no clear co-localization with filopodial extensions could be identified (Figures S5A–S5I). In a second approach, we expressed a GFP-tagged secreted Wnt receptor SFRP1a-GFP in HEK-293 cells and collected the supernatant, then applied it on fixed floating brain sections. As a positive control, lipofected cells with Wnt8a-mCherry did not show a strong specific co-localization of SFRP1a-GFP (Figures S5J–S5L). Cells lipofected with Fyn-RFP to visualize the filopodia did not reveal co-localization of the SFRP1a-GFP (Figures S5J–S5L). We therefore conclude that with the methods used here, filopodial extensions in adult NSCs do not seem to convey Wnt signaling.

The localization of the EGF receptors was probed with an AlexaFluor 488-EGF complex that binds EGF receptor (EGFR) (Pastrana et al., 2009). Sections with cells lipofected with mtdTomato were incubated with the green fluorescent complex, revealing the localization of EGFR on the radial glia (Figures S5P–S5W). The AlexaFluor 488-EGF complex did not co-localize specifically with filopodial extensions. Hence, potential signals relayed via filopodia to neighboring radial glia remain to be determined in further studies.

As we were looking for signals involved in the regulation of recruitment to the cell cycle, we next focused on pathways differentially regulated in young and old brains.

The IGF Signaling Pathway Diminishes with Age, and the Mitotic Response to IGF2b Becomes Incomplete

The differential protein content in young and old surface fractions revealed an enrichment in proteins involved in G₁/S transition in the young brain, and an enrichment in proteins involved in the P21 (CDKN1A) pathway in the old brain (Tables S3 and S4), in accordance with previously observed age-related decrease in mitotic activity (Edelmann et al., 2013). Hierarchical clustering and principal component analysis revealed consistent results between replicates (Figures 3A and 3B). The proteins up- and

radial glia are labeled by the gfap:GFP transgene. (C) A small, variable number of cells per brain were labeled by the *in vivo* lipofection (maximum 12 cells per brain); their somata and branched radial processes into the parenchyme are visible (inset is a higher magnification), revealing the soma at the top (apical side) and the radial process in the parenchyme with numerous branches. All lipofected cells displayed this radial process, but it is not visible on all pictures. (D) Merged channels. (E–G) Apical surface of one radial glia, viewed from the top, depicting the existence of lamellipodia extending laterally (arrow in F and G). (H–J) Apical surface of one radial glia, depicting the existence of filopodia (arrow in I and J). (K–M) Filopodia are also extending from the basolateral cell surface toward apical locations on neighboring cells (arrow in L and M). (N–P) The longest filopodia span below 4 cell diameters. (Q–S) lipofection with Lifeact-RFP also reveals basolateral extensions (arrows in R and S). (T–V) Apical view on a cell co-lipofected with the membrane-localized Lyn-GFP (T) and the F-actin localized Lifeact-RFP (U) revealing the presence of filopodial extensions with F-actin (yellow arrows) or without (white arrow). (V') Lateral view of the same cell. Green lines in (K), (N), and (Q) depict the ventricular surface. Scale bars, 100 μ m (D) and 10 μ m (G, J, M, P, S, and V).

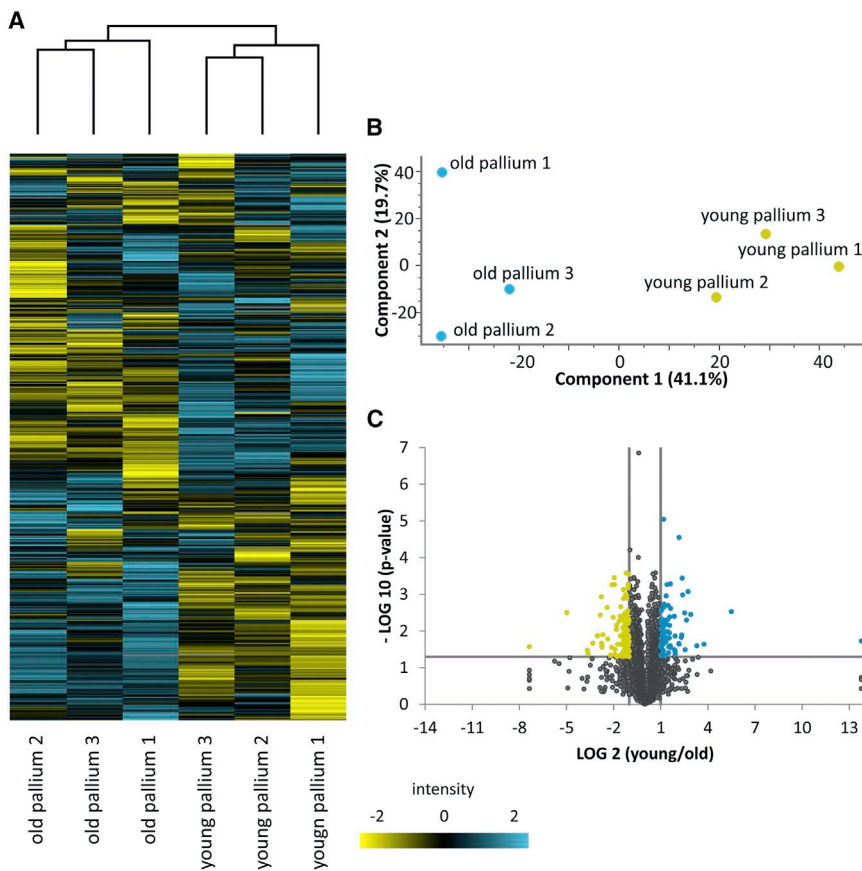


Figure 3. Expression Changes with Age in the Ventricular Zone

(A) Hierarchical clustering of all proteins in the ventricular zone using normalized \log_2 transformed abundances of three old and three young brain samples (high-abundance proteins colored blue, low-abundance proteins yellow).

(B) Principal component analysis of the three samples of old brain and three samples of young brain.

(C) Volcano plot analysis: ratios of the means of all protein abundances in the three old compared with the three young brain samples were plotted against the corresponding negative \log_{10} transformed p value.

downregulated with age were evenly distributed (Figure 3C). Several components of N-Cadherin signaling were upregulated in young surfaces (N-Cadherin signaling components, p value 6.14×10^{-3} : DAGLA, CDH2, CDC42, CTNNA1, KIF5B), suggesting that cell-cell interactions might be modified with age. However, other components of this signaling pathway remained unchanged (CTNNA1, CNR1, GRIA2, CTTN, GSN, GJA1).

Proteins on the NSCs' surface and in the lysate revealed a decrease in IGF signaling with age (Figures 4A and 4B), especially for the receptors IGF1R and insulin receptors. In zebrafish, two *igf1r* genes, *igf1ra* and *igf1rb*, are orthologous to the mammalian IGF1R and play complementary roles during development (Schlueter et al., 2006). Both were decreased on the surface fraction of aged brains. The insulin receptor InsR-B also declined with age, while the level of InsR-A expression did not change. IGF ligands were not detected in the proteomic analysis, but were detected by RNA *in situ* hybridization (Figure S6), suggesting that they might act as autocrine or paracrine factors, as in mammalian adult neurogenic areas (Bracko et al., 2012; Lehtinen et al., 2011). Phosphorylated (phospho)-IGF1R expression was visible in immunostainings in the layer of radial glia, as well as in a few closely located cells in the pa-

renchyme in young brains (Figures 4C–4F and 5A–5D), while in aged brains only a few plasma membrane-localized dots and a weak cytoplasmic expression were visible in the radial glia (Figures 4G–4J and 5I–5L).

IGF2b was cloned into a $5 \times$ UAS plasmid for overexpression by *in vivo* lipofections. Fish were lipofected with a red-labeling plasmid alone or in combination with *igf2b*. Control

lipofections with two differently colored plasmids resulted in cells receiving both plasmids in 90% of the cases (27 of 30 cells co-lipofected with plasmids for a green cytoplasmic staining and for a membrane-bound red staining revealed expression of both colors). After 2–4 days, we observed an increased expression of phospho-IGF1R in the cells lipofected with *igf2b* (Figures 5E–5H, arrows in 5G and 5H) as well as in their neighbors, indicating the expected effect of IGF2b expression. The phospho-IGF1R expression in aged brains, upon either control lipofections (Figures 5I–5L) or *igf2b* lipofections (Figures 5M–5P), showed a lower basal expression than in young brains, and IGF2b overexpression was able to induce a few dots of phospho-IGF1R expression (arrows in Figures 5O and 5P). However, the expression was not as strongly increased as in young brains, in line with the decreased receptor expression with age observed by mass spectrometry. Quantification of the fluorescence confirmed higher expression levels in *igf2b*-lipofected cells compared with control lipofections in young brains, but no significantly detectable change in old brains (Figure 5Q). We tested another downstream target of IGF2b signaling, phosphorylated Akt (Ser473), which revealed only very low levels of expression (Figure S7).

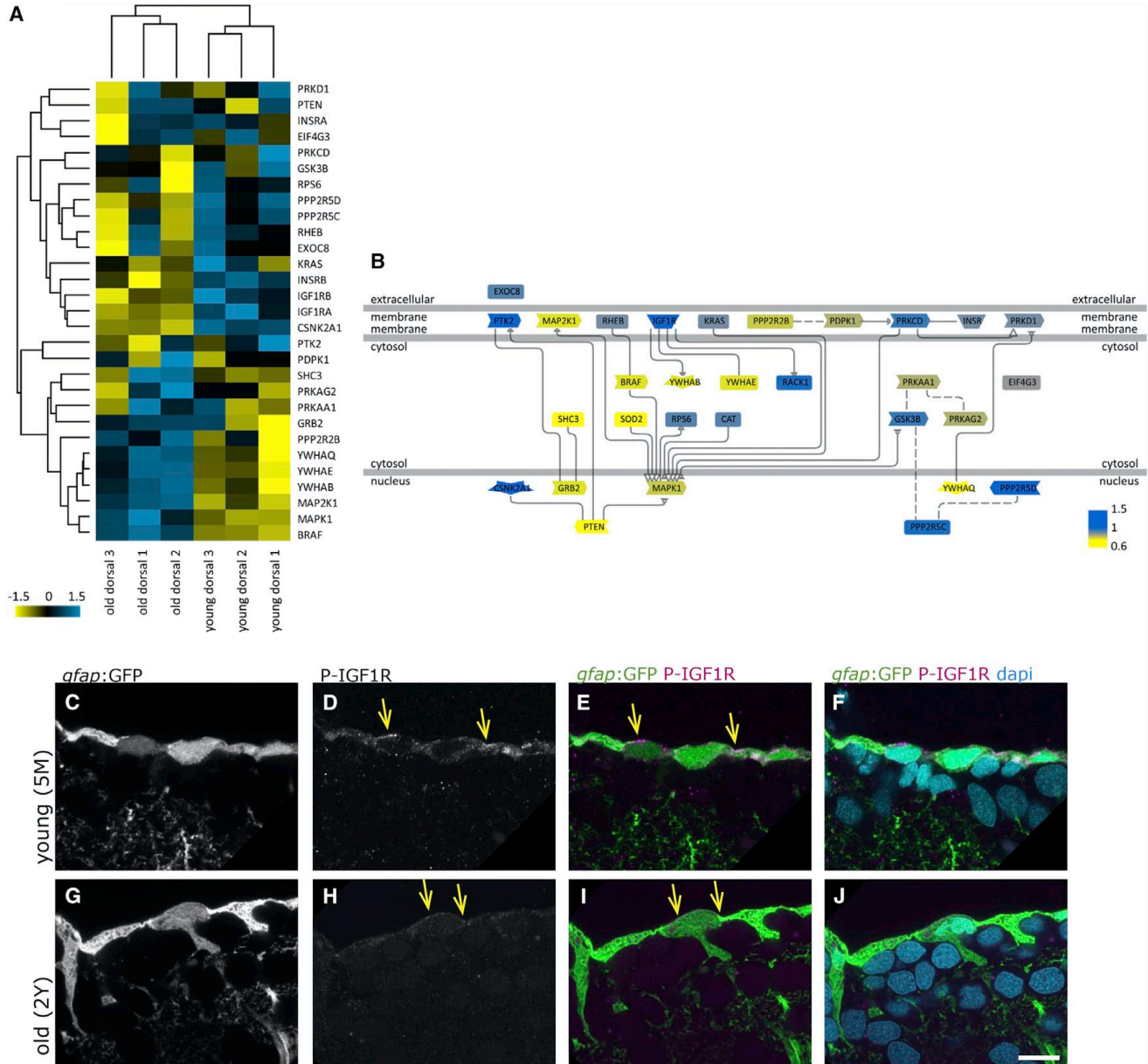


Figure 4. The IGF Signaling Pathway Declines with Age

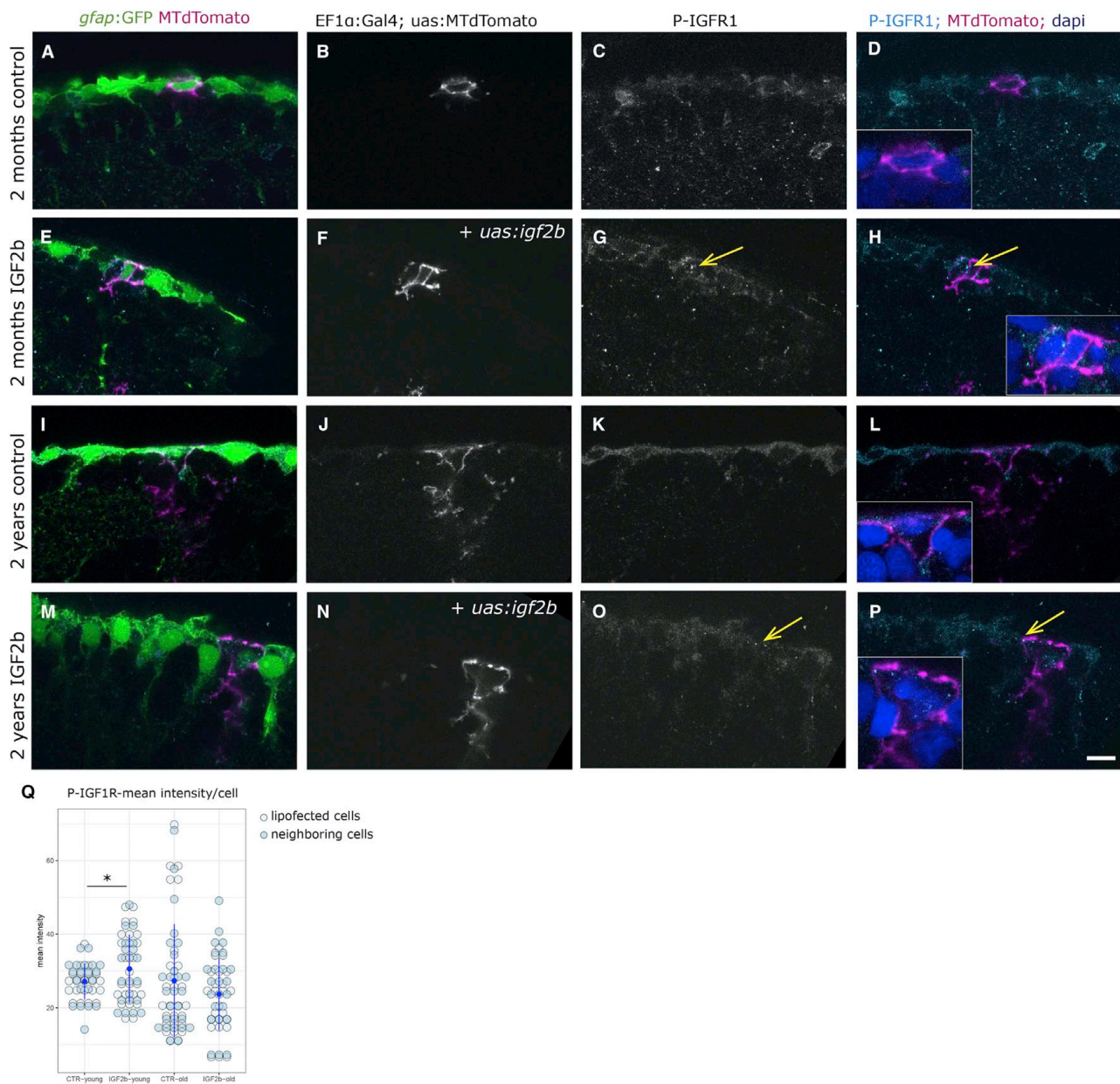
(A) Hierarchical clustering of the IGF, Insulin, and Akt pathway protein members identified in the surface fraction, revealing the differential expressions in young and old dorsal surface fractions (scale: log₂ young/old). Insulin receptor B, as well as IGF1 receptors a and b, are downregulated with age, while some other components are upregulated (i.e., MAP2K1 and BRAF).

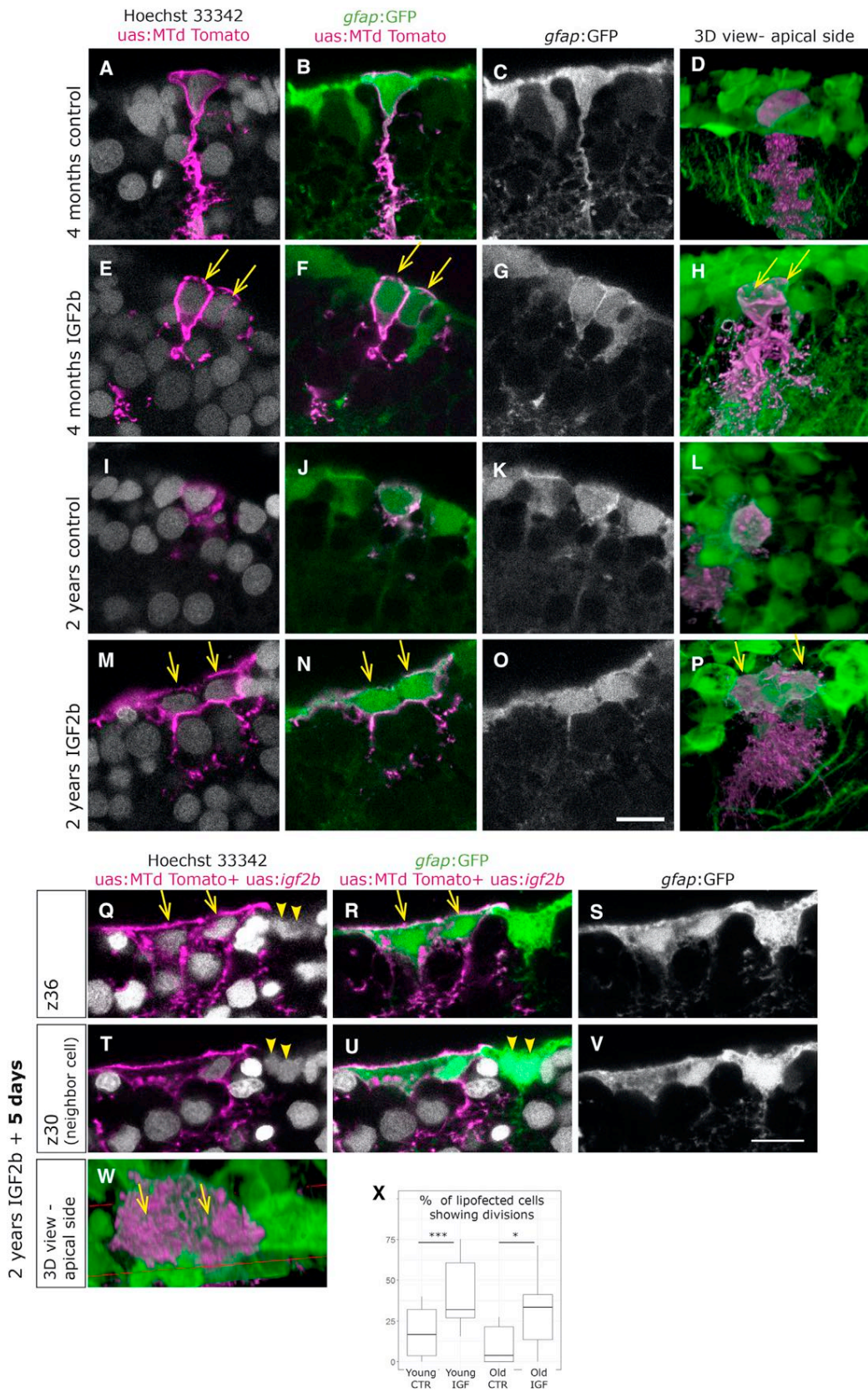
(B) Representation of the signaling pathway with color coding (blue, upregulated young; yellow, upregulated old).

(C–J) Phosphorylated IGF1R (P-IGF1R) immunohistochemistry (Tyr1161) on young (5 months, C–F) and old (2 years, G–J) brains as a close-up view on the ventricular surface of the dorsal pallium depicted as single confocal planes. The radial glia somata, located at the border of the ventricle, express P-IGF1R (yellow arrows). We observe the distinct expression levels of P-IGF1R in young and old brains in a total of 4 young and 4 old immunosamples. Scale bar, 10 μm.

To test for functional downstream effects of IGF in the adult NSCs, we analyzed the putative proliferative effect 2–5 days after lipofection in 6 independent experiments. Overexpression of IGF2b in young brains (2–4 months

old) resulted in a higher proportion of lipofected cells that revealed a recent mitosis, being visible as two neighboring cells immediately abutting each other (Figures 6A–6H and 6X; Table S5). Even if the cell division response to





(legend on next page)



IGF2b was indeed observed in a higher proportion than in control cells, it did not occur in all transfected cells, suggesting that the cells do not all have the same capacity to respond. Note that in Figures 5E–5H, the lipofected cell has divided and encompasses two cell bodies, even if the two cells are incompletely covered by the membrane staining. Overexpression of IGF2b in old brains was able to also induce the formation of two nuclei; however the division was incomplete, lacking cytokinesis, and led to the formation of very large cells (Figures 6I–6P and 6X). More time might be required for old cells to undergo cytokinesis, so we extended the lapse to 5 days, which revealed, however, the same effect of binucleation in old cells (Figures 6Q–6S and 6W). We also observed that some cells next to the *igf2b*-lipofected cells revealed the same phenotype of binucleated cells, as they might respond in a paracrine manner to IGF (Figures 6T–6V). The incomplete divisions might be the result of the lowered levels of IGF receptor, and the exact downstream mechanism will require closer examination. Together, our results show that aged cells are not competent to respond and divide properly to an increase of growth signals encountered, hence indicating significant cell-intrinsic alteration in the course of aging.

DISCUSSION

With the aim of understanding better how NSCs communicate and organize their cell-cycle entries, we identified the proteins expressed on their surface in young and aged brains. The use of the zebrafish brain, offering direct access to NSCs without preceding dissociation, combined with a biotinylation method, permitted us to obtain the surface proteome of an intact NSC population. From there we showed the presence of apically located filopodial structures and a changing response to IGF with age. Hence, two important aspects are revealed herein: a possible path of intercellular communication via cellular extensions, and cell-intrinsic alterations impacting on the proliferative competence of aging cells.

One of the two biotinylation protocols employed in this study, involving a covalent binding reaction between glycosylated residues and biotin, revealed a strong bias for proteins increased in aged samples, suggesting increased glycosylation patterns with aging. Age-related changes in glycosylation patterns in the brain have previously been reported (Miura and Endo, 2016), and a closer investigation of these alterations will be important.

The identified proteins in the surface fraction were in accordance with previous findings in the zebrafish or other adult neurogenic systems. For instance, Connexin 43, identified here on the adult radial glia in zebrafish, plays a role in the adult neuroepithelium in mammals (Lacar et al., 2011). The representation of exosome components in our study is interesting in the context of their newly described roles in adult neurogenesis (Batiz et al., 2015). We also identified Notch3 and Dner, in keeping with the role for the Notch signaling pathway described in previous studies (Alunni et al., 2013; Chapouton et al., 2010; Ehm et al., 2010; Hsieh et al., 2013; Katz et al., 2016).

Our study reveals protein members that allow defining an epithelial identity of the adult NSCs, a question that was also addressed by Grupp et al. (2010), who observed the presence of ZO-1 in those cells. A new feature of the cells described here is the presence of lateral lamellipodial and filopodial extension from the somata of the radial glia. The filopodial extensions are contacting neighboring cells further than the next neighbor (up to the fourth, most frequently the second), an aspect that might be important for cell-to-cell communication over several cell distances. Filopodia can convey signals in developing tissues (Prols et al., 2016), such as Wnt signals (Stanganello et al., 2015) or Notch signals (Cohen et al., 2010). Such signals remain to be identified in these adult cells, and could possibly be involved in coordinating the cell-cycle activity. A feedback signaling between cycling cells and their neighbors has been proposed previously in this system via the Notch signaling pathway (Chapouton et al., 2010).

The activity of the insulin and IGF signaling pathway is important in several developmental and regenerating

Figure 6. Overexpression of IGF2b Induces Complete Cell Division in Young Cells, but Incomplete Division in Old Cells

(A–P) Brains were lipofected *in vivo* 4 days prior to fixation with mtdTomato (control, A–D and I–L) or with mtdTomato and *igf2b* (IGF2b, E–H and M–P). Single confocal planes are displayed in the left panels and 3D reconstructions in the rightmost panels (D, H, L, and P). Cell nuclei (Hoechst, gray) and membrane labeling of the lipofected cells (magenta) are shown in (A), (E), (I), and (M). (A–D) Young control lipofected cells reveal infrequent cell division events, while young cells with IGF2b overexpression (E–H) reveal a higher incidence of cell division events, being visible as two neighboring cells immediately abutting each other (E–H, arrows). (M–P) Old control lipofected cells with IGF2b overexpression result in large cells with two nuclei, indicating an incomplete division (arrows in M, N, and P).

(Q–W) Brains fixed 5 days after *igf2b* lipofection also reveal binucleated large cells (arrows in Q, R, and W), visible here in two distinct confocal planes (Q–S and T–V). Some neighboring cells reveal the same phenotype (arrowheads in Q, T, and U).

(X) Cells having divided after lipofection were quantified in 6 experiments with a total of 69 young-control, 114 young-*igf2b*, 64 old-control, and 71 old-*igf2b* cells. The significance was calculated by a chi-squared test (young, *** $p = 0.7 \times 10^{-3}$; old, * $p = 0.01$).

Scale bars, 10 μm .



systems and shows multiple effects at distinct ages. These pathways are generally associated with nutrient sensing, growth, and metabolism, and play important roles in the homeostasis of NSCs (Rafalski and Brunet, 2011; Ziegler et al., 2015). IGF signaling induces proliferation and regulates the length of the cell cycle (Hodge et al., 2004; Mairet-Coello et al., 2009; Nieto-Estevez et al., 2016; Popken et al., 2004; Yuan et al., 2015), in some instances acting in combination with other growth factors, such as the EGFR (Alagappan et al., 2014). With age, systemic and brain levels of IGF ligands are reduced (Rafalski and Brunet, 2011; Shetty et al., 2005). These properties suggest that a maintained IGF pathway would be advantageous for counteracting an age-related proliferative decline. Indeed, infusion of IGF could restore higher levels of proliferation and neurogenesis in aged rats (Lichtenwalner et al., 2001). In contrast, most of the current literature suggests that inhibition of this pathway is beneficial for animals' longevity (Kappeler et al., 2008; Lopez-Otin et al., 2016), an effect also being observed in dwarf mutant mice (Sun, 2006). For instance, neurogenesis is maintained longer when IGF1R is conditionally deleted in the hypothalamus (Chaker et al., 2016) and SVZ (Chaker et al., 2015). Our results add a new aspect, as they show that NSCs lose their responsiveness to the IGF pathway with age. The reduction takes place both at the level of expression of the receptors and at the level of the proliferative response, remaining incomplete in old brains. Hence, we identify a cell-intrinsic change that might represent a protective response of cells. Collectively these observations lead to the concept that declining levels of neurogenesis with age could be, as opposed to a deficit, an actual benefit linked with healthy aging, whereby cells reduce at the same time their proliferative and general metabolic activity (see Hamilton et al., 2013). Thus, some of the changes observed with age might be the ones that promote longevity.

We have previously shown that aged radial glia are activated in lower percentage by an injury protocol than are young cells (Edelmann et al., 2013). Together with the results presented here, this indicates significant cell-intrinsic changes with age. It will be fundamental in the future to understand the respective contributions of cell-intrinsic changes and signals received from the neighborhood in order to understand under which conditions manipulations to rejuvenate aging tissue can be successful.

EXPERIMENTAL PROCEDURES

See [Supplemental Information](#) for details of all experimental procedures.

Animal Maintenance

Zebrafish were bred and maintained in the animal facility of the Helmholtz Zentrum München. Wild-type zebrafish (AB) or

the transgenic line *gfap:GFP* (Bernardos and Raymond, 2006) (mi2001) in the AB background were used. Animal experiments were conducted in accordance with the laws of the government of Oberbayern (animal protocol 55.2-1-54-2531-83-14).

Further information and requests for resources and reagents should be directed to and will be fulfilled by P.C. (chapouton@helmholtz-muenchen.de).

SUPPLEMENTAL INFORMATION

Supplemental Information includes Supplemental Experimental Procedures, seven figures, and six tables and can be found with this article online at <https://doi.org/10.1016/j.stemcr.2018.12.005>.

AUTHOR CONTRIBUTIONS

J.O. performed the gene ontology analysis, generated all graphs representing the proteomics dataset, and wrote the proteomics methods; F.W. produced the SFRP-EGFP construct; A.K. contributed to the FACS experiments; A.Z. performed the RNA-seq experiments on FACS isolated cells; J.N. analyzed the RNA-seq results; S.M.H. designed the biotinylation protocols and analyzed the mass spectrometry data; P.C. conceived the study, performed the experiments, prepared the figures, and wrote the manuscript.

ACKNOWLEDGMENTS

We are thankful to Leanne Godinho for providing several constructs and for critical reading of the manuscript, Christian Stigloher for helpful comments on the manuscript, Oriol Viader-Llagues and Reinhard Köster for providing pCS2-lifeact-RFP constructs, and Steffen Scholpp for providing the pCS2-Wnt8-mcherry plasmid. We thank Ayla Schröder, Sebnem Akbas, and Kathrin Edelmann who performed experiments during their respective practical courses, and Jennifer Behler and Fabian Gruhn for technical help in S.M.H.'s lab. We thank Andreas Ettinger and Maria-Elena Torres-Padilla for access to their confocal microscope. We acknowledge the work of the animal keepers. This work was performed in the lab of Hernán Lopez-Schier. This work was supported by Deutsche Forschungsgemeinschaft grants (HA6014/2-2 and PR 1248/2-2) and by intramural funding from Helmholtz Zentrum München – GmbH, Germany, which is funded by the German Federal Ministry of Education and Research (BMBF) and the State of Bavaria.

Received: July 20, 2017

Revised: October 12, 2018

Accepted: December 11, 2018

Published: January 10, 2019

REFERENCES

- Adolf, B., Chapouton, P., Lam, C.S., Topp, S., Tannhauser, B., Strahle, U., Gotz, M., and Bally-Cuif, L. (2006). Conserved and acquired features of adult neurogenesis in the zebrafish telencephalon. *Dev. Biol.* 295, 278–293.
- Alagappan, D., Ziegler, A.N., Chidambaram, S., Min, J., Wood, T.L., and Levison, S.W. (2014). Insulin-like growth factor receptor



- signaling is necessary for epidermal growth factor mediated proliferation of SVZ neural precursors in vitro following neonatal hypoxia-ischemia. *Front. Neurol.* 5, 79.
- Alunni, A., and Bally-Cuif, L. (2016). A comparative view of regenerative neurogenesis in vertebrates. *Development* 143, 741–753.
- Alunni, A., Krecsmarik, M., Bosco, A., Galant, S., Pan, L., Moens, C.B., and Bally-Cuif, L. (2013). Notch3 signaling gates cell cycle entry and limits neural stem cell amplification in the adult pallium. *Development* 140, 3335–3347.
- Barbosa, J.S., Sanchez-Gonzalez, R., Di Giaimo, R., Baumgart, E.V., Theis, F.J., Gotz, M., and Ninkovic, J. (2015). Neurodevelopment. Live imaging of adult neural stem cell behavior in the intact and injured zebrafish brain. *Science* 348, 789–793.
- Batiz, L.F., Castro, M.A., Burgos, P.V., Velasquez, Z.D., Munoz, R.I., Lafourcade, C.A., Troncoso-Escudero, P., and Wyneken, U. (2015). Exosomes as novel regulators of adult neurogenic niches. *Front. Cell Neurosci.* 9, 501.
- Baumgart, E.V., Barbosa, J.S., Bally-Cuif, L., Gotz, M., and Ninkovic, J. (2012). Stab wound injury of the zebrafish telencephalon: a model for comparative analysis of reactive gliosis. *Glia* 60, 343–357.
- Bernardos, R.L., and Raymond, P.A. (2006). GFAP transgenic zebrafish. *Gene Expr. Patterns* 6, 1007–1013.
- Bracko, O., Singer, T., Aigner, S., Knobloch, M., Winner, B., Ray, J., Clemenson, G.D., Jr., Suh, H., Couillard-Despres, S., Aigner, L., et al. (2012). Gene expression profiling of neural stem cells and their neuronal progeny reveals IGF2 as a regulator of adult hippocampal neurogenesis. *J. Neurosci.* 32, 3376–3387.
- Calzolari, F., Michel, J., Baumgart, E.V., Theis, F., Gotz, M., and Ninkovic, J. (2015). Fast clonal expansion and limited neural stem cell self-renewal in the adult subependymal zone. *Nat. Neurosci.* 18, 490–492.
- Capilla-Gonzalez, V., Cebrian-Silla, A., Guerrero-Cazares, H., Garcia-Verdugo, J.M., and Quinones-Hinojosa, A. (2014). Age-related changes in astrocytic and ependymal cells of the subventricular zone. *Glia* 62, 790–803.
- Carlen, M., Meletis, K., Goritz, C., Darsalia, V., Evergren, E., Tanigaki, K., Amendola, M., Barnabe-Heider, F., Yeung, M.S., Naldini, L., et al. (2009). Forebrain ependymal cells are Notch-dependent and generate neuroblasts and astrocytes after stroke. *Nat. Neurosci.* 12, 259–267.
- Chaker, Z., Aid, S., Berry, H., and Holzenberger, M. (2015). Suppression of IGF-I signals in neural stem cells enhances neurogenesis and olfactory function during aging. *Aging Cell* 14, 847–856.
- Chaker, Z., George, C., Petrovska, M., Caron, J.B., Lacube, P., Caille, I., and Holzenberger, M. (2016). Hypothalamic neurogenesis persists in the aging brain and is controlled by energy-sensing IGF-I pathway. *Neurobiol. Aging* 41, 64–72.
- Chapouton, P., Skupien, P., Hesl, B., Coolen, M., Moore, J.C., Madelaine, R., Kremmer, E., Faus-Kessler, T., Blader, P., Lawson, N.D., et al. (2010). Notch activity levels control the balance between quiescence and recruitment of adult neural stem cells. *J. Neurosci.* 30, 7961–7974.
- Cohen, M., Georgiou, M., Stevenson, N.L., Miodownik, M., and Baum, B. (2010). Dynamic filopodia transmit intermittent Delta-Notch signaling to drive pattern refinement during lateral inhibition. *Dev. Cell* 19, 78–89.
- Daynac, M., Morizur, L., Chicheportiche, A., Mouthon, M.A., and Boussin, F.D. (2016). Age-related neurogenesis decline in the subventricular zone is associated with specific cell cycle regulation changes in activated neural stem cells. *Sci. Rep.* 6, 21505.
- Daynac, M., Pineda, J.R., Chicheportiche, A., Gauthier, L.R., Morizur, L., Boussin, F.D., and Mouthon, M.A. (2014). TGFbeta lengthens the G1 phase of stem cells in aged mouse brain. *Stem Cells* 32, 3257–3265.
- Diotel, N., Rodriguez Viales, R., Armant, O., Marz, M., Ferg, M., Rastegar, S., and Strahle, U. (2015). Comprehensive expression map of transcription regulators in the adult zebrafish telencephalon reveals distinct neurogenic niches. *J. Comp. Neurol.* 523, 1202–1221.
- Dray, N., Bedu, S., Vuillemin, N., Alunni, A., Coolen, M., Krecsmarik, M., Supatto, W., Beaurepaire, E., and Bally-Cuif, L. (2015). Large-scale live imaging of adult neural stem cells in their endogenous niche. *Development* 142, 3592–3600.
- Edelmann, K., Glashauser, L., Sprungala, S., Hesl, B., Fritschle, M., Ninkovic, J., Godinho, L., and Chapouton, P. (2013). Increased radial glia quiescence, decreased reactivation upon injury and unaltered neuroblast behavior underlie decreased neurogenesis in the aging zebrafish telencephalon. *J. Comp. Neurol.* 521, 3099–3115.
- Ehm, O., Goritz, C., Covic, M., Schaffner, I., Schwarz, T.J., Karaca, E., Kempkes, B., Kremmer, E., Pfrieger, F.W., Espinosa, L., et al. (2010). RBPJkappa-dependent signaling is essential for long-term maintenance of neural stem cells in the adult hippocampus. *J. Neurosci.* 30, 13794–13807.
- Encinas, J.M., Michurina, T.V., Peunova, N., Park, J.H., Tordo, J., Peterson, D.A., Fishell, G., Koulakov, A., and Enikolopov, G. (2011). Division-coupled astrocytic differentiation and age-related depletion of neural stem cells in the adult hippocampus. *Cell Stem Cell* 8, 566–579.
- Fuentealba, L.C., Obernier, K., and Alvarez-Buylla, A. (2012). Adult neural stem cells bridge their niche. *Cell Stem Cell* 10, 698–708.
- Galant, S., Furlan, G., Coolen, M., Dirian, L., Foucher, I., and Bally-Cuif, L. (2016). Embryonic origin and lineage hierarchies of the neural progenitor subtypes building the zebrafish adult midbrain. *Dev. Biol.* 420, 120–135.
- Ganz, J., Kaslin, J., Hochmann, S., Freudenreich, D., and Brand, M. (2010). Heterogeneity and Fgf dependence of adult neural progenitors in the zebrafish telencephalon. *Glia* 58, 1345–1363.
- Goncalves, J.T., Schafer, S.T., and Gage, F.H. (2016). Adult neurogenesis in the hippocampus: from stem cells to behavior. *Cell* 167, 897–914.
- Grandel, H., and Brand, M. (2013). Comparative aspects of adult neural stem cell activity in vertebrates. *Dev. Genes Evol.* 223, 131–147.
- Grandel, H., Kaslin, J., Ganz, J., Wenzel, I., and Brand, M. (2006). Neural stem cells and neurogenesis in the adult zebrafish brain: origin, proliferation dynamics, migration and cell fate. *Dev. Biol.* 295, 263–277.
- Grupp, L., Wolburg, H., and Mack, A.F. (2010). Astroglial structures in the zebrafish brain. *J. Comp. Neurol.* 518, 4277–4287.



- Hamilton, L.K., Joppe, S.E., M Cochard, L., and Fernandes, K.J. (2013). Aging and neurogenesis in the adult forebrain: what we have learned and where we should go from here. *Eur. J. Neurosci.* *37*, 1978–1986.
- Hodge, R.D., D’Ercole, A.J., and O’Kusky, J.R. (2004). Insulin-like growth factor-I accelerates the cell cycle by decreasing G1 phase length and increases cell cycle reentry in the embryonic cerebral cortex. *J. Neurosci.* *24*, 10201–10210.
- Hsieh, F.Y., Ma, T.L., Shih, H.Y., Lin, S.J., Huang, C.W., Wang, H.Y., and Cheng, Y.C. (2013). Dner inhibits neural progenitor proliferation and induces neuronal and glial differentiation in zebrafish. *Dev. Biol.* *375*, 1–12.
- Kang, W., and Hebert, J.M. (2015). FGF signaling is necessary for neurogenesis in young mice and sufficient to reverse its decline in old mice. *J. Neurosci.* *35*, 10217–10223.
- Kappeler, L., De Magalhaes Filho, C., Dupont, J., Leneuve, P., Cervera, P., Perin, L., Loudes, C., Blaise, A., Klein, R., Epelbaum, J., et al. (2008). Brain IGF-1 receptors control mammalian growth and lifespan through a neuroendocrine mechanism. *PLoS Biol.* *6*, e254.
- Kaslin, J., Ganz, J., Geffarth, M., Grandel, H., Hans, S., and Brand, M. (2009). Stem cells in the adult zebrafish cerebellum: initiation and maintenance of a novel stem cell niche. *J. Neurosci.* *29*, 6142–6153.
- Kaslin, J., Kroehne, V., Ganz, J., Hans, S., and Brand, M. (2017). Distinct roles of neuroepithelial-like and radial glia-like progenitor cells in cerebellar regeneration. *Development* *144*, 1462–1471.
- Katz, S., Cussigh, D., Urban, N., Blomfield, I., Guillemot, F., Bally-Cuif, L., and Coolen, M. (2016). A nuclear role for miR-9 and argonaute proteins in balancing quiescent and activated neural stem cell states. *Cell Rep.* *17*, 1383–1398.
- Kazanis, I., Lathia, J.D., Vadakkan, T.J., Raborn, E., Wan, R., Mughal, M.R., Eckley, D.M., Sasaki, T., Patton, B., Mattson, M.P., et al. (2010). Quiescence and activation of stem and precursor cell populations in the subependymal zone of the mammalian brain are associated with distinct cellular and extracellular matrix signals. *J. Neurosci.* *30*, 9771–9781.
- Kroehne, V., Freudenreich, D., Hans, S., Kaslin, J., and Brand, M. (2011). Regeneration of the adult zebrafish brain from neurogenic radial glia-type progenitors. *Development* *138*, 4831–4841.
- Kuhn, H.G., Dickinson-Anson, H., and Gage, F.H. (1996). Neurogenesis in the dentate gyrus of the adult rat: age-related decrease of neuronal progenitor proliferation. *J. Neurosci.* *16*, 2027–2033.
- Lacar, B., Young, S.Z., Platel, J.C., and Bordey, A. (2011). Gap junction-mediated calcium waves define communication networks among murine postnatal neural progenitor cells. *Eur. J. Neurosci.* *34*, 1895–1905.
- Lehtinen, M.K., Zappaterra, M.W., Chen, X., Yang, Y.J., Hill, A.D., Lun, M., Maynard, T., Gonzalez, D., Kim, S., Ye, P., et al. (2011). The cerebrospinal fluid provides a proliferative niche for neural progenitor cells. *Neuron* *69*, 893–905.
- Lichtenwalner, R.J., Forbes, M.E., Bennett, S.A., Lynch, C.D., Sonntag, W.E., and Riddle, D.R. (2001). Intracerebroventricular infusion of insulin-like growth factor-I ameliorates the age-related decline in hippocampal neurogenesis. *Neuroscience* *107*, 603–613.
- Lim, D.A., and Alvarez-Buylla, A. (2016). The adult ventricular-subventricular zone (V-SVZ) and olfactory bulb (OB) neurogenesis. *Cold Spring Harb. Perspect. Biol.* *8*. <https://doi.org/10.1101/cshperspect.a018820>.
- Lopez-Otin, C., Galluzzi, L., Freije, J.M., Madeo, F., and Kroemer, G. (2016). Metabolic control of longevity. *Cell* *166*, 802–821.
- Maggi, R., Zasso, J., and Conti, L. (2014). Neurodevelopmental origin and adult neurogenesis of the neuroendocrine hypothalamus. *Front. Cell Neurosci.* *8*, 440.
- Mairet-Coello, G., Tury, A., and DiCicco-Bloom, E. (2009). Insulin-like growth factor-1 promotes G(1)/S cell cycle progression through bidirectional regulation of cyclins and cyclin-dependent kinase inhibitors via the phosphatidylinositol 3-kinase/Akt pathway in developing rat cerebral cortex. *J. Neurosci.* *29*, 775–788.
- März, M., Chapouton, P., Diotel, N., Vaillant, C., Hesl, B., Takamiya, M., Lam, C.S., Kah, O., Bally-Cuif, L., and Strahle, U. (2010). Heterogeneity in progenitor cell subtypes in the ventricular zone of the zebrafish adult telencephalon. *Glia* *58*, 870–888.
- Mirzadeh, Z., Merkle, F.T., Soriano-Navarro, M., Garcia-Verdugo, J.M., and Alvarez-Buylla, A. (2008). Neural stem cells confer unique pinwheel architecture to the ventricular surface in neurogenic regions of the adult brain. *Cell Stem Cell* *3*, 265–278.
- Miura, Y., and Endo, T. (2016). Glycomics and glycoproteomics focused on aging and age-related diseases—glycans as a potential biomarker for physiological alterations. *Biochim. Biophys. Acta* *1860*, 1608–1614.
- Nieto-Estevéz, V., Defterali, C., and Vicario-Abejon, C. (2016). IGF-I: a key growth factor that regulates neurogenesis and synaptogenesis from embryonic to adult stages of the brain. *Front. Neurosci.* *10*, 52.
- Pastrana, E., Cheng, L.C., and Doetsch, F. (2009). Simultaneous prospective purification of adult subventricular zone neural stem cells and their progeny. *Proc. Natl. Acad. Sci. U S A* *106*, 6387–6392.
- Popken, G.J., Hodge, R.D., Ye, P., Zhang, J., Ng, W., O’Kusky, J.R., and D’Ercole, A.J. (2004). In vivo effects of insulin-like growth factor-I (IGF-I) on prenatal and early postnatal development of the central nervous system. *Eur. J. Neurosci.* *19*, 2056–2068.
- Porlan, E., Marti-Prado, B., Morante-Redolat, J.M., Consiglio, A., Delgado, A.C., Kypta, R., Lopez-Otin, C., Kirstein, M., and Farinas, I. (2014). MT5-MMP regulates adult neural stem cell functional quiescence through the cleavage of N-cadherin. *Nat. Cell Biol.* *16*, 629–638.
- Prols, F., Sagar, and Scaal, M. (2016). Signaling filopodia in vertebrate embryonic development. *Cell Mol. Life Sci.* *73*, 961–974.
- Rafalski, V.A., and Brunet, A. (2011). Energy metabolism in adult neural stem cell fate. *Prog. Neurobiol.* *93*, 182–203.
- Recabal, A., Caprile, T., and Garcia-Robles, M.L.A. (2017). Hypothalamic neurogenesis as an adaptive metabolic mechanism. *Front. Neurosci.* *11*, 190.
- Rothensaigner, I., Krecsmarik, M., Hayes, J.A., Bahn, B., Lepier, A., Fortin, G., Gotz, M., Jagasia, R., and Bally-Cuif, L. (2011). Clonal analysis by distinct viral vectors identifies bona fide neural stem cells in the adult zebrafish telencephalon and characterizes their division properties and fate. *Development* *138*, 1459–1469.



- Schlueter, P.J., Royer, T., Farah, M.H., Laser, B., Chan, S.J., Steiner, D.F., and Duan, C. (2006). Gene duplication and functional divergence of the zebrafish insulin-like growth factor 1 receptors. *FASEB J.* *20*, 1230–1232.
- Shetty, A.K., Hattiangady, B., and Shetty, G.A. (2005). Stem/progenitor cell proliferation factors FGF-2, IGF-1, and VEGF exhibit early decline during the course of aging in the hippocampus: role of astrocytes. *Glia* *51*, 173–186.
- Stanganello, E., Hagemann, A.I., Mattes, B., Sinner, C., Meyen, D., Weber, S., Schug, A., Raz, E., and Scholpp, S. (2015). Filopodia-based Wnt transport during vertebrate tissue patterning. *Nat. Commun.* *6*, 5846.
- Sun, L.Y. (2006). Hippocampal IGF-1 expression, neurogenesis and slowed aging: clues to longevity from mutant mice. *Age (Dordr)* *28*, 181–189.
- Than-Trong, E., and Bally-Cuif, L. (2015). Radial glia and neural progenitors in the adult zebrafish central nervous system. *Glia* *63*, 1406–1428.
- Villeda, S.A., Luo, J., Mosher, K.I., Zou, B., Britschgi, M., Bieri, G., Stan, T.M., Fainberg, N., Ding, Z., Eggel, A., et al. (2011). The ageing systemic milieu negatively regulates neurogenesis and cognitive function. *Nature* *477*, 90–94.
- Wullimann, M.F., and Mueller, T. (2004). Teleostean and mammalian forebrains contrasted: evidence from genes to behavior. *J. Comp. Neurol.* *475*, 143–162.
- Yamada, T., Kerever, A., Yoshimura, Y., Suzuki, Y., Nonaka, R., Higashi, K., Toida, T., Mercier, F., and Arikawa-Hirasawa, E. (2017). Heparan sulfate alterations in extracellular matrix structures and FGF-2 signaling impairment in the aged neurogenic niche. *J. Neurochem.* *142*, 534–544.
- Yuan, H., Chen, R., Wu, L., Chen, Q., Hu, A., Zhang, T., Wang, Z., and Zhu, X. (2015). The regulatory mechanism of neurogenesis by IGF-1 in adult mice. *Mol. Neurobiol.* *51*, 512–522.
- Ziegler, A.N., Levison, S.W., and Wood, T.L. (2015). Insulin and IGF receptor signalling in neural-stem-cell homeostasis. *Nat. Rev. Endocrinol.* *11*, 161–170.

Stem Cell Reports, Volume 12

Supplemental Information

**The Surface Proteome of Adult Neural Stem Cells in Zebrafish Unveils
Long-Range Cell-Cell Connections and Age-Related Changes
in Responsiveness to IGF**

Jara Obermann, Felicia Wagner, Anita Kociaj, Alessandro Zambusi, Jovica Ninkovic, Stefanie M. Hauck, and Prisca Chapouton

Experimental procedures

Biotinylation of the zebrafish brain surface

a- Biotinylation via glycosyl side chains

Brains (3 replicates of 6 two-years-old; 3 replicates of 6 four-months-old brains) were dissected and incubated in 330µl biotinylation reagent (20 mM NaIO₄, 100 µM biotin (both Gentaur, Aachen, Germany) and 10 mM aniline (Sigma Aldrich, Deisenhofen, Germany) in PBS pH 6.7) in the dark for 30 minutes at 4°C. The reaction was quenched with 1mM glycerol for 5 minutes. Brains were dissected into dorsal (pallium) and ventral (subpallium) part, lysed in 100µl lysis buffer containing 1% NP-40, sonicated and centrifuged. The supernatant was incubated with 10µl washed streptavidin beads for two hours at 4°C and frozen at -20°C. Streptavidin beads were washed (with 500µl 1xTBS and with 500µl UC buffer (5M urea, 100mM Tris-HCl, pH8.5). Beads were incubated with 200µl UC buffer containing 100mM DTT for 30 minutes at room temperature, washed with 500µl UC buffer, incubated with 200µl UC buffer containing 50mM iodacetamide for 30 minutes at room temperature, washed with 200µl UC buffer containing 100mM DTT, with 500µl 5M NaCl, with 500µl 100mM Na₂CO₃ (pH 11.5) and twice with 500µl 100mM Tris-HCl, pH 8.5). After digestion overnight at 37°C in 40µl 50 mM Tris-HCl, pH 8.5, containing 1µg trypsin (Promega, Mannheim, Germany) beads were centrifuged and the supernatant containing tryptic peptides was transferred to a new tube. Beads were resuspended once with 20µl 50 mM Tris-HCl, pH 8.5, centrifuged and the supernatant was pooled with the first tryptic fraction, centrifuged through FASP filter and acidified with TFA (pH2).

b- Biotinylation via amino groups

Biotinylation via amino groups was performed with a cell surface protein isolation kit (Thermo scientific 89881) coupling biotin on NH₂ residues via EZ-Link™ Sulfo-NHS-SS-Biotin labelling. Brains (3 replicates of 6x two-year-old brains; 3 replicates of 7x four-month-old brains) were dissected in cold PBS (-Ca²⁺;-Mg²⁺) and the hemispheres of the telencephalon gently pulled apart from each other in order to disrupt partly the tela choroida and allow for the penetration of the biotinylation reagent into the ventricle. The brains were incubated in 12 ml Sulfo-NHS-SS-Biotin reagent per tube for 30 minutes at 4°C and the biotinylation reaction stopped with 200µl quenching solution (50mM Glycine in PBS), brains were washed with TBS, and telencephalons dissected into dorsal (dorsal pallium) and ventral (subpallium) part, then collected in 500µl lysis buffer (provided by the kit).

The tissue was transferred to 2 ml Precellys tubes, containing 12 small ceramic and 3 big ceramic beads, and lysed in the tissue homogenizer Precellys. Cell lysates were centrifuged at 10,000 ×g for 10 minutes at 4°C and the clarified supernatant was frozen at -20°C. 50µL of the NeutrAvidin Agarose

slurry (provided by the kit) was added to each column, washed and clarified cell lysate was added to the gel. After incubation for 60 minutes at room temperature with end-over-end mixing and following centrifugation for 1 minute at 1000 ×g, flow-through (intracellular fraction) was collected in separate tubes and stored at -20°C with Protease inhibitors. 50µL sample buffer (62.5mM Tris HCl, pH 6.8, 1% SDS, 10% Glycerol) containing 50 mM DTT was added to the gel and mixed end-over-end for 60 minutes at room temperature. After centrifugation, eluates were collected and frozen at -20°C.

Mass spectrometry

The identification of the isolated proteins was performed by LC-MS mass spectrometry on an LTQ OrbitrapXL (Thermo Fisher Scientific Inc.) (Grosche et al. 2016), or on a Q Exactive HF (Thermo Fisher Scientific). Digested peptides were loaded automatically onto an Ultimate3000 nano HPLC system (Dionex, Sunnyvale, CA) equipped with a nanotrap column (300 µm inner diameter × 5 mm, packed with Acclaim PepMap100 C18, 5 µm, 100 Å; LC Packings, Sunnyvale, CA) at a flow rate of 30µl/min in HPLC buffer containing 0.1% trifluoroacetic acid (TFA) for 5 minutes.

Different concentrations of buffer A (LTQ OrbitrapXL: 5% ACN in 0.1% formic acid (FA); Q Exactive HF: 2% ACN in 0.1% FA) and buffer B (LTQ OrbitrapXL: 80% ACN in 0.1% FA; Q Exactive HF: 100% ACN in 0.1% FA) were used to separate the peptides by increasing ACN concentrations on a reversed phase chromatography (LTQ OrbitrapXL: 75 µm inner diameter x 15 cm, Acclaim PepMap100 C18, 3 µm, 100A, Dionex; Q Exactive H: AcquityMST3 column, 25 cm, 1.8 µm, Waters) over 120 (LTQ OrbitrapXL) or 130 (Q Exactive HF) minutes at a flow rate of 250 nl/min.

From the high resolution MS prescan the 10 most abundant peptide ions for fragmentation in the HCD cell were acquired.

Survey full scan MS spectra (from m/z 200 to 1500) were measured with high-resolution (60,000 full-width half maximum). Target peptides already selected for MS/MS were dynamically excluded for 30 seconds.

Label-free quantification

LC-MS/MS-derived MS/MS spectra were directly imported as raw files into Progenesis Q1 software for proteomics (Version 2.5, Nonlinear Dynamics, Waters, Newcastle upon Tyne, U.K.) and label-free quantification was performed as previously described (Grosche et al. 2016). Briefly, profile data of the MS scans as well as MS/MS spectra were transformed to peak lists with respective m/z values, intensities, m/z width and abundances. The most complex sample was set as a reference, and the retention times of all other samples within the experiment were aligned (3 to 5 manual landmarks, followed by automatic alignment) to create maximal overlay of the two-dimensional feature maps. Features with charge scores of one or above 7 were excluded from further analysis. Subsequently,

samples were grouped (young or old, respectively) and all features were normalized. Peptide identification was performed with Mascot (Matrix Science, Version 2.2.06) using the Ensembl zebrafish public database (genome assembly Zv9; http://www.ensembl.org/Danio_rerio/) and setting trypsin as digestion enzyme and allowing fragment ion mass tolerances of 0.6 Da (Orbitrap XL data) or 20mmu (Q Exactive HF data) and parent ion tolerances of 10 ppm. One missed cleavage was allowed and iodoacetamide derivatives of cysteines were set as stable modifications as well as oxidation of methionine and deamidation of asparagine and glutamine as variable modifications. A Mascot-integrated decoy database search calculated an average false discovery (FDR) of <1.2% when searches were performed with a mascot percolator score cut-off of 13 and an appropriate significance threshold p.

Peptide assignments were reimported into Progenesis Q1 and all normalized abundances of unique peptides of an identified protein are summed for the total cumulative normalized of the respective protein.

Gene Ontology (GO) and Phobius algorithm

Proteins identified by LC-MS/MS were analyzed for the presence of transmembrane domains and/or signal peptides by the Phobius algorithm based on the amino acid sequence of a protein (Käll et al. 2004). Identified proteins were also analyzed by the Genomatix (GO) software suite to determine their “cellular components” either directly from the entries in the zebrafish database or by searching orthologue entries in the human database. Proteins annotated with GO terms “extracellular region”, “membrane” and/or “plasma membrane” were considered as being potentially located on the cell surface in addition to those with transmembrane domains or secretion signal peptides.

List of proteins were examined for overrepresented signaling pathways in the Genomatix Generanker and GePS (Genomatix Pathway Sytem) analyses tools.

Statistical analysis

Normalized abundances of the identified proteins of young and aged neural stem cells were compared and proteins which were 2 fold up- or downregulated were accepted as differentially expressed. Proteins without unique peptides were excluded of the analysis. Normal distribution was assumed and significance was determined by Student’s t-test. Proteins with p-values lower than 0.05 were regarded as significantly changed.

Hierarchical clustering based on Euclidean distance and Principal Component analysis (PCA) was performed with Perseus (Tyanova et al. 2016) including log2 transformed normalized abundances of all identified proteins.

Plasmids

Igf1, *igf2a*, *igf2b*, *igf1Ra* and *igf1rb* were cloned from zebrafish embryonic cDNA into the Strataclone PCR cloning vector PSC-A for generation of antisense-RNA probes for in situ-hybridization, using the following primers: IGF1FW: 5' ATGTCTAGCGGTCATTTCTCCAGG 3'; IGF1R: 5' CTACATGCGATAGTTTCTGCCCCCT 3'; IGF2aFW: 5' ATGGATGATTACCATGTATTCTGTGCATC 3'; IGF2aR: 5' TCATTTTCGGGATGTGCTGATCTG.3' IGF2bFW: 5' ATGGAGGACCAACTAAAACATCATTCTGT 3'; IGF2bR: 5' TCACTTGTGGCTAACGTAGTTTTCTGTG 3'; IGF1raFW: 5' CGAGGGATGTTTGGACCTATTTTG 3'; IGF1raR: 5' GACGAAGTCCACCTCGCTGGG 3'; IGF1rbFW: 5' AGCAAACAGAGGCGATATT 3'; IGF1rbR 5' GTGCACAACATGCTGACAGACACAC 3'. IGF2b was subcloned into pBH-5xuas with sma1 /Cla1 for use in Lipofections.

For lipofections (Supplementary information), EF1 α : gal4 was combined to 14xuas: MtdTomato and pBH 5x uas: IGF2b.

Further plasmids lipofected: pCS2-wnt8a-mcherry, pCS2-lynGFP, pCS2: FynRFP.

Sfrp1a was cloned from zebrafish embryonic cDNA and fused in 3' to EGFP in the pCDNA-EGFP vector using the Gibson cloning kit (NEB) using the following primers: FW-pCDNA3-sfrp1a:

GACCCAAGCTTGCCACCATGAAGTCCCTTGCATCTTTGTC; RV-Sfrp1a-Gly-egfp:

CCCTTGCTCACCATGCCCTTGAAGACATTCTCATAGGCAGG; FW- Gly-epfp:

GGCATGGTGAGCAAGGGCGAGG; RV-pCDNA3-stop-egfp:

CTATAGAATAGGGCCCTCTAGATTAGAATTCCTTGTACAGCTCGTCCA. In order to enable zebrafish SFRP1-

GFP to be secreted in the supernatant of mammalian cell lines the zebrafish specific signal peptide

sequence was exchanged with a murine IgG kappa-leader sequence in pCR3-SFRP-GFP, using the

following oligonucleotides and a Gibson cloning assembly: IgG-kappa-leader sequence:

ATGGAGACAGACACACTCCTGCTATGGGTACTGCTGCTCTGGGTTCCAGGTTCCACTGGTGAC; IgG-kappa-

fw: AGGGAGACCCAAGCTTGCCACCATGGAGACAGACACACTCCTG; IgG-kappa-rv:

GCCAGCCATACTCAAATGTCTGGTCAACAGTGGAACTGGAAC; SFRP1.1_GFP-fw:

CAGACATTTGAGTATGGCTGGCC; SFRP1.1_GFP-rv: CATAGAAGGCGGCGGTGGAAT; SFRP1.2_GFP-fw:

TTCGAAATGACCGACCAAGC; SFRP1.2_GFP-rv: CATGGTGGCAAGCTTGGGT.

Lipofections *in vivo*

1.5 μ g of each plasmid in a total of 5 μ l dd Ambion H₂O was given to a solution containing 2 μ l of EBSS and 3 μ l of Lipofectamine 2000, briefly vortexed and incubated at room temperature for 20 minutes.

Fish were anesthetized in 0.02 % MS222 and transferred into a wet foam piece. A thin whole was pierced into the skull by a thin needle (27G) and a small volume (less than 1 μ l) of lipofection solution

was gently injected through a micro capillary into the brain ventricle by pressure injection, as

previously described (Chapouton et al. 2010).

Transfection and expression of the SFRP1a-EGFP construct

6x10⁵ HEK 293T cells were seeded on 6-well plates in full medium and transfected the next day with 6 µg pCR3-IgGK-SFRP-GFP using Fugene HD transfection reagent (Promega) according to the manufacturer's instructions. 24h post transfection cells were washed with PBS and further cultured in FBS-free medium. The supernatant was harvested 48h post transfection.

In situ hybridisation

Brains were dissected and fixed in 4% Paraformaldehyde over night at 4°C. Gelatin albumin sections (100µm) were cut at the vibratome and in situ hybridization were performed using dig-labelled antisense RNA probes, as described in (Chapouton et al. 2011).

Immunohistochemistry

Dissected brains were fixed over-night in 4% PFA at 4°C, washed and embedded in 3% agarose. Vibratome sections (100µm) were prepared and blocked in 10% Normal goat serum with 0.5% Tritonx100. Immunohistochemistry was performed using following primary antibodies: Rabbit-anti Phospho-Tyr1161-IGF-1R, Assaybiotech A7114 (1:100) and Rabbit-anti-Phospho Akt (Ser473), Cell Signaling #9271 (1: 50), the Alexa 488-EGF complex, Thermo Fisher Scientific E13345 (1:1000) or the SFRP1a-GFP supernatant on floating vibratome sections in 24-well plates. Goat-anti-rabbit –Alexa561 or- Alexa633 (Thermo Fisher Scientific) were used at a dilution of 1:1000. Streptavidin-Alexa555 (Thermo Fisher Scientific) was diluted 1:1000.

Fluorescence Activated Cell Sorting (FACS) of adult neural stem cells

20 telencephalons per experiment were dissected in cold HBSS (Hank's balanced salt solution, Life Technologies, Cat. num. 24020). 5 telencephalons per tube were covered with 3 ml dissociation solution (10% (vol/vol) HBSS (Hank's balanced salt solution, Life Technologies, Cat. num. 24020), 1,8% (vol/vol) D-(+)- glucose (SIGMA®, Cat. num. G8769), 1,5% (vol/vol) HEPES (Life Technologies, Cat. num. 15630-080), 0.002% Trypsin-EDTA (Life Technologies, Cat. Num. 25300-054), pH 7.5). The tissue and cells were dissociated for 20 min at 30°C. After 10 min the tissue was mechanically dissociated with a fire-polished, medium coated Pasteur pipette and incubated for additional 10 min. The enzymatic reaction was stopped with 3ml of stop solution (2% (vol/vol) HEPES (Life Technologies, Cat. num. 15630-080), 4% (wt/vol) Bovine serum albumin (SIGMA-ALDRICH®, Cat. num. [A4503](#)) and EBSS (Earle's Balanced Salt Solution) (Life technologies, Cat. num. [14155063](#)). The cell suspension was filtered through a 70 µm strainer and centrifuged for 7 min at 1500 rpm/min. The pellet was washed twice with 500 µl of Dulbecco's Phosphate Buffered saline (Life Technologies, Cat. num. 14190-094), filtered again, resuspended into 2ml PBS and sorted at the FACS Aria III Cell Sorter (BD). Sorting gates

were set according to the WT tissue expressing no fluorescent marker and neural stem cells were sorted according to the GFP levels. Cellular debris were eliminated based on the positivity for propidium iodide. After the sorting, cells were centrifuged for 7min at 1500 rpm/min and either immediately stored at -80°C for protein extraction or plated on poly-D-lysine coated coverslips for fixation and image acquisition. 4 replicates containing 50.000 to 100.000 cells each (respectively GFP-positive and GFP-negative cells) were lysed and analyzed by mass spectrometry.

For RNA isolation, cells were directly sorted into extraction buffer and total RNA was isolated using the PicoPure RNA isolation kit, according to the manufacturer's instructions (Thermo Fisher Scientific).

Libraries for deep sequencing of FACS sorted cells

The quality and concentration of RNA was assessed on Agilent 2100 Bioanalyzer. Only RNA with RIN value higher than 8 were used for libraries preparation cDNA was synthesized from 1ng of total RNA using SMART-Seq v4 Ultra Low Input RNA kit for Sequencing (Clontech), according to the manufacturer's instructions. The quality and concentration of cDNA was assessed on Agilent 2100 Bioanalyzer before proceeding to library preparation using MicroPlex Library Preparation kit v2 (Diagenode). All libraries (minimum of 3 biological replicates per condition) were processed together to minimize batch effects. Final libraries were evaluated and quantified using an Agilent 2100 Bioanalyzer and the concentration was measured additionally with Quant-iT PicoGreen dsDNA Assay Kit (Thermo Fisher Scientific) before sequencing. The uniquely barcoded libraries were multiplexed onto one lane and 50-bp paired-end deep sequencing was carried out on HiSeq 4000 (Illumina) that generated approximately 20 million reads per sample.

The Kallisto pipeline (Bray et al. 2016) was then used to quantify the expression of transcripts. The Sleuth pipeline (Pimentel et al. 2017) was used for the statistical analysis. For the quantification, we aligned 30-kmers of 150 bp reads to the zebrafish Zv9 transcriptome containing both protein coding and non-coding genome using 100 bootstraps for every biological replicate (4 in total for each population). The most expressed isoform of gene was then used to generate the heatmap. The data in the heatmap (mean value of the replicates) is shown as log₂ of transcript per million.

Image acquisition and analysis

Vibratome sections or whole-mount brains were mounted in Vectashield (Vector Laboratories). Pictures were taken at the Leica SP5 or SP6 inverted confocal microscopes with the 63x glycerol immersion and 20x immersion objectives. In situ Hybridizations pictures were taken at the Zeiss axioplan with a matrix meteor video camera.

Confocal pictures were analyzed with ImageJ (Fiji). Filopodia were measured using the simple neurite tracer plugin. Mean fluorescence intensities were measured on manually defined ROIs (the whole cell soma in 3 different z-planes) on images taken with a hybrid detector. The 3D-viewer plugin was used to visualize all sides of the cells. Stackreg plugin was employed in case of deviation during z-stack acquisition (P. Thévenaz, U.E. Ruttimann, M. Unser A Pyramid Approach to Subpixel Registration Based on Intensity IEEE Transactions on Image Processing vol. 7, no. 1, pp. 27-41, January 1998).

Figures preparation

Figures were prepared in Adobe InDesign. Venn Diagramms were made with the Venny open source tool: <http://bioinfogp.cnb.csic.es/tools/venny/>, or with the Genomatix software. Graphs were prepared in Excel, Perseus (version 1.5.3.2; Computational Systems Biochemistry, Germany) and R Studio (RStudio Team (2015). RStudio: Integrated Development for R. RStudio, Inc., Boston, MA URL <http://www.rstudio.com/>) with the ggplot2 package.

References in the Supplementary Material:

- Bray NL, Pimentel H, Melsted P, Pachter L. 2016. Near-optimal probabilistic RNA-seq quantification. *Nat Biotechnol* **34**: 525-527.
- Chapouton P, Skupien P, Hesl B, Coolen M, Moore JC, Madelaine R, Kremmer E, Faus-Kessler T, Blader P, Lawson ND et al. 2010. Notch activity levels control the balance between quiescence and recruitment of adult neural stem cells. *J Neurosci* **30**: 7961-7974.
- Chapouton P, Webb KJ, Stigloher C, Alunni A, Adolf B, Hesl B, Topp S, Kremmer E, Bally-Cuif L. 2011. Expression of hairy/enhancer of split genes in neural progenitors and neurogenesis domains of the adult zebrafish brain. *J Comp Neurol* **519**: 1748-1769.
- Grosche A, Hauser A, Lepper MF, Mayo R, von Toerne C, Merl-Pham J, Hauck SM. 2016. The Proteome of Native Adult Muller Glial Cells From Murine Retina. *Molecular & cellular proteomics : MCP* **15**: 462-480.
- Käll L, Krogh A, Sonnhammer EL. 2004. A combined transmembrane topology and signal peptide prediction method. *Journal of molecular biology* **338**: 1027-1036.
- Pimentel H, Bray NL, Puente S, Melsted P, Pachter L. 2017. Differential analysis of RNA-seq incorporating quantification uncertainty. *Nat Methods* **14**: 687-690.
- Tyanova S, Temu T, Sinitcyn P, Carlson A, Hein MY, Geiger T, Mann M, Cox J. 2016. The Perseus computational platform for comprehensive analysis of (prote) omics data. *Nature methods* **13**: 731-740.

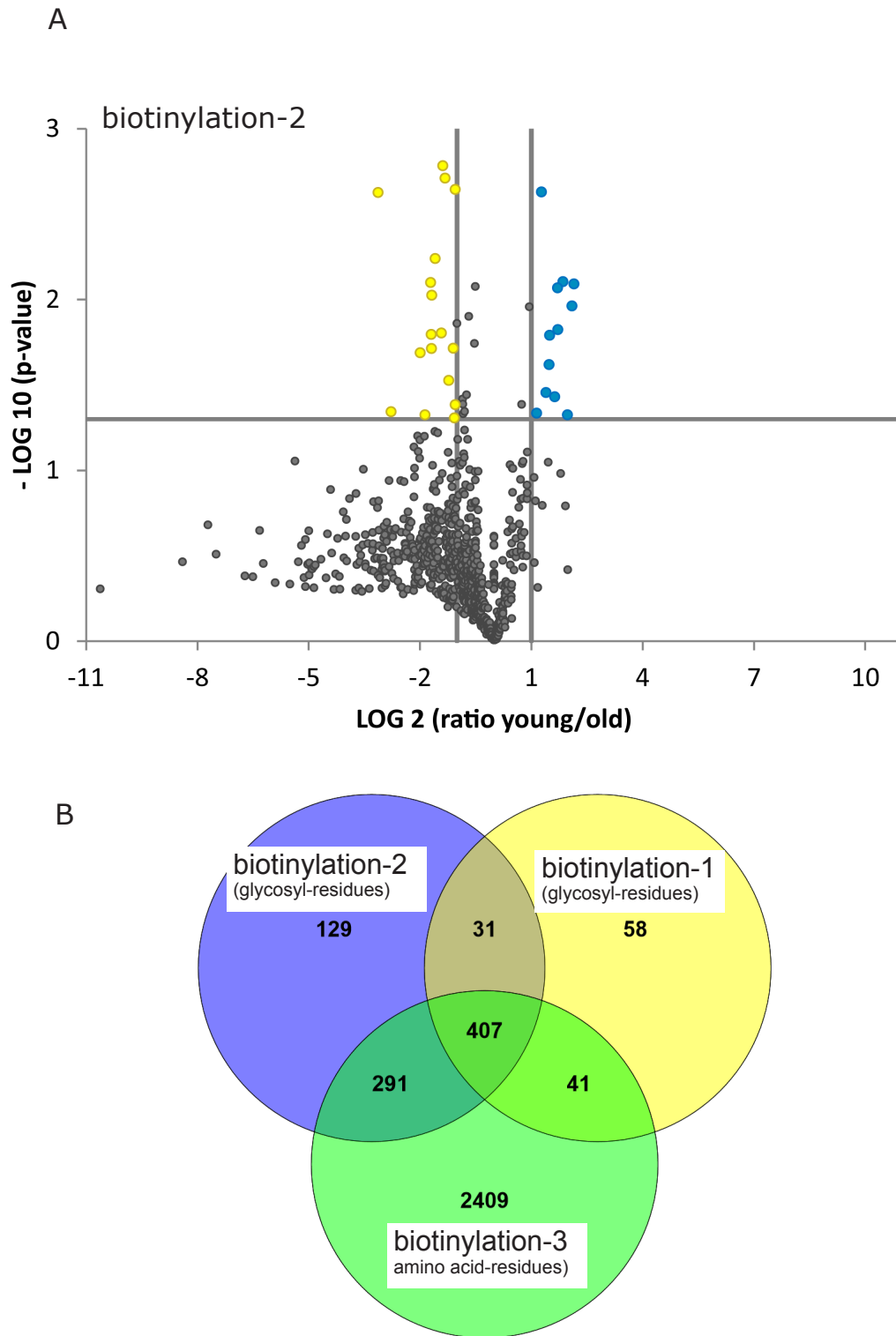


Figure S1: Proteins retrieved by two different biotinylation protocols

A: Volcano plot representation of the proteins identified by the glycosylation-dependent biotinylation, depicting young versus old ratios. Note the bias towards proteins with increased expression in aged brains (left side). B: Venn diagram of three experiments. The majority of proteins identified by the glycosylation-dependent biotinylations (1 and 2) are also identified in the amino-acid bound biotinylation (3). A higher number of proteins were identified in the latter approach.

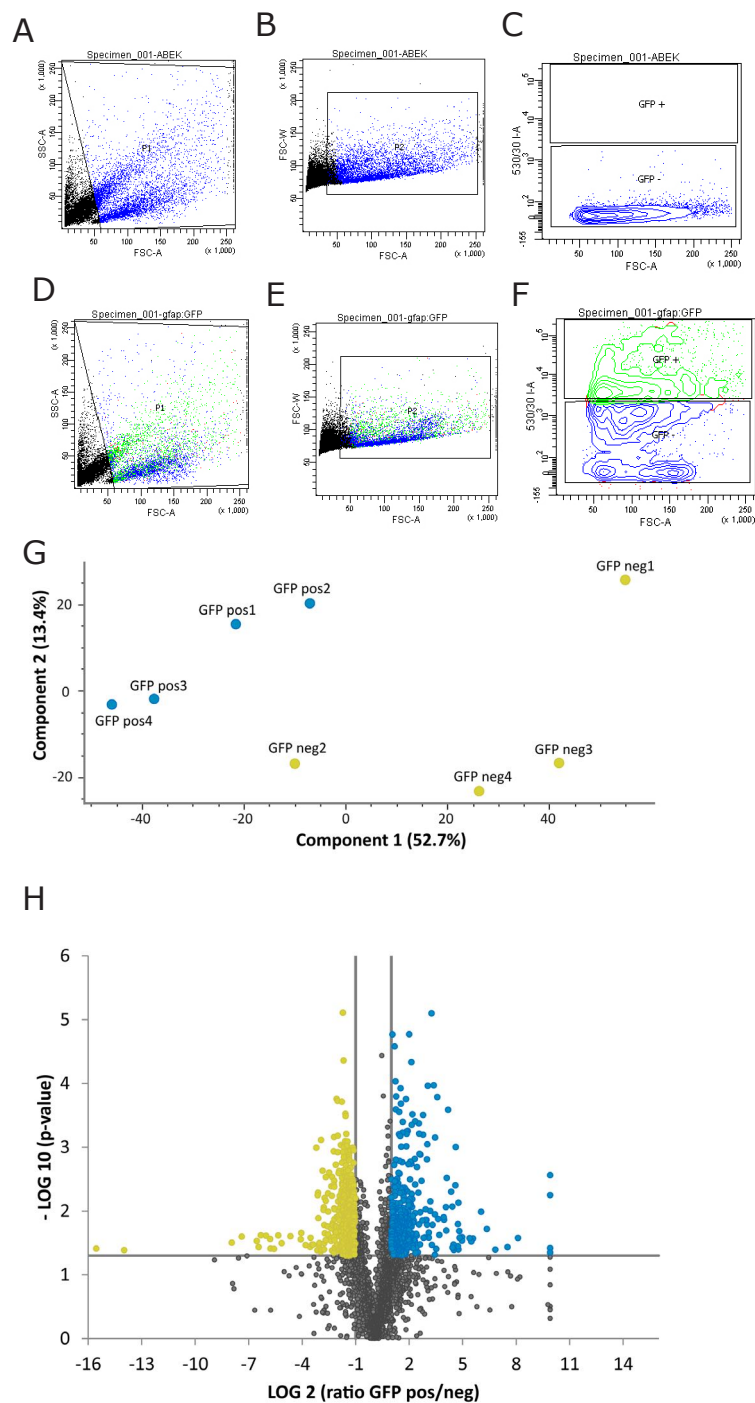
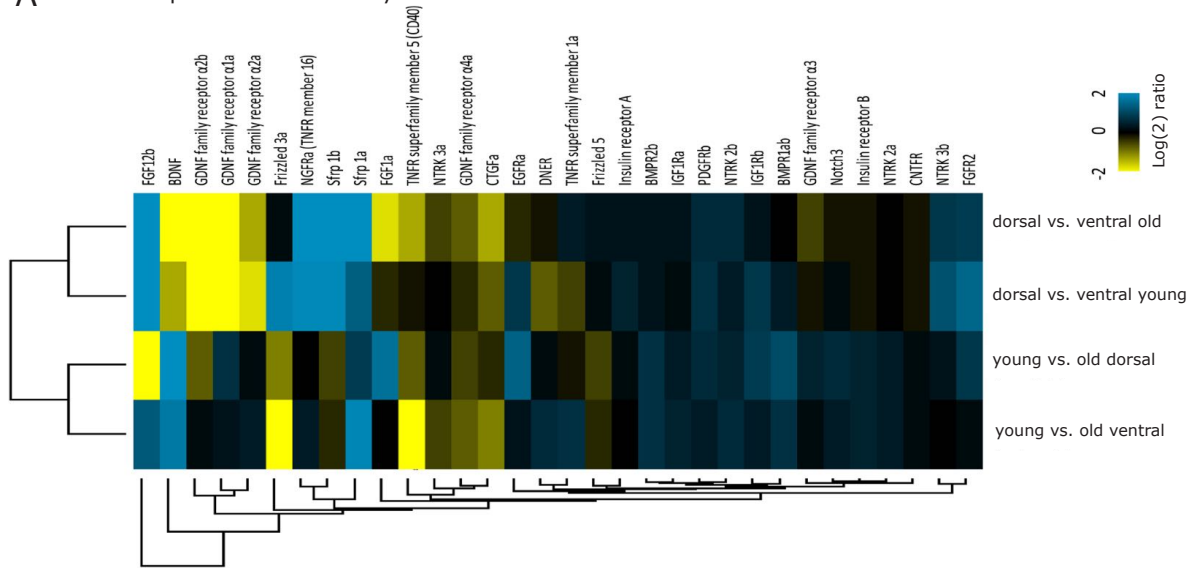


Figure S2: FACS isolation of cells and protein identification thereafter

A-F: dissociated cells were selected by forward scatter (FSC-A) and side scatter (SSC-A), P1 gate. B, E: Cellular aggregates are excluded on FSC-W and FSC-A gate, (P2). C: Gates for gfap:GFP sorting were based on AB wild-type zebrafish, which are negative for GFP. F: Plot depicting cells which do not express (GFP-negative gate) and cells that express GFP (GFP-positive gate). G: principal component analysis of the proteins identified in consecutive sorting experiments, depicting a consistent clustering of the fractions. H: volcano plot of the proteins upregulated in the GFP-positive fraction versus proteins upregulated in the GFP-negative fraction, revealing similar number of proteins on both sides.

Obermann et al., **Figure S4**: Surface receptors and ligands isolated as proteins in the biotinylated fraction and as RNA in FACS-sorted cells

A Isolated proteins from biotinylated brains



B RNA-seq data on FACS-sorted cells

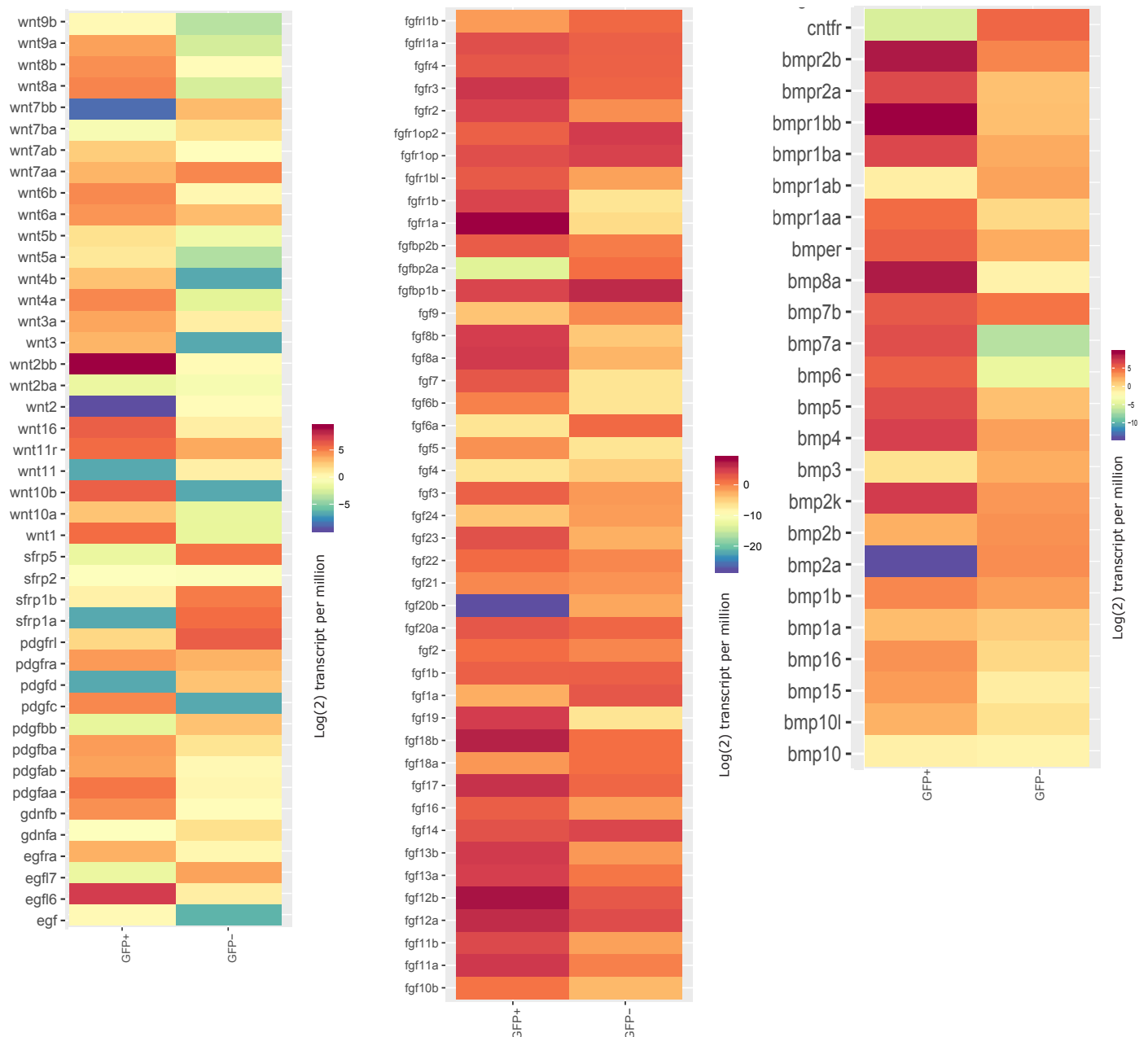


Figure S4: Surface receptor and ligands isolated as proteins in the biotinylated fraction and as RNA in FACS-sorted cells.

A: Surface receptors, as well as some ligands were clustered. Log (2) ratios of the expression levels are depicted. B: cDNA produced from sorted gfap:GFP-positive and -negative cells was sequenced and quantified. Members of the Wnt, PDGF, EGF, FGF, CNTF and BMP signal pathways are represented as log(2) transcripts per million.

Obermann et al., **Figure S5:**

Neither Wnt nor EGF signaling co-localize with filopodial extensions of adult radial glia

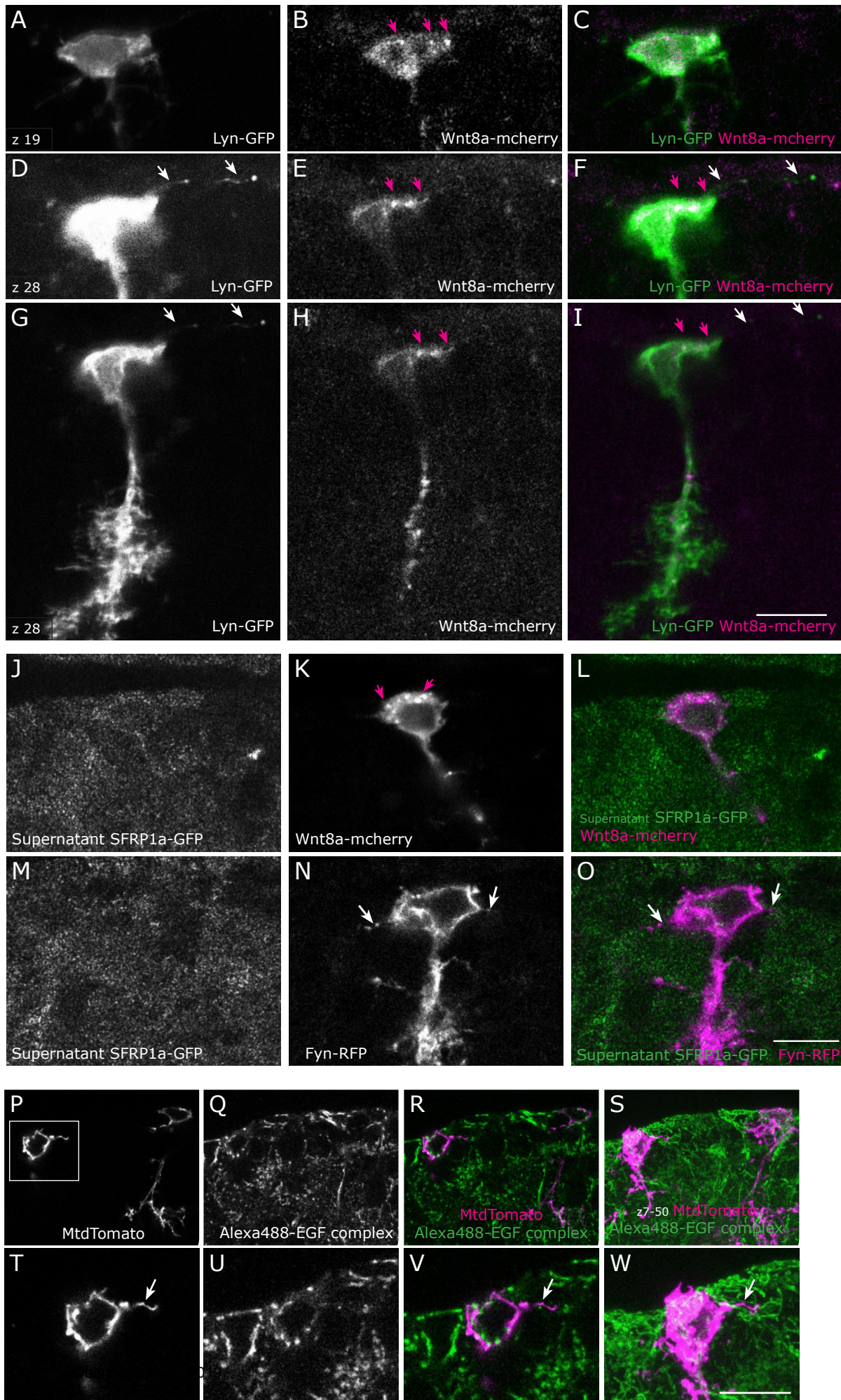


Figure S5: Neither Wnt nor EGF signaling co-localizes with filopodial extensions in adult radial glia.

A-I: Example of a cell in a 3-months-old wild-type (AB) brain co-lipofected with pCS2-lyn-GFP and pCS2-wnt8a-mcherry as single confocal planes (z19 in A-C and z28 in D-I). Wnt8a-mcherry localizes in a non-homogeneous manner in the radial glia and can be found at edges of the cytoplasm (pink arrows), however it does not localize in thin filopodial extensions labelled by Lyn-GFP (white arrows). Number of cells analyzed: 8. J-O: The supernatant of Hek-293 cells transfected with sfrp1a-GFP was applied on brain sections containing cells lipofected with pCS2-Wnt8a-mcherry (J-L), or with pCS2-fyn-RFP (M-O). The SFRP-GFP protein does not co-localize strongly with Wnt8a-mCherry (pink arrows in K), and does not co-localize with filopodia visible on Fyn-RFP-transfected cells (white arrows in N, O). Number of cells analyzed: 8. P: Staining of a 3-month-old wild-type brain section with the Alexa Fluor 488-EGF complex, which binds to the EGF receptor. Two lipofected cells are visible as a single confocal plane in P-R and as a maximum intensity projection in S. T-W: higher magnification of the inset region depicted in P showing the soma and a filopodial extension (arrow). The EGF-Alexa-488 complex does not co-localize with filopodial extensions. Number of cells analyzed: 12. Scale bars: 10 μ m.

Obermann et al., **Figure S6:**

Expression of *igf1*, *igf2a* and *-2b*, *igf1ra* and *igf1rb* in the adult telencephalon

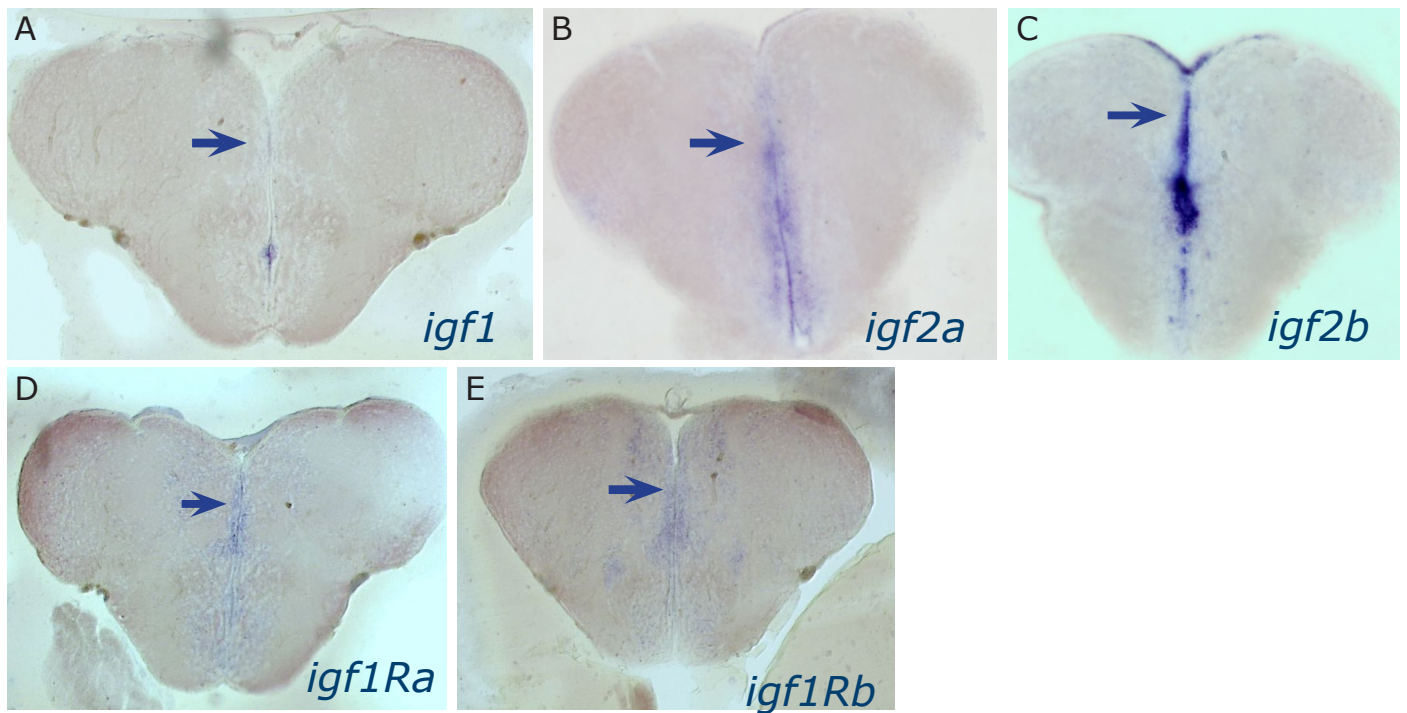


Figure S6: Expression of *igf 1*, *igf2a*, *igf2b*, *igf1ra* and *igf1rb* in the adult telencephalon.

In situ hybridization was performed on gelatin-albumine frontal sections of adult brains, with antisense probes as indicated in the panels. Expression is detected in the telencephalic ventricular zone (with a stronger expression level in the midline compared to the dorsal surface, where the signal was difficult to detect).

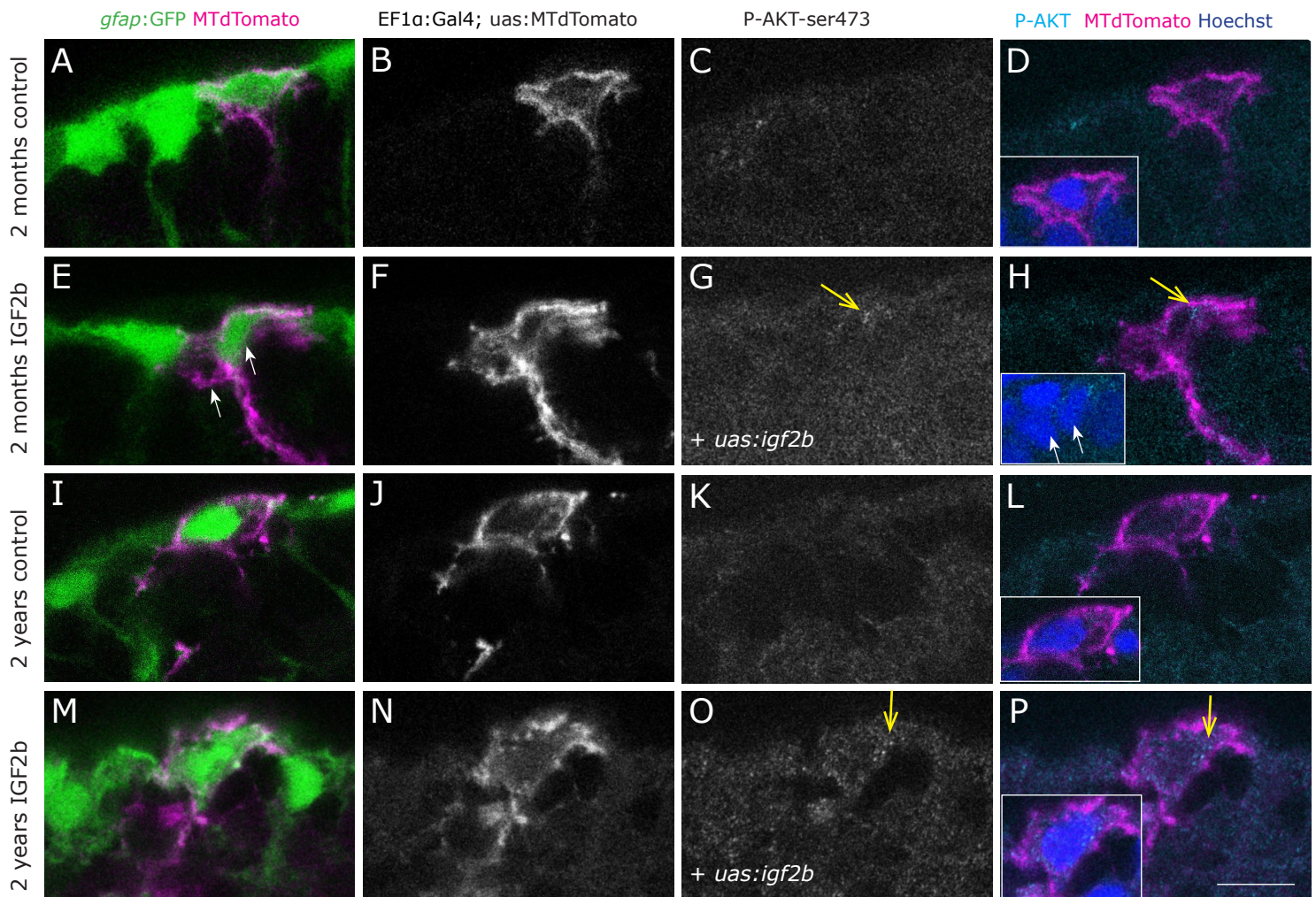


Figure S7: IGF2b overexpression reveals a moderate increase of phospho-Akt immunostaining. Phosphorylated-AKT (Ser473) immunohistochemistry on young (A-H) and old (I-P) brains as a close-up view on the ventricular surface of the pallium. The radial glia somata, located at the border of the ventricle, are labelled in green by the *gfap:GFP* transgenic line. Single cells stained in magenta have been lipofected *in vivo* 4 days prior to brain fixation with MTdTomato (control, A-D; I-L) or with MTdTomato and *igf2b* (IGF2b, E-H; M-P) and are depicted as single confocal plane, highlighting primarily the cell soma (the radial process is not always in the plane of the optical section, therefore not always visible, but it is present below all the somata of lipofected cells). Dots of expression of P-Akt are visible in IGF2b lipofected cells (arrows in G, H, O, P). Insets in D, H, L and P are higher magnifications of the lipofected cells, the nuclei in blue are stained by DAPI. Single confocal planes are displayed, examples are taken out of 3 brains for each condition. Scale bar: 10µm

Aim of the study III

The aim of the study is to investigate:

The activation states of microglia in response to injury, the importance of regulating the clearance of phase-separated TDP-43 condensates for the de-activation of immune response, and the functional role of granulins in regulating these processes in the adult zebrafish telencephalon.

Phase-separated TDP-43 regulates the activation states of microglia after traumatic brain injury

Alessandro Zambusi*, Klara Tereza Novoselec*, Christina Koupourtidou, Sofia Kalpazidou, Saskia Hutten, Lara Silva, Bettina Schmid, Claire Delbridge, Jürgen Schlegel, Hananeh Aliee, Fabian Theis, Dorothee Dormann and Jovica Ninkovic.

* These authors contributed equally to the manuscript

For this paper I was involved in performing and analyzing all the experiments together with Klara Tereza Novoselec, except for staining of brain tissues from patients with stroke (Figure 7), performed by Sofia Kalpazidou and Claire Delbridge. All the materials required to study the phase-separation of TDP-43 and FUS were provided by Dr. Saskia Hutten, Lara Silva and Prof. Dr. Dorothee Dormann.

I was also involved in writing, editing and reviewing the paper, together with Prof. Dr. Jovica Ninkovic and Klara Tereza Novoselec.

The paper is currently in revision in Nature Neuroscience.

1 **Phase-separated TDP-43 regulates the activation states of microglia**
2 **after traumatic brain injury**

3 Alessandro Zambusi^{1,2*}, Klara Tereza Novoselc^{1,2*}, Christina Koupourtidou^{1,2}, Sofia
4 Kalpazidou¹, Saskia Hutten¹, Lara Silva¹, Bettina Schmid³, Claire Delbridge⁴, Jürgen
5 Schlegel⁴, Hananeh Aliee⁵, Fabian Theis⁵, Dorothee Dormann^{1,7} and Jovica
6 Ninkovic^{1,6,7,8#}

7
8 ¹ Biomedical Center Munich (BMC), Department of Cell Biology and Anatomy, LMU,
9 Munich, Germany

10 ² Graduate School of Systemic Neurosciences, LMU, Munich, Germany.

11 ³ German Center for Neurodegenerative Diseases (DZNE), Munich, Germany

12 ⁴ Institute of Pathology, Faculty of Medicine, TUM, Munich, Germany

13 ⁵ Institute of Computational Biology, Helmholtz Zentrum Munich, Munich, Germany

14 ⁶ Biomedical Center Munich (BMC), Faculty of Medicine, LMU, Munich, Germany

15 ⁷ Munich Cluster for Systems Neurology SYNERGY, LMU, Munich, Germany

16 ⁸ Institute of Stem Cell Research, Helmholtz Zentrum Munich, Munich, Germany

17
18 * these authors equally contributed to the work

19 #Correspondence to: ninkovic@helmholtz-muenchen.de

20
21 **Abstract**

22
23 Inactivation of pathology-activated microglia is crucial to prevent chronic
24 neuroinflammation and tissue scarring. We identified an injury-induced microglial state
25 at the transition between activation and homeostasis in injured zebrafish brains, which
26 was characterized by accumulation of lipid droplets and phase-separated TDP-43
27 condensates. Granulin-mediated clearance of both lipid droplets and TDP-43
28 condensates was necessary and sufficient to promote this microglial transition and the
29 return to homeostatic function. Clearance of phase-separated TDP-43 condensates
30 promoted both the return of activated microglia back to homeostasis and scarless
31 regeneration. Importantly, the activated state of microglia also correlated with the
32 accumulation of lipid droplets, TDP-43 condensates and stress granules in patients
33 with ischemic stroke, thus supporting the existence of a similar regulatory mechanism
34 in humans. Together, our results identified a drug-targetable mechanism required for
35 the inactivation of microglia, which is necessary to avoid chronic neuroinflammation
36 and has high potential for new therapeutic applications in humans.

1 Main

2
3 Regeneration of the damaged adult mammalian central nervous system (CNS),
4 including that in humans, is largely limited^{1,2}. Despite the injury-induced enhancement
5 of adult neurogenesis and neuronal migration to injury sites, young neurons fail to
6 integrate into pre-existing neural circuits and to survive³⁻⁷. Similarly, the numbers of
7 transplanted neurons decrease over time, and their functional benefits decline in
8 different models of neurodegenerative diseases^{8,9}. This response is largely due to an
9 adverse environment generated by prolonged neuroinflammation and glial scar
10 formation^{10,11}. Both neuroinflammation and the glial scarring are initially beneficial in
11 limiting the expansion of the damage, but they later hinder functional recovery by
12 tissue remodeling and result in the generation of an inflamed environment^{2,12-14}.

13 Under physiological conditions, microglia, the brain-resident immune cells, are
14 dynamically activated by environmental and microglia-intrinsic pathways and
15 subsequently surveil the local environment and shape the organization and
16 functionality of neural circuits¹⁵⁻²¹. Microglial activation is, however, tightly controlled
17 by the balance between activating “ON” and inactivating “OFF” signals. Indeed, the
18 loss of “OFF” signals, such as TREM2, leads to the development of disease-
19 associated microglia, which can enhance the progression of neurodegenerative
20 phenotypes²²⁻²⁷. Importantly, the injury-induced inflammatory response activated in
21 the mammalian brain lacks “OFF” signals, thus leading to persistent
22 neuroinflammation and cellular stress.

23 In contrast to that in mammals, the injured CNS in adult zebrafish displays
24 exceptional regenerative capacity, including the generation of long-lasting neurons
25 from endogenous neural stem cell pools (restorative neurogenesis) in different areas
26 of the brain and the spinal cord^{28,29,38,30-37}. Injury in the zebrafish CNS induces only
27 transient neuroinflammation, which is terminated in a timely manner, promoting
28 neuronal integration and the resolution of scar tissue^{29-31,39-43}. Therefore,
29 understanding of the cellular dynamics and signaling cues underlying the resolution of
30 the inflammatory cascade in the zebrafish CNS is crucial to ameliorate the
31 regenerative outcomes in the mammalian CNS in response to traumatic brain injury
32 and neurodegenerative diseases.

33 Here, we sought to investigate the microglial dynamics in the injured adult
34 zebrafish telencephalon. We identified the transient state of activated pro-regenerative
35 microglia that spontaneously return to homeostasis in a granulin-dependent manner.
36 Furthermore, we demonstrated that granulin-mediated clearance of phase-separated
37 TDP-43 condensates in microglial cells is fundamental for the activation of “OFF”
38 signals in activated microglia and the scarless regeneration in the adult zebrafish CNS.
39 These results highlight liquid-liquid phase separation (LLPS) of TDP-43 as valuable
40 target for new approaches to improve CNS regeneration in response to traumatic brain
41 injury and neurodegenerative diseases. The translational value of our research is
42 strengthened by the observation of high microglial reactivity correlating with the
43 presence of TDP-43 condensates and lipid droplets in human patients with stroke.
44

45 **Stab wound injury induces a pro-regenerative signature in a *granulin a*-** 46 **expressing microglial subpopulation**

47
48 The activation state of microglia is a key regulator of neuroinflammation during aging,
49 neurodegeneration and CNS injuries⁴⁴⁻⁵⁰. Moreover, injury-induced activation of
50 immune cells is necessary to initiate restorative programs in regeneration-competent

1 species such as zebrafish ³⁰. However, little is known about the mechanisms
2 promoting the transition of activated microglia back to homeostasis, and the avoidance
3 of long-lasting and chronic neuroinflammation. Therefore, we first analyzed the
4 dynamics of the microglial response to injury in the adult zebrafish telencephalon (Fig.
5 1A), on the basis of the expression of 4C4, an established marker for labeling immune
6 cells in the zebrafish telencephalon ²⁹. Indeed, we observed ramified, homeostatic
7 microglia throughout the intact telencephalic parenchyma (Fig. 1A). Stab wound injury
8 through the zebrafish nostrils induced an immediate microglial response that reached
9 a maximum intensity 3 days post-injury (dpi), as evidenced by the accumulation of
10 activated 4C4⁺ microglial cells at injury sites (red square in Fig. 1A). However, the
11 4C4⁺ microglial cell accumulation was only transient and resolved by 7 dpi, in
12 agreement with the observation of complete scarless tissue regeneration at the same
13 time point (Fig. 1A, Extended Data Fig. 1A, B). Microglial activation was restricted to
14 the site of the injury, because reactive microglia were not detected far from it (blue
15 square in Fig. 1A). This finding is consistent with recent observations that different
16 microglial populations emerge after brain injury and neurodegenerative diseases, and
17 have distinct dynamics and roles in regulating neuroinflammation, including the
18 modulation of other scar-forming cells ^{51,52}.

19 To assess the composition of microglia and identify the molecular pathways
20 controlling their dynamics during scarless regeneration, we followed the transcriptional
21 changes at the single-cell level in the whole zebrafish telencephalon in response to
22 brain injury. We isolated cells from intact and injured wildtype (Wt) telencephali (3 and
23 7 dpi) and compared their transcriptomes with a droplet-based single cell RNA-
24 sequencing (scRNA-seq) platform (10x Genomics Chromium) (Fig. 1B, Extended Data
25 Fig. 1A). After applying quality control filters, we identified 29603 single cells uniformly
26 distributed over different conditions (Extended Data Fig. 1C). Unsupervised clustering
27 of single cells according to their transcriptomes revealed 30 distinct clusters (Fig. 1B,
28 Extended Data Fig. 1A). We identified neuronal clusters as well as distinct glial
29 populations, including microglia, oligodendrocyte lineage cells and radial glial cells
30 (RGCs), on the basis of the expression of established markers characterizing these
31 populations (Fig. 1B, Extended Data Fig. 1A, D). We first analyzed changes in the
32 abundance of cellular populations (Extended Data Fig. 1B). We detected an increase
33 in microglial and oligodendroglial cell abundance at 3 dpi (Extended Data Fig. 1B) and
34 a concomitant decrease in RGCs, findings that may be explained by direct damage to
35 RGC processes spanning the parenchyma and subsequent RGC death. The
36 abundance of oligodendroglial and microglial cells decreased at 7 dpi and almost
37 reached the levels detected in intact brains (Extended Data Fig. 1B). The observed
38 kinetics of microglial cells was compatible with the hypothesis that regeneration-
39 competent species have mechanisms that prevent the prolonged activation and
40 amplification of immune cells, and subsequent chronic neuroinflammation. Therefore,
41 we focused our analysis on the transcriptional changes in microglial cells (cluster 17
42 in Fig. 1B) during the course of regeneration. We identified 420 differentially expressed
43 genes (DEGs) ($\log_2FC \geq 1$; $FDR \leq 0.05$) at 3 dpi compared with other conditions (intact
44 and 7 dpi) (Extended Data Fig. 1E; Supplementary Table 1). GO term analysis (DAVID
45 6.8) of enriched DEGs identified innate immunity (Toll-like receptor (TLR) signaling
46 pathway), inflammation (cytokine-cytokine receptor interaction), lipid metabolism,
47 extracellular matrix remodeling (collagen trimer) and phospholipase inhibitor activity
48 as enriched processes (Fig. 1C; Supplementary Table 1). These processes have been
49 associated with pro-regenerative microglia emerging after spinal cord injury in mice ⁵¹.
50 Interestingly, the comparison between microglial cells isolated from intact and injured

1 telencephali at 7 dpi revealed only a limited number of DEGs without any GO term
2 enrichment (Extended Data Fig. 1E), in line with the transient activation and timely
3 transition of microglia to the homeostatic state observed in our previous
4 immunohistochemical analysis (Fig. 1A).

5 To further gain insights into the transient microglial activation and its importance
6 in scarless tissue restoration, we isolated cells belonging to microglial cluster 17,
7 performed unsupervised subclustering and identified six distinct states with specific
8 transcriptional signatures (Fig. 1D, E; Supplementary Table 2). RNA velocity-based
9 analysis of cellular dynamics^{53,54} revealed three parallel, non-overlapping trajectories
10 (Wt-MG4 \Rightarrow Wt-MG1 \Rightarrow Wt-MG2; Wt-MG3 \Rightarrow Wt-MG2; Wt-MG5 \Rightarrow Wt-MG0 \Rightarrow Wt-
11 MG2) (Fig. 1F). Numerous pro-inflammatory programs associated with immune cell
12 activation, including tumor necrosis factor (TNF), TLR, NOD-like receptor and IL1-
13 dependent signaling pathways, were detected with different patterns in distinct
14 subclusters (Supplementary Table 2). The IL1-dependent signaling pathway was
15 enriched in Wt-MG3, whereas the TNF- and TLR-dependent signaling pathways were
16 enriched exclusively in Wt-MG0. Interestingly, the TNF-, TLR- and NOD-signaling
17 pathways were downregulated in Wt-MG4 (Supplementary Table 2), thus suggesting
18 that microglial cells belonging to this trajectory might have anti-inflammatory
19 properties. These observations are consistent with distinct activated microglia
20 emerging after injury in the adult zebrafish telencephalon and suggest that specific
21 regulatory mechanisms may be involved in their return to a homeostatic state.

22 Interestingly, all three trajectories converged on the Wt-MG2 state, the most abundant
23 state in the intact brain (Fig. 1E, F). Functional analysis of genes enriched in Wt-MG2
24 microglia revealed over-representation of glycolysis, vacuolar acidification and
25 lysosome composition, and under-representation of pro-inflammatory cytokines
26 (Supplementary Table 2), findings indicative of *in vivo* homeostatic microglia involved
27 in tissue surveillance⁵⁵⁻⁵⁸. Therefore, we further analyzed injury-induced microglial
28 states transitioning back to Wt-MG2 (homeostatic microglia) to reveal the mechanisms
29 promoting the inactivation of microglial cells in the zebrafish CNS at 3 dpi. We
30 particularly focused on the Wt-MG0 state, because it displayed a significant increase
31 in proportion at 3 dpi, coinciding with the peak of microglial accumulation at injury sites,
32 followed by a significant decrease and return to normal levels at 7 dpi, thus faithfully
33 reproducing the dynamics of 4C4⁺ microglial cells at injury sites observed by
34 immunohistochemistry (Fig. 1A, E). Wt-MG0 cells displayed enriched expression of
35 genes identified in pro-regenerative microglia induced after spinal cord injury in
36 neonatal mice⁵¹, including *ctsba*, *anxa1*, *anxa2* and *anxa5* (Fig. 1G). Moreover, the
37 Wt-MG0 state was characterized by high expression of *granulin a* (*grna*) (Fig. 1H),
38 encoding a secreted factor that regulates inflammation, promotes wound healing and
39 modulates the formation of lipid droplets, first-line intracellular defenses that activate
40 innate immunity and sequester cytotoxic compounds detrimental to other cells
41^{46,59,68,60-67}. Indeed, Wt-MG0 cells were also enriched in genes associated with lipid
42 droplet-accumulating microglia (Fig. 1I, Extended Data Fig. 1F). On the basis of these
43 results, we propose that Wt-MG0 cells are the population of microglial cells that
44 accumulate at injury sites and activate specific programs promoting regeneration.
45 When regeneration is terminated, activated Wt-MG0 cells require the initiation of anti-
46 inflammatory programs, including granulins (Grns), to transition back to the
47 homeostatic Wt-MG2 state. In line with this hypothesis, we detected significant
48 upregulation of different members of the granulin family (*grna*, *grnb* and *grn1-2*) at 3
49 dpi and their return to basal levels at 7 dpi (Fig. 1J, Extended Data Fig. 1G).

1 Granulins are necessary and sufficient to limit prolonged microglial activation 2 at injury sites

3
4 To address the hypothesis that granulins are required for the transition from a pro-
5 inflammatory to a homeostatic microglial state, we assessed the microglial reactivity
6 to stab wound injury in granulin-deficient zebrafish^{69,70}. Because Wt-MG0 microglia
7 express both *grna* and *grnb* (gene duplication of mammalian progranulin (PGRN)), we
8 used a composite mutant (Grn-deficient) to avoid possible compensatory
9 mechanisms. As expected, 4C4⁺ microglial cells accumulated at injury sites in Wt
10 animals at 3 dpi and we did not detect any 4C4⁺ microglial cell accumulation at the
11 injury site at 7 dpi (Fig. 2A). Interestingly, Grn-deficient microglia accumulated at injury
12 sites in a manner indistinguishable from that of Wt microglia at 3 dpi, thus supporting
13 that the injury-induced activation of microglial cells is Grn independent (Fig. 2A).
14 However, Grn-deficient microglial cell accumulation, in contrast to that of Wt cells, was
15 still detected at injury sites at 7 dpi (Fig. 2A). Because scRNA-seq analysis revealed
16 numerous genes associated with high lipid droplet content in Wt-MG0 microglia (Fig.
17 1I), thus indicating their activated state⁴⁶, we assessed the lipid droplet formation in
18 Wt and Grn-deficient brains in response to injury by using an antibody against the lipid
19 droplet surface protein perilipin 3 (Plin3) (Fig. 2A-C, Extended Data Fig. 2A, B) or
20 BODIPY (Extended Data Fig. 2C). Plin3⁺ lipid droplets were nearly absent from both
21 Wt and Grn-deficient intact brains (Fig. 2A). Plin3⁺ lipid droplets were detected after
22 injury, almost exclusively in the 4C4⁺ microglial cells accumulating at injury sites at 3
23 dpi in both Wt and Grn-deficient animals (Fig. 2A-C, Extended Data Fig. 2B). In line
24 with their prolonged retention at injury sites, Grn-deficient 4C4⁺ microglia maintained
25 elevated numbers of Plin3⁺ and BODIPY⁺ lipid droplets at 7 dpi, whereas lipid droplets
26 were completely cleared in Wt animals (Fig. 2A-C, Extended Data Fig. 2C). To further
27 substantiate these observations, we isolated microglial cells identified by scRNA-seq
28 from Wt (Fig. 1B, D) and Grn-deficient telencephali (Extended Data Fig. 4A-D), and
29 analyzed the expression of genes enriched in lipid droplet-accumulating microglia⁴⁶.
30 The expression of these genes was comparable in microglia isolated from the intact
31 brains of both genotypes (Fig. 2D). Similarly, this set of genes was comparably
32 induced in Wt and Grn-deficient microglia at 3 dpi. However, whereas the expression
33 of most lipid droplet-related genes returned to normal levels in Wt microglia at 7 dpi, it
34 persisted at high levels in Grn-deficient microglia (Fig. 2D), in agreement with the
35 immunohistochemistry results for Plin3⁺ and BODIPY⁺ lipid droplets in the injured
36 brains of Wt and Grn-deficient animals (Fig. 2A, Extended Data Fig. 2C). Quantitative
37 lipid content analysis of intact and injured (7 dpi) Wt and Grn-deficient telencephali
38 revealed an increase in the relative abundance of triacylglycerols (TAGs) and
39 diacylglycerols (DAGs), major components of lipid droplets, in the injured brains of
40 Grn-deficient animals compared with Wt brains at 7 dpi (Fig. 2E, Extended Data Fig.
41 2D). These results were similar to the changes reported in lipidomic analysis of
42 progranulin (PGRN)-deficient mouse brains⁷¹.

43 To verify the direct roles of granulins in regulating lipid droplet clearance and
44 transition to a homeostatic state of microglial cells at injury sites, we injected
45 recombinant progranulin (PGRN) while performing injury in Grn-deficient animals (Fig.
46 2F). Intraparenchymal injection of recombinant PGRN was sufficient to resolve the
47 microglial cell accumulation at injury sites and to promote the clearance of lipid
48 droplets in Grn-deficient microglia at 7 dpi (Fig. 2G-I), with similar kinetics to that in Wt
49 animals.

1 Collectively, our data support the roles of granulins in clearing injury-induced
2 lipid droplets in microglial cells and promoting their transition back to a homeostatic
3 state.

4 5 **Granulin deficiency-induced neuroinflammation prolongs glial reactivity at** 6 **injury sites and impairs restorative neurogenesis**

7
8 The interaction of immune cells with resident parenchymal glia is the key determinant
9 of scar formation in the mammalian brain after stroke or traumatic brain injury ². The
10 prolonged accumulation of 4C4⁺ microglial cells at injury sites and the excessive lipid
11 droplet formation in Grn-deficient animals prompted us to investigate whether this
12 prolonged neuroinflammation changed glial reactivity in response to injury, possibly
13 through causing the scarless regeneration in zebrafish to transition to a scarring model
14 typical of the mammalian CNS. To examine the reaction of parenchymal cells
15 belonging to the oligodendrocyte lineage, we used the pan-oligodendrocyte marker
16 Sox10 ⁷² and followed the reaction of Sox10⁺ cells to injury in Wt and Grn-deficient
17 animals (Fig. 3A, B, Extended Data Fig. 3A-C; Supplementary Videos 1-3). Wt Sox10⁺
18 oligodendroglial cells responded to the injury with similar kinetics to that in 4C4⁺
19 microglial cells (Fig. 1A, 3A). Despite the transient accumulation of Sox10⁺ cells at
20 injury sites at 3 dpi, we observed no glial cell accumulation at 7 or 21 dpi in Wt brains
21 (Fig. 3A, B; Supplementary Video 1). Grn-deficient Sox10⁺ oligodendroglial cells
22 accumulated similarly to Wt cells at injury sites at 3 dpi, thus further supporting a Grn-
23 independent initial glial response to injury (Fig. 3A, B). However, Sox10⁺ cell
24 accumulation still occurred at injury sites in Grn-deficient animals, in contrast to Wt
25 animals, at 7 dpi and 31 dpi (Fig. 3A, B; Supplementary Videos 2, 3). The phenotype
26 observed in the Grn-deficient CNS resembled the neuroinflammation-driven prolonged
27 reactivity of glial cells observed in the mammalian brain in response to injury. These
28 data support the hypothesis that a failure to promote the transition of microglial cells
29 back to the homeostatic state accounts for the prolonged glial cell reactivity at injury
30 sites. To further test this hypothesis, we prevented the exacerbated inflammatory
31 response and long-lasting inflammation in Grn-deficient animals through treatment
32 with dexamethasone, an anti-inflammatory drug known to block microglial activation
33 in the adult zebrafish telencephalon after injury ³⁰. We pretreated Grn-deficient animals
34 for 10 days with either dexamethasone or methanol (MeOH, as solvent control),
35 injured them, and analyzed 4C4 and Sox10 immunoreactivity at 3 dpi and 7 dpi (Fig.
36 3C-E, Extended Data Fig. 3D-F). Importantly, MeOH treatment did not alter the
37 reactivity of glial cells (microglia and oligodendroglia), because we observed
38 prolonged accumulation of glial cells at injury sites in MeOH-treated Grn-deficient
39 animals at 7 dpi (Fig. 3D, E). Strikingly, dexamethasone treatment rescued the
40 prolonged accumulation of 4C4⁺ microglial and Sox10⁺ oligodendroglial cells at injury
41 sites in Grn-deficient animals (Fig. 3D, E). Cell densities of 4C4⁺ microglia and Sox10⁺
42 oligodendroglia at injury sites in dexamethasone-treated Grn-deficient animals were
43 comparable to those detected in Wt animals at 7 dpi (Fig. 3B, E). Together, these
44 results demonstrate that prolonged activation of microglia, caused by Grn-deficiency,
45 is sufficient to prevent the resolution of the glial cell accumulation at injury sites, thus
46 transforming the scarless regeneration in the zebrafish CNS into a scarring model.

47 Because glial scarring in the mammalian CNS hinders functional regeneration
48 ^{2,73}, we set out to address whether prolonged accumulation of glial cells (microglia and
49 oligodendroglia) at injury sites might impair the injury-induced generation and/or the
50 survival of new neurons, a key feature in regeneration in the adult zebrafish CNS ⁴³.

1 We kept Wt and Grn-deficient injured animals for 3 days in 5-bromo-2'-deoxyuridine
2 (BrdU) water to label the injury-activated stem cell population and the newly formed
3 neurons migrating to the brain parenchyma generated by the injury-activated stem cell
4 population (Fig. 3F, G). On the basis of the immunoreactivity of neural HUC and HUD
5 proteins (HuC/D), we observed significantly fewer newly formed BrdU⁺/HuC/D⁺
6 neurons in Grn-deficient animals than in Wt animals at 31 dpi (Fig. 3H, I). Together,
7 these results demonstrate that the prolonged neuroinflammation and glial cell
8 accumulation in Grn-deficient animals generate an environment not permissive to
9 restorative neurogenesis in the zebrafish brain, similarly to the observed reaction to
10 injury in the mammalian brain.

11 12 **Activated microglia fail to transition back to the homeostatic state in the Grn-** 13 **deficient injured CNS**

14
15 On the basis of previous results, we reasoned that excessive neuroinflammation
16 leading to prolonged glial cell accumulation at injury sites and impaired regeneration
17 might be caused by specific microglial states present in the Grn-deficient brain. To
18 address this question, we isolated and re-clustered all microglial cells identified by
19 scRNA-seq from Wt and Grn-deficient telencephali (Fig. 4A, Extended Data Fig. 4D,
20 E). We identified eight subclusters representing distinct microglial states (Fig. 4A),
21 which we were able to directly relate to those identified in Wt brains through cluster
22 similarity matrix analysis (Extended Data Fig. 4F, G). Importantly, six of these clusters
23 were previously identified in Wt brains, whereas two clusters appeared only after the
24 analysis that included Grn-deficient microglia (Fig. 4A, B, Extended Data Fig. 4D-F).
25 The identified states contained different numbers of cells derived from Wt and Grn-
26 deficient brains (Fig. 4B, Extended Data Fig. 4E). The MG4 state, corresponding to
27 the pro-regenerative Wt-MG0 state, and the MG3 state, corresponding to the
28 homeostatic Wt-MG2 state (Fig. 4A, Extended Data Fig. 4F, G), were largely under-
29 represented in Grn-deficient brains at both 3 dpi and 7 dpi (Fig. 4B, Extended Data
30 Fig. 4E). We identified activated microglia of both genotypes within the MG1 state,
31 which had a high similarity score with respect to the Wt-MG4 cluster (Fig. 1D, 4A, B,
32 Extended Data Fig. 4D-G). As expected, in the velocity analysis, activated Wt
33 microglial cells from the MG4 and MG1 clusters projected toward the MG3 cluster,
34 which was mainly composed of homeostatic microglia at 7 dpi (Fig. 4B, C, Extended
35 Data Fig. 4E-G). In contrast, Grn-deficient activated microglia projected towards
36 clusters MG5 and MG0, which contained almost exclusively Grn-deficient cells (Fig.
37 4B, C, Extended Data Fig. 4E). Interestingly, the MG0 and MG5 microglial states
38 displayed enrichment in numerous genes associated with innate immunity, lysosomes,
39 phagosomes and apoptosis (Supplementary Table 3), thus contributing to the
40 activated signature detected at 7 dpi in Grn-deficient microglial cells, as compared with
41 the homeostatic signature of Wt microglial cells at the same time point (Fig. 4D, E;
42 Supplementary Table 3). Additionally, microglia from the MG0 and MG5 clusters were
43 enriched in numerous genes associated with lipid droplet formation, and cellular and
44 mechanical stress, including several members of the Hsp70 family (Fig. 4F, G). Our
45 findings thus support that Grn-deficient microglia fail to transition back to homeostasis
46 and remain activated at 7 dpi.

47 Together, these results suggest that dysregulated injury-induced cellular stress
48 in Grn-deficient brains promotes long-lasting pro-inflammatory microglial cell
49 accumulation at injury sites. Grn-deficient pro-inflammatory microglia do not fully

1 transition back to homeostasis and induce long-lasting glial cell accumulation, thus
2 causing detrimental consequences in neuronal regeneration.

3 4 **Clearance of extranuclear TDP-43 condensates formed through LLPS is** 5 **required for termination of microglia-driven neuroinflammation**

6
7 Analysis of microglial populations revealed that MG0 and MG5 microglial cells in Grn-
8 deficient brains displayed dysregulated lipid metabolism, were unable to dissolve lipid
9 droplets and underwent cellular stress. Therefore, we aimed at identifying signals
10 leading to lipid droplet formation and cellular stress after brain injury. The RNA-binding
11 protein TAR DNA binding protein of 43 kDa (TDP-43) is a pathological marker protein
12 associated with neurodegeneration and brain injury⁷⁴⁻⁷⁷. In several
13 neurodegenerative diseases, including amyotrophic lateral sclerosis (ALS) and
14 frontotemporal dementia (FTD), and after traumatic brain injury, TDP-43 relocates
15 from the nucleus to the cytoplasm, forms cytoplasmic condensates or aggregates
16 through LLPS, and colocalizes with stress granules (SGs). Granulins have been
17 demonstrated to alter the solubility of TDP-43, modulating its LLPS and aggregation
18 behavior⁷⁸⁻⁸⁰. Therefore, we analyzed TDP-43 immunoreactivity in response to injury
19 in Wt and Grn-deficient brains (Fig. 5A, Extended Data Fig. 5A, B). In intact brains, we
20 observed TDP-43 signal exclusively in cell nuclei, mostly in HuC/D⁺ neuronal cells
21 (Extended Data Fig. 5A). Interestingly, the nuclear TDP-43 signal was complemented
22 by extranuclear TDP-43⁺ condensates in both Wt and Grn-deficient brains at injury
23 sites at 3 dpi (Fig. 5A, B, Extended Data Fig. 5B). Importantly, a proportion of TDP-
24 43⁺ condensates colocalized with 4C4⁺ microglia (Extended Data Fig. 5B).
25 Unexpectedly, whereas extranuclear TDP-43⁺ condensates were cleared at 7 dpi in
26 Wt animals, they were detected at injury sites in Grn-deficient animals at the same
27 time point (Fig. 5A, B), in a manner following Plin3⁺ lipid droplet kinetics (Fig. 2A, B).
28 Therefore, we hypothesized that Wt microglia upregulate granulins to clear potentially
29 cytotoxic TDP-43 condensates. Indeed, intraparenchymal injection of recombinant
30 PGRN in Grn-deficient brains was sufficient to clear extranuclear TDP-43⁺
31 condensates at 7 dpi (Extended Data Fig. 5C-E).

32 Because granulins regulate the LLPS behavior of TDP-43⁸⁰, we hypothesized that the
33 balance between granulins and LLPS-driven TDP-43⁺ condensates might define the
34 activation state of microglial cells in response to injury. In the absence of granulins,
35 TDP-43 was expected to form long-lasting condensates via LLPS, thus causing
36 cellular stress, and prolonged microglial activation and accumulation at injury sites. To
37 test this hypothesis, we made use of the finding that TDP-43 fused to maltose binding
38 protein (MBP) via a TEV proteolytic site does not undergo LLPS (Extended Data Fig.
39 6B, C). The proteolytic removal of MBP is sufficient to induce LLPS of TDP-43⁸¹⁻⁸⁴.
40 We injected TDP-43 (containing the maltose binding protein (MBP) tag preventing
41 LLPS) and phase-separated TDP-43 (MBP tag cleaved off) proteins while performing
42 injury in Wt brains (Fig. 5C-E, Extended Data Fig. 6A-D), aiming to oversaturate the
43 system with phase-separated TDP-43 and bypass available granulins. Injection of
44 both versions of TDP-43 prolonged microglial accumulation at injury sites at 7 dpi in
45 Wt animals, although a stronger reaction was observed when we injected phase-
46 separated TDP-43 (Fig. 5E, Extended Data Fig. 6D). In line with our hypothesis, only
47 the injection of phase-separated TDP-43 induced excessive formation of Plin3⁺ lipid
48 droplets and extranuclear TDP-43⁺ condensates, which colocalized primarily with 4C4⁺
49 microglial cells at injury sites (Fig. 5E-G, Extended Data Fig. 6D, E), thus mimicking
50 the phenotype of the reaction observed in Grn-deficient brains in response to injury.

1 Because we detected numerous cytosolic TDP-43 condensates in 4C4⁺ cells after
2 injection of phase-separated TDP-43 in Wt animals, and we did not observe any
3 upregulation of TDP-43 mRNA in microglial cells during the course of regeneration
4 (Extended Data Fig. 6F), we speculate that microglial cells accumulate at injury sites,
5 phagocytose TDP-43 released by dying neurons and do not dissolve LLPS-driven
6 TDP-43⁺ condensates when the amount of phase-separated TDP-43 is in excess or
7 when granulin levels are low.

8 To determine whether the phenotype detected in Grn-deficient animals was
9 specifically associated with the dysregulation of LLPS of TDP-43, we injected the
10 neurodegeneration-linked RNA-binding protein Fused in Sarcoma (FUS) or phase-
11 separated FUS while performing injury in Wt brains (Extended Data Fig. 6A, G, H). In
12 contrast to TDP-43, injections of FUS and phase-separated FUS promoted only mild
13 reactivity of microglial cells at injury sites and did not affect the number of Plin3⁺ lipid
14 droplets in Wt microglia at 7 dpi (Extended Data Fig. 6H-J). Therefore, we propose
15 that the phenotype observed in Grn-deficient animals is not caused by general
16 dysregulation of LLPS but instead may be caused by dysregulation of LLPS of specific
17 proteins, including TDP-43, thus leading to an excess of cytotoxic extranuclear TDP-
18 43⁺ condensates.

19 20 **Prevention of excessive LLPS-mediated formation of SGs is sufficient to** 21 **terminate prolonged neuroinflammation in Grn-deficient animals**

22
23 We hypothesized that Grn-controlled LLPS of TDP-43 must be tightly regulated to
24 successfully clear the TDP-43⁺ condensates formed in response to brain injury in
25 microglial cells and enable their return to the homeostatic state. To directly test this
26 hypothesis, we interfered with the formation of SGs, phase-separated cytosolic
27 condensates, in injured Grn-deficient brains through the administration of lipoamide
28 (Fig. 6A, B), a newly identified agent that decreases SG formation⁸⁵. We kept Grn-
29 deficient animals in either DMSO- or lipoamide-containing water for 7 days after injury
30 and assessed the formation of TDP-43⁺ condensates and the accumulation of 4C4⁺
31 microglial cells and Plin3⁺ lipid droplets at injury sites at that time point (Fig. 6C, D).
32 As expected, injured Grn-deficient animals kept in the DMSO-containing water
33 displayed prolonged accumulation of extranuclear TDP-43⁺ condensates and lipid
34 droplet-accumulating 4C4⁺ microglial cells at injury sites at 7 dpi (Fig. 6B-D). In
35 contrast, treatment of Grn-deficient animals with lipoamide resolved the accumulation
36 of lipid droplet-accumulating 4C4⁺ microglial cells at injury sites (Fig. 6B-D). Moreover,
37 we did not observe extranuclear TDP-43⁺ condensates at injury sites in lipoamide-
38 treated Grn-deficient animals (Fig. 6B-D), thus suggesting that lipoamide treatment
39 rescues the phenotype generated by Grn deficiency and promotes the return of
40 microglial cells to the homeostatic state. To verify this, we compared the reaction of
41 Grn-deficient microglia to injury after lipoamide treatment (*LipoGrn*-deficient cells) to
42 the reaction of microglia isolated from untreated Wt and Grn-deficient animals at 7 dpi
43 by using scRNA-seq analysis (Fig. 6E). *LipoGrn*-deficient microglia were identified
44 within the cluster of activated microglia (MG1 and MG5), and, in a lower proportion,
45 within the cluster composed of homeostatic microglia (MG3) (Fig. 6F, G). Interestingly,
46 lipoamide treatment significantly decreased the number of Grn-deficient microglia
47 within the pro-inflammatory MG0 cluster, which contained almost exclusively Grn-
48 deficient cells that did not fully transition back to the homeostatic state (Fig. 6F, G,
49 Extended Data Fig. 4E). Moreover, the relative number of *LipoGrn*-deficient microglial
50 cells returned to normal after lipoamide treatment at 7 dpi and was comparable to the

1 microglial abundance detected in Wt brains at the same time point. In line with this
2 analysis, *LipoGrn*-deficient microglia did not show upregulation of the inflammatory
3 pathways enriched in *Grn*-deficient microglia (Fig. 4D; Supplementary Table 3), as
4 compared with Wt microglia at 7 dpi. However, we detected 1349 significantly
5 downregulated genes in *LipoGrn*-deficient microglia compared with untreated *Grn*-
6 deficient microglia at the same time point. This regulated gene set was enriched in GO
7 processes associated with microglial functions, microglial activation and lipid
8 metabolism (Fig. 6H). Lastly, we observed lower expression of numerous genes
9 associated with lipid droplet-accumulating microglia (Fig. 6I) and cellular-stress (Fig.
10 6J) in *LipoGrn*-deficient microglia than in untreated *Grn*-deficient microglia at 7 dpi,
11 thus suggesting that the *LipoGrn*-deficient microglial cell reactivity and transcriptome
12 are more similar to those of Wt microglia.

13 Collectively, these results demonstrate that in Wt microglia, LLPS-mediated
14 TDP-43⁺ condensates form only transiently and are cleared in a timely manner, thus
15 leading to scarless regeneration in the zebrafish brain. Granulin deficiency impairs the
16 ability of microglia to clear the LLPS-mediated extranuclear TDP-43⁺ condensates
17 accumulating in SGs, thus leading to a cascade that locks microglial cells in their pro-
18 inflammatory state and prevents them from transitioning back to homeostasis.

19

20 **Stroke induces lipid droplet and SG formation in the human brain**

21

22 The gene signature conservation previously reported between zebrafish pro-
23 regenerative, lipid droplet-forming microglia and pro-regenerative microglia detected
24 in response to spinal cord injury in neonatal mice (Fig. 1G)⁵¹ prompted us to assess
25 whether CNS damage might induce similar formation of lipid droplets, TDP-43⁺
26 condensates and SGs in the human brain. Therefore, we assessed the reactivity of
27 IBA1⁺ microglial cells, PLIN3⁺ lipid droplets, TDP-43⁺ and G3BP⁺ SGs in post-mortem
28 brain tissues obtained from patients several weeks after ischemic stroke (Fig. 7A, B).
29 Notably, we detected neuroinflammation in the penumbra, as characterized by the
30 high expression of the microglial marker IBA1 (Fig. 7B). High IBA1 immunoreactivity
31 of microglial cells located in the penumbra was accompanied by morphological
32 changes indicative of their activated state (Fig. 7A, B). Importantly, the penumbra
33 containing highly activated microglia was also enriched in TDP-43⁺, PLIN3⁺ and
34 G3BP⁺ signals (Fig. 7B), in line with our data implicating their roles in maintaining long-
35 lasting neuroinflammation.

36

37 **Discussion**

38

39 Our data support a model of CNS regeneration wherein injury causes the release of
40 intracellular proteins able to undergo LLPS (including TDP-43) into the extracellular
41 space. These proteins are subsequently phagocytosed by pro-regenerative activated
42 microglia at injury sites. Granulins regulate the clearance of phagocytosed proteins
43 and condensates, which is necessary to allow activated microglia to transition back to
44 the homeostatic state. A failure to clear TDP-43⁺ condensates locks pro-regenerative
45 microglia in a pro-inflammatory, disease-associated state. Pro-inflammatory microglia
46 further enhance the transition of the remaining microglial cells to an activated state
47 (positive feedback loop) and prolong the accumulation of oligodendrocyte lineage cells
48 at injury sites, thus leading to long-term neuroinflammation and glial scar formation.
49 According to this model, microglial cells have several partially overlapping roles
50 defined by their activation state. In line with their known physiological roles in the intact

1 brain, microglia are dynamically activated by “ON” signals and inactivated by “OFF”
2 signals in an array of functions, such as phagocytosis of cellular debris, trophic support
3 of neurons, synaptic organization and the regulation of neuronal excitability^{15,61,86–88}.
4 The tight balance between activating “ON” and inactivating “OFF” signals, such as
5 cytokines and chemokines, ATP, PAMPs and TREM2^{23,25,27,89–91}, allows microglia to
6 perform their scavenging functions without generating chronic neuroinflammation. In
7 regeneration-competent species, such as zebrafish, CNS injuries induce the activation
8 of homeostatic microglial cells. However, immune cell activation is only transient and
9 is terminated in a timely manner, thereby enabling long-term integration and survival
10 of new neurons necessary for full tissue restoration and neuronal replacement at injury
11 sites^{30,43}. Interestingly, we identified different subpopulations of activated microglia
12 that returned to the homeostatic state through parallel, possibly independent,
13 trajectories, thus suggesting that distinct microglial cells may have different functions
14 in the injured CNS, and specific regulatory mechanisms may ensure the timely
15 termination of their activated state. Indeed, different activation states were also
16 characterized by the enrichment and downregulation of specific neuroinflammatory
17 programs. TNF-, TLR-, NOD- and IL1-dependent pro-inflammatory cascades are
18 major drivers of long-term neuroinflammation and scar formation in the mammalian
19 brain^{92,93}. Their separation and unique combinations in different microglial
20 subpopulations might possibly determine the overall activation state of single
21 microglial cells, thus facilitating their return to the homeostatic state after regeneration
22 is completed. The return of all activated microglial subpopulations to the homeostatic
23 state, however, involves a tight regulation of lysosomal functions and lytic vacuoles as
24 well as a return to glycolysis as a major energy supply source. These features have
25 recently been associated with the homeostatic scavenger function of microglia
26 detected in the mammalian brain^{56,94}. Because the trajectories describing microglial
27 dynamics do not overlap, these processes appear to be independently regulated along
28 each trajectory, in line with their specific roles in defining the activation state of
29 microglia. Interestingly, one population of transiently activated microglia in the
30 zebrafish telencephalon (Wt-MG0, mostly enriched at 3 dpi) expressed genes that
31 have recently been associated with pro-regenerative microglia emerging after spinal
32 cord injury in a neonatal mouse model⁵¹. These observations suggest the intriguing
33 possibility that both mammals and zebrafish may share several programs underlying
34 the transition of microglia to the activated state necessary for early beneficial effects
35^{10,45}. Furthermore, these results suggest that the regulatory mechanisms required for
36 the inactivation and the return of pro-regenerative microglia to the homeostatic state,
37 as observed in regeneration-competent species, were lost not during evolution but
38 during mammalian development and aging. Accordingly, long-term neuroinflammation
39 after CNS injury, aging and neurodegenerative diseases may be considered a
40 consequence of the aging-associated loss of “OFF” signals in microglial cells, whose
41 chronic activation hinders glial scar resolution and the functionality of neuronal circuits
42^{2,11,27,12–14,22–26}.

43 Interestingly, the subpopulation of Wt-MG0 pro-regenerative microglial cells, which
44 partially shares a signature with mammalian neonatal pro-regenerative microglia,
45 displayed elevated expression of genes associated with lipid droplet-accumulating
46 microglia⁴⁶, thus supporting the possibility that the timely inactivation of this specific
47 subpopulation is the key regulatory mechanism preventing chronic neuroinflammation.
48 Lipid droplets are among the first-line intracellular defenses that activate innate
49 immunity and sequester cytotoxic compounds detrimental to other cells^{46,68}. However,
50 the excessive production of lipid droplets in microglial cells during aging and

1 degenerative diseases, such as atherosclerosis, has been demonstrated to be
2 detrimental to cell functionality^{46,95}. Indeed, our findings that granulins regulate lipid
3 droplet resolution and microglial transition back to the homeostatic state, together with
4 previously demonstrated roles of granulins in the regulation of the inflammatory
5 response and microglial lipid metabolism^{46,59–61,63,65–67}, further support the importance
6 of the granulin-mediated return of Wt-MG0 microglial cells to homeostasis in limiting
7 long-lasting neuroinflammation. In fact, unbiased single-cell transcriptomic analysis
8 focusing on microglial subpopulations in Wt and Grn-deficient animals showed a
9 significant underrepresentation of homeostatic and pro-regenerative microglia in Grn-
10 deficient brains in response to injury. A large proportion of Grn-deficient microglial cells
11 are “locked” in an activated state after injury and do not fully transition back to the
12 homeostatic state. Because lipid droplets are composed of acyl-glycerols that are
13 synthesized by diacylglycerol transferases, converting DAGs to TAGs, which fill the
14 lipid droplet core⁹⁶, an increase in DAGs after injury in Grn-deficient animals suggests
15 an even more severe impairment of lipid metabolism than that in other
16 neuropathological states⁹⁶.

17 We showed that the prolonged neuroinflammation in Grn-deficient animals was
18 accompanied by prolonged accumulation of oligodendroglial cells at injury sites,
19 thereby mimicking the common features of the glial scar generated in response to
20 injury in the mammalian CNS^{2,11,97}. This data set further strengthens the key
21 regulatory role of the Wt-MG0 microglial state and underscores the need for deeper
22 understanding of Wt-MG0 microglial dynamics and regulation.

23 We propose that Grn-regulated LLPS of TDP-43 defines the activation state of
24 Wt-MG0 microglia. We showed that extranuclear TDP-43⁺ condensates (possibly
25 derived from TDP-43 released by dying neurons) were also present during the course
26 of normal regeneration in the adult zebrafish telencephalon. However, in the absence
27 of granulins, extranuclear TDP-43⁺ condensates persisted at injury sites along with
28 activated lipid droplet-accumulating microglia. This cascade of detrimental events was
29 prevented by inhibition of LLPS-mediated SG formation through administration of
30 lipoamide⁸⁵ or exogenous PGRN. Indeed, inflammation has recently been associated
31 with SG-mediated cellular stress⁹⁸, a process that may contribute to long-term
32 neuroinflammation and the persistence of glial scars. In line with that possibility,
33 traumatic brain injury has been reported to induce SG formation^{67,76,77}. In a survival
34 mechanism, after stress, cells inhibit global protein translation by sequestering RNA-
35 protein complexes involved in the pre-initiation of protein synthesis into SGs^{99,100}. SGs
36 are dynamic membrane-less cytoplasmic condensates that form through a process of
37 LLPS, a reversible unmixing of molecules into two separate phases, a dilute and
38 condensed phase, that are in constant exchange with each other^{101,102}. LLPS is
39 important in a variety of cellular functions, such as metabolism, transcriptional and
40 translational regulation, signal transduction and cellular motility^{101,103}. Moreover, LLPS
41 has been suggested to be involved in the development of various neurodegenerative
42 diseases, including ALS and FTD¹⁰⁴. ALS-causing mutations in RNA-binding proteins
43 have been shown to alter LLPS *in vitro* and to result in the localization of RNA-binding
44 proteins, including TDP-43, to SGs^{105–113}. Furthermore, cells exposed to chronic
45 stress form SGs and persistent TDP-43 condensates, thus suggesting that chronic
46 stress and SG localization leads to disease-like aggregation of TDP-43^{113–116}. Finally,
47 TDP-43 solubility, aggregation and LLPS properties, as well as its levels and toxicity,
48 have been shown to be influenced by granulins^{78–80}. Together, these results support
49 our model of development of chronic neuroinflammation. However, how LLPS-
50 mediated TDP-43⁺ condensate formation in activated microglia regulates and

1 coordinates glial reactivity during scar formation remains unclear. A growing body of
2 evidence suggests that lipid droplet composition changes depending on the
3 physiological state of the cell and that lipid droplets could serve as signaling mediators
4 in cellular communication ¹¹⁷, including non-cell autonomous glial scar cellular
5 interactions. In addition, SG-related proteins have been associated with the regulation
6 of translation and cell motility via mTORC signaling ¹¹⁸. Finally, SG proteins are
7 associated with microtubules and centrosomes, crucial structures for cellular migration
8 ^{119,120}. Therefore, SG-mediated alterations in microglial cell motility may account for
9 the persistence of these cells at injury sites and the induction of chronic
10 neuroinflammation.

11 Overall, our model provides new insights into basic regulatory mechanisms that
12 may prevent long-term neuroinflammation and promote CNS regeneration. Our new
13 findings on the crosstalk between granulins and the LLPS of TDP-43 could potentially
14 be targeted to develop new approaches to improve CNS regeneration in response to
15 traumatic brain injury and neurodegenerative diseases in mammalian species,
16 including humans.

17 **Methods**

18 **Human post-mortem brain tissues**

19
20
21
22 Brain tissue was collected several weeks after infarction of the right arteria cerebri
23 media with hemiparesis. Tissue was fixed in 4% PFA and embedded in paraffin.
24 Sample collection was performed according to the legal guidelines of Government of
25 Upper Bavaria (BayKrG Art. 27 Abs. 4).

26 **Zebrafish lines**

27
28
29 *Zebrafish from the $grna^{+/+};grnb^{+/+}$, $grna^{-/-};grnb^{-/-}$ and AB/EK strains and from the*
30 *transgenic strains Tg(olig2:DsRed), Tg(mpeg1:mCherry),*
31 *Tg(olig2:DsRed; $grna^{-/-};grnb^{-/-}$) and Tg(mpeg1:mCherry; $grna^{-/-};grnb^{-/-}$) were used in*
32 *all experiments. All experiments were performed in 3-5-month-old animals, as in this*
33 *range we do not observe any age-associated differences. Wildtype and Granulin-*
34 *deficient intact, injured and treated animals were sex-mixed littermates in individual*
35 *experiments. 4-5 independent biological replicates were used in every experiment (the*
36 *exact number of analyzed animals is specified in each dot plot) and analysis was*
37 *performed blindly. All animals were kept under standard husbandry conditions and*
38 *experiments were performed according to the handling guidelines and regulations of*
39 *EU and the Government of Upper Bavaria (AZ 55.2-1-54-2532-0916).*
40

41 **Treatment with dexamethasone**

42
43 3-5-month-old, mixed-sex zebrafish from specific genotypes were immersed for 10
44 days in dexamethasone-containing (15 mg/L) or MeOH-containing (0.0001%) aerated
45 water. Animals were immersed in dexamethasone- or MeOH-containing water for the
46 whole duration of the experiment until sacrifice (time point indicated in the
47 experimental paradigm). Water was changed daily and animals were fed every second
48 day, 4 hours prior the water change.

1 Treatment with lipoamide

2
3 3-5-month-old, mixed-sex zebrafish from specific genotypes were immersed for the
4 whole duration of the experiment in lipoamide-containing (20 μ M) or DMSO-containing
5 aerated water until sacrifice (time point indicated in the experimental paradigm). Water
6 was changed daily and animals were fed 4 hours prior the water change.

7 8 Genotype identification

9
10 Genotyping was performed by cutting a small part of the zebrafish tail fin. REDExtract-
11 N-Amp Tissue Kit (Sigma-Aldrich) was used to extract genomic DNA according to
12 manufacturer's instructions. Isolated genomic DNA was amplified by PCR and Sanger
13 sequencing was performed to compare the nucleotide sequences and identify the
14 selected mutations for *grna* and *grnb*. Mutations selected are the following: mde54a
15 and mde360 for *grna* and *grnb* respectively, as indicated in ZFIN database
16 (<https://zfin.org/action/publication/ZDB-PUB-200208-2/feature-list>).

17 18 Stab wound injury

19
20 Stab wound injury from zebrafish nostrils was performed in both telencephalic
21 hemispheres according to previous publication²⁹. 100 x 0.9 mm glass capillary needle
22 (KG01, A. Hartenstein) was used. The needle was pulled on a Narishige Puller (model
23 PC-10) with "one-stage" pull setting at 63.5°C. The needle used to perform the stab
24 wound injury resulted in 5 mm length and 0.1 mm diameter.

25 26 Tissue preparation and immunohistochemistry

27
28 Animals were sacrificed by MS222 overdose of tricaine methane sulfonate (MS222,
29 0,2%) by prolonged immersion. Tissue processing was performed as described
30 previously²⁹. Immunodetection of BrdU required a pretreatment with 4 N HCl followed
31 by washes with borate buffer and PBS before placing sections in anti-BrdU antibody.

32 33 BrdU labeling experiment

34
35 To assess the number of newly formed neurons in response to injury (restorative
36 neurogenesis), zebrafish from specific genotypes were immersed, immediately after
37 stab wound injury, in BrdU-containing aerated water (10 mM) for 16 h/day during 3
38 consecutive days. During the 8 hours outside BrdU-containing water, fish were kept in
39 fresh water and fed. Animals were sacrificed 28 days after BrdU treatment (3 days
40 BrdU water + 28 days chase) to allow the incorporation of BrdU in activated stem cells
41 that would generate neurons in response to injury and the migration of newly formed
42 BrdU⁺ neurons at injury sites in the brain parenchyma.

43 44 Lipidomic analysis

45
46 Single telencephali were isolated and completely dissolved with mechanical
47 homogenization procedures in D-PBS without Mg, Ca to reach the final concentration
48 of 4-5 mg/mL (tissue wet weight per volume). Mass spectrometry-based analysis was
49 performed by Lipotype GmbH.

50

1 **Injection of recombinant Progranulin (mPGRN)**

2
3 Intraparenchymal injection of recombinant mPGRN was performed while we executed
4 stab wound injury. 5 μ L of recombinant mPGRN (dilution of 1:250 from stock solution
5 of 250 ng/ μ L, reconstituted in sterile PBS) were injected in both hemispheres of the
6 zebrafish telencephalon.

7 8 **Protein expression**

9
10 TDP-43-MBP-His6 was purified according to ⁸¹ with slight adaptations. Expression
11 was performed in E. coli BL21-DE3 Rosetta 2 using 0.5 mM IPTG overnight at 16°C.
12 Cells were lysed in purification buffer (20 mM Tris pH 8, 1 M NaCl, 10 mM imidazole,
13 10 % (v/v) glycerol, 4 mM β -mercaptoethanol and 1 μ g/ml each of aprotinin, leupeptin
14 hemisulfate and pepstatin A) supplemented with 0.1 mg/ml RNase A using lysozyme
15 and sonication. Afterwards, the protein was purified by Ni-NTA agarose (Qiagen) and
16 eluted using 300 mM imidazole. Finally, eluates were further purified using size
17 exclusion chromatography (Hiload 16/600 Superdex 200 pg, GE Healthcare) in
18 storage buffer (20 mM Tris pH 8, 300 mM NaCl, 10% (v/v) glycerol supplemented with
19 2 mM TCEP) in order to obtain monomeric TDP-43-MBP-His₆.

20 For MBP-FUS-His6 ¹²¹, protein expression was induced in E. coli Rosetta-LysS after
21 cold shock using 100 nM IPTG overnight at 12°C. Protein was purified as described
22 above for TDP-43-MBP. SEC eluates were additionally purified using amylose HS
23 (NEB) in amylose binding buffer (20 mM Tris pH6, 150 mM NaCl, 5% (v/v) glycerol
24 supplemented with 2 mM DTT and 1 μ g/ml each of aprotinin, leupeptin hemisulfate
25 and pepstatin A and eluted using 10 mM maltose in storage buffer.

26 Purified protein was concentrated using Amicon ultra centrifugal filters, flash frozen
27 and stored at -80°C. Protein concentration was determined by measuring absorbance
28 at 280 nm using the respective extinction coefficient (ϵ) predicted by the ProtParam
29 tool. A260/280 ratio of purified protein was between 0.5-0.7, showing deprivation of
30 nucleic acids.

31 Purified TDP-43-TEV-MBP-His6 was exchanged to Hepes buffer (20 mM Hepes, pH
32 7.5, 150 mM NaCl, 1 mM DTT). For visualization of condensates the reaction was
33 setup directly in a Uncoated μ -Slide 18 Well - Flat chambers (Cat.No: 81821, Ibidi),
34 where protein was diluted to a concentration of 5 μ M and phase separation was
35 induced by addition of 100 μ g/ml His6-TEV protease at RT. After ~20 min, imaging
36 was performed by bright field microscopy using a widefield microscope.

37 38 **Injection of TDP-43 and FUS proteins**

39
40 TDP-43-MBP and MBP-FUS proteins were independently incubated for 30 min at RT
41 with TEV and TEV buffer (Tris 20 mM pH 8.0, 300mM NaCl, 2mM dTT in H₂O) to
42 cleave the MBP tag. 5 μ L of uncleaved and cleaved TDP-43 (20 μ M) and FUS (20 μ M)
43 proteins were independently injected in both hemispheres of the zebrafish
44 telencephalon while performing the injury. 5 μ L of TEV+TEV buffer were also injected
45 in control animals to account for possible changes in reactivity due to the injection.

46 47 **Tissue dissociation**

48

1 Cells were isolated from zebrafish telencephali (n=4) and dissociated into single cell
2 suspension using the papain kit (Worthington) according to manufacturer's
3 instructions. Incubation in dissociating enzyme was performed for 30 min.

4 5 **Library preparation and sequencing**

6
7 Single cell suspensions were loaded into 10x Genomics Single Cell 3' Chips according
8 to manufacturer's instruction for Chromium Single Cell 3' Reagent Kits v3 (10x
9 Genomics) to generate single cell bead emulsion (GEMs). cDNA synthesis was
10 carried out according to 10x Genomics guidelines. Libraries were pooled and
11 sequenced on NovaSeq6000 (Illumina) with the recommended number of cycles (28-
12 8-91) according to Chromium Single Cell 3' Reagent Kits v3. Sequencing was
13 performed by the Core Sequencing Facility at the Helmholtz Zentrum München.

14 15 **Alignment and data analysis**

16
17 Transcriptome alignment of single cell data was performed using Cell Ranger 4.0.0
18 against the Danio rerio reference genome assembly GRCz11 (Ensembl Release 100).
19 Quality Control (QC) of mapped cells was performed adjusting the recommendations
20 from previous publication (gene counts ≥ 350 ; $40000 \leq$ reads per cell ≥ 800 ;
21 mitochondrial fraction ≤ 0.2)¹²². Batch-correction and integration of different scRNA-
22 seq datasets was performed using Scanorama¹²³. Unsupervised clustering of cells
23 was performed using the Louvain algorithm (<https://doi.org/10.5281/zenodo.595481>),
24 implemented in SCANPY with resolution parameter of 1 and 0.8 when the
25 unsupervised cell clustering was applied to all cells or to microglia-only cells,
26 respectively. Marker genes specific for each cluster were identified using t-test
27 between the counts of each gene in a cell cluster against all other clusters with the
28 function *rank_genes_groups* in SCANPY. Visualization of cell clusters was performed
29 with Uniform Manifold Approximation and Projection (UMAP)¹²⁴ in SCANPY. Velocity
30 analysis⁵⁴ to identify differences in the dynamics of microglial cells reactivity to injury
31 was performed following the instructions from previous publication using *scvelo*
32 package in SCANPY⁵³.

33 34 **Tissue preparation and immunohistochemistry of human brain tissues with 3,3'- 35 diaminobenzidine (DAB) development**

36
37 Sections were deparaffinized in xylene and rehydrated in 96% and 70% EtOH. Antigen
38 retrieval was then performed for 30 min with the use of citrate buffer (10 mM, pH: 6,0)
39 and washing steps with bidistilled water followed. Tissue was incubated in 4%
40 hydrogen peroxidase solution for 10 min at RT, washed with bidistilled water and
41 subsequently blocked for 30 min in RT in Blocking Buffer (1X PBS, 2.5% normal horse
42 serum, 1% BSA, 0.1% Triton x-100, 0.2% Gold Fish Gelatine and 0.02% sodium azide
43 solution (10%) and Avidin). Primaries were diluted in Blocking buffer with biotin and
44 an overnight incubation at 4°C was carried out. On the following day, the primaries
45 were washed with PBS and biotinylated secondary antibodies (1:400 in blocking
46 buffer) were applied and incubated for 30 min at RT. Washing steps with PBS followed
47 and incubation with the Avidin-Biotin Complex (ABC) for 30 min at RT was carried out.
48 After extensive washing with PBS, DAB solution was applied to the samples
49 (ImmPACT DAB, SK4104 Vector). Stainings were checked under the microscope and
50 the reaction was stopped in bidistilled water. 3 min in haematoxylin allowed the

1 counterstaining of samples. Dehydration in 70% and 96% EtOH and incubation in
2 xylene were performed and the samples were then coverslipped.

3 4 **Quantification and statistical analysis**

5
6 Statistical analyses were performed with Prism 8 software (GraphPad Software).
7 Individual animal experiments were performed with 4 or 5 zebrafish per group
8 (identified by genotype and by condition, i.e. intact/injured). The specific number of
9 animals analyzed is specified in each dot plot and quantifications were performed
10 blindly. Data of same experimental groups derived from multiple experiments with
11 identical conditions were combined and analyzed statistically to determine normality
12 ($n \geq 8$). All data analyzed passed normality test and for this reason unpaired t test,
13 ordinary one-way ANOVA and two-way ANOVA were used when 2 groups, more than
14 2 groups from different genotypes or conditions (i.e. intact, injured, drug-treated) or
15 more than 2 groups from different genotypes and conditions were statistically
16 analyzed, respectively. Statistical tests and post-hoc tests for multiple comparisons
17 are indicated in the figure legends. Each data point is obtained by quantifying multiple
18 sections (from zebrafish telencephalon) per biological replicate. Data are presented
19 as the mean \pm standard error of the mean (SEM).

20 21 **Data and software availability**

22
23 The scRNA-seq data has been deposited in GEO under accession code GEO:
24 pending.

25 The analysis was performed by following the guidelines obtained from previously
26 released as open source codes on GitHub at the following
27 links:[https://github.com/theislab/single-cell-](https://github.com/theislab/single-cell-tutorial/blob/master/latest_notebook/Case-study_Mouse-intestinal-epithelium_1906.ipynb)
28 [tutorial/blob/master/latest_notebook/Case-study_Mouse-intestinal-](https://github.com/theislab/single-cell-tutorial/blob/master/latest_notebook/Case-study_Mouse-intestinal-epithelium_1906.ipynb)
29 [epithelium_1906.ipynb](https://github.com/brianhie/scanorama), <https://github.com/brianhie/scanorama>,
30 https://github.com/theislab/scvelo_notebooks/blob/master/VelocityBasics.ipynb.

31 32 **Contact for reagent and resource sharing**

33
34 Further information and requests for resources and reagents should be directed to and
35 will be fulfilled by the Lead Contact, Prof. Jovica Ninkovic ([ninkovic@helmholtz-](mailto:ninkovic@helmholtz-muenchen.de)
36 [muenchen.de](mailto:ninkovic@helmholtz-muenchen.de)).

37 38 **References**

- 39
40 1. Dimou, L. & Gotz, M. Glial cells as progenitors and stem cells: new roles in the
41 healthy and diseased brain. *Physiol Rev* **94**, 709–737 (2014).
42 2. O’Shea, T. M., Burda, J. E. & Sofroniew, M. V. Cell biology of spinal cord injury
43 and repair. *J Clin Invest* **127**, 3259–3270 (2017).
44 3. Arvidsson, A., Collin, T., Kirik, D., Kokaia, Z. & Lindvall, O. Neuronal
45 replacement from endogenous precursors in the adult brain after stroke. *Nat*
46 *Med* **8**, 963–970 (2002).
47 4. Thored, P. *et al.* Long-term neuroblast migration along blood vessels in an
48 area with transient angiogenesis and increased vascularization after stroke.
49 *Stroke* **38**, 3032–3039 (2007).

- 1 5. Thored, P. *et al.* Persistent production of neurons from adult brain stem cells
2 during recovery after stroke. *Stem Cells* **24**, 739–747 (2006).
- 3 6. Ernst, A. *et al.* Neurogenesis in the striatum of the adult human brain. *Cell* **156**,
4 1072–1083 (2014).
- 5 7. Winpenny, E. *et al.* Sequential generation of olfactory bulb glutamatergic
6 neurons by Neurog2-expressing precursor cells. *Neural Dev* **6**, 12 (2011).
- 7 8. Henriques, D., Moreira, R., Schwamborn, J., Pereira de Almeida, L. &
8 Mendonça, L. S. Successes and Hurdles in Stem Cells Application and
9 Production for Brain Transplantation. *Frontiers in Neuroscience* (2019)
10 doi:10.3389/fnins.2019.01194.
- 11 9. Grade, S. & Götz, M. Neuronal replacement therapy: previous achievements
12 and challenges ahead. *Regen Med* (2017).
- 13 10. Adams, K. L. & Gallo, V. The diversity and disparity of the glial scar. *Nature*
14 *Neuroscience* vol. 21 9–15 (2018).
- 15 11. Frik, J. *et al.* Cross-talk between monocyte invasion and astrocyte proliferation
16 regulates scarring in brain injury. *EMBO Rep* **19**, (2018).
- 17 12. Anderson, M. A. *et al.* Astrocyte scar formation AIDS central nervous system
18 axon regeneration. *Nature* (2016) doi:10.1038/nature17623.
- 19 13. Goritz, C. *et al.* A pericyte origin of spinal cord scar tissue. *Science* (80-.).
20 **333**, 238–242 (2011).
- 21 14. Dias, D. O. *et al.* Reducing Pericyte-Derived Scarring Promotes Recovery after
22 Spinal Cord Injury. *Cell* **173**, 153-165 e22 (2018).
- 23 15. Badimon, A. *et al.* Negative feedback control of neuronal activity by microglia.
24 *Nature* (2020) doi:10.1038/s41586-020-2777-8.
- 25 16. Helmut, K., Hanisch, U. K., Noda, M. & Verkhratsky, A. Physiology of
26 microglia. *Physiol. Rev.* (2011) doi:10.1152/physrev.00011.2010.
- 27 17. Hanisch, U. K. Microglia as a source and target of cytokines. *GLIA* (2002)
28 doi:10.1002/glia.10161.
- 29 18. Koizumi, S., Ohsawa, K., Inoue, K. & Kohsaka, S. Purinergic receptors in
30 microglia: Functional modal shifts of microglia mediated by P2 and P1
31 receptors. *Glia* (2013) doi:10.1002/glia.22358.
- 32 19. Fontainhas, A. M. *et al.* Microglial morphology and dynamic behavior is
33 regulated by ionotropic glutamatergic and GABAergic neurotransmission.
34 *PLoS One* (2011) doi:10.1371/journal.pone.0015973.
- 35 20. Pocock, J. M. & Kettenmann, H. Neurotransmitter receptors on microglia.
36 *Trends in Neurosciences* (2007) doi:10.1016/j.tins.2007.07.007.
- 37 21. Michell-Robinson, M. A. *et al.* Roles of microglia in brain development, tissue
38 maintenance and repair. *Brain* (2015) doi:10.1093/brain/awv066.
- 39 22. Colonna, M. & Butovsky, O. Microglia function in the central nervous system
40 during health and neurodegeneration. *Annual Review of Immunology* (2017)
41 doi:10.1146/annurev-immunol-051116-052358.
- 42 23. Song, W. M. & Colonna, M. The identity and function of microglia in
43 neurodegeneration. *Nature Immunology* (2018) doi:10.1038/s41590-018-0212-
44 1.
- 45 24. Krasemann, S. *et al.* The TREM2-APOE Pathway Drives the Transcriptional
46 Phenotype of Dysfunctional Microglia in Neurodegenerative Diseases.
47 *Immunity* (2017) doi:10.1016/j.immuni.2017.08.008.
- 48 25. Deczkowska, A. *et al.* Disease-Associated Microglia: A Universal Immune
49 Sensor of Neurodegeneration. *Cell* (2018) doi:10.1016/j.cell.2018.05.003.
- 50 26. Fetler, L. & Amigorena, S. Brain under surveillance: The microglia patrol.

- 1 *Science* (2005) doi:10.1126/science.1114852.
- 2 27. Casano, A. M., Albert, M. & Peri, F. Developmental Apoptosis Mediates Entry
3 and Positioning of Microglia in the Zebrafish Brain. *Cell Rep.* (2016)
4 doi:10.1016/j.celrep.2016.06.033.
- 5 28. Barbosa, J. S. S. *et al.* Single-cell in vivo imaging of adult neural stem cells in
6 the zebrafish telencephalon. *Nat Protoc* **11**, 1360–1370 (2016).
- 7 29. Baumgart, E. V. V *et al.* Stab wound injury of the zebrafish telencephalon: a
8 model for comparative analysis of reactive gliosis. *Glia* **60**, 343–357 (2012).
- 9 30. Kyritsis, N. *et al.* Acute inflammation initiates the regenerative response in the
10 adult zebrafish brain. *Science* (80-.). **338**, 1353–1356 (2012).
- 11 31. Kroehne, V., Freudenreich, D., Hans, S., Kaslin, J. & Brand, M. Regeneration
12 of the adult zebrafish brain from neurogenic radial glia-type progenitors.
13 *Development* **138**, 4831–4841 (2011).
- 14 32. Kishimoto, N., Shimizu, K. & Sawamoto, K. Neuronal regeneration in a
15 zebrafish model of adult brain injury. *Dis Model Mech* **5**, 200–209 (2012).
- 16 33. Becker, C. G. & Becker, T. Growth and pathfinding of regenerating axons in
17 the optic projection of adult fish. *J. Neurosci. Res.* **85**, 2793–2799 (2007).
- 18 34. Becker, T. & Becker, C. G. Regenerating descending axons preferentially
19 reroute to the gray matter in the presence of a general macrophage/microglial
20 reaction caudal to a spinal transection in adult zebrafish. *J Comp Neurol* **433**,
21 131–147 (2001).
- 22 35. Becker, C. G. & Becker, T. Neuronal Regeneration from Ependymo-Radial
23 Glial Cells: Cook, Little Pot, Cook! *Dev. Cell* **32**, 516–527 (2015).
- 24 36. Reimer, M. M. *et al.* Motor neuron regeneration in adult zebrafish. *J Neurosci*
25 **28**, 8510–8516 (2008).
- 26 37. Lindsey, B. W. *et al.* Midbrain tectal stem cells display diverse regenerative
27 capacities in zebrafish. *Sci. Rep.* (2019) doi:10.1038/s41598-019-40734-z.
- 28 38. Fleisch, V. C., Fraser, B. & Allison, W. T. Investigating regeneration and
29 functional integration of CNS neurons: Lessons from zebrafish genetics and
30 other fish species. *Biochimica et Biophysica Acta - Molecular Basis of Disease*
31 (2011) doi:10.1016/j.bbadis.2010.10.012.
- 32 39. Guarino, A. M. *et al.* YB-1 recruitment to stress granules in zebrafish cells
33 reveals a differential adaptive response to stress. *Sci. Rep.* (2019)
34 doi:10.1038/s41598-019-45468-6.
- 35 40. Acosta, J. R. *et al.* Mutant human FUS is ubiquitously mislocalized and
36 generates persistent stress granules in primary cultured transgenic zebrafish
37 cells. *PLoS One* (2014) doi:10.1371/journal.pone.0090572.
- 38 41. Zampedri, C. *et al.* Zebrafish P54 RNA helicases are cytoplasmic granule
39 residents that are required for development and stress resilience. *Biol. Open*
40 (2016) doi:10.1242/bio.015826.
- 41 42. R., W., H., Z., J., D. & J., X. Heat resilience in embryonic zebrafish revealed
42 using an in vivo stress granule reporter. *J. Cell Sci.* (2019).
- 43 43. Di Giaimo, R. *et al.* The Aryl Hydrocarbon Receptor Pathway Defines the Time
44 Frame for Restorative Neurogenesis. *Cell Rep* **25**, 3241–3251 e5 (2018).
- 45 44. Zambusi, A. & Ninkovic, J. Regeneration of the central nervous system-
46 principles from brain regeneration in adult zebrafish. *World Journal of Stem*
47 *Cells* (2020) doi:10.4252/wjsc.v12.i1.8.
- 48 45. Burda, J. E. & Sofroniew, M. V. Reactive gliosis and the multicellular response
49 to CNS damage and disease. *Neuron* **81**, 229–248 (2014).
- 50 46. Marschallinger, J. *et al.* Lipid-droplet-accumulating microglia represent a

- 1 dysfunctional and proinflammatory state in the aging brain. *Nat. Neurosci.*
2 (2020) doi:10.1038/s41593-019-0566-1.
- 3 47. Mazaheri, F. *et al.* TREM2 deficiency impairs chemotaxis and microglial
4 responses to neuronal injury. *EMBO Rep* **18**, 1186–1198 (2017).
- 5 48. Schlepckow, K. *et al.* Enhancing protective microglial activities with a dual
6 function TREM 2 antibody to the stalk region. *EMBO Mol. Med.* (2020)
7 doi:10.15252/emmm.201911227.
- 8 49. Zhou, X. *et al.* Loss of Tmem106b exacerbates FTLN pathologies and causes
9 motor deficits in progranulin-deficient mice. *EMBO Rep.* **21**, (2020).
- 10 50. Werner, G. *et al.* Loss of TMEM 106B potentiates lysosomal and FTLN-like
11 pathology in progranulin-deficient mice. *EMBO Rep.* **21**, (2020).
- 12 51. Li, Y. *et al.* Microglia-organized scar-free spinal cord repair in neonatal mice.
13 *Nature* **587**, 613–618 (2020).
- 14 52. Masuda, T. *et al.* Spatial and temporal heterogeneity of mouse and human
15 microglia at single-cell resolution. *Nature* **566**, 388–392 (2019).
- 16 53. Bergen, V., Lange, M., Peidli, S., Wolf, F. A. & Theis, F. J. Generalizing RNA
17 velocity to transient cell states through dynamical modeling. *Nat. Biotechnol.*
18 (2020) doi:10.1038/s41587-020-0591-3.
- 19 54. La Manno, G. *et al.* RNA velocity of single cells. *Nature* (2018)
20 doi:10.1038/s41586-018-0414-6.
- 21 55. Lauro, C. & Limatola, C. Metabolic Reprogramming of Microglia in the
22 Regulation of the Innate Inflammatory Response. *Frontiers in Immunology*
23 (2020) doi:10.3389/fimmu.2020.00493.
- 24 56. Bernier, L. P. *et al.* Microglial metabolic flexibility supports immune surveillance
25 of the brain parenchyma. *Nat. Commun.* (2020) doi:10.1038/s41467-020-
26 15267-z.
- 27 57. Majumdar, A. *et al.* Activation of microglia acidifies lysosomes and leads to
28 degradation of Alzheimer amyloid fibrils. *Mol. Biol. Cell* (2007)
29 doi:10.1091/mbc.E06-10-0975.
- 30 58. Dou, Y. *et al.* Microglial migration mediated by ATP-induced ATP release from
31 lysosomes. *Cell Res.* (2012) doi:10.1038/cr.2012.10.
- 32 59. Altmann, C. *et al.* Progranulin promotes peripheral nerve regeneration and
33 reinnervation: Role of notch signaling. *Mol. Neurodegener.* **11**, 69 (2016).
- 34 60. He, Z., Ong, C. H. P., Halper, J. & Bateman, A. Progranulin is a mediator of
35 the wound response. *Nat. Med.* **9**, 225–229 (2003).
- 36 61. Lui, H. *et al.* Progranulin Deficiency Promotes Circuit-Specific Synaptic
37 Pruning by Microglia via Complement Activation. *Cell* **165**, 921–935 (2016).
- 38 62. Rhinn, H. & Abeliovich, A. Differential Aging Analysis in Human Cerebral
39 Cortex Identifies Variants in TMEM106B and GRN that Regulate Aging
40 Phenotypes. *Cell Syst.* **4**, 404-415.e5 (2017).
- 41 63. Tanaka, Y., Matsuwaki, T., Yamanouchi, K. & Nishihara, M. Exacerbated
42 inflammatory responses related to activated microglia after traumatic brain
43 injury in progranulin-deficient mice. *Neuroscience* **231**, 49–60 (2013).
- 44 64. Valenzano, D. R. *et al.* The African Turquoise Killifish Genome Provides
45 Insights into Evolution and Genetic Architecture of Lifespan. *Cell* **163**, 1539–
46 1554 (2015).
- 47 65. Wils, H. *et al.* Cellular ageing, increased mortality and FTLN-TDP-associated
48 neuropathology in progranulin knockout mice. *J. Pathol.* **228**, 67–76 (2012).
- 49 66. Yin, F. *et al.* Exaggerated inflammation, impaired host defense, and
50 neuropathology in progranulin-deficient mice. *J. Exp. Med.* **207**, 117–128

- 1 (2010).
- 2 67. Zhang, J. *et al.* Neurotoxic microglia promote TDP-43 proteinopathy in
3 progranulin deficiency. *Nature* **588**, (2020).
- 4 68. Bosch, M. *et al.* Mammalian lipid droplets are innate immune hubs integrating
5 cell metabolism and host defense. *Science* (80-.). **370**, (2020).
- 6 69. Solchenberger, B., Russell, C., Kremmer, E., Haass, C. & Schmid, B. Granulin
7 Knock Out Zebrafish Lack Frontotemporal Lobar Degeneration and Neuronal
8 Ceroid Lipofuscinosis Pathology. *PLoS One* **10**, e0118956 (2015).
- 9 70. Zambusi, A., Pelin Burhan, Ö., Di Giaimo, R., Schmid, B. & Ninkovic, J.
10 Granulins Regulate Aging Kinetics in the Adult Zebrafish Telencephalon. *Cells*
11 (2020) doi:10.3390/cells9020350.
- 12 71. Evers, B. M. *et al.* Lipidomic and Transcriptomic Basis of Lysosomal
13 Dysfunction in Progranulin Deficiency. *Cell Rep.* **20**, 2565–2574 (2017).
- 14 72. Simon, C., Lickert, H., Gotz, M. & Dimou, L. Sox10-iCreERT2 : a mouse line to
15 inducibly trace the neural crest and oligodendrocyte lineage. *Genesis* **50**, 506–
16 515 (2012).
- 17 73. Buffo, A. *et al.* Expression pattern of the transcription factor Olig2 in response
18 to brain injuries: implications for neuronal repair. *Proc Natl Acad Sci U S A*
19 **102**, 18183–18188 (2005).
- 20 74. Thammisetty, S. S. *et al.* Age-related deregulation of TDP-43 after stroke
21 enhances NF- κ B-mediated inflammation and neuronal damage 11 Medical and
22 Health Sciences 1109 Neurosciences. *J. Neuroinflammation* **15**, (2018).
- 23 75. Heyburn, L., Sajja, V. S. S. S. & Long, J. B. The role of TDP-43 in military-
24 relevant TBI and chronic neurodegeneration. *Frontiers in Neurology* vol. 10
25 (2019).
- 26 76. Anderson, E. N. *et al.* Traumatic injury induces stress granule formation and
27 enhances motor dysfunctions in ALS/FTD models. *Hum. Mol. Genet.* **27**,
28 1366–1381 (2018).
- 29 77. Wiesner, D. *et al.* Reversible induction of TDP-43 granules in cortical neurons
30 after traumatic injury. *Exp. Neurol.* **299**, 15–25 (2018).
- 31 78. Salazar, D. A. *et al.* The progranulin cleavage products, granulins, exacerbate
32 TDP-43 toxicity and increase TDP-43 levels. *J. Neurosci.* **35**, 9315–9328
33 (2015).
- 34 79. Beel, S. *et al.* Progranulin reduces insoluble TDP-43 levels, slows down axonal
35 degeneration and prolongs survival in mutant TDP-43 mice 11 Medical and
36 Health Sciences 1109 Neurosciences. *Mol. Neurodegener.* **13**, (2018).
- 37 80. Bhopatkar, A. A., Uversky, V. N. & Rangachari, V. Granulins modulate liquid–
38 liquid phase separation and aggregation of the prion-like C-terminal domain of
39 the neurodegeneration-associated protein TDP-43. *J. Biol. Chem.* **295**, 2506–
40 2519 (2020).
- 41 81. Wang, A. *et al.* A single N-terminal phosphomimic disrupts TDP-43
42 polymerization, phase separation, and RNA splicing. *EMBO J.* **37**, (2018).
- 43 82. Fox, J. D. & Waugh, D. S. Maltose-binding protein as a solubility enhancer.
44 *Methods Mol. Biol.* **205**, 99–117 (2003).
- 45 83. Nallamsetty, S. & Waugh, D. S. Solubility-enhancing proteins MBP and NusA
46 play a passive role in the folding of their fusion partners. *Protein Expr. Purif.*
47 **45**, 175–182 (2006).
- 48 84. Nallamsetty, S., Austin, B. P., Penrose, K. J. & Waugh, D. S. Gateway vectors
49 for the production of combinatorially-tagged His₆-MBP fusion proteins in the
50 cytoplasm and periplasm of *Escherichia coli*. *Protein Sci.* **14**, 2964–2971

- 1 (2005).
- 2 85. Wheeler, R. J. *et al.* Small molecules for modulating protein driven liquid-liquid
3 phase separation in treating neurodegenerative disease. *bioRxiv* (2019)
4 doi:10.1101/721001.
- 5 86. Lalancette-Hébert, M., Gowing, G., Simard, A., Yuan, C. W. & Kriz, J.
6 Selective ablation of proliferating microglial cells exacerbates ischemic injury in
7 the brain. *J. Neurosci.* **27**, 2596–2605 (2007).
- 8 87. Paolicelli, R. C. *et al.* Synaptic pruning by microglia is necessary for normal
9 brain development. *Science (80-.)*. **333**, 1456–1458 (2011).
- 10 88. Brown, G. C. & Neher, J. J. Microglial phagocytosis of live neurons. *Nat. Rev.*
11 *Neurosci.* **15**, 209–216 (2014).
- 12 89. Hanisch, U.-K. & Kettenmann, H. Microglia: active sensor and versatile effector
13 cells in the normal and pathologic brain. *Nat Neurosci* **10**, 1387–1394 (2007).
- 14 90. Davalos, D. *et al.* ATP mediates rapid microglial response to local brain injury
15 in vivo. *Nat. Neurosci.* (2005) doi:10.1038/nn1472.
- 16 91. Nimmerjahn, A., Kirchhoff, F. & Helmchen, F. Resting microglial cells are
17 highly dynamic surveillants of brain parenchyma in vivo. *Neuroforum* (2005)
18 doi:10.1515/nf-2005-0304.
- 19 92. Dinarello, C. A. Overview of the IL-1 family in innate inflammation and acquired
20 immunity. *Immunological Reviews* vol. 281 (2018).
- 21 93. Lucas, K. & Maes, M. Role of the toll like receptor (TLR) radical cycle in
22 chronic inflammation: Possible treatments targeting the TLR4 pathway.
23 *Molecular Neurobiology* vol. 48 (2013).
- 24 94. Song, Q., Meng, B., Xu, H. & Mao, Z. The emerging roles of vacuolar-type
25 ATPase-dependent Lysosomal acidification in neurodegenerative diseases.
26 *Translational Neurodegeneration* vol. 9 (2020).
- 27 95. Childs, B. G. *et al.* Senescent intimal foam cells are deleterious at all stages of
28 atherosclerosis. *Science (80-.)*. **354**, 472–477 (2016).
- 29 96. Harris, C. A. *et al.* DGAT enzymes are required for triacylglycerol synthesis
30 and lipid droplets in adipocytes. *J. Lipid Res.* **52**, 657–667 (2011).
- 31 97. Mori, T., Buffo, A. & Gotz, M. The novel roles of glial cells revisited: the
32 contribution of radial glia and astrocytes to neurogenesis. *Curr Top Dev Biol*
33 **69**, 67–99 (2005).
- 34 98. Herman, A. B. *et al.* Regulation of stress granule formation by inflammation,
35 vascular injury, and atherosclerosis. *Arterioscler. Thromb. Vasc. Biol.* (2019)
36 doi:10.1161/ATVBAHA.119.313034.
- 37 99. Ivanov, P., Kedersha, N. & Anderson, P. Stress granules and processing
38 bodies in translational control. *Cold Spring Harb. Perspect. Biol.* **11**, (2019).
- 39 100. Jaud, M. *et al.* Translational Regulations in Response to Endoplasmic
40 Reticulum Stress in Cancers. *Cells* **9**, 540 (2020).
- 41 101. Alberti, S., Gladfelter, A. & Mittag, T. Considerations and Challenges in
42 Studying Liquid-Liquid Phase Separation and Biomolecular Condensates. *Cell*
43 vol. 176 419–434 (2019).
- 44 102. Boeynaems, S. *et al.* Protein Phase Separation: A New Phase in Cell Biology.
45 *Trends in Cell Biology* vol. 28 420–435 (2018).
- 46 103. Shin, Y. & Brangwynne, C. P. Liquid phase condensation in cell physiology
47 and disease. *Science* vol. 357 (2017).
- 48 104. Alberti, S. & Dormann, D. Liquid–Liquid Phase Separation in Disease. *Annu.*
49 *Rev. Genet.* **53**, 171–194 (2019).
- 50 105. Protter, D. S. W. & Parker, R. Principles and Properties of Stress Granules.

- 1 *Trends in Cell Biology* vol. 26 668–679 (2016).
- 2 106. Molliex, A. *et al.* Phase Separation by Low Complexity Domains Promotes
3 Stress Granule Assembly and Drives Pathological Fibrillization. *Cell* **163**, 123–
4 133 (2015).
- 5 107. Lin, Y., Protter, D. S. W., Rosen, M. K. & Parker, R. Formation and Maturation
6 of Phase-Separated Liquid Droplets by RNA-Binding Proteins. *Mol. Cell* **60**,
7 208–219 (2015).
- 8 108. Murakami, T. *et al.* ALS/FTD Mutation-Induced Phase Transition of FUS Liquid
9 Droplets and Reversible Hydrogels into Irreversible Hydrogels Impairs RNP
10 Granule Function. *Neuron* **88**, 678–690 (2015).
- 11 109. Patel, A. *et al.* A Liquid-to-Solid Phase Transition of the ALS Protein FUS
12 Accelerated by Disease Mutation. *Cell* **162**, 1066–1077 (2015).
- 13 110. Conicella, A. E., Zerbe, G. H., Mittal, J. & Fawzi, N. L. ALS Mutations Disrupt
14 Phase Separation Mediated by α -Helical Structure in the TDP-43 Low-
15 Complexity C-Terminal Domain. *Structure* **24**, 1537–1549 (2016).
- 16 111. Lee, K. H. *et al.* C9orf72 Dipeptide Repeats Impair the Assembly, Dynamics,
17 and Function of Membrane-Less Organelles. *Cell* **167**, 774-788.e17 (2016).
- 18 112. Wang, J. *et al.* A Molecular Grammar Governing the Driving Forces for Phase
19 Separation of Prion-like RNA Binding Proteins. *Cell* **174**, 688-699.e16 (2018).
- 20 113. McGurk, L. *et al.* Poly(ADP-Ribose) Prevents Pathological Phase Separation
21 of TDP-43 by Promoting Liquid Demixing and Stress Granule Localization.
22 *Mol. Cell* **71**, 703-717.e9 (2018).
- 23 114. Gasset-Rosa, F. *et al.* Cytoplasmic TDP-43 De-mixing Independent of Stress
24 Granules Drives Inhibition of Nuclear Import, Loss of Nuclear TDP-43, and Cell
25 Death. *Neuron* **102**, 339-357.e7 (2019).
- 26 115. Fernandes, N. *et al.* Stress granule assembly can facilitate but is not required
27 for TDP-43 cytoplasmic aggregation. *Biomolecules* **10**, 1–19 (2020).
- 28 116. Hayashi, Y., Ford, L. K., Fioriti, L., McGurk, L. & Zhang, M. Liquid-Liquid
29 Phase Separation in Physiology and Pathophysiology of the Nervous System.
30 *J. Neurosci.* **41**, JN-SY-1656-20 (2021).
- 31 117. Cruz, A. L. S., Barreto, E. de A., Fazolini, N. P. B., Viola, J. P. B. & Bozza, P.
32 T. Lipid droplets: platforms with multiple functions in cancer hallmarks. *Cell*
33 *Death and Disease* vol. 11 (2020).
- 34 118. Prentzell, M. T. *et al.* G3BPs tether the TSC complex to lysosomes and
35 suppress mTORC1 signaling. *Cell* **184**, (2021).
- 36 119. Kolobova, E. *et al.* Microtubule-dependent association of AKAP350A and
37 CCAR1 with RNA stress granules. *Exp. Cell Res.* **315**, (2009).
- 38 120. Youn, J. Y. *et al.* High-Density Proximity Mapping Reveals the Subcellular
39 Organization of mRNA-Associated Granules and Bodies. *Mol. Cell* **69**, (2018).
- 40 121. Hofweber, M. *et al.* Phase Separation of FUS Is Suppressed by Its Nuclear
41 Import Receptor and Arginine Methylation. *Cell* **173**, 706-719.e13 (2018).
- 42 122. Luecken, M. D. & Theis, F. J. Current best practices in single-cell RNA-seq
43 analysis: a tutorial. *Mol. Syst. Biol.* **15**, e8746 (2019).
- 44 123. Hie, B., Bryson, B. & Berger, B. Efficient integration of heterogeneous single-
45 cell transcriptomes using Scanorama. *Nat. Biotechnol.* **37**, 685–691 (2019).
- 46 124. McInnes, L., Healy, J., Saul, N. & Großberger, L. UMAP: Uniform Manifold
47 Approximation and Projection. *J. Open Source Softw.* **3**, 861 (2018).
- 48 125. Deka, K. & Saha, S. Regulation of Mammalian HSP70 Expression and Stress
49 Response. in 3–25 (Springer, Cham, 2018). doi:10.1007/978-3-319-74715-
50 6_1.

1 **Acknowledgments**

2
3 We are particularly grateful to Dr. Magdalena Götz and Dr. Stefan Stricker (Ludwig-
4 Maximilians-University, Munich) for the valuable support toward this study,
5 experimental suggestions and critical reading of the manuscript. We would also like to
6 thank Dr. Michael Kiebler (Ludwig-Maximilians-University, Munich) for the critical
7 reading of the manuscript. Lastly, we thank all the members of the Neurogenesis and
8 Regeneration group for experimental inputs, discussions and critical reading of the
9 manuscript. We acknowledge the support of the following core facilities: the
10 Bioimaging Core Facility at the BioMedical Center of LMU Munich and the Sequencing
11 Facility at the Helmholtz Zentrum München.

12 This work was supported by the German research foundation (DFG) by the SFB 870;
13 TRR274; SPP 1738 “Emerging roles of non-coding RNAs in nervous system
14 development, plasticity & disease”, SPP1757 “Glial heterogeneity”; SPP2191
15 “Molecular mechanisms of functional phase separation” (ID 402723784) and the
16 Excellence Strategy within the framework of the Munich Cluster for Systems
17 Neurology (EXC 2145/1010 SyNergy – ID 390857198) and Ampro Helmholtz Alliance.
18

19 **Author contributions**

20
21 A.Z., K.T.N. and J.N. conceived the project and experiments. A.Z., K.T.N., S.K., S.H.,
22 L.S., C.D. performed the experiments and analyzed the data; A.Z., K.T.N., C.K., H.A.
23 and F.T. performed the bioinformatic analyses. A.Z., K.T.N., and J.N. wrote the
24 manuscript with inputs from B.S., J.S., and D.D. J.N. and D.D. supervised research
25 and acquired funding.
26

27 **Declaration of Interests**

28
29 The authors declare no competing interests.
30

31 **Supplementary information**

32
33 **Supplementary Table 1:** GO Terms (p-value < 0.05 and fold enrichment > 1.5) from
34 enriched genes in Wt microglia at 3 dpi. Related to Fig. 1.
35

36 **Supplementary Table 2:** GO Terms (p-value < 0.05 and fold enrichment > 1.5) from
37 upregulated and downregulated genes identified comparing each Wt microglia cluster
38 with all the others. Related to Fig. 1.
39

40 **Supplementary Table 3:** GO Terms (p-value < 0.05 and fold enrichment > 1.5) from
41 enriched genes in Grn-deficient vs Wt microglia at 7 dpi and in MG0 vs MG3 microglial
42 clusters. Related to Fig. 4.
43

44 **Supplementary Video 1:** Microglial and oligodendroglial cell reactivity in Wt
45 telencephalon at 7 dpi. Related to Fig. 3.
46

47 **Supplementary Video 2:** Microglial and oligodendroglial cell reactivity in Grn-deficient
48 telencephalon at 7 dpi. Related to Fig. 3.

1 **Supplementary Video 3:** Microglial and oligodendroglial cell reactivity in *Grn*-deficient
2 telencephalon at 31 dpi. Related to Fig. 3.

3 4 **Figures**

5 6 **Fig. 1: Stab wound injury induces a pro-regenerative signature in a *granulin a*- 7 expressing microglial subpopulation**

8 (A) Representative images of 4C4⁺ microglia (white) at different time points after injury
9 in the adult zebrafish telencephalon. Red and blue framed images are magnifications
10 of brain parenchyma near (red) and far from (blue) from injury sites. Scale bars, 100
11 μm or 20 μm (magnifications).

12 (B) UMAP plot depicting color-coded cellular clusters identified through single-cell
13 transcriptome analysis of Wt cells, isolated from intact and injured (3 and 7 dpi)
14 zebrafish telencephali. Cells are colored according to their cell type identity; each point
15 represents a single cell.

16 (C) Dot plot depicting representative GO terms enriched in the gene set identifying
17 microglial cells (cluster 17, Fig. 1B) at 3 dpi. GO Terms include Kyoto Encyclopedia of
18 Genes and Genomes (KEGG) pathways, Molecular Function (MF)- and Cellular
19 Component (CC)-related terms. Dot color, p-value; dot size, number of genes.

20 (D) Subclustering of Wt microglial cells (cluster 17, Fig. 1B) isolated from intact and
21 injured telencephali and combined. Cells are colored according to their microglial
22 subcluster identity; each point represents a single cell.

23 (E) Abundance of Wt microglial subclusters (from Fig. 1E) in different conditions: intact
24 (top), 3 dpi (middle), 7 dpi (bottom).

25 (F) Velocity analysis depicting Wt microglial dynamics in response to injury. Each dot
26 represents a single cell.

27 (G-J) Dot plots depicting the expression of genes associated with pro-regenerative
28 mouse microglia⁵¹ (G), identified as significantly enriched in MGO activated microglia
29 (H), associated with lipid droplet formation⁴⁶ (I), and depicting the expression of
30 granulin genes in different conditions (J). Dot color, mean expression; dot size, fraction
31 of cells.

32 33 **Fig. 2: Granulins are necessary and sufficient to limit prolonged microglial 34 activation at injury sites**

35 (A) Representative images of 4C4 (red) and Plin3 (cyan) immunoreactivity in intact
36 parenchyma and at injury sites in Wt and *Grn*-deficient brains. Scale bars, 20 μm .

37 (B, C) Dot plots depicting the total number of Plin3⁺ droplets (B) and number of Plin3⁺
38 droplets within 4C4⁺ microglia (C) at injury sites in Wt and *Grn*-deficient brains. Data
39 are shown as mean \pm SEM. Each point represents one animal. Significance was
40 calculated with ordinary two-way ANOVA, and post-hoc Tukey test was used for
41 multiple comparison. * $p < 0.05$, ** $p < 0.01$.

42 (D) Dot plot depicting the expression of genes associated with lipid droplet formation
43⁴⁶ in Wt and *Grn*-deficient microglia. Dot color, mean expression; dot size, fraction of
44 cells.

45 (E) Heatmaps depicting triacylglycerols (TAGs) and diacylglycerols (DAGs) content in
46 intact and injured Wt and *Grn*-deficient telencephali (7 dpi). Scale bar, z-score.

47 (F) Experimental paradigm of intraparenchymal recombinant progranulin (PGRN)
48 injections in the adult *Grn*-deficient zebrafish.

1 (G) Representative images of 4C4 (red) and Plin3 (cyan) immunoreactivity at injury
2 sites in vehicle- and PGRN-injected Grn-deficient animals. Scale bars, 100 μm or 20
3 μm (magnifications).
4 (H, I) Dot plots showing the number of total Plin3⁺ droplets (H) and Plin3⁺ droplets
5 within 4C4⁺ microglia (I) at injury sites of Wt, Grn-deficient and mPGRN-injected Grn-
6 deficient animals at 7 dpi. Data are shown as mean \pm SEM. Each point represents
7 one animal. Significance was calculated with ordinary one-way ANOVA, and post-hoc
8 Tukey test was used for multiple comparison. * $p < 0.05$, ** $p < 0.01$, *** $p < 0.001$.

9

10 **Fig. 3: Granulin deficiency-induced neuroinflammation prolongs glial reactivity**
11 **at injury sites and impairs restorative neurogenesis**

12 (A) Representative images of 4C4 (red) and Sox10 (cyan) immunoreactivity of injured
13 Wt and Grn-deficient telencephalic hemispheres at different time points (3, 7 and 21
14 dpi). Boxed areas representing injury site are magnified. Scale bars, 100 μm or 20 μm
15 (magnifications).

16 (B) Dot plot depicting the number of Sox10⁺ cells at injury sites in Wt and Grn-deficient
17 animals. Data are shown as mean \pm SEM. Each point represents one animal.
18 Significance was calculated with ordinary two-way ANOVA, and post-hoc Tukey test
19 was used for multiple comparison. * $p < 0.05$, ** $p < 0.01$.

20 (C) Scheme depicting the experimental timeline of methanol/dexamethasone
21 manipulations in the adult Grn-deficient brain.

22 (D) Representative images of 4C4 (red) and Sox10 (cyan) of
23 methanol/dexamethasone-treated Grn-deficient animals at 7 dpi. Scale bars, 100 μm
24 or 20 μm (magnifications).

25 (E) Dot plot depicting the number of Sox10⁺ cells injury sites in
26 methanol/dexamethasone-treated Grn-deficient animals at 7 dpi. Data are shown as
27 mean \pm SEM. Each point represents one animal. Significance was calculated with
28 unpaired Student's t-test. * $p < 0.05$, ** $p < 0.01$.

29 (F, G) Schemes depicting the experimental paradigm (F) and brain areas analyzed
30 (G) to assess restorative neurogenesis in Wt and Grn-deficient animals.

31 (H) Representative images and orthogonal projections of HuC/D (green) and BrdU
32 (magenta) immunoreactivity in the telencephalic parenchyma of Wt and Grn-deficient
33 animals. Boxed areas are magnified. Scale bars, 100 μm or 20 μm (magnifications).

34 (I) Dot plot depicting the number of HuC/D⁺BrdU⁺ cells in the telencephalic
35 parenchyma of Wt and Grn-deficient animals. Data are shown as mean \pm SEM. Each
36 point represents one animal. Significance was calculated with unpaired Student's T-
37 test. * $p < 0.05$, ** $p < 0.01$.

38

39 **Fig. 4: Activated microglia fail to transition back to the homeostatic state in the**
40 **Grn-deficient injured CNS**

41 (A) UMAP plot depicting subclustering of merged Wt and Grn-deficient microglial cells
42 isolated from intact and injured (3 dpi and 7 dpi) telencephali on the basis of their
43 transcriptomes. Cells are colored according to their microglial subcluster identity; each
44 point represents a single cell.

45 (B) UMAP plots depicting color-coded microglia from Wt or Grn-deficient zebrafish
46 telencephali (intact and injured conditions were merged). Cells are colored according
47 to which genotype they are isolated from; each point represents a single cell.

48 (C) Velocity analysis depicting microglial dynamics in response to injury in Wt and Grn-
49 deficient microglia. Each dot represents a single cell. Dot color, p-value; dot size,
50 number of genes.

1 (D, E) Dot plots depicting representative GO terms enriched in the upregulated gene
2 set in Grn-deficient microglia compared with Wt microglia at 7 dpi (D) and enriched in
3 MGO cells vs MG3 cells (E). Dot color, p-value; dot size, number of genes.
4 (F, G) Dot plots depicting the expression of genes associated with lipid droplet
5 formation⁴⁶ (F) and stress related genes¹²⁵ (G). Dot color, mean expression; dot size,
6 fraction of cells.

7

8 **Fig. 5: Clearance of extranuclear TDP-43 condensates formed through LLPS is**
9 **required for termination of microglia-driven neuroinflammation**

10 (A) Representative images of 4C4 (magenta), Plin3 (green) and TDP-43 (cyan) Wt
11 and Grn-deficient injured telencephali at 3 dpi and 7 dpi. Scale bar, 20 μ m.

12 Yellow arrowheads indicate examples of extranuclear TDP-43⁺ condensates; white
13 arrowheads indicate examples of nuclear TDP-43⁺ signal.

14 (B) Dot plot depicting numbers of TDP-43⁺ condensates at injury sites in Wt and Grn-
15 deficient animals. Data are shown as mean \pm SEM. Each point represents one animal.
16 Significance was calculated with ordinary two-way ANOVA, and post-hoc Tukey test
17 was used for multiple comparison. *p < 0.05, **p < 0.01, ***p < 0.001, ****p < 0.0001.

18 (C) Scheme of experimental paradigm of intraparenchymal injections of vehicle/TDP-
19 43 (uncleaved)/phase-separated TDP-43 (cleaved) in Wt zebrafish.

20 (D) Schematic representation of TDP-43 (containing MBP tag) and phase-separated
21 TDP-43 (MBP tag cleaved off).

22 (E) Representative images of 4C4 (magenta) and Plin3 (green) in Wt injured (7 dpi)
23 telencephali injected with vehicle, TDP-43 or phase-separated TDP-43 proteins. Scale
24 bar, 20 μ m.

25 (F, G) Dot plots depicting total numbers of Plin3⁺ droplets (F) and numbers of Plin3⁺
26 droplets within 4C4⁺ microglia (G) at injury sites in vehicle/TDP-43-injected Wt
27 animals. Data are shown as mean \pm SEM. Each point represents one animal.
28 Significance was calculated with ordinary one-way ANOVA, and post-hoc Tukey test
29 was used for multiple comparison. *p < 0.05, **p < 0.01.

30

31 **Fig. 6: Prevention of excessive LLPS-mediated formation of SGs is sufficient to**
32 **terminate prolonged neuroinflammation in Grn-deficient animals**

33 (A) Scheme of experimental timeline of lipoamide/DMSO administration in injured Grn-
34 deficient animals.

35 (B) Representative images of 4C4 (magenta), TDP-43 (cyan) and Plin3 (green) in
36 injured (7 dpi) Grn-deficient animals treated with DMSO/lipoamide. Scale bar, 20 μ m.

37 (C, D) Dot plots depicting the total number of TDP-43⁺ condensates (C) and the
38 number of Plin3⁺ droplets within 4C4⁺ microglia (D) at injury sites at 7 dpi in Wt, Grn-
39 deficient and lipoamide-treated Grn-deficient animals. Data are shown as mean
40 \pm SEM. Each point represents one animal. Significance was calculated with ordinary
41 one-way ANOVA, and post-hoc Tukey test was used for multiple comparison. *p <
42 0.05, **p < 0.01, ***p < 0.001, ****p < 0.0001.

43 (E) UMAP plot depicting subclustering of merged Wt and Grn-deficient (including
44 lipoamide-treated cells) microglial cells isolated from intact and injured (3 dpi and 7
45 dpi) telencephali on the basis of their transcriptomes. Cells are colored according to
46 their microglial subcluster identity; each point represents a single cell.

47 (F) UMAP plot depicting color coded microglia from lipoamide-treated Grn-deficient
48 zebrafish telencephali (for lipoamide-treated microglia, only 7 dpi was included). Cells
49 are colored according to which condition and genotype they are isolated from; each
50 point represents a single cell.

1 (G) Abundance of microglial subclusters (from Fig. 6E) in different conditions:
2 untreated Grn-deficient (top) and lipoamide-treated Grn-deficient microglia (bottom) at
3 7 dpi.
4 (H) Dot plot depicting representative GO terms enriched in the downregulated gene
5 set of lipoamide-treated Grn-deficient microglia at 7 dpi (compared with untreated Grn-
6 deficient microglia at the same time point). GO Terms include Kyoto Encyclopedia of
7 Genes and Genomes (KEGG) pathways, Molecular Function (MF)- and Cellular
8 Component (CC)-related terms. Dot color, p-value; dot size, number of genes.
9 (I, J) Dot plots depicting the expression of genes associated with lipid droplet formation
10 ⁴⁶ (I) and stress-related genes ¹²⁵ (J) in untreated Grn-deficient and lipoamide-treated
11 Grn-deficient microglia at 7 dpi. Dot color, mean expression; dot size, fraction of cells.
12

13 Fig. 7: Stroke induces lipid droplet and SG formation in the human brain

14 (A, B) Representative images of IBA1, PLIN3, TDP-43 and G3BP immunoreactivity in
15 healthy area distant from stroke area (A) and penumbra area (B) from post-mortem
16 human brain tissues obtained from patients with ischemic stroke. Scale bar, 200 μ m
17 or 20 μ m (magnifications).
18

19 Extended Data Figures

20 Extended Data Fig. 1: Extended scRNA-seq analysis of Wt cells

21 (A) UMAP plot depicting color-coded cellular clusters identified on the basis of the
22 single-cell transcriptome analysis of cells isolated from intact and injured (3 and 7 dpi)
23 Wt zebrafish telencephali. Cells are colored according to their cell type identity; each
24 point represents a single cell.
25 (B) Injury response kinetics of indicated cell types relative to intact condition.
26 (C) UMAP plots depicting color-coded Wt conditions (intact, 3 dpi, 7 dpi). Cells are
27 colored according to the condition they are isolated from; each point represents a
28 single cell.
29 (D) UMAP plots depicting characteristic cell-type marker gene expression (identifying
30 microglial, radial glial, oligodendroglial and neuronal clusters) in single cells isolated
31 from intact and injured (3 and 7 dpi) Wt telencephali. Scale, normalized expression
32 level; each point represents a single cell.
33 (E) Table depicting the number of differentially upregulated genes in specific condition
34 in microglia isolated from Wt telencephali.
35 (F-G) Dot plots depicting the expression of genes associated with lipid droplet
36 formation in different conditions (Marschallinger et al., 2020) (F) and expression of
37 granulin genes in different microglial subclusters (G). Dot color, mean expression; dot
38 size, fraction of cells.
39
40

41 Extended Data Fig. 2: Lipid composition of Wt and Grn-deficient telencephali

42 (A) Representative images of 4C4 (red) and Plin3 (cyan) immunoreactivity with
43 orthogonal projections at injury sites in Wt and Grn-deficient brains displaying
44 colocalization of Plin3⁺ lipid droplets with 4C4⁺ microglial cells. Scale bars, 20 μ m.
45 (B) Dot plot showing the proportion of Plin3⁺4C4⁺ double-positive lipid droplets among
46 total Plin3⁺ droplets at injury sites in Wt and Grn-deficient brains. Data are shown as
47 mean \pm SEM. Each point represents one animal. Significance was calculated with
48 ordinary two-way ANOVA, and post-hoc Tukey test was used for multiple comparison.
49 (C) Representative images of 4C4 (red) and BODIPY (cyan) reactivity at injury sites
50 in Wt and Grn-deficient brains. Scale bars, 20 μ m.

1 (D) Heatmaps depicting phosphatidylcholine (PC), cholesteryl ester (CE) and
2 phosphatidylethanolamine (PE) content in intact and injured (7 dpi) Wt and Grn-
3 deficient telencephali. Scale bar, z-score.

4
5 **Extended Data Fig. 3: Extended characterization of wound healing progression**
6 **in Wt and Grn-deficient CNS**

7 (A) Representative images of 4C4 (red) and Sox10 (cyan) immunoreactivity in intact
8 Wt and Grn-deficient telencephalic hemispheres. Boxed areas are magnified. Scale
9 bars, 100 μ m or 20 μ m (magnifications).

10 (B) Dot plot depicting the number of Sox10⁺ cells in intact Wt and Grn-deficient brains.
11 Data are shown as mean \pm SEM. Each point represents one animal. Significance was
12 calculated using Student's t-test.

13 (C) Representative images of DAPI (white) labelling in intact and injured (3 and 7 dpi)
14 Wt and Grn-deficient telencephali. Scale bars, 100 μ m.

15 (D) Scheme depicting the experimental timeline of dexamethasone/methanol
16 manipulations in the adult Grn-deficient brain at 3 dpi.

17 (E) Representative images of 4C4 (red) and Sox10 (cyan) of
18 methanol/dexamethasone-treated Grn-deficient animals at 3 dpi. Scale bars, 100 μ m
19 or 20 μ m (magnifications).

20 (F) Dot plot depicting the number of Sox10⁺ cells at injury sites in
21 methanol/dexamethasone-treated Grn-deficient animals at 3 dpi. Data are shown as
22 mean \pm SEM. Each point represents one animal. Significance was calculated using
23 Student's t-test.

24
25 **Extended Data Fig. 4: Extended scRNA-seq analysis of Wt and Grn-deficient**
26 **cells**

27 (A) UMAP plot depicting color-coded cellular clusters identified on the basis of the
28 single-cell transcriptome analysis of cells, isolated from intact and injured (3 and 7 dpi)
29 Wt and Grn-deficient zebrafish telencephali. Cells are colored according to their cell
30 type identity; each point represents a single cell.

31 (B) UMAP plots depicting color-coded intact and injured (3 and 7 dpi) conditions from
32 Wt and Grn-deficient zebrafish telencephali. Cells are colored according to the
33 condition they are isolated from; each point represents a single cell.

34 (C) UMAP plots depicting characteristic cell-type marker gene expression (identifying
35 microglial, radial glial, oligodendroglial and neuronal clusters) in single cells isolated
36 from intact and injured (3 and 7 dpi) Wt and Grn-deficient zebrafish telencephali.
37 Scale, normalized expression level; each point represents a single cell.

38 (D) UMAP plot depicting subclustering of Wt and Grn-deficient microglial cells in intact
39 an injured telencephali based on their transcriptome. Cells are colored according to
40 their microglial subcluster identity; each point represents a single cell. (Same as Fig.
41 4A).

42 (E) Abundance of microglial subclusters (from Fig. S4D) from different Wt and Grn-
43 deficient conditions: intact (left), 3 dpi (middle) and 7 dpi (right).

44 (F) Similarity matrix depicting correlation between Wt-only microglial subclusters (from
45 Fig. 1) and merged (Wt and Grn-deficient) microglial subclusters (from Fig. 4). Scale
46 bar, similarity index.

47 (G) UMAP plots depicting the cell identity of Wt microglia to correlate Wt-only
48 microglial subclusters (from Fig. 1) and merged (Wt and Grn-deficient) microglial
49 subclusters (from Fig. 4).

50

1 **Extended Data Fig. 5: Characterization of TDP-43⁺ condensate formation and**
2 **clearance in response to brain injury**

3 (A) Representative images of HuC/D (magenta) and TDP-43 (cyan) immunoreactivity
4 in intact zebrafish telencephalon. Scale bar, 100 μ m or 20 μ m (magnifications).

5 (B) Representative images of 4C4 (magenta) and TDP-43 (cyan) immunoreactivity
6 with orthogonal projections at injury sites of Wt and Grn-deficient brains displaying
7 colocalization of TDP-43⁺ condensates with 4C4⁺ microglial cells. Scale bar, 20 μ m.

8 (C) Experimental paradigm of the intraparenchymal recombinant progranulin (PGRN)
9 injections in the adult Grn-deficient zebrafish.

10 (D) Representative images of 4C4 (magenta) and TDP-43 (cyan) immunoreactivity at
11 injury sites of vehicle- and PGRN-injected Grn-deficient animals. Scale bars, 100 μ m
12 or 20 μ m (magnifications).

13 (E) Dot plot depicting the numbers of TDP-43⁺ condensates at injury sites of Wt, Grn-
14 deficient and PGRN-injected Grn-deficient animals at 7 dpi. Data are shown as mean
15 \pm SEM. Each point represents one animal. Significance was calculated with ordinary
16 one-way ANOVA, and post-hoc Tukey test was used for multiple comparison. *p <
17 0.05, **p < 0.01, ***p < 0.001, ****p < 0.0001.

18

19 **Extended Data Fig. 6: Specificity of phase-separated TDP-43 overload in**
20 **promoting persistent neuroinflammation**

21 (A) Scheme depicting the experimental paradigm of intraparenchymal injections of
22 vehicle/uncleaved/cleaved TDP-43 and FUS in Wt zebrafish.

23 (B) Coomassie blue-stained SDS-PAGE gel of different intraparenchymal injection
24 solutions: vehicle (buffer + TEV), TDP-43 (uncleaved) and phase-separated TDP-43
25 (cleaved).

26 (C) Representative bright field microscopy images of phase-separated TDP-43
27 (cleaved) and unseparated TDP-43 (uncleaved). Scale bar, 50 μ m or 25 μ m
28 (magnifications).

29 (D) Representative images of 4C4 (magenta) and TDP-43 (cyan) in injured (7 dpi) Wt
30 telencephali injected with TDP-43 (uncleaved) or phase-separated (cleaved) TDP-43.
31 Scale bar, 20 μ m.

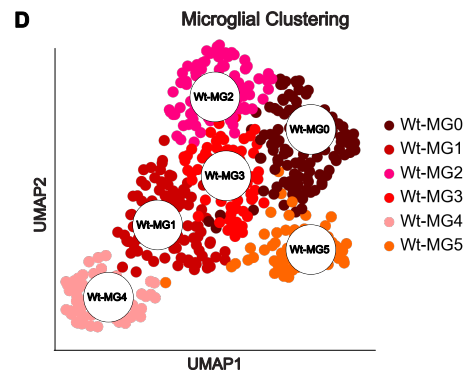
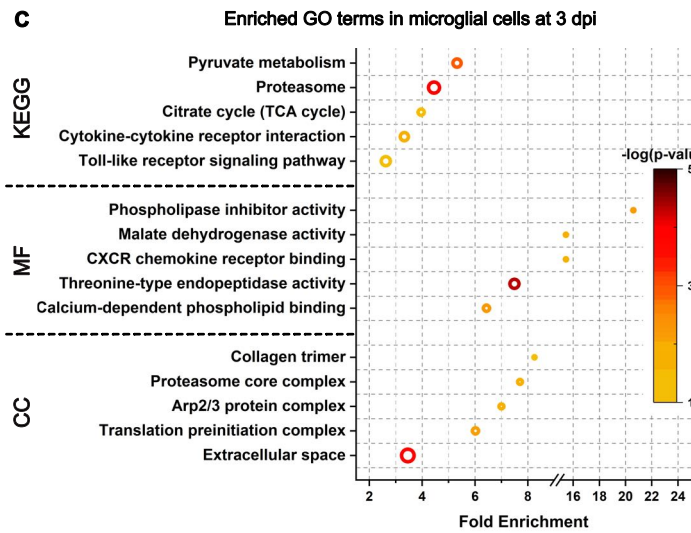
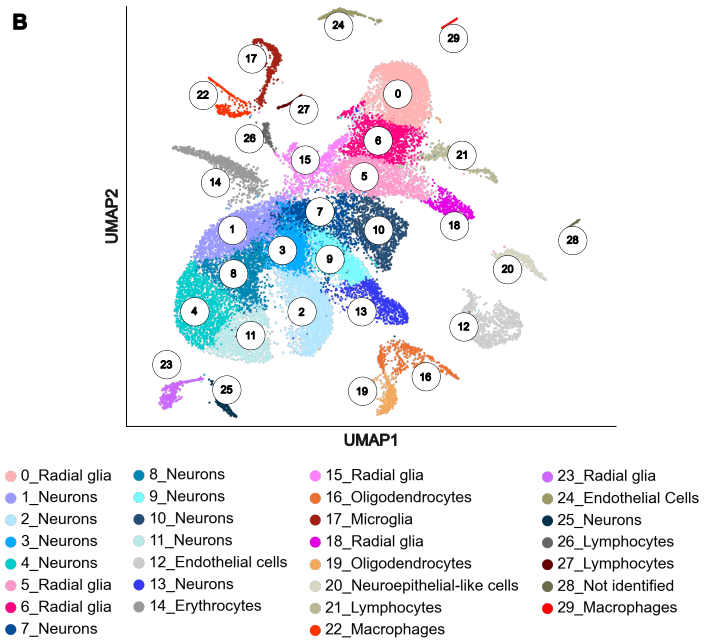
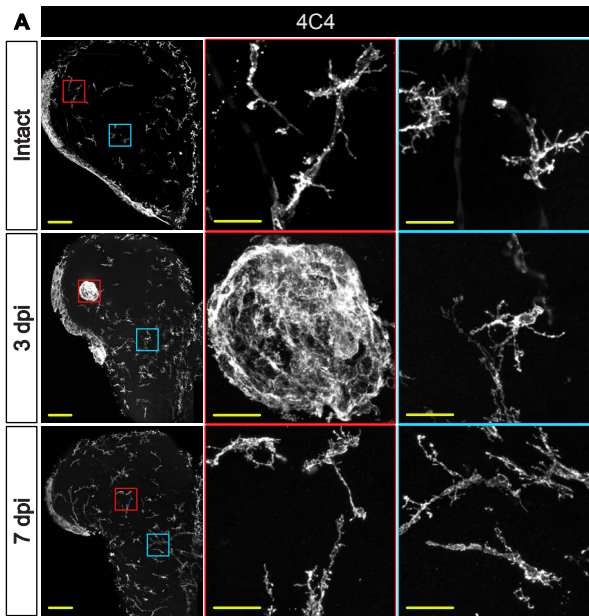
32 (E) Dot plot depicting the total number of TDP-43⁺ condensates at injury sites in
33 vehicle-, TDP-43- and phase-separated TDP-43-injected Wt animals at 7 dpi. Data are
34 shown as mean \pm SEM. Each point represents one animal. Significance was
35 calculated with ordinary one-way ANOVA, and post-hoc Tukey test was used for
36 multiple comparison. *p < 0.05, **p < 0.01.

37 (F) Dot plot depicting the expression of *tardbp* and *tardbpl* genes in microglia in
38 different Wt conditions. Dot color, mean expression; dot size, fraction of cells.

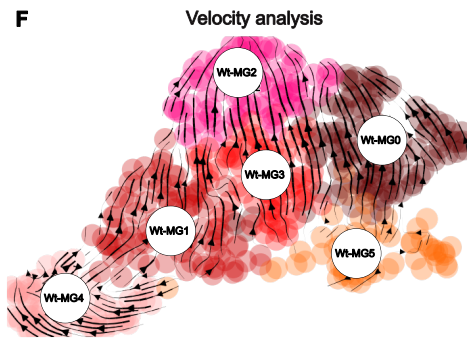
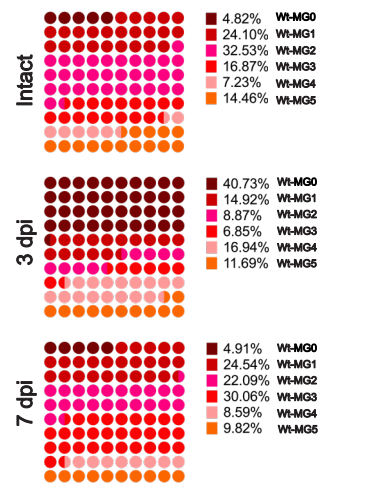
39 (G) Schematic representation of FUS (containing MBP tag) and phase-separated
40 (MBP tag cleaved off) FUS proteins.

41 (H) Representative images of 4C4 (magenta) and Plin3 (green) in Wt injured (7 dpi)
42 telencephali injected with FUS (uncleaved) or phase-separated (cleaved) FUS. Scale
43 bar, 20 μ m.

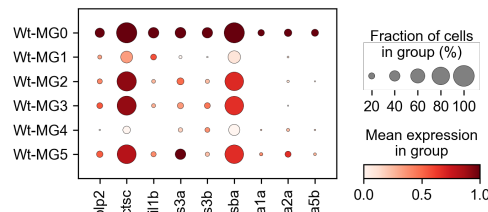
44 (I-J) Dot plots depicting the total numbers of Plin3⁺ lipid droplets (I) and numbers of
45 Plin3⁺ lipid droplets within 4C4⁺ microglia (J) at injury sites in vehicle/FUS-injected
46 Wt animals. Data are shown as mean \pm SEM. Each point represents one animal.
47 Significance was calculated with ordinary one-way ANOVA, and post-hoc Tukey test
48 was used for multiple comparison.



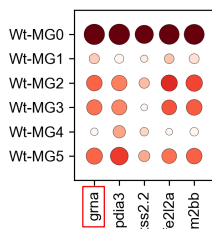
E Cell proportion in microglial clusters



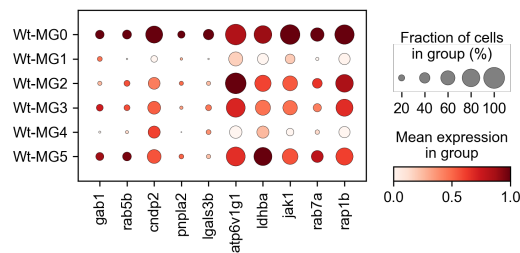
G Conserved genes in regenerative mouse microglia



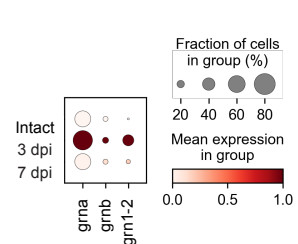
H Top 5 significant genes in Wt-MG0

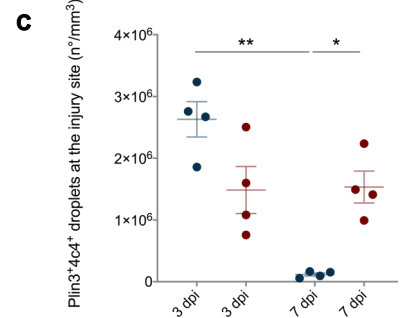
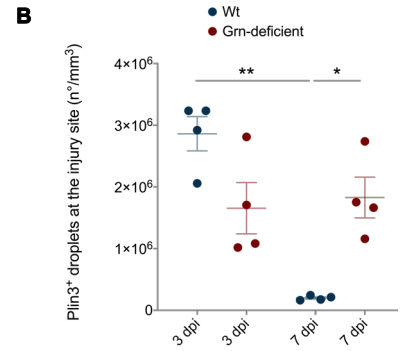
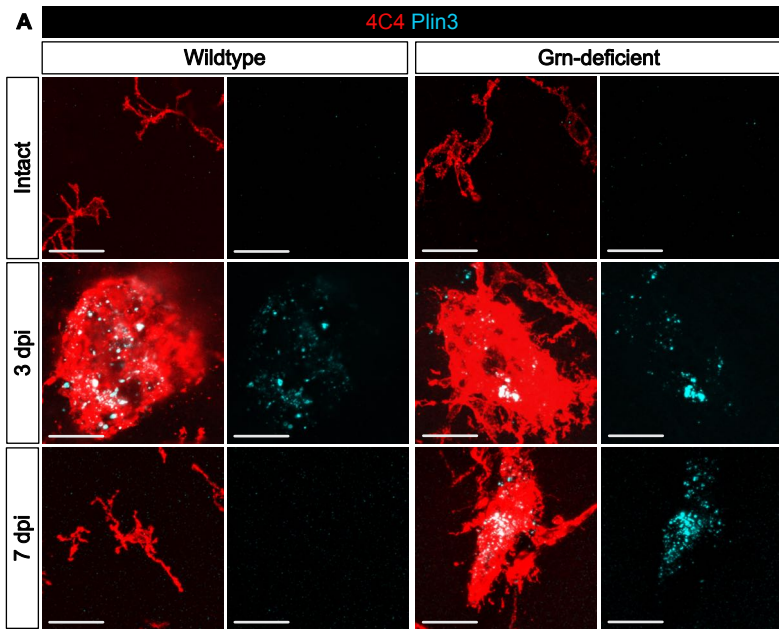


I Enriched genes in lipid droplet-accumulating microglia

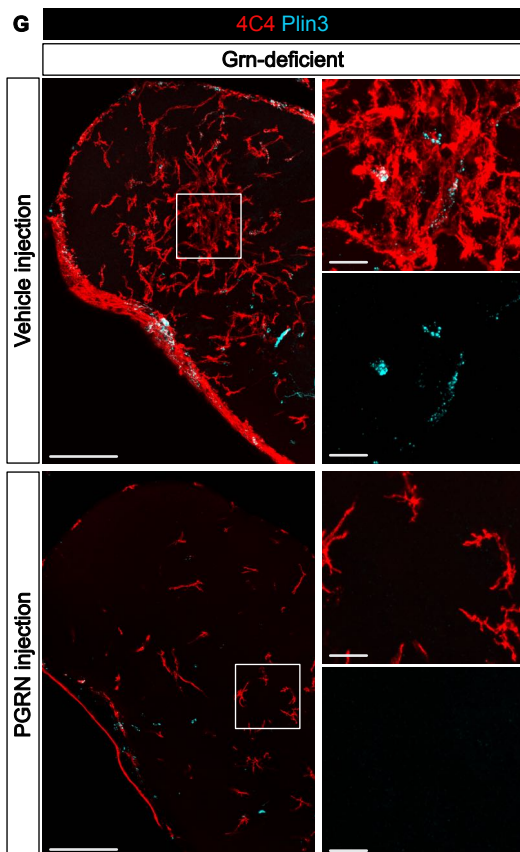
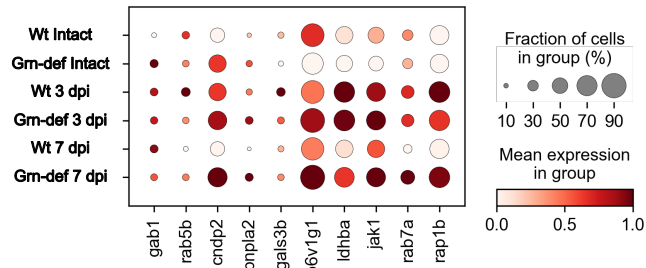


J Granulin expression in response to injury

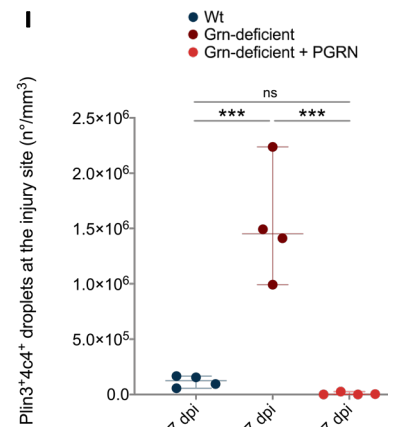
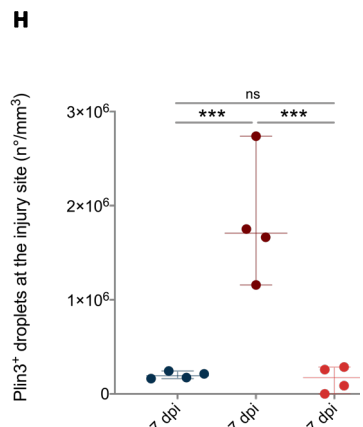
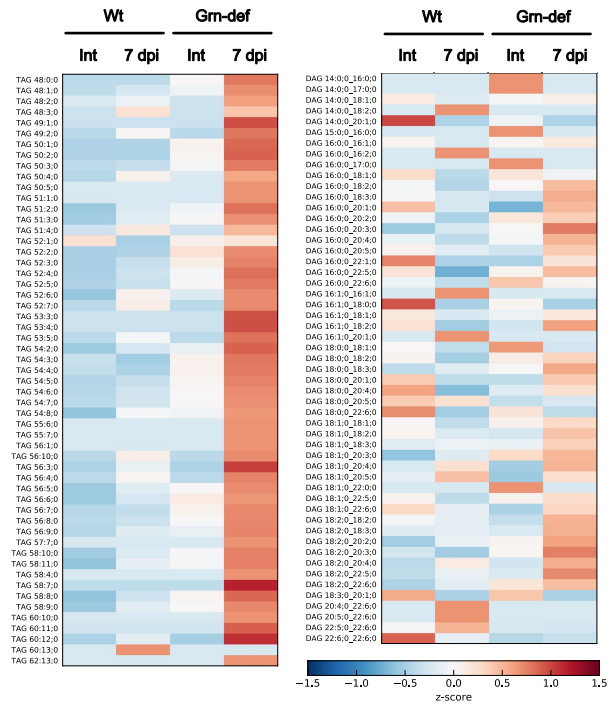


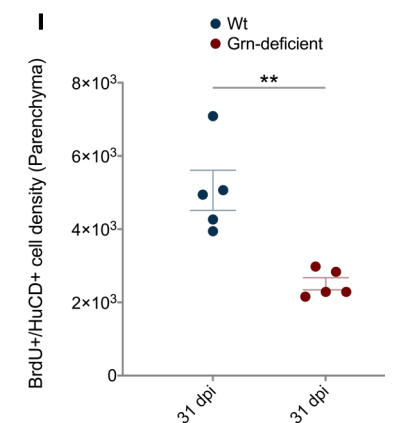
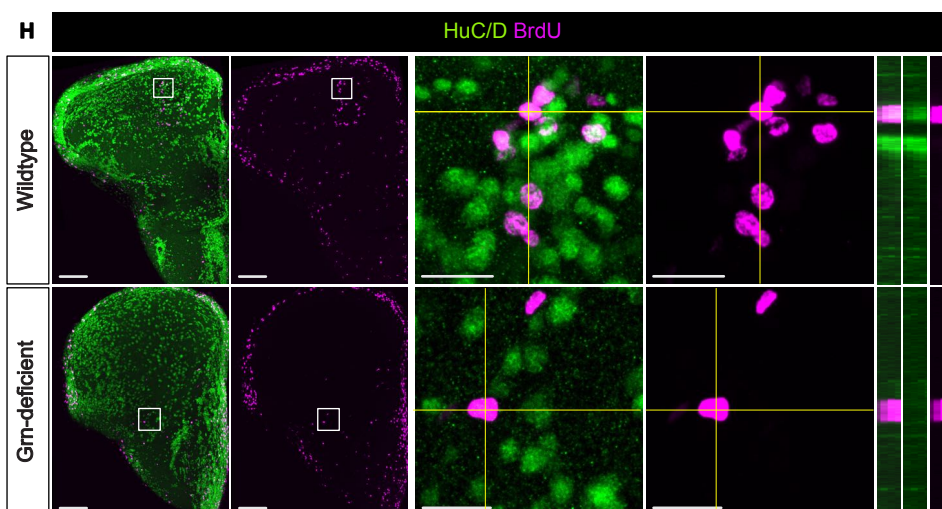
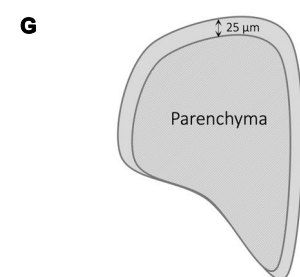
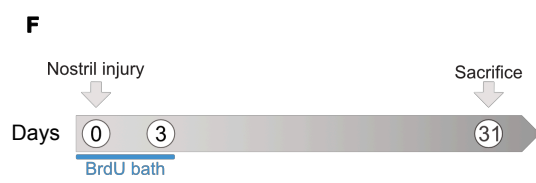
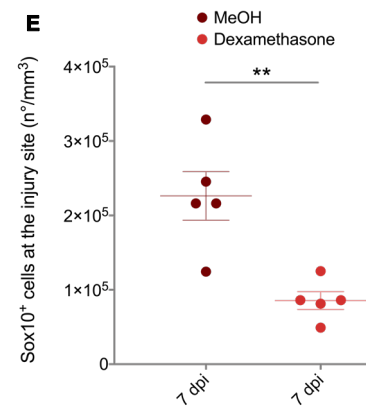
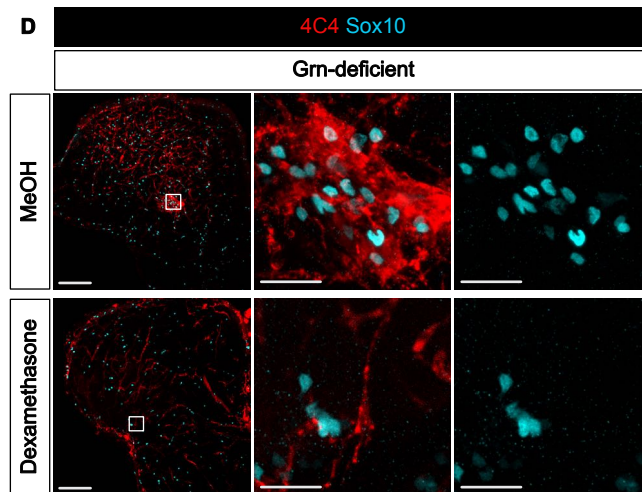
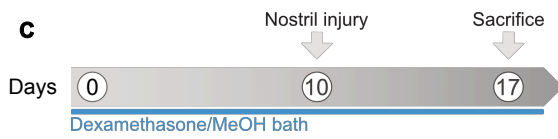
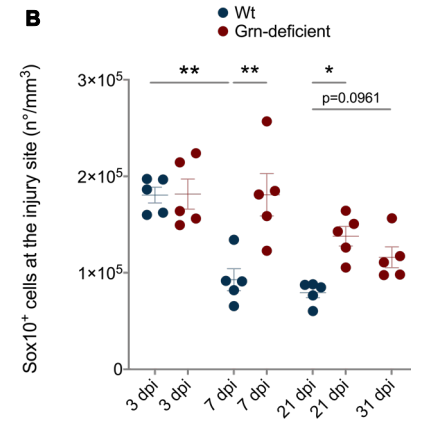
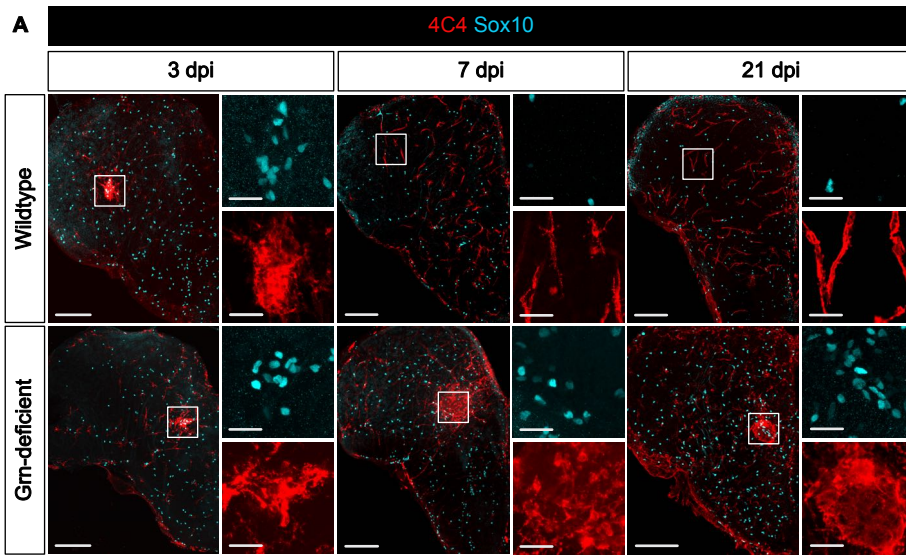


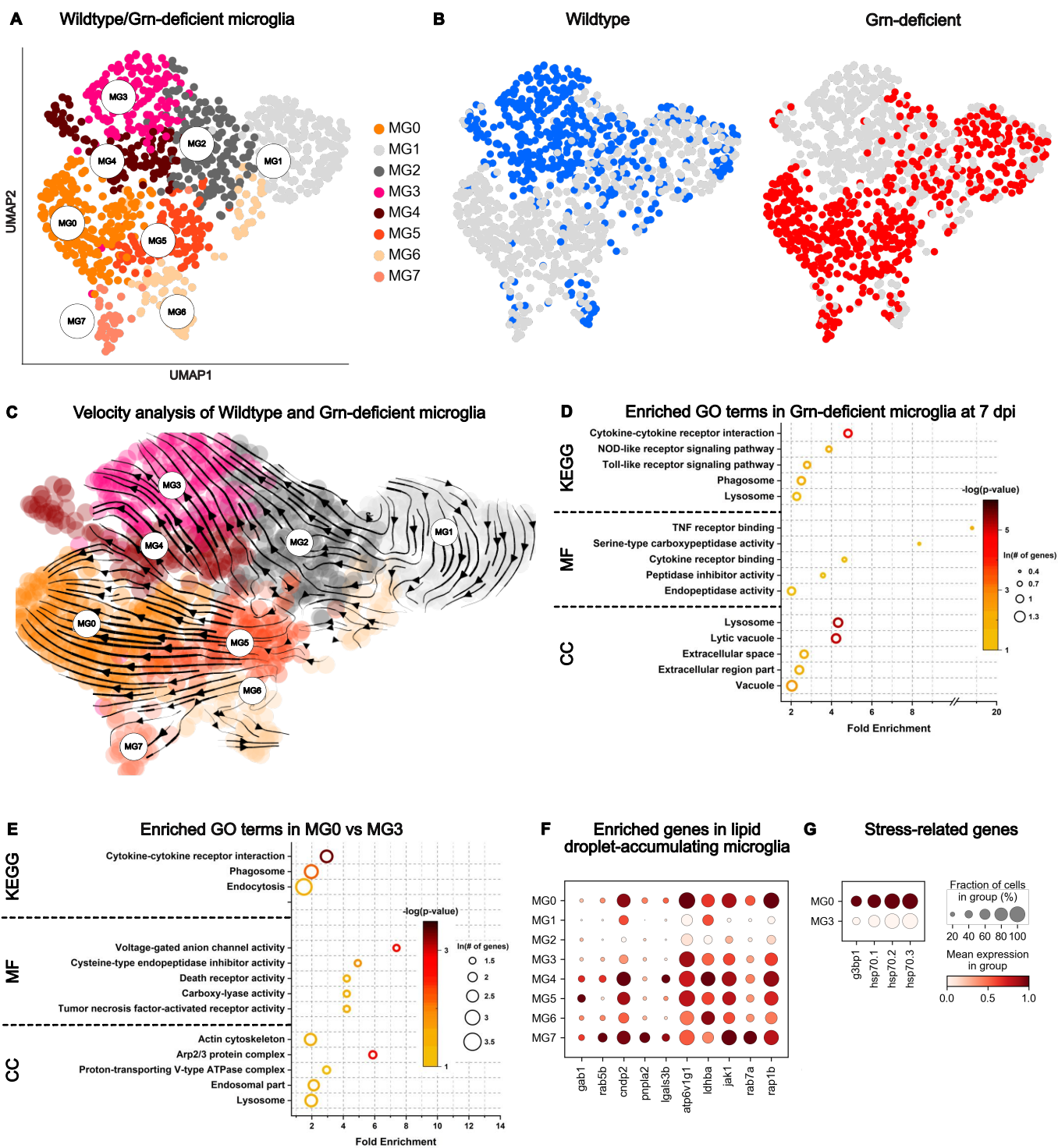
D Enriched genes in lipid droplet-accumulating microglia

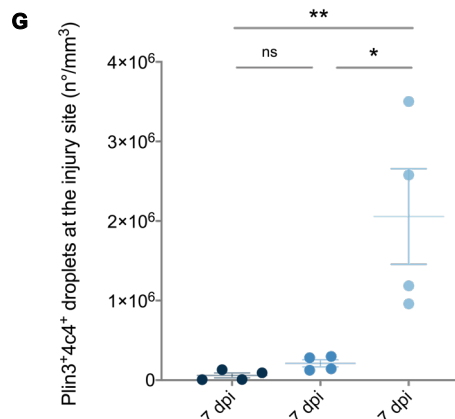
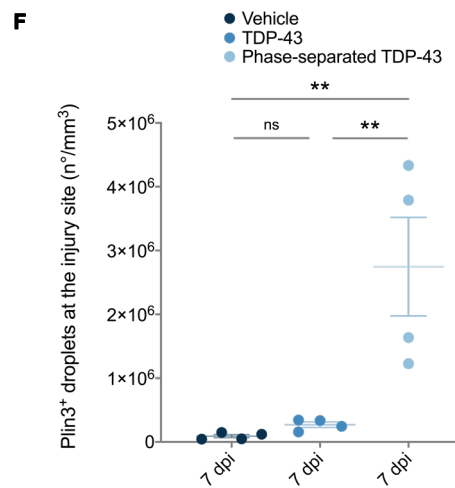
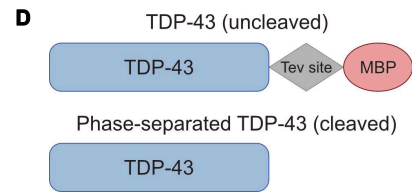
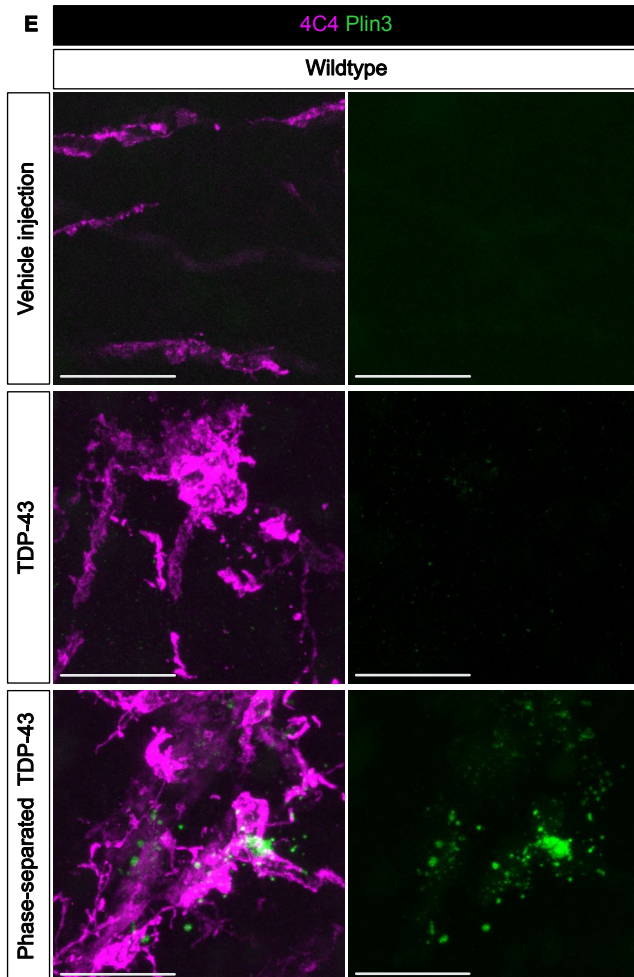
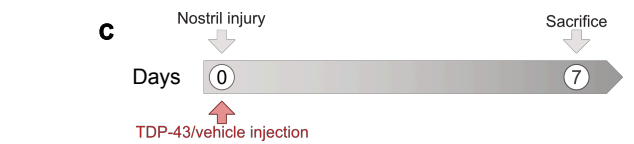
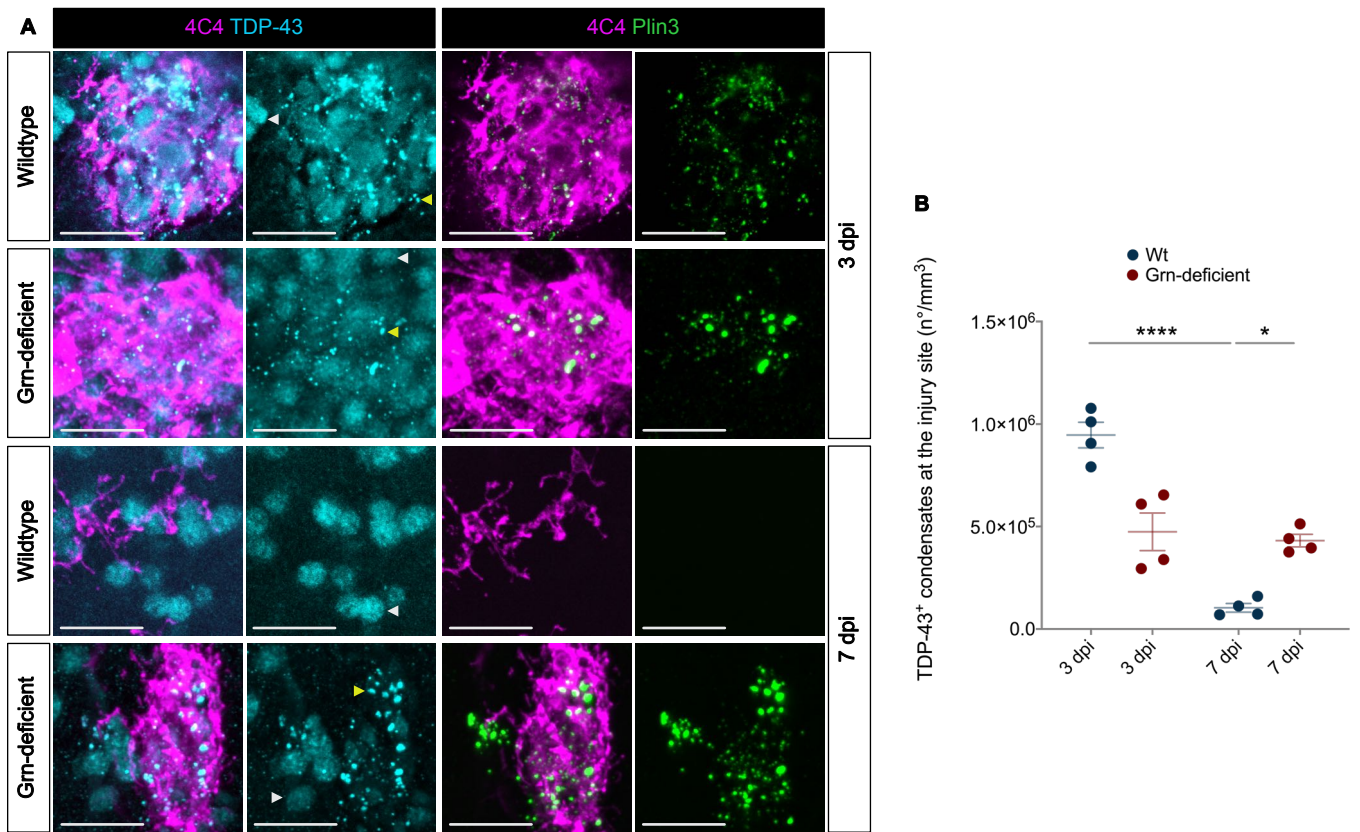


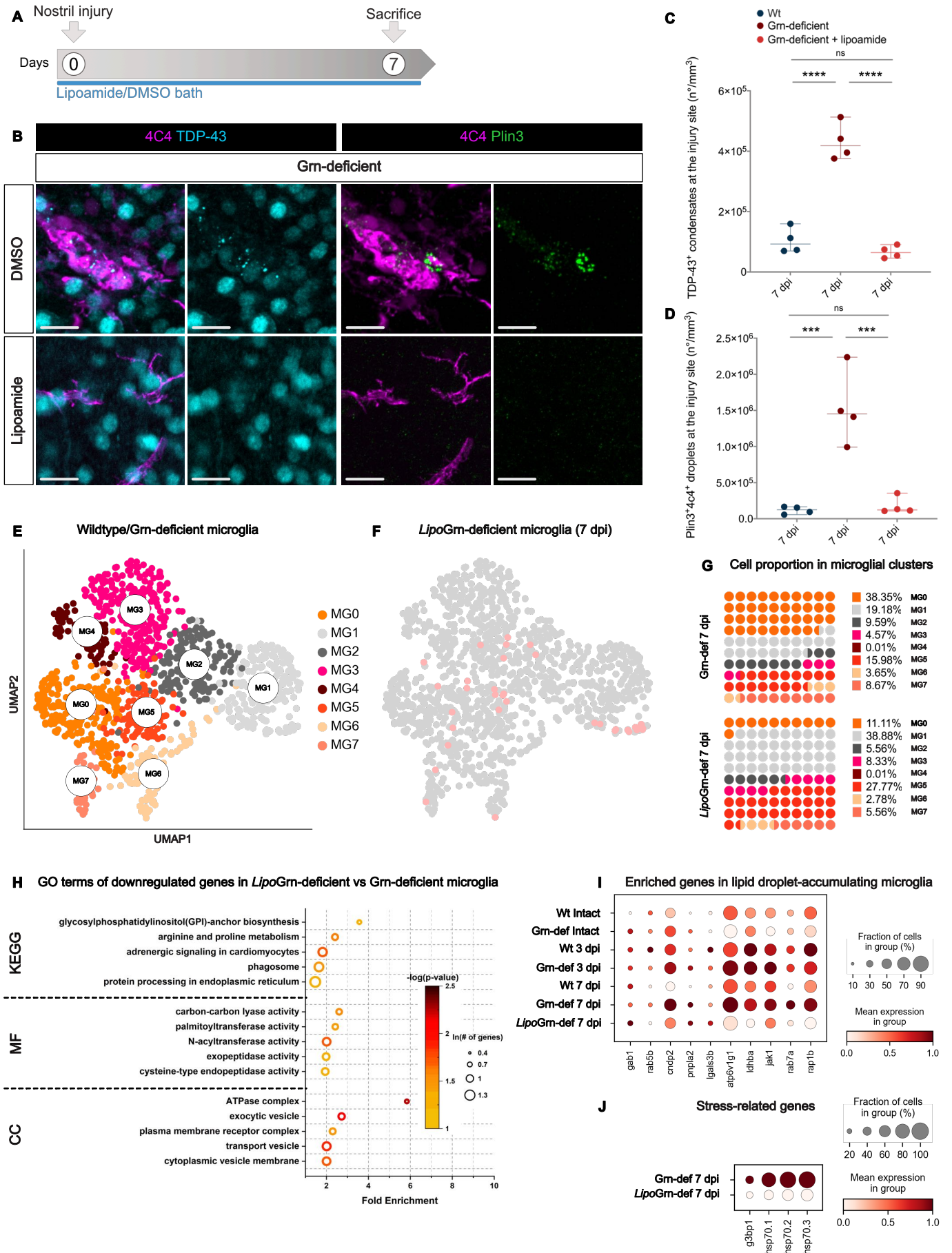
E Lipidomic analysis of zebrafish telencephali



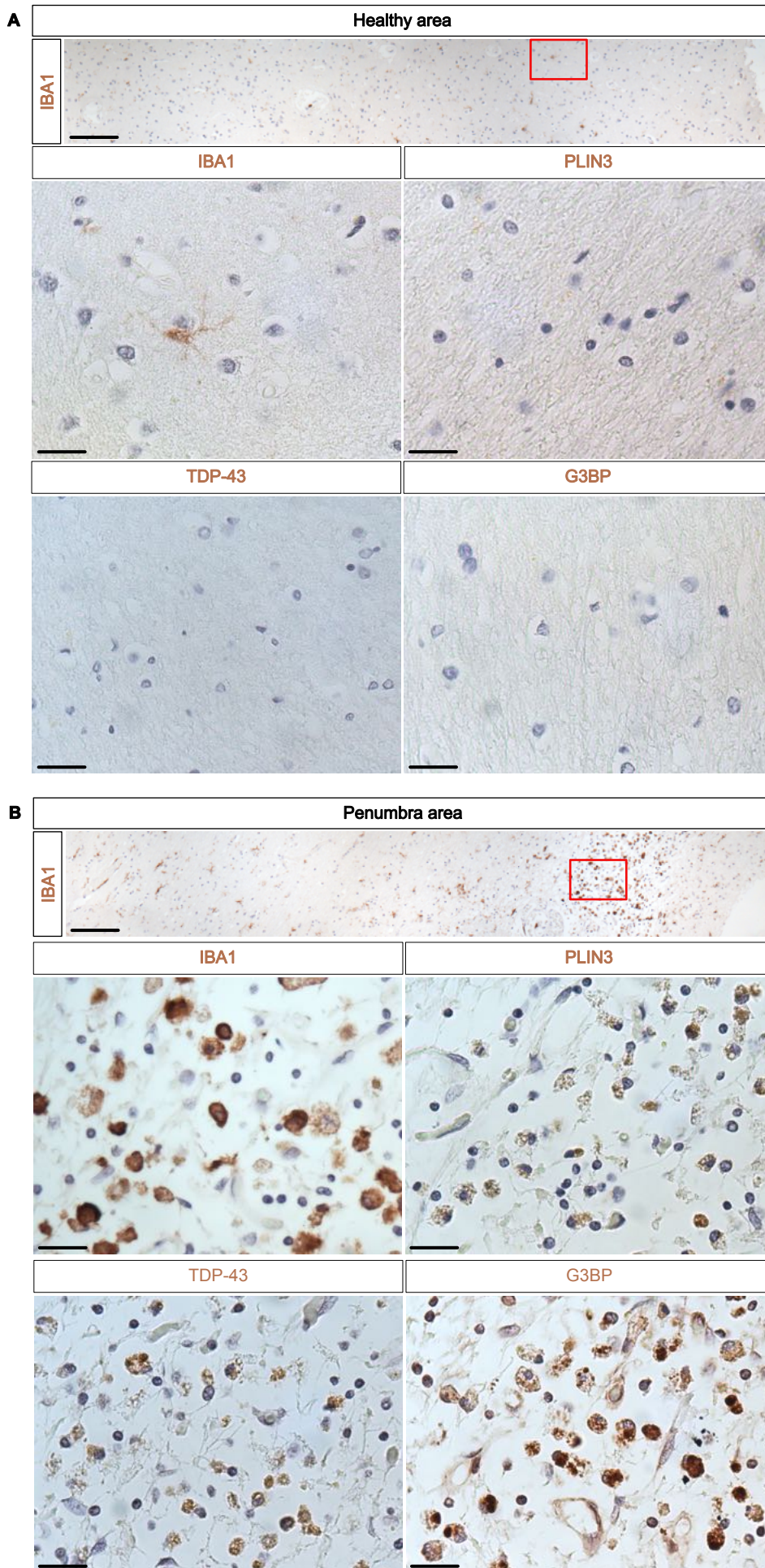


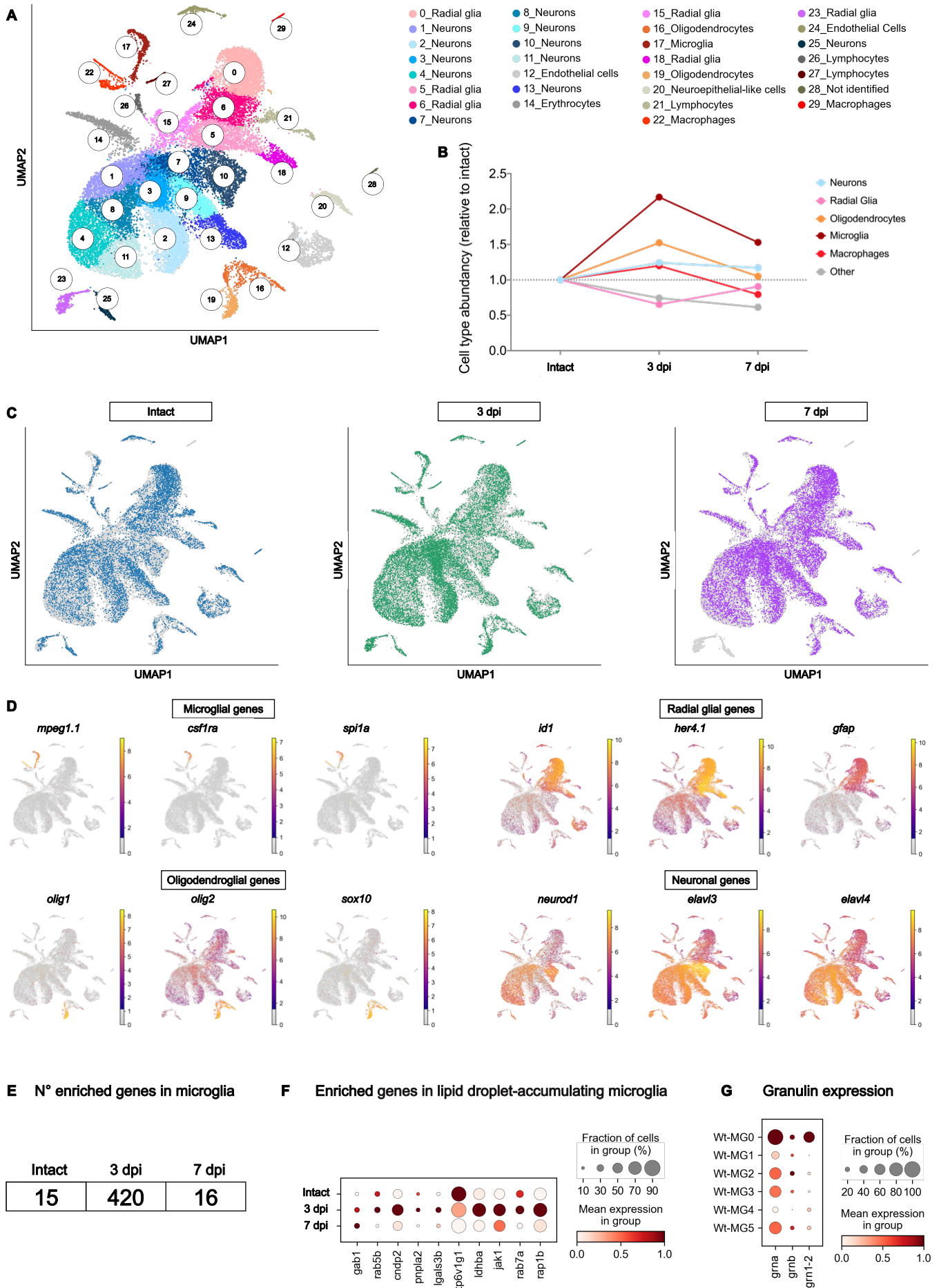


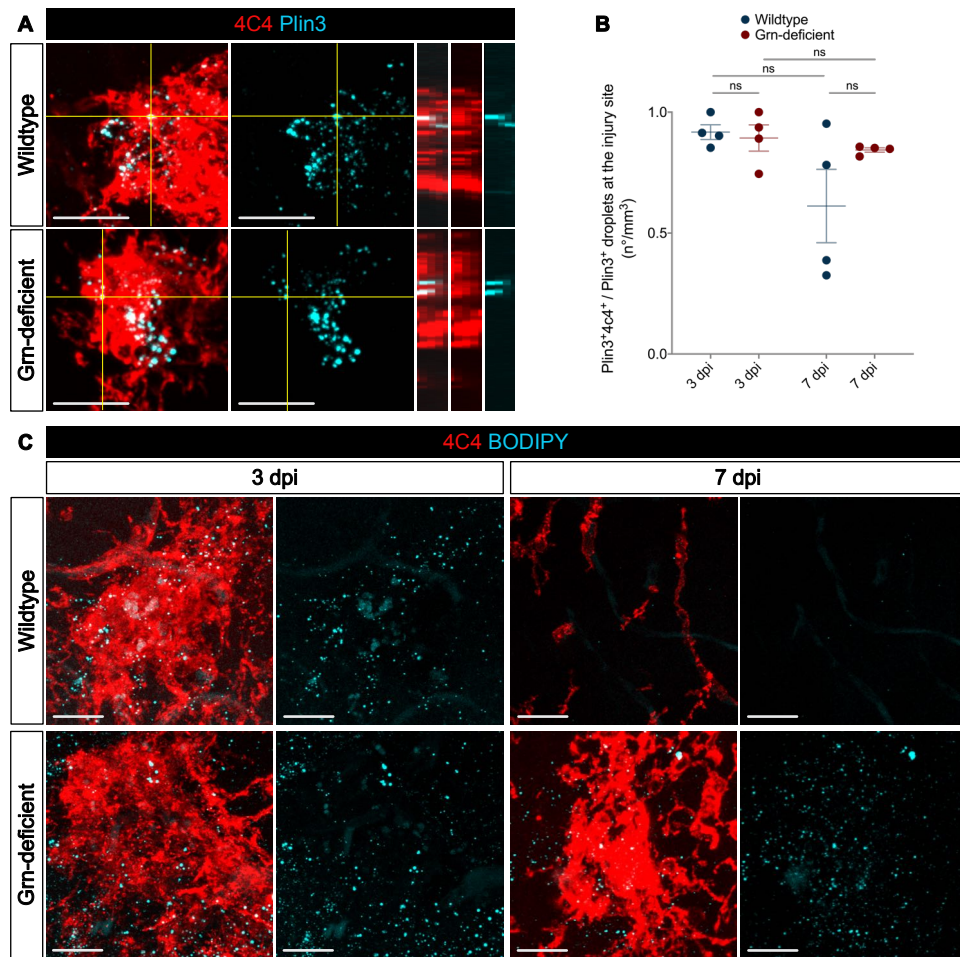


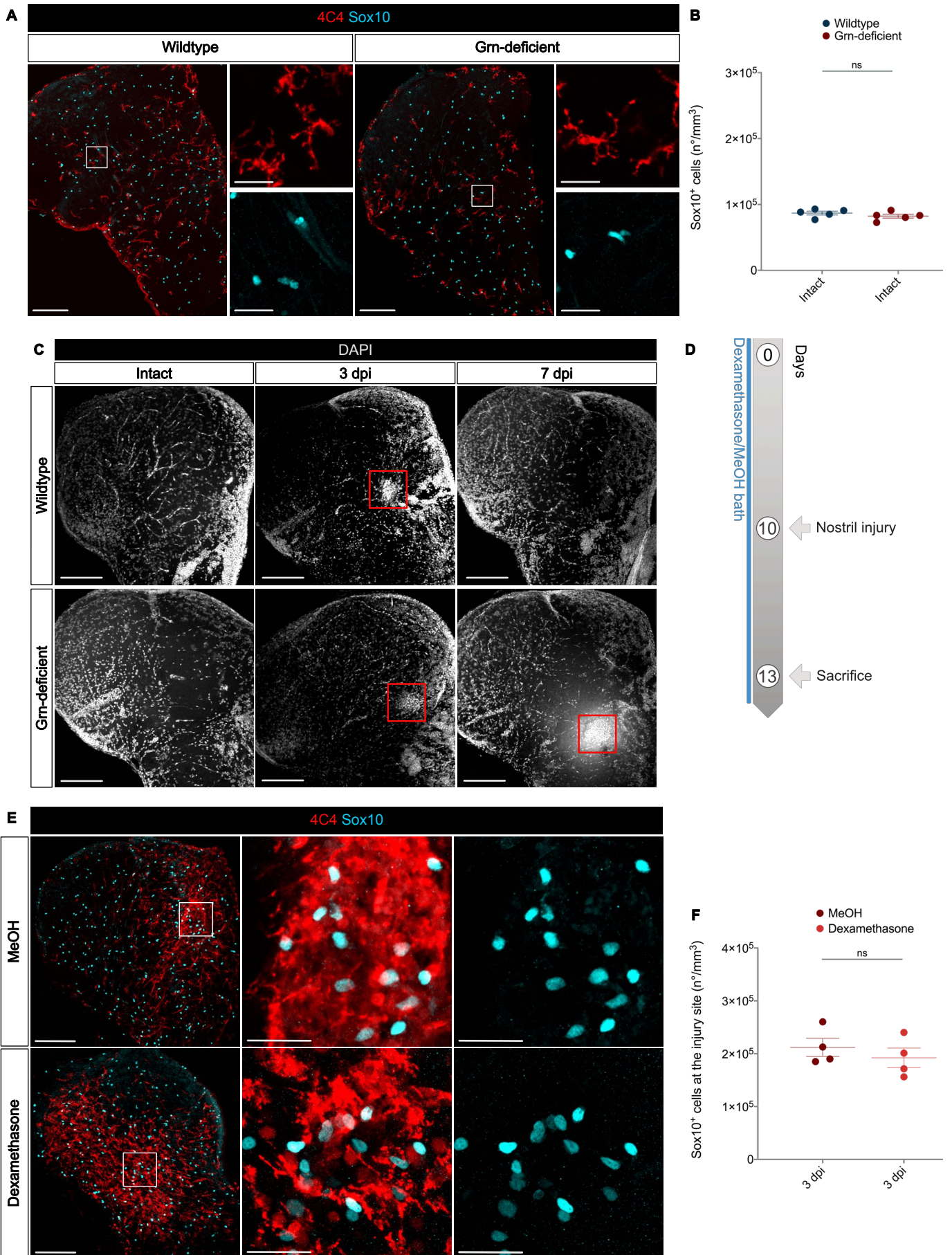


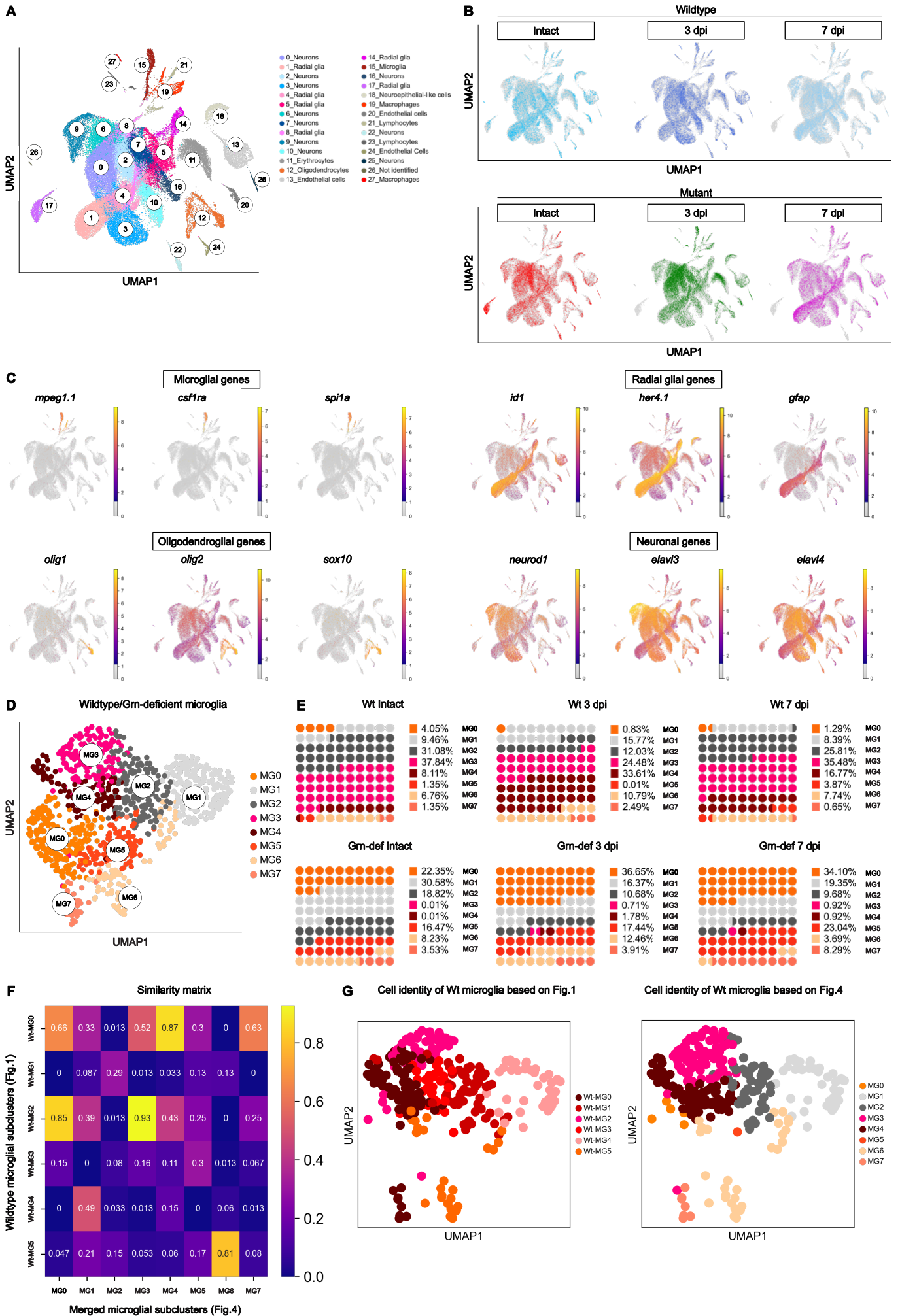
Zambusi, Novoselc et al., Fig. 6

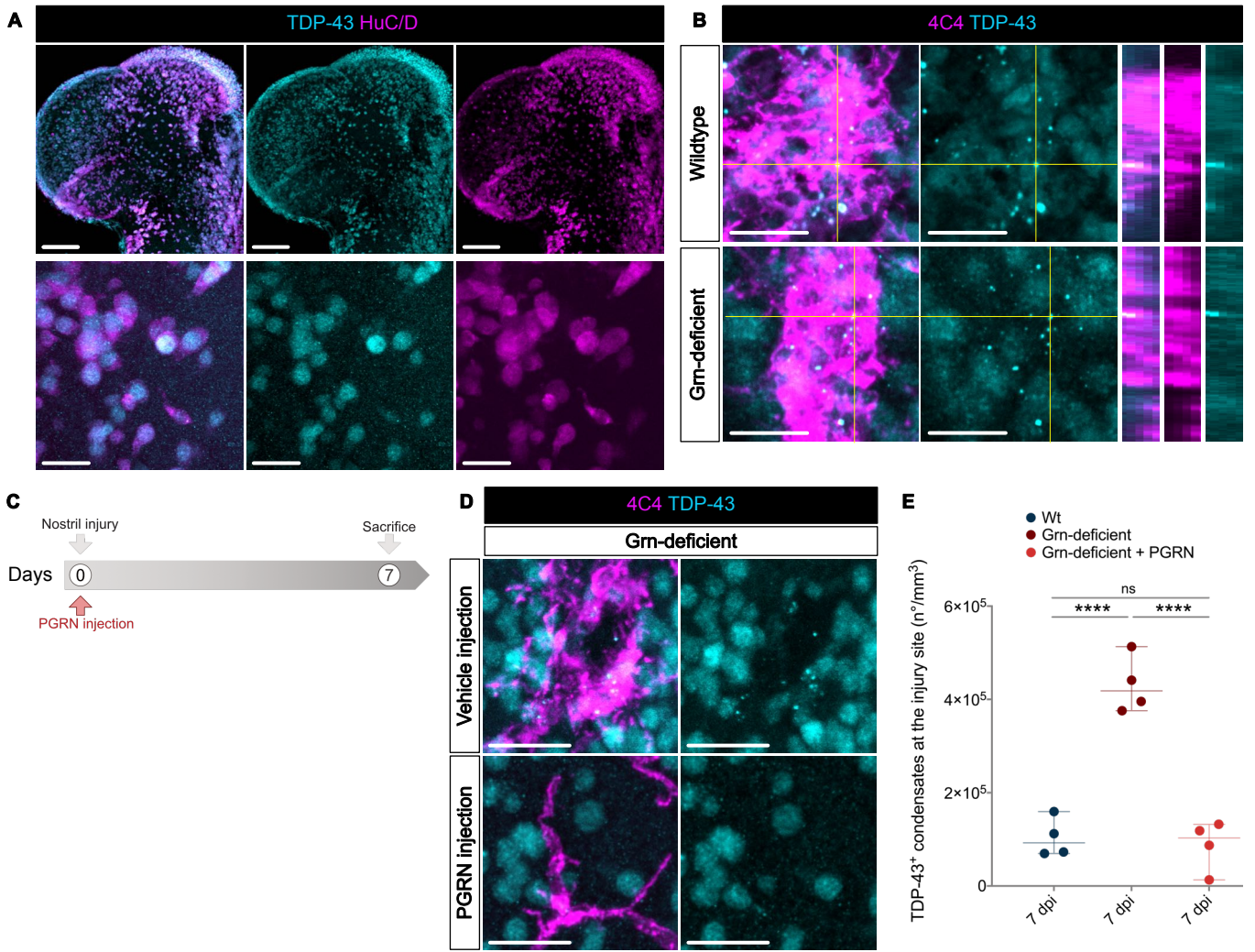


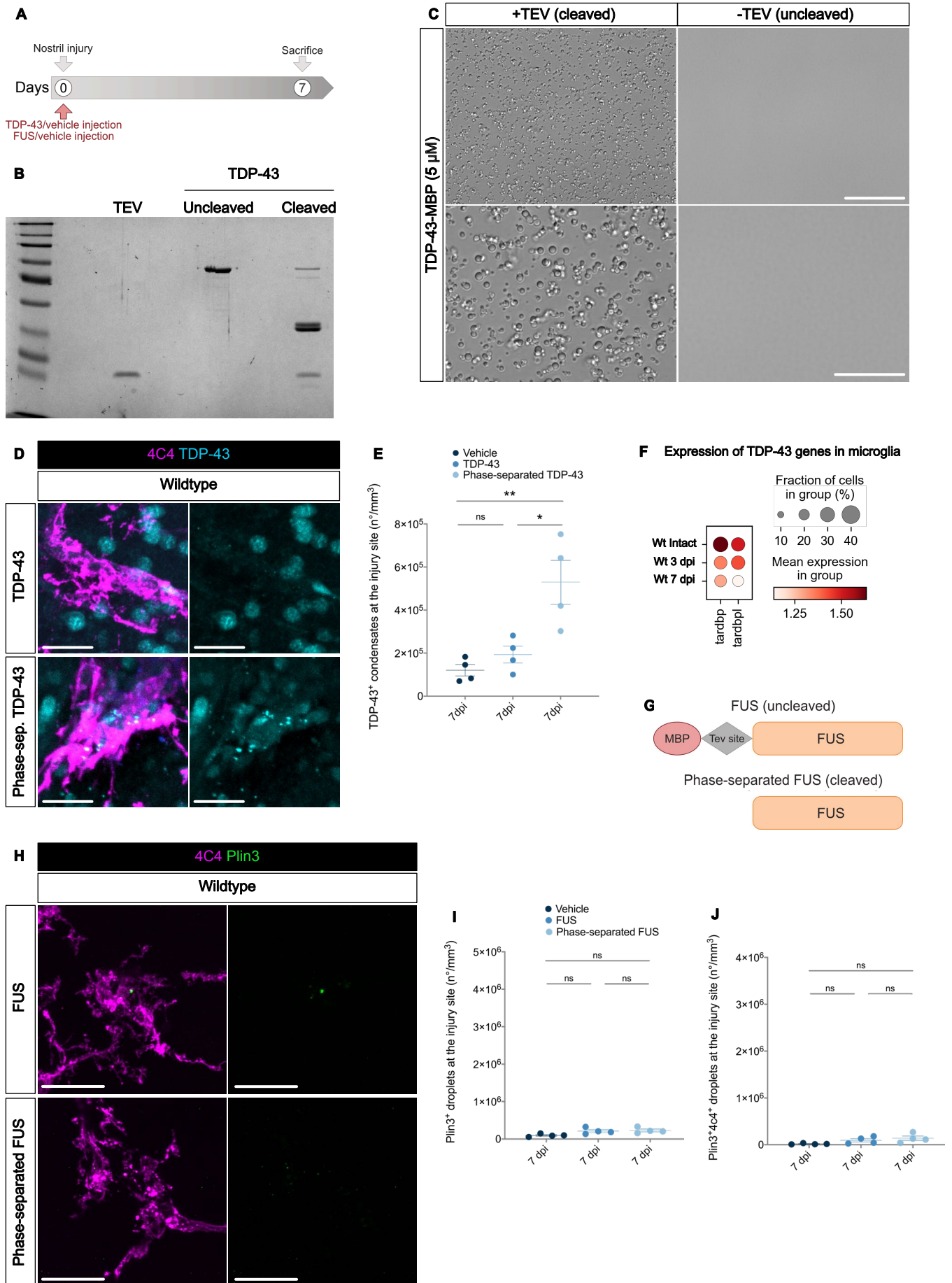












Aim of the study IV

The aim of the study is to investigate:

The functional role of innate immunity in a model of telencephalic injury characterized by prolonged glial cell accumulation and neuroinflammation.

Activation of innate immune pathways after brain injury promotes scar formation and impairs tissue recovery

Rosario Sanchez-Gonzalez, Christina Koupourtidou, Tjasa Lepko, **Alessandro Zambusi**, Klara Tereza Novoselc, Tamara Durovic, Sven Aschenbroich, Veronika Schwarz, Christopher Breunig, Hans Straka, Hagen Huttner, Martin Irmeler, Johannes Beckers, Wolfgang Wurst, Andreas Zwergal, Tamas Schauer, Tobias Straub, Tim Czopka, Dietrich Trümbach, Magdalena Götz, Stefan Stricker, Jovica Ninkovic.

For this paper I was involved in performing FACS sorting and preparing RNA-Seq libraries from FACS isolated cells.

I was also involved in editing and reviewing the paper.

The paper has been resubmitted after revision to EMBO Journal.

1 **Activation of innate immune pathways after brain injury promotes scar**
2 **formation and impairs tissue recovery**

3 **Authors:** Rosario Sanchez-Gonzalez^{1,2}, Christina Koupouridou^{1,3,4}, Tjasa Lepko^{1,3,4},
4 Alessandro Zambusi^{1,3,4}, Klara Tereza Novoselc^{1,3,4}, Tamara Durovic^{1,3,4}, Sven
5 Aschenbroich^{1,3,4}, Veronika Schwarz^{1,3,4}, Christopher T Breunig^{5,6}, Hans Straka², Hagen B.
6 Huttner⁷, Martin Irmeler⁸, Johannes Beckers^{8,9,10}, Wolfgang Wurst^{11,12,13,14}, Andreas Zwergal¹⁵,
7 Tamas Schauer¹⁶, Tobias Straub¹⁶, Tim Czopka¹⁷, Dietrich Trümbach¹¹, #, Magdalena
8 Götz^{1,12,18}, Stefan H Stricker^{5,6}, Jovica Ninkovic^{1,3,12*}

9 **Affiliations:**

10 ¹ Institute of Stem Cell Research, Helmholtz Center Munich, Germany

11 ² Department Biology II, University of Munich, Germany

12 ³ Biomedical Center (BMC), Division of Cell Biology and Anatomy, Faculty of Medicine,
13 LMU Munich, Germany

14 ⁴ Graduate School Systemic Neurosciences, LMU, Munich, Germany.

15 ⁵ Reprogramming and Regeneration, Biomedical Center (BMC), Physiological Genomics,
16 Faculty of Medicine, LMU Munich

17 ⁶ Epigenetic Engineering, Institute of Stem Cell Research, Helmholtz Center Munich,
18 Germany

19 ⁷ Department of Neurology, Justus-Liebig-University Giessen, Giessen

20 ⁸ Institute of Experimental Genetics, Helmholtz Center Munich, Germany

21 ⁹ German Center for Diabetes Research (DZD), Germany

22 ¹⁰ Chair of Experimental Genetics, School of Life Sciences Weihenstephan, Technical
23 University Munich, Germany

24 ¹¹ Institute of Developmental Genetics, Helmholtz Center Munich, Germany

25 ¹² Munich cluster for Systems Neurology SYNERGY, LMU, Munich, Germany

26 ¹³ Chair of Developmental Genetics c/o Helmholtz Zentrum München, School of
27 Life Sciences Weihenstephan, Technical University Munich, Germany

28 ¹⁴ German Center for Neurodegenerative Diseases (DZNE), Site Munich, Germany

29 ¹⁵ Department of Neurology, Ludwig-Maximilians University, Campus Grosshadern,
30 Munich, Germany

31 ¹⁶ Biomedical Center (BMC), Bioinformatic Core Facility, Faculty of Medicine, LMU
32 Munich, Germany

33 ¹⁷ Centre for Clinical Brain Sciences, University of Edinburgh, Edinburgh, UK

34 ¹⁸ Biomedical Center (BMC), Division of Physiological Genomics, Faculty of Medicine,
35 LMU Munich, Germany

36 *Correspondence to: ninkovic@helmholtz-muenchen.de

37 # Present address: Institute of Metabolism and Cell Death, Helmholtz Center, Munich,
38 Germany

1 **Summary**

2 Scar formation is a major hindrance to central nervous system recovery after traumatic injury
3 with glial cells as a key player. Here, we used the regenerative potential of zebrafish
4 telencephalon to identify specific molecular and cellular mechanisms regulating glial scar
5 formation. We demonstrated that the influx of the cerebrospinal fluid into the brain parenchyma
6 after injury simultaneously activates toll-like receptor 2 (Tlr2) and the chemokine receptor 3
7 (Cxcr3) innate immunity pathways, leading to the initiation of a glial scar. These pathways
8 were critical for scarring even after ablation of microglia and infiltrating monocytes. Our data
9 support a specific role for the injury-induced Tlr1/2 and Cxcr3 signaling pathways in
10 controlling the proliferation of oligodendrocyte progenitors and thereby exacerbated glial
11 reactivity, contributing to scar formation. Interference with the Tlr1/2 and Cxcr3 pathways after
12 injury alleviated glial scar formation, increased new neuron recruitment and improved tissue
13 restoration.

14

1 **Introduction**

2 The ability to heal the wound and re-establish tissue function is critical after a traumatic
3 injury. Wound closure in the mammalian central nervous system (CNS) is often accompanied
4 by the formation of non-functional tissue known as glial scar^{1,2}. Glial cells play a critical role
5 during the wound healing and scarring response. Initial glial activation is essential for wound
6 closure and restoration of the normal brain milieu³⁻⁶. However, long-term effects include
7 aversive extracellular matrix modifications and exacerbated inflammation⁷⁻⁹. Broad
8 interference with initial glial activation after mammalian CNS injuries hampers the
9 regenerative response in both brain¹⁰ and spinal cord^{9,11}. Therefore, there is a need to identify
10 pathways that specifically lead to prolonged glial activation, scar formation and restricted
11 regeneration.

12 In contrast to mammals, zebrafish have mechanisms to restore brain tissue after
13 inserting a capillary through the nostrils^{6,12-18}, and to functionally recover spinal cord circuitry
14 after full or partial trans-section^{12,13}. Functional recovery in the zebrafish CNS correlates with
15 the capacity to regulate the neuroinflammatory landscape and induce the restorative
16 neurogenesis (neuronal replacement) from endogenous sources¹⁴. The basis for neuronal
17 replacement resides in the injury-induced activation of neural stem cell-like ependymogial
18 cells¹⁵. The initial microglial reaction to injury activates developmental and/or injury-specific
19 regulatory pathways in ependymogial cells¹⁵, regulating the timely production of new neurons
20 necessary for tissue recovery¹⁹. Interference with the crosstalk between microglia and
21 ependymogial cells or with timely resolution of neuroinflammation, leads to aberrant
22 neurogenesis and neuronal cell death, similar to observations in the mammalian brain^{16,17,20}.
23 Although several regulatory mechanisms mediating the crosstalk between immune and
24 ependymogial cells have been identified¹⁵, little is known about the mechanisms that restrict
25 the initial phase of neuroinflammation, introducing a permissive time window for the
26 integration of new neurons.

27 The induction of the glial scar has been associated with activation of particular glial
28 cell types such as astrocytes, oligodendrocyte progenitors (OPCs) and pericytes⁶. The absence
29 of protoplasmic astrocytes has been proposed as a possible reason for scarless regeneration in
30 the zebrafish brain⁶. However, recent studies suggest that the scarring process is defined by a
31 specific, temporarily regulated inflammatory signature, rather than by the cellular milieu
32 present prior to injury²¹. Indeed, the zebrafish telencephalon exhibits different regenerative
33 outcomes depending on the injury paradigm. While injuries performed rostro-caudally through

1 the nostrils regenerate in a scarless manner as described above^{14,19,22}, injuries along the dorso-
2 ventral axis induce exacerbated and prolonged reaction of oligodendroglia and microglia
3 around the injury site²³. These two injury paradigms offer an ideal comparative model by which
4 to identify specific scarring pathways using identical starting cellular milieus in the zebrafish
5 telencephalon. Moreover, the comparison between permissive and detrimental injury-induced
6 environment might shed light on the mechanisms regulating tissue restoration and neuronal
7 integration.

8 We applied a comparative analysis of scarless versus scarring zebrafish forebrain tissue
9 to identify novel molecular mechanisms regulating the tight balance between wound closure
10 and formation of scar tissue. We identified toll-like receptor 2 (Tlr2) and chemokine receptor
11 3 (Cxcr3) innate immune pathways as key regulators of glial scar formation. Interference with
12 these signaling pathways after injury not only alleviated glial scar formation but also improved
13 wound healing and restorative neurogenesis. We also showed that prolonged exposure of
14 activated glial cells to cerebrospinal fluid content activated Tlr2/Cxcr3 signaling and in turn
15 triggered the scarring process. Taken together, we identified signaling pathways and the source
16 of their ligands leading to glial scar formation, opening a new avenue for targeting therapies.
17

1 **Results**

2

3 **Scarring and scarless models of zebrafish telencephalon injury differ in the kinetics of** 4 **the glial reaction**

5 To identify the cellular and molecular basis for scar formation, we set out to follow the
6 reaction of different cell types to an injury in the zebrafish telencephalon using two paradigms
7 in parallel, one with long-term glial reactivity (referred to as skull injury, Figure 1A) and the
8 other resulting in scarless regeneration (referred to as nostril injury, Figure 1B). The rupture of
9 the blood brain barrier (Appendix Figure S1) and the expression of damage-associated
10 molecules trigger the early inflammatory response that induces the recruitment of peripheral
11 neutrophils into the injury site, and the subsequent activation of macrophages and resident
12 microglia in the mammalian brain²⁴. In zebrafish, we observed Lys⁺ neutrophils already 12h
13 after both injuries in the brain parenchyma (Appendix Figure S2A, D). Interestingly, Lys⁺ cells
14 accumulated at the injury site after the nostril injury (Appendix Figure S2B), while they were
15 dispersed throughout the injured parenchyma after the skull injury (Appendix Figure S2D).
16 Moreover, Lys⁺ neutrophil accumulation resolved 24h after nostril injury and we could not
17 detect any difference 48h after injury (Appendix Figure S2C) compared to the intact brain. In
18 contrast, we did not observe the fast clearance of Lys⁺ cells after skull injury (Appendix Figure
19 S2E).

20 As neutrophils regulate the activity state of microglia and extravasating macrophages and
21 consequently the regenerative response²⁴, we further analyzed both populations based on the
22 expression of two different immunohistochemical markers (4C4 and L-plastin) as well as the
23 transgenic line *Tg(mpeg1:mCherry)*²⁵ after both injury paradigms (Appendix Figure S2F-H’’’).
24 In the intact condition, the majority of microglia co-expressed all three markers although at the
25 different levels (Appendix Figure S2F-F’’’). 3 days after injury, both paradigms displayed
26 similar changes in the immune cell expression pattern (Appendix Figure S2G-H’’’). Most of
27 the labeled immune cells expressed the 4C4 marker and only a proportion of them colocalized
28 with L-plastin and/or with *mpeg1:mCherry*⁺ cells. Taken together, these data suggest that 4C4
29 was the broadest marker to identify the immune cell population and, therefore, we used it
30 further in our study. While the initial activation pattern of 4C4⁺ cells after the skull injury was
31 similar to the nostril paradigm with the first signs of reactivity detectable already at 24 h after
32 injury (Appendix Figure S2J, L), the skull injury induced stronger reactivity and long-lasting
33 accumulation of 4C4⁺ cells at the injury site (Figure 1E-M’).

1 The reactivity of cells belonging to the oligodendrocyte lineage (labeled using the transgenic
2 lines [*Tg(Olig2:GFP)* or *Tg(Olig2:DsRed)*]²⁶ and the immunoreactivity to Sox10²⁷) was
3 slightly delayed in comparison with those of the immune cells (Appendix Figure S2I, K).
4 Olig2:GFP⁺ cells were increased at the injury site 3 days after both skull (Figure 1F, G, N) and
5 nostril injury (Figure 1H, I, O), although to different extents. The accumulation of Olig2:GFP⁺
6 cells, as we observed for 4C4⁺ cells, was rapidly resolved and returned to pre-injury conditions
7 within 7 days after the nostril injury (Figure 1L-M', O), in agreement with previous reports of
8 scarless regeneration in the adult zebrafish telencephalon^{14,19,22}. In contrast, the density of
9 Olig2:GFP⁺ cells further increased in the skull injury paradigm (Figures 1J-K', N). We
10 analyzed coronal brain sections depicting the skull injury in its full extent, but only part of the
11 nostril injury. Therefore, the accumulation of both 4C4⁺ and Olig2:GFP⁺ cells observed
12 exclusively after skull injury could be a consequence of a bias in the analysis. To exclude any
13 technical bias, the number of Olig2:GFP⁺ cells accumulating at the nostril injury site was also
14 analyzed in sagittal sections depicting the full extent of the nostril injury (Appendix Figure
15 S3A-D). No statistical differences compared to the analysis of coronal sections were observed
16 at any of the analyzed time points (Appendix Figure S3E). Moreover, injury sites were
17 analyzed in BABB-cleared brains. While we could observe a clear accumulation of Sox10⁺ and
18 4C4⁺ cells 3 days after nostril injury, 7 days after injury Sox10⁺ and 4C4⁺ cells showed
19 distributions that were indistinguishable from samples of intact brains (Movies EV1-3).

20 The zebrafish telencephalon does not contain protoplasmic astrocytes^{14,28-30}, and the classical
21 astrocytic markers are expressed by GFAP⁺ ependymoglia populations, resident neural stem
22 cells^{28,29} and radial glia-like astrocytes³¹. So next, we used the *Tg(gfap:GFP)* transgenic line³²
23 to label and characterize the reactivity of ependymoglia cells after both types of injury.
24 Gfap:GFP⁺ cell bodies line up at the ventricular wall of the brain surface with processes
25 reaching basement membrane (Appendix Figure S4A); therefore, after a nostril injury, only
26 some processes of ependymoglia, located in the deep parenchyma were wounded (Appendix
27 Figure S4B, C). Importantly, no sign of damage was observed at 7 days after nostril injury
28 (Appendix Figure S4F). On the other hand, upon skull injury, the ependymoglia cell layer was
29 disrupted, opening the telencephalic ventricle to the parenchyma (Appendix Figure S4D, E).
30 The ependymoglia cell layer was restored 7 days after skull injury (Appendix Figure S4G).
31 However, we still observed hypertrophic processes and misplaced Gfap:GFP⁺ cells at the injury
32 site (Appendix Figure S4H). The delay in tissue restoration observed after skull injury was
33 accompanied by the reorganization of the extracellular matrix (ECM) as early as 1 day after
34 the skull injury (Figure 1P) that was still detectable after 7 days (Figure 1Q).

1 The accumulation of Olig2:GFP⁺ and immune 4C4⁺ cells is resolved by 28 days after the skull
2 injury (Figure 1R), resembling the behavior of OPCs and microglia in the injured mammalian
3 cerebral cortex, where a permanent scar persists^{33,34}. However, even after the accumulation of
4 Olig2:GFP⁺ and immune 4C4⁺ cells was resolved, the tissue architecture was not fully restored,
5 based on the Gfap:GFP⁺ ependymogial cell morphology. To assess the ependymogial
6 morphology, we labelled ependymogial cells by electroporation of the TdTomatomem
7 plasmid both after nostril and skull injury and analyzed their morphology and localization 28
8 dpi. In line with previous reports^{35,14}, the nostril injury did not change the morphology or the
9 localization of ependymogial cells compared to the intact brain. As in the intact brain, we
10 found ependymogial cell bodies lining up at the telencephalic ventricular wall with processes
11 mostly spanning the brain parenchyma and anchoring at the basement membrane 28 dpi (Figure
12 1T, T'). However, after skull injury several of the labelled ependymogial cells had bushy
13 morphology and did not reach the basement membrane (Figure 1S; Movie EV4).

14 These data demonstrate, for the first time, a prolonged glial accumulation associated
15 with long-term changes and impaired tissue restoration in the teleost fish brain, recapitulating
16 the typical scarring wound closure in mammalian brain.

17

18 **Activation of innate immunity pathways induces gliosis after injury in the zebrafish** 19 **telencephalon**

20 In view of the above findings, comparing the transcriptome following nostril versus
21 skull injury offers a unique opportunity to disentangle the specific molecular programs
22 inducing exacerbated glial reactivity from the beneficial pathways activating scarless wound
23 healing. We reasoned that some signaling pathways activated after skull injury, but not after
24 nostril injury, could account for the prolonged glial accumulation and the absence of full tissue
25 restoration at the injury site. Therefore, we analyzed the gene expression during regeneration
26 (1, 2, 3, and 7 dpi) after nostril or skull brain injury in the telencephalon, using the Affymetrix
27 Zebrafish Gene ST 1.0 array (Figure 2A). Both types of injuries initially induced comparable
28 transcriptome changes, as reflected by a similar number of significantly regulated genes (fold
29 change >1.6, $p < 0.05$) and a large overlap in significantly overrepresented Gene Ontology
30 (GO) terms (based on DAVID analysis, fold enrichment ≥ 2 ; $p < 0.01$) at 1 and 2 dpi (Figure
31 2B). However, we observed a striking difference in the number of regulated GO terms after
32 nostril and skull injury at 3 dpi (Figure 2B), with 1012 transcripts regulated after a skull but
33 not nostril injury (Figure 2C). Interestingly, this large number of uniquely regulated genes at 3
34 dpi correlates with differences in the reaction of Olig2:GFP⁺ cells and immune cells between

1 the two injury paradigms (Figure 1N, O), supporting the idea that understanding these
2 transcriptional differences could identify scarring specific programs. To further validate the
3 applicability of this approach we analyzed the differential expression of genes involved in the
4 ECM modifications, as the specific ECM changes could be associated with the scar formation⁸.
5 Towards this end, we selected genes related to the GO terms “Extracellular matrix”
6 (GO_0031012) and “Extracellular region” (GO_0005576) and analyzed their expression at 3
7 days post skull and nostril injury. Among all the regulated ECM-related transcripts (131), 69
8 of them were exclusively regulated after the skull injury (Figure 2D). These transcripts were
9 overrepresented in GO terms related to the immune response, regulation of immune system
10 process and proteolysis (Figure 2E), processes implicated in tissue scarring. Moreover, some
11 of these genes encoded for factors reported to regulate either glial reactivity (Ptpn6, Cst B,
12 C1qa, C1qb, Mmp9, Fga)³⁶⁻⁴⁰ or fibrotic scar formation⁴¹⁻⁴⁵ (Figure 2F). Because the two types
13 of injuries show different kinetics in cellular response, some genes could still be differentially
14 regulated at different time points after nostril injury. Therefore, we filtered out from the 1012
15 transcript set (Figure 2C) all transcripts regulated after nostril injury at any analyzed time point.
16 We identified 812 transcripts regulated 3 days after skull injury but not at any time point after
17 nostril injury (Figure 2G). Most of the GO terms significantly enriched in this gene set (2-fold
18 enrichment and $p < 0.01$) were related to metabolism, immune, and innate immune response
19 (Figure 2H). In particular, we observed upregulation of genes indicative of activation of the
20 Toll-like receptor, Tlr, (*mx*, *mxe*, *irf7*, *irf2*)⁴⁶⁻⁴⁸ and chemokine family 11 (*cxcl11.1*, *cxcl11.5*,
21 *cxcl11.6like*, and *cxcl13*)⁴⁹ mediated innate immune response, at 3 days after skull injury
22 (Figure 2I). Innate immunity orchestrates the initial events of wound healing after skin⁵⁰,
23 heart⁵¹, and CNS⁵² injury, and its regulation determines the extent of tissue restoration⁵³.
24 Therefore, we set out to address whether activation of either Tlr- or Cxcl11 family-mediated
25 innate immunity leads to induction of exacerbated glial reactivity in the zebrafish
26 telencephalon. We first activated the Tlr-mediated innate immune response by ventricular
27 injection of zymosan A microparticles⁵⁴ and investigated the glial response after nostril
28 (scarless) injury (Figure 2J). Indeed, zymosan A treatment induced an exacerbated
29 accumulation of both 4C4⁺ and Olig2:GFP⁺ cells at the injury site (Figure 2K-M', Q) 5 dpi
30 after nostril injury compared with the vehicle (artificial cerebrospinal fluid, aCSF) treatment,
31 turning the scarless regeneration into prolonged and exacerbated activation of glial cells at the
32 injury site. Toll-like receptor 2 (Tlr2) mediates the sterile inflammation induced by zymosan
33 A in other systems^{46,55}, and Tlr2 is expressed in the intact as well as the injured zebrafish
34 telencephalon (EV 1A). Therefore, we tested whether interfering with Tlr1/2 pathway

1 activation using a Tlr1/2-specific competitive inhibitor (CU CPT22) would abolish the capacity
2 of zymosan A to induce a prolonged glial reaction after nostril injury (EV 1B). Indeed,
3 interference with activation of the Tlr1/2 pathways prevented accumulation of Olig2:GFP⁺
4 cells at the injury site after zymosan A injection (EV 1C-G), suggesting that activation of Tlr2
5 is sufficient to induce the accumulation of Olig2:GFP⁺ cells and immune cells at the injury site.
6 Similar to Tlr2-induced innate immunity, we set out to test whether the Cxcl11 family has a
7 role in prolonged glial activation, in line with induction of these ligands exclusively after skull
8 injury. As up-regulated Cxcl11-family ligands (Figure 2I) signal through the same chemokine
9 receptor, Cxcr3⁵⁶, we analyzed the ability of a specific Cxcr3 agonist (VUF 11222⁵⁷) to induce
10 glial accumulation in the scarless injury paradigm (Figure 2N). Similar to the reactivity
11 observed upon Tlr2 pathway activation (Figures 2K-M', Q), treatment with the Cxcr3 agonist
12 was sufficient to trigger exacerbated 4C4⁺ and Olig2:GFP⁺ cell accumulation at the injury site
13 at 5 dpi (Figures 2O-Q).

14 Taken together, our data suggest that activation of either Tlr2 or Cxcr3 is sufficient to
15 induce exacerbated glial reactivity after injury.

16

17 **Tlr1/2 and Cxcr3 pathways cooperatively control glial scar formation after injury in the** 18 **zebrafish telencephalon**

19 Because activation of either Tlr2 or Cxcr3 signaling induced prolonged glial reactivity
20 in the nostril injury and transcriptome analysis demonstrated activation of both pathways
21 exclusively after skull injury, we asked whether interference with these pathways would block
22 prolonged glial reactivity after skull injury. We inhibited the activation of the two signaling
23 pathways by using specific inhibitors: CU CPT22 for the Tlr1/2⁵⁸ pathway and NBI-74330 for
24 the Cxcr3⁵⁹ pathway (Figure 3A). Strikingly, interference with the Tlr1/2 pathway did not
25 change accumulation of Olig2:GFP⁺ cells after skull injury (Figure 3A-C, F), despite a
26 significant reduction of area covered by 4C4⁺ immune cells (EV 2A-C, F). Similarly, inhibition
27 of the Cxcr3 pathway did not affect accumulation of either 4C4⁺ or Olig2:GFP⁺ cells (Figure
28 3D, F and EV 2D, F). The fact that inhibition of either Tlr1/2 or Cxcr3 did not abolish
29 Olig2:GFP⁺ glia accumulation after skull injury, despite their ability to induce prolonged
30 reactivity after nostril injury, suggested that the two signaling pathways might be functionally
31 redundant in controlling glial reactivity. To assess their redundancy, we simultaneously
32 inhibited Tlr1/2 and Cxcr3 pathways with respective inhibitors after skull injury (Figure 3A).
33 Indeed, we observed a significant decrease in the number of Olig2:GFP⁺ cells accumulating at
34 the injury site by 4 dpi in inhibitor-treated animals compared to controls (Figure 3E, F).

1 Moreover, Sox10⁺ cells, representing oligodendrocyte lineage cells⁶⁰, showed a similar
2 reduction, supporting the idea that the effect of inhibitors on the oligodendrocyte lineage was
3 mainly in regulating their accumulation at the injury site, rather than affecting Olig2-driven
4 expression of GFP (Figure 3B-E). In addition, the area covered by 4C4⁺
5 microglia/macrophages was significantly reduced after inhibitor treatment (EV 2E, F). A
6 reduction in glial reactivity was also observed after Tlr1/2 inhibitor treatment (CU CPT22)
7 combined with a different Cxcr3 inhibitor (AMG-487⁴⁴) (EV 2G-J). Thus, the possibility of
8 this phenotype being induced by off-target effects of our pharmacological treatment is rather
9 low. These effects of the inhibitor cocktail on alleviating Olig2:GFP⁺ glia and microglia
10 accumulation persisted also at later time points as no sign of Olig2:GFP⁺ cell accumulation
11 was detectable following the inhibitor treatment 7 dpi in the skull injury paradigm (Figure 3G-
12 J).

13 The reduction in the number of reactive glial cells accumulating at the injury site after
14 inhibitor treatment suggests a role of these pathways in the initial induction of exacerbated
15 gliosis, their maintenance at the injury site, or both. To further disentangle the role of Tlr1/2
16 and Cxcr3 signaling in prolonged glial activation, we pharmacologically blocked both
17 pathways after the initial accumulation of Olig2:GFP⁺ cells at 4 dpi (Figure 3K). Once glial
18 cells had accumulated at the injury site (4 dpi), interference with activation of both pathways
19 failed to resolve the accumulation of Olig2⁺ cells 7 dpi (Figure 3L, M), in strong contrast to the
20 improvement observed in the early inhibition protocol (Figure 3G, J). Taken together, these
21 data support the role of Tlr1/2 and Cxcr3 signaling during the initial phase of glial activation
22 and accumulation. The extent of the glial scar is defined by the initial neuroinflammatory
23 reaction, in line with recent findings in the mammalian cerebral cortex³⁴.

24 Because immunohistochemical analysis showed a similar initial accumulation of glial cells in
25 the injury site at 3 dpi following nostril and skull injury (Figure 1N, O), we asked whether
26 interference with Tlr1/2 and Cxcr3 signaling could alter the initial accumulation of Olig2:GFP⁺
27 cells in the scarless injury paradigm. To address this question, we treated nostril-injured
28 animals with Tlr1/2 and Cxcr3 inhibitors and assessed accumulation of Olig2:GFP⁺ cells at the
29 injury site (EV 2K). We observed similar initial accumulation of Olig2:GFP⁺ at the injury site
30 in untreated and vehicle-treated animals (EV 2L-L', N). Importantly, double-inhibitor treatment
31 did not interfere with this initial accumulation of Olig2:GFP⁺ cells (EV 2M-N), in agreement
32 with the absence of the transcriptional signature indicative of skull injury-induced innate
33 immunity activation after the nostril injury. Next, we analyzed the integrity of the blood brain
34 barrier (BBB) to validate that the lack of effect observed upon Tlr1/2 and Cxcr3 inhibitor

1 treatment after the nostril injury was not due to restricted BBB permeability. We used
2 cadaverine as an indicator for BBB leakage and the absence of the cadaverine in the blood
3 vessels labelled by Fli1:GFP line indicates the BBB leakage. The BBB was restored 4-7 dpi in
4 the case of the nostril injury and at 7 dpi after the skull injury, later than any of our treatments
5 (Appendix Figure S1). In conclusion, these data validated our hypothesis that the scarless
6 response and exacerbated gliosis wound closure rely largely on different molecular
7 mechanisms.

8 The simultaneous activation of Tlr1/2 and Cxcr3 during the wound healing period is
9 sufficient and necessary to induce a prolonged accumulation of both microglial and
10 Olig2:GFP⁺ cells at the injury site, leading to exacerbated glial reaction.

11

12 **Reduction in glial accumulation correlates with better tissue recovery**

13 The reduction in the exacerbated accumulation of Olig2:GFP⁺ and microglia after
14 double-inhibitor treatment following skull injury prompted us to investigate the effect of
15 prolonged injury-induced gliosis on brain regeneration by measuring the volume of the injured
16 tissue (Figure 4A, B). We observed a significant reduction in the size of the injured tissue 7 dpi
17 after double-inhibitor treatment compared with vehicle treatment (Figure 4B and Movies EV5,
18 6). Animals treated only with the Tlr1/2 pathway inhibitor (CU CPT22), maintaining the
19 Olig2:GFP cell accumulation, showed no improvement in tissue recovery, as assessed by the
20 volume of injury (Figure 4B), despite the reduction in microglial reactivity observed at 4 dpi
21 (EV 2C, F). This finding supports the hypothesis that the decrease in the number of reactive
22 Olig2:GFP⁺ cells at the injury site leads to improved tissue restoration.

23 We next tested whether the improved tissue recovery induced by the double-inhibitor
24 treatment was accompanied by an addition of new, adult-generated HuC/D⁺ neurons to the
25 injured brain parenchyma (restorative neurogenesis). As ependymogial cells lining the
26 ventricle surface increase their proliferation and generate new neurons in response to an
27 injury^{14,22,54}, we used BrdU-based birth dating to determine whether the decreased glial
28 reactivity after double-inhibitor treatment also correlated with improved restorative
29 neurogenesis. To assess injury-induced neurogenesis, BrdU was added to the fish water during
30 the first 3 days after injury to label all cells synthesizing DNA; that is, mostly dividing
31 progenitors. The BrdU-incorporation phase was followed by a 4-day chase period, allowing
32 progenitor differentiation and correlating with the resolution of the glial scar upon inhibitor
33 treatment (Figure 4C). We previously showed that the majority of newly generated neurons in
34 the intact brain (BrdU⁺ and HuC/D⁺) reside in the ventricular zone (hemisphere periphery,

1 Figure 4G) and display very low migratory potential³⁵. Therefore, we analyzed the proportion
2 of HuC/D⁺ and BrdU⁺ cells residing outside this neurogenic zone, as we observed migration of
3 new neurons towards this area only after injury³⁵. Both control and inhibitor-treated animals
4 generated similar total numbers of new neurons (HuC/D⁺ and BrdU⁺) after injury (Figure 4D-
5 F). However, we observed a significantly increased proportion of new neurons located in the
6 brain parenchyma after double-inhibitor treatment (HuC/D⁺ and BrdU⁺ located in the
7 parenchyma in respect to all HuC/D⁺ and BrdU⁺ cells) (Figure 4G, H). As we did not observe
8 any difference in the total number of generated neurons between control and inhibitor-treated
9 animals, our data exclude an effect of inhibitor treatment on injury-mediated stem cell
10 activation, but rather support the interpretation that the reduced gliosis contributed to the better
11 recruitment, survival or integration of newly generated neurons into the injured brain
12 parenchyma.

13 The reactivity of Olig2:GFP⁺ and 4C4⁺ cells after skull injury showed detrimental
14 effects associated with the harmful scar-induced environment⁵². These aversive effects were
15 alleviated by inhibition of the injury-induced Tlr1/2 and Cxcr3 pathways, suggesting that
16 Olig2:GFP⁺ and 4C4⁺ cells contribute to the development of non-functional scarring tissue in
17 zebrafish and that the Tlr1/2 and Cxcr3 pathways play a pivotal role in scar formation.

18

19 **Microglial depletion does not alter innate immunity regulated glial scar formation**

20 Simultaneous inhibition of Tlr1/2 and Cxcr3 improved tissue regeneration. However,
21 decreasing only 4C4⁺ cell reactivity with the Tlr1/2 inhibitor without changing Olig2:GFP⁺ cell
22 accumulation showed no beneficial effect on infarct tissue volume (Figure 4B). These data
23 suggest that microglia might be unnecessary for scarring response regulated by the Tlr1/2 and
24 Cxcr3 signaling pathways. To directly assess this hypothesis, we analyzed the glial scar
25 response in zebrafish brains depleted of microglia. A combination of Clodrosome and a Ccr2
26 inhibitor prior to skull injury depleted 95% of 4C4⁺ cells (microglia and infiltrating monocytes,
27 EV 3C-F). The 4C4-free condition was then maintained by continuously blocking monocyte
28 extravasation through Ccr2 inhibitor (EV 3G-I). Microglial depletion did not alter Olig2:GFP⁺
29 cell accumulation at 4 days after skull injury compared with the control Encapsome treatment
30 (Figure 4I, J, L and EV 3J, K). Importantly, inhibition of Tlr1/2 and Cxcr3 successfully blocked
31 scar formation in microglia/monocyte-depleted brains (Figure 4K, L). Consistent with this, our
32 expression analysis of FACS-purified Olig2:DsRed⁺ cells (labeling the same oligodendroglia
33 population as Olig2:GFP⁺) showed that they express Cxcr3 (Cxcr3.2 and Cxcr3.3) and Tlr2
34 (Tlr18) isoforms in both intact and injured brains (EV 3L). Moreover, RNAscope analysis

1 revealed expression of genes involved in both innate immune pathways (*Cxcr3.2*, *Tlr8b*,
2 *MYD88* and *Mxc*) in the Olig2:GFP⁺ population after skull injury (EV 3M-R). These data
3 support the concept that the activation of microglia and/or invading monocytes is not necessary
4 for injury-induced oligodendroglial reactivity and their initial accumulation at the injury site in
5 zebrafish.

6 We next tested the effect of microglia depletion on the incorporation of new neurons at
7 the injury site. To this end, we combined the microglia/monocyte depletion protocol with the
8 BrdU-based neuronal birth dating used previously (Figure 4M). The initial depletion of injury-
9 activated microglia did not alter incorporation of new neurons (Figure 4N-O') compared with
10 untreated control animals (compare Veh in Figure 4H and 4R), supporting the hypothesis that
11 the activated microglia is not the only population contributing to the adverse environment
12 restricting new neuron recruitment. Importantly, the inhibition of the Tlr1/2 and Cxcr3
13 pathways in immune cell-depleted brains still improved the integration of new neurons (Figure
14 4M-R), similar to the beneficial effects observed in animals with an intact immune system and
15 further associating the beneficial effects of the inhibitor treatment with resolution of prolonged
16 Olig2:GFP⁺ cell accumulations.

17 Taken together, our results support the hypothesis that Tlr1/2 and Cxcr3 pathways
18 regulate the two hallmarks of the glial scar: accumulation of Olig2:GFP⁺ cells at the injury site
19 and injury-induced impairment of neuronal recruitment to the injury.

20

21 **Olig2:dsRed⁺ cells activate both innate immunity pathways and cell proliferation** 22 **transcription programs in response to an injury**

23 Given the above data identifying the role of innate immunity pathways in accumulation
24 of Olig2:GFP⁺ cells during scar formation after skull injury, we analyzed the injury-induced
25 transcriptomic changes in Olig2⁺ cells acutely isolated from the injured zebrafish telencephalon
26 3 days after either vehicle or inhibitor treatment. The FACS-based purification of Olig2:dsRed⁺
27 cells enriched for OPCs, as we have previously demonstrated⁶¹. We observed 1649
28 significantly regulated transcripts in Olig2:dsRed⁺ cells after injury in vehicle-treated brains
29 compared with intact brains (EV 4A). Interestingly, a minority of transcripts were
30 downregulated (114), suggesting that upon injury OPCs still maintain their oligodendrocyte
31 lineage identity and gain additional features, leading to their reactivity. The distribution of
32 upregulated genes in the biological pathways (Panther-based analysis) revealed activation of
33 FGF-, EGF-, PDGF-signaling pathways (EV 4B), which have previously been implicated in
34 the proliferation of OPCs⁶²⁻⁶⁵. In line with those activated pathways, GO term analysis revealed

1 enrichment of processes involved in scar formation, such as cell migration and response to
2 cytokines and chemokines (EV 4C). Surprisingly, most of the enriched GO terms were related
3 to inflammation (63% of all enriched terms, EV 4C), including the activation of innate
4 immunity. Importantly, genes belonging to both cytokine and toll-like receptor signaling were
5 upregulated in response to injury (EV 4B, C). Moreover, 45% of ECM related genes
6 specifically regulated at 3 days after skull injury were regulated in the Olig2:dsRed⁺ cell
7 population (EV 4D). This unbiased transcriptome analysis further corroborated our hypothesis
8 that cells of the oligodendrocyte lineage activate molecular pathways of the innate immune
9 response, including Tlr2 and Cxcr3, which allows their microglia/macrophage-independent
10 reaction and accumulation at the injury site.

11 The transcriptomic changes after skull injury, supporting the activation of innate
12 immunity pathways directly in Olig2⁺ cells, prompted us to further analyze the effect of the
13 inhibitor cocktail on gene expression in Olig2⁺ cells isolated from injured brains. Interestingly,
14 the inhibitor treatment didn't change the overall transcriptome of Olig2⁺ cells. Approximately
15 80% of regulated transcripts after inhibitor treatment were also regulated in vehicle-treated
16 brains (Figure 5A, EV 4A, E). This suggests that the inhibitor cocktail treatment did not change
17 the overall transcriptome of Olig2:dsRed⁺ cells, but rather restricted regulatory pathways
18 involved in long-term glial accumulation and scar formation. Importantly, both cytokine
19 receptor signaling and toll-like receptor signaling were no longer regulated in Olig2:dsRed⁺
20 cells after inhibitor treatment (Figure 5A, B). However, regulation of number of biological
21 processes linked to the immune response was still present (Source Data), supporting the
22 specific role of Tlr1/2- and Cxcr3-mediated immunity in scar formation. Comparison of injury-
23 regulated genes in Olig2⁺ cells isolated from vehicle- and inhibitor cocktail-treated brains
24 identified a set of 510 genes (597 transcripts) exclusively regulated after brain injury and
25 vehicle treatment (Figure 5A) and, therefore, likely involved in scar formation downstream of
26 the Tlr1/2 and Cxcr3 pathways. These genes were overrepresented in GO terms related to
27 proliferation and cell migration (Figure 5B, Source Data), both being biological processes at
28 the core of the oligodendroglial reaction to injury and glial scar formation in mammals^{66,67}.

29

30 **Regulation of oligodendrocyte progenitor cell proliferation by Tlr1/2 and Cxcr3** 31 **signaling**

32 Transcriptome data support the role of Tlr1/2 and Cxcr3 signaling pathways in direct
33 regulation of OPC proliferation during the scarring process. Therefore, we first assessed the
34 proliferation of Olig2:GFP⁺ cells during scar formation in the zebrafish telencephalon.

1 Accordingly, we labeled all cells undergoing S-phase by BrdU within 5 days after the skull
2 injury, the time point corresponding to the scarring accumulation of oligodendroglia at the
3 injury site (Figure 5C). As expected, we observed accumulation of Olig2:GFP⁺ cells at the
4 injury site, indicating that the BrdU treatment did not alter the behavior of Olig2:GFP⁺ cells.
5 Importantly, we observed that 45% of all Olig2:GFP⁺ cells at the injury site were BrdU⁺ and
6 hence went through at least one cell cycle during 5 days of labelling (Figure 5D-F), supporting
7 the concept that the Olig2:GFP⁺ accumulation at the skull injury site was, at least in part,
8 achieved by increased proliferation. Considering the key role of the Olig2:GFP⁺ cells during
9 the scar formation, we next analyzed if the skull injury had an impact not only on the activation
10 of the OPCs but also on the mature oligodendrocyte population. We made use of the transgenic
11 line *Tg(Mbp:nls-GFP)*⁶⁸ and a BrdU-based birth dating protocol to identify the proportion of
12 the injury-activated OPCs that mature into oligodendrocytes seven days after the skull injury
13 (EV 4F). We did not observe a significant increase in the total number of oligodendrocytes nor
14 in the proportion of newly matured oligodendrocytes upon skull injury (EV 4G-K), supporting
15 the concept that OPCs and not mature oligodendrocytes accumulate at the injury site⁶⁹.

16 Next, we analyzed whether the inhibitor cocktail treatment may alter the proliferation
17 of Olig2:GFP⁺ cells as the cellular basis for reduction in scar formation. As Olig2:GFP⁺ cells
18 display the first signs of exacerbated reactivity 3 days after skull injury, yet without the
19 significant change in total number of Olig2:GFP⁺ cells, we analyzed the proliferation of
20 Olig2:GFP⁺ cells 3 dpi after vehicle and inhibitor treatment (Figure 5G). This experiment
21 revealed a significant reduction in the total number of BrdU⁺ Olig2:GFP⁺ cells after inhibitor
22 cocktail treatment compared with the vehicle treatment (Figure 5H-L). To confirm the
23 activation of Tlr1/2 and Cxcr3 scarring pathways directly on OPCs, we made use of a murine
24 *in vitro* system that allowed us to exclude any paracrine effects. Moloney murine leukemia
25 virus (MLV)-based clonal analysis was performed in pure primary OPC cultures isolated from
26 P0 mouse cerebral cortex after vehicle or double inhibitor treatment (Figure 5M). OPCs were
27 permanently labeled with GFP expressing retrovirus and the size of clones produced by
28 transduced progenitors within 5 days was measured (Figure 5N-P). Inhibitor treatment reduced
29 the GFP⁺ clone size produced by OPCs, supporting a role of Tlr1/2 and Cxcr3 pathways in
30 OPC proliferation (Figure 5P).

31 Taken together, our data indicate a direct role of Tlr1/2 and Cxcr3 pathways in
32 regulating Olig2⁺ OPCs proliferation during the glial scar formation in the zebrafish
33 telencephalon.

34

1 **Cerebrospinal fluid induces exacerbated glial reactivity by increasing OPC proliferation**

2 To identify the source and nature of ligands activating scarring pathways after brain
3 injury, we first examined the size of the skull versus nostril injury. As the volume of the skull
4 injury is larger than that of the nostril injury (Figure 6A), we first set out to determine whether
5 this is the cause of scarring. We reduced the volume of the skull injury to one-third (small skull
6 injury) using the same glass capillary as for the nostril injury (Figure 6B). The small skull
7 injury still induced strong reactivity of both 4C4⁺ and Olig2:GFP⁺ cells (Figure 6C, D). This
8 reaction was comparable to the outcome of the initial skull injury, allowing us to exclude the
9 size of the injury as a major determinant of differential glial reactivity to injury.

10 We next hypothesized that an injury-induced ligand that activates the scarring pathways
11 must be present only after skull injury. The telencephalic ventricle is located dorsally in the
12 zebrafish brain^{70,71} and, therefore, is exclusively damaged during the dorso-ventrally performed
13 skull injury. Cerebrospinal fluid (CSF), which is confined to the ventricles, is rich in cytokines
14 and growth factors that maintain normal homeostasis and nurture the brain; however, direct
15 interaction with the brain parenchyma is restricted and regulated by the CSF–brain barrier⁷².
16 Rupture of the ventricular barrier might allow influx of CSF-derived molecules into the brain
17 parenchyma, potentially explaining the activation of Tlr1/2 and Cxcr3 pathways only after skull
18 injury. To validate the scarring potential of CSF, we injected human CSF in the nostril injury
19 site and analyzed glial reactivity (Figure 6E). Notably, we observed an 8-fold increase in the
20 number of Olig2:GFP⁺ cells accumulating at the injury site (Figure 6F, M). However, this
21 dramatic effect was not observed upon administration of human plasma or heat inactivated
22 human CSF (Appendix Figure S5), indicating that the reactive gliosis was not due to xenograft-
23 induced inflammation. The extraordinary scarring potential of the CSF in the otherwise scarless
24 injury paradigm prompted us to investigate the cellular basis for the Olig2:GFP⁺ cell
25 accumulation in response to the CSF. As the scarring response observed after a skull injury
26 was achieved, at least in part, by an increased proliferation of OPCs (Figure 5C-F), we assessed
27 whether the proliferation of Sox10⁺ cells was also induced by the CSF injection into the nostril
28 injury site (Figure 6G). Indeed, we observed that the majority of Sox10⁺ cells accumulating
29 around the injury site incorporated BrdU during the initial 3 days after the injury and CSF
30 administration (Sox10⁺ and BrdU⁺ cells in respect to all Sox10⁺ cells) (Figure 6H, H', J). The
31 induced proliferation was not, however, observed after injection of heat-inactivated CSF
32 (Figure 6I- J), in line with the significantly smaller accumulation of Olig2:GFP⁺ cells at the
33 injury site observed after heat-inactivated CSF treatment (Appendix Figure S5D). The
34 similarity in OPC reaction induced by CSF injection into the nostril injury and the skull injury

1 motivated us to assess whether CSF-induced scarring potential involved the activation of the
2 Tlr1/2 and Cxcr3 pathways. Therefore, we inhibited Tlr1/2 and Cxcr3 pathways together with
3 administration of human CSF after nostril injury (Figure 6K). Importantly, the accumulation
4 of Olig2:GFP⁺ cells was prevented upon Cxcr3 and Tlr1/2 inhibition, despite the accessibility
5 of the CSF at the injury site (Figure 6L, M). Taken together, these data suggest that the scarring
6 wound closure observed upon skull injury is likely triggered by leakage of CSF into the brain
7 parenchyma and subsequent activation of the Tlr1/2 and Cxcr3 pathways.

8 To identify potential ligands activating innate immunity pathways in the CSF, we setup
9 an in vitro system that relays on the proliferation of a murine OPC cell line (OliNeu).
10 Importantly, addition of CSF to the OliNeu culture medium induced dose-dependent increase
11 in proportion of proliferating, phospho-histone H3 (pH3) positive cells (Figure 7A-D), in line
12 with our data that human CSF can directly regulate OPCs proliferation in vivo (Figure 6J).
13 Moreover, this dose-dependent response was completely abolished in the double Tlr2 and
14 Cxcr3 knockout clones generated using CRISPR-Cas9 technology (Figure 7D, Q; EV 5). These
15 results not only confirmed the pivotal role of Tlr2 and Cxcr3 signaling in the CSF induced
16 proliferation of OPCs, but also additionally validated the specificity of our pharmacological
17 inhibitor treatment in vivo.

18 As cytokines have been reported to activate both Cxcr3 and Tlr2 signaling^{50,56,73}, we
19 first studied the composition of four healthy donor-derived CSFs using a cytokine antibody
20 array (Figure 7E, F). It is important to mention that all four samples turned nostril injury into
21 a scarring phenotype after injecting at the injury site. Strikingly, 90% of the analyzed cytokines
22 were present in at least one of the samples and 57% in all four samples (Figure 7E, F). Out of
23 these cytokines, we pre-selected 30 potential candidates (Figure 7E) that were present in at
24 least one CSF sample and available as recombinant protein for further functional screening
25 using OliNeu proliferation as a read-out (Figure 7G). We used 3 different concentration of the
26 selected candidates and six of them (Ccl5, EGF, Ccl7, IL-10, Cxcl9 and IL-3) significantly
27 increased the proportion of mitotic pH3⁺ cells (Figure 7G), including a known Cxcr3 ligand
28 (Cxcl9). Interestingly, some candidates like Cxcl9 were not detected in all CSF samples despite
29 the ability of all 4 CSF samples to induce the accumulation of Olig2:GFP⁺ cells, suggesting
30 redundancy of ligands in their capacity to activate OPC proliferation.

31 Taken together our data suggest that the CSF cytokines activate the innate immunity to
32 regulate OPC proliferation in a redundant manner and therefore regulate the scarring process.

33

1 **Discussion**

2 Despite the general agreement that removing or minimizing non-functional scar tissue
3 is at the center of functional regeneration, there are only a few therapeutically applicable tools
4 to specifically interfere with the detrimental aspects of the glial scar. Comparative studies
5 analyzing regeneration competent and incompetent species failed to identify specific
6 mechanisms regulating the scar response^{74–79}, even after comparing evolutionarily close
7 species^{80–82}. This is not only due to the complexity of the scarring response that involves a
8 number of molecular pathways and different cell types^{6,52}, but also due to redundancies
9 between processes active during wound healing and scarring wound closure²⁵². To overcome
10 these limitations, we performed a comparative analysis of gliotic (glial scar formation) and
11 scarless wound closure in the same organ and model organism. In contrast to the previously
12 described nostril “scarless” injury of brain parenchyma^{14,19,22}, skull injury showed more
13 similarities to the scarring process reported in mammals, such as prolonged glial accumulation,
14 lack of tissue restoration, extracellular modifications, and exacerbated inflammatory
15 response^{6,83}. Therefore, our data demonstrate, for the first time, that the zebrafish telencephalon
16 can also present the main hallmark of the mammalian CNS reaction to traumatic brain injury—
17 the glial scar.

18 Comparative analysis (scarless vs. scarring) revealed a shared cellular reaction and
19 large overlap in gene regulation shortly after injury, further highlighting the common features
20 of initial wound healing processes⁵². Importantly, a unique molecular signature, including
21 specific innate immunity pathways, was expressed 3 days after the scar-inducing injury,
22 correlating with the first signs of the exacerbated glial reaction. These pathways were never
23 regulated during the scarless wound healing, validating the theory that the glial scar is induced
24 by a specific molecular program independent of the initial wound healing response. Our study
25 does not support the concept that the regenerative capacity of the CNS is an evolutionarily
26 fixed feature of a given species^{84,85}; rather, it is a highly regulated, adaptive response to a
27 specific type of injury. This concept is shared with skin regeneration, in which the depth of the
28 injury determines the scar response⁸⁶.

29 We identified two receptors, Tlr1/2 and Cxcr3, as main regulators of the scarring
30 signature, as their injury-induced activation leads to scar formation. Interestingly, inhibition of
31 either of the two pathways separately showed no beneficial effect, whereas activation of either
32 Tlr2 or Cxcr3 in the scarless paradigm was sufficient to induce gliosis. Hence, both signaling
33 pathways control glial scar formation in a redundant and synergistic manner. The complex
34 cross-regulation of immune cells (macrophages and microglia) and glia after brain injury is

1 crucial for the scar formation^{34,87-89}. The classical inflammatory cascade is initiated by
2 activation and polarization of microglia and invading monocytes. Consequently, these cells
3 regulate the reactivity of astrocytes that, in turn, limits the inflammatory response^{9,34,90,91}.
4 However, our data demonstrate, for the first time, that immune cells are not essential for
5 initiation of the glial scar and that Tlr1/2 and Cxcr3 pathways can be directly regulated in
6 OPCs, a cell type that contributes to the glial scarring response⁶. Our study, therefore, brings
7 forth a new concept that OPCs can sense and react to injury-induced signals independent of
8 microglia and invading monocytes. However, we cannot exclude any involvement of the
9 immune cells in other aspects of the scarring response, such as scar maintenance. As we did
10 not perform cell-specific interference and because both receptors are expressed in several cell
11 types (microglia/macrophages^{92,93}; astrocytes^{94,95}; oligodendroglia⁹⁵; neurons^{94,96}), we cannot
12 exclude the possibility that other cell types contribute to the induction of the scar via Tlr1/2
13 and Cxcr3 signaling pathways. However, our knockout in vitro model validated the role of Tlr2
14 and Cxcr3 pathways in directly activating OPC proliferation and hence, demonstrating that
15 they are clearly involved in a crucial manner in the scarring process. Moreover, the
16 improvement in tissue recovery (reduced injured volume and enhanced restorative
17 neurogenesis) observed after inhibitor treatment correlates nicely with a reduction in the
18 number of scarring Olig2⁺ cells. Our data and the fact that the zebrafish telencephalon does not
19 possess protoplasmic astrocytes support the hypothesis that the detrimental environment
20 classically associated with the glial scar might be driven specifically by reactive OPCs.

21 The central role of Tlr1/2 and Cxcr3 pathways in regulating glial scar and tissue
22 restoration motivated us to investigate injury-induced mechanisms. Our study suggests that the
23 ligand(s) activating the scarring Tlr1/2 and Cxcr3 pathways are part of the CSF that leaks into
24 the CNS parenchyma upon traumatic injury⁹⁷. The capability of the CSF to directly induce
25 OPC proliferation in a Tlr2 and Cxcr3 dependent manner, further corroborates the pivotal role
26 of OPCs in initiating the scarring response and generating a harmful environment. Although
27 the specific CSF-derived molecule/s driving the scarring response in vivo remain unidentified,
28 our in vitro screening suggests that some of the cytokines present in the CSF could be
29 responsible for the OPC activation induced by the traumatic brain injury. These data support a
30 central regulatory role of CSF in controlling not only the activation of neural stem cells in the
31 intact brain, but also the activation state of CNS glia after injury^{98,99}. Overall, our work
32 highlights novel pathways in scar formation as potential targets for developing efficient
33 therapies improving regeneration in the mammalian brain.

34

1 Main Figures Legends

2 **Figure 1. Distinct injury paradigms in the zebrafish telencephalon led to either scarless** 3 **regeneration or prolonged glial reactivity.**

4 (A, B) Schemes depicting skull (A) and nostril (B) injury paradigms. Red triangle (A) and red
5 line (B) illustrate the injury track. (C, D) Micrographs of a telencephalic section showing the
6 distribution of Olig2:GFP⁺ oligodendroglia and 4C4⁺ immune cells in the intact brain. (E, F)
7 Images of 3 dpi skull-injured sections (4C4⁺ and Olig2:GFP⁺ cells) at the level of the injury
8 core delineated by white line (E) and lateral to injury depicting first signs of Olig2:GFP⁺ cell
9 accumulation indicated by boxed area (F). (H) Image showing the distribution of Olig2:GFP⁺
10 and 4C4⁺ cells at 3 dpi after a nostril injury. G and I are magnifications of the boxed areas in
11 F and H, depicting Olig2:GFP⁺ cell distribution. (J-M') Images showing the reactivity of 4C4⁺
12 and Olig2:GFP⁺ cells at 7 days after skull (J) and nostril (L) injury. K, K' and M, M' are
13 magnifications of the boxed area in the respective images. (N, O) Graphs depicting the number
14 of Olig2:GFP⁺ cells at the injury site after skull (N) and nostril (O) injury. Data are shown as
15 mean \pm SEM; each data point represents one animal. Statistical analysis is based on non-
16 parametric Kruskal-Wallis Test (p-value= 0.0021) with post-hoc Dunn test (many-to-one) in N
17 and one-way ANOVA (p-value=2.483e-05) with post-hoc Dunnett test (many-to-one) in O. (P,
18 Q) Brightfield images of AFOG staining after skull injury at 1 dpi (P) and 7 dpi (Q). Black
19 arrows indicate collagen deposition. (R) The accumulation of 4C4⁺ and Olig2:GFP⁺ cells
20 resolved at 28 days after skull injury. (S-T') Images showing morphology of ependymoglia
21 cells (labelled by electroporation of TdTomatomem) 28 days after skull (S) and nostril injury
22 (T, T'). While we observed restoration of radial morphology of labelled ependymoglia that
23 contacts basement membrane after nostril injury (similar to the intact brain), ependymoglia
24 after skull injury failed to restore radial morphology and built extensive contacts with Fli1-
25 positive blood vessels. All images are full z-projections of confocal stack; insets indicate the
26 rostro-caudal levels of the sections. Scale bars in C, E, F, H, J, L, R, S, T, T' = 100 μ m; Scale
27 bars in D, G, I, K, K', M, M', P, Q = 20 μ m. Abbreviations: OB: olfactory bulb, OT: optic
28 tectum, dpi: days post-injury; AFOG: acid fuchsin orange G. Symbol description: black
29 triangle: skull injury; black circle: nostril injury.

1 **Figure 2. Activation of innate immunity pathways after injury induced gliosis in the**
2 **zebrafish telencephalon.**

3 (A) Experimental design to analyze transcriptome changes occurring upon nostril and skull
4 injury. (B) Table depicting the number of significantly regulated Gene Ontology (GO) terms
5 (Injury vs. Intact) at different time points after nostril and skull injury. (C) Comparative
6 analysis using a Venn diagram illustrating the number of genes exclusively regulated 3 days
7 after skull injury (Skull vs. Intact) and not after nostril 3 dpi (Nostril vs. Intact). (D) Venn
8 diagram depicting the overlap between ECM-related genes regulated at 3 days after skull and
9 nostril injury. Regulated genes were defined by a p-value <0.05, fold-change >1.6, and linear
10 average expression >20. (E) Significantly enriched GO terms of biological processes (color
11 indicates p-values and symbol size number of identified genes within the term) in an ECM-
12 related gene set regulated exclusively 3 days after skull injury (69 genes in panel D). (F) Chord
13 diagram depicting selection of regulated ECM-related genes and associated GO terms
14 biological processes. (G) Venn diagram depicting the overlap between genes exclusively
15 regulated at 3 days after skull injury and genes regulated after the nostril injury at any time
16 point. Note that 80% of the genes were exclusively regulated after skull injury at 3 dpi but were
17 never regulated after nostril injury. (H) Plot showing significantly enriched (p-values indicated
18 on bars) GO terms biological processes in a gene set regulated exclusively 3 days after skull
19 injury (Skull 3 dpi vs. Nostril at any time point), correlating with glial scar initiation. (I)
20 Histogram depicting the regulation of genes related to Cxcr3 and Tlr signatures after nostril
21 and skull injury. The gray line shows the 1.6 fold-change cut off. (J) Scheme of the
22 experimental design to analyze the ability of the Tlr2 agonist to induce glia accumulation after
23 nostril injury. (K, L) Images of 5-day-injured telencephalic sections in the *Tg(Olig2:GFP)* line
24 after nostril injury and aCSF (K) or zymosan A injections (L). (M, M') Magnifications of the
25 boxed area in L depict the exacerbated accumulation of Olig2:GFP⁺ (M) and 4C4⁺ (M') cells
26 at the injury site. (N) Scheme representing the experimental design to analyze the capacity of
27 the Cxcr3 agonist (VUF 11222) to induce a reactive gliosis. (O) Micrograph illustrating the
28 reactivity of Olig2:DsRed⁺ and 4C4⁺ cells after Cxcr3 activation. (P) Magnification of injured
29 area in O. (Q) Graph showing the density of Olig2:GFP⁺ cells in the injured area 5 days after
30 nostril injury with aCSF, Cxcr3 or Tlr2 agonist treatments. Data are shown as mean ± SEM;
31 each data point represents one animal. p-values are based on One-way ANOVA (p-value=
32 1.183e-05) with post-hoc Dunnett test (many-to-one). All images are full z-projections of
33 confocal stack. Insets indicate the rostro-caudal levels of the sections. Scale bars in K, L and

1 O = 100 μm ; scale bars in M, M' and P = 20 μm ; Abbreviations: dpi: days post-injury, N3d:
2 nostril 3 dpi, S3d: skull 3 dpi; Ctrl: control; aCSF: artificial cerebrospinal fluid. Symbol
3 description: orange square: ventricular injection of aCSF; orange circle: ventricular injection
4 of zymosan A (Tlr2 agonist); green circle: VUF 11222 (Cxcr3 agonist); black circle: nostril
5 injury.

6

7 **Figure 3. Tlr1/2 and Cxcr3 pathways redundantly control glial scar formation but not**
8 **scar maintenance after injury in the zebrafish telencephalon.**

9 (A) Scheme of the experimental setup to address the role of Cxcr3 and Tlr1/2 in glial scar
10 formation. (B-E) Micrographs of telencephalic sections obtained after 4 dpi depicting
11 Olig2:GFP⁺ and Sox10⁺ oligodendroglia reactivity after vehicle (B), Tlr1/2 inhibitor (C),
12 Cxcr3 inhibitor (D), and double-inhibitor (E) treatments. (F) Graph showing the number of
13 Olig2:GFP⁺ cells located at the injury site after vehicle, Tlr1/2 inhibitor (CU CPT22), Cxcr3
14 inhibitor (NBI 74330) and double-inhibitor combination (NBI 74330 + CU CPT22 treatment).
15 Note that only the double-inhibitor cocktail reduces the number of Olig2:GFP⁺ cells
16 accumulating at the injury site. Data shown as mean \pm SEM; each data point represents one
17 animal. p-values are based on One-way ANOVA (p-value= 4.074e-03) with post-hoc Dunnett
18 test (many-to-one). (G) Experimental outline to assess the effect of vehicle and double-
19 inhibitor treatment 7 dpi. (H, I) Micrographs of telencephalic sections 7 days after skull injury
20 depicting Olig2:GFP⁺ and Sox10⁺ oligodendroglia after vehicle (H) and inhibitor cocktail (NBI
21 74330 and CU CPT22) (I) treatment. (J) Graph illustrating the number of Olig2:GFP⁺ cells
22 located within the injured volume after vehicle and double-inhibitor treatment. An equal
23 volume was quantified in both conditions (p-values is based on Student's t-test with equal
24 variances). (K) Scheme depicting the experimental design to assess the capacity of the vehicle
25 and double inhibitors treatment to resolve glial scar. (L, M) Micrographs showing
26 telencephalic sections 7 days after skull injury and vehicle (L) or double-inhibitor (M)
27 treatment. White arrows indicate the injury site. Note that both vehicle and inhibitor treatments
28 failed to resolve Olig2:GFP⁺ accumulation. All images are full z-projections of confocal stack.
29 The level of the cross-section is indicated in the inset. Scale bars in L and M = 100 μm ; scale
30 bars in B, C, D, E, H, and I = 20 μm . Abbreviations: dpi: days post-injury, Inh: inhibitor, Veh:
31 vehicle. Symbol description: red triangle: vehicle; dark blue triangle: Tlr1/2 inhibitor, CU

1 CPT22; green triangle: Cxcr3 inhibitor, NBI 74330; light blue triangle: double inhibitors, NBI
2 74330 and CU CPT22.

3

4 **Figure 4. Activation of Tlr1/2 and Cxcr3 creates a detrimental environment by inducing**
5 **oligodendroglia accumulation in a microglia-independent manner.**

6 (A) Scheme of the experimental design to analyze the consequences of double-inhibitor
7 treatment (NBI 74330 and CU CPT22). (B) Graph illustrating the size of the injured volume 7
8 days after skull injury and vehicle, Tlr1/2 inhibitor (CU CPT22), or double Tlr1/2 and Cxcr3
9 inhibitor (NBI 74330 and CU CPT22) treatment. p-values are based on One-way ANOVA (p-
10 value= 1.971e-04) with post-hoc Dunnett test (many-to-one). (C) Experimental scheme
11 designed to study restorative neurogenesis upon different treatments. (D, E) Images depicting
12 HuC/D⁺ and BrdU⁺ cells located in the parenchyma following vehicle (D) and double-inhibitor
13 (E) treatment. (F) Dot-plot showing the total density (whole telencephalon) of HuC/D⁺ and
14 BrdU⁺ after vehicle and Tlr1/2 and Cxcr3 inhibitor treatment. p-value is based on Welch's t-
15 test with unequal variances. (G) Diagram illustrating the ventricular zone (25 μm from the
16 ventricle surface) and the parenchyma (blue area) in the telencephalic region. Restorative
17 neurogenesis was measured by the proportion of newly generated neurons (HuC/D⁺ and BrdU⁺)
18 that migrated towards the parenchyma with respect to the total number (ventricular zone and
19 parenchyma) of new neurons. (H) Graph depicting the proportion of HuC/D⁺ and BrdU⁺ cells
20 located in the telencephalic parenchyma after vehicle and Tlr1/2 and Cxcr3 inhibitor treatment.
21 p-value is based on Student's t-test with equal variances. (I) Design of the experimental
22 workflow to analyze the effect of Tlr1/2 and Cxcr3 inhibitors on scar formation after immune
23 cell depletion. (J, K) Micrographs depicting the reactivity of Olig2:GFP⁺ cells after skull injury
24 at 4 dpi with immune cell depletion and vehicle (J) or Tlr1/2 and Cxcr3 inhibitor treatments
25 (K). (L) Graph illustrating the density of Olig2:GFP⁺ cells at the injury site at 4 dpi following
26 Clodrosome + Ccr2 (MK-0812) inhibitor treatment (immune depletion protocol), Encapsome
27 (empty liposomes, control for Clodrosome; ventricular injection) and Clodrosome + Ccr2 +
28 Tlr1/2 (CU CPT22) + Cxcr3 (NBI 74330) inhibitor treatments. The decrease in glial scar
29 formation after Tlr1/2 and Cxcr3 inhibitor treatment was maintained in microglia/monocyte-
30 depleted brain. p-values are based on One-way ANOVA (p-value= 7.957e-03) with post-hoc
31 Tukey Test (all pairs). (M) Design of the experimental protocol used to analyze injury-induced
32 neurogenesis (BrdU-based birth dating) in immune cell-depleted brains treated with vehicle or

1 Tlr1/2 and Cxcr3 inhibitor cocktail. (N, P) Micrographs of injured telencephala at 7 dpi
2 showing the generation of new neurons (HuC/D⁺/BrdU⁺) after vehicle (N) and Tlr1/2 and
3 Cxcr3 inhibitor (P) treatment in immune cell-depleted brains. O, O', Q and Q' are
4 magnifications of the areas boxed in N and P, respectively. White arrowheads depict double
5 HuC/D⁺ and BrdU⁺ cells. The level of the cross-section is indicated in the inset. (R) Graph
6 depicting the proportion of HuC/D⁺ and BrdU⁺ cells located in the telencephalic parenchyma
7 after vehicle and Tlr1/2 and Cxcr3 inhibitor treatment. p-value is based on Student's t-test with
8 equal variances. All images are full z-projections of confocal stack. Data are shown as mean ±
9 SEM; each data point represents one animal. Scale bars in N and P = 100 μm; scale bars in D,
10 E, J, K, O, O', Q and Q' = 20 μm. Abbreviations: dpi: days post-injury; Veh: vehicle; Inh:
11 inhibitors. Symbol description: black triangle: skull injury; red triangle: vehicle; dark blue
12 triangle: Tlr1/2 inhibitor (CU CPT22); green triangle: Cxcr3 inhibitor (NBI 74330); light blue
13 triangle: double inhibitors (NBI 74330 and CU CPT22); orange triangle: ventricular
14 Clodrosome injection; purple triangle: intraperitoneal Ccr2 inhibitor injection (MK-0812).

15

16 **Figure 5. Transcriptome analysis of zebrafish oligodendrocyte lineage cells reveals**
17 **activation of innate immunity and cell cycle pathways after skull injury.**

18 (A) Venn diagram of genes regulated at 3 dpi in Olig2-GFP⁺ cells after vehicle (red) and Tlr1/2
19 and Cxcr3 inhibitor (cyan) treatment. (B) Histogram depicting GO terms biological process
20 significantly enriched (p-values indicated on bars) in a gene set (597 genes in A) normalized
21 after inhibitor treatment and therefore regulated exclusively after vehicle treatment. GO terms
22 related to inflammatory response are shown by gray bars; patterned bars indicate processes
23 previously reported to be activated in response to injury. Note that both innate immunity and
24 cytokine-mediated signaling pathways are normalized upon inhibitor treatment. (C) Scheme
25 depicting the experimental design to analyze the proliferative capacity of Olig2:GFP⁺ cells
26 during the first 5 days after skull injury. (D) Micrograph of injured section 5 days after skull
27 injury stained for GFP and BrdU. (E, E') Magnification of the oligodendroglial scar boxed in
28 D. Double Olig2:GFP⁺BrdU⁺ cells are marked with white arrows. (F) Graph illustrating the
29 proportion of Olig2:GFP⁺BrdU⁺ cells located at the injury site and in an equivalent uninjured
30 volume in the same section. Note that 45% of Olig2:GFP⁺ cells at the injury site proliferated
31 after skull injury. (G) Scheme of experimental design to assess proliferation of Olig2-GFP⁺
32 cells after vehicle and inhibitors treatment. (H, J) Images of telencephalic sections 3 days after

1 skull injury and BrdU bath with vehicle (**H**) and double inhibitors (**J**) treatments. (**I**, **K**)
2 Micrographs with orthogonal projections of BrdU⁺ and Olig2:GFP⁺ cells after vehicle (**I**) and
3 Tlr1/2 and Cxcr3 inhibitor (**K**) treatment. (**L**) Graph depicting the total numbers of Olig2:GFP⁺
4 and BrdU⁺ cells 3 dpi in vehicle and Tlr1/2 and Cxcr3 inhibitor treated animals. (**M**)
5 Experimental design to measure the clonal growth of murine OPCs primary cultures after
6 vehicle and Tlr1/2 and Cxcr3 inhibitor cocktail. OPCs were permanently labeled with GFP
7 expressing retrovirus. (**N**, **O**) Micrographs depicting OPC derived clones 5 days after retroviral
8 infection in vehicle (**N**) and Tlr1/2 and Cxcr3 inhibitor (NBI 74330 & CU CPT22) cocktail (**O**)
9 treated primary OPCs culture. (**P**) Graph depicting the frequency of different clone sizes in the
10 vehicle (CTR) and Tlr1/2 and Cxcr3 inhibitor cocktail (INH) treated primary OPCs culture.
11 Data are shown as mean ± SEM; each data point represents one animal. p-values are based on
12 Student's t-test with equal variances. All images are full z-projections of confocal stack. The
13 level of the cross-section is indicated in the inset. Scale bars in D, H, J = 100 μm; scale bars in
14 N, O = 50μm, scale bars in E, E' = 20 μm; scale bars in I, K = 10 μm. Abbreviations: dpi: days
15 post-injury; Veh: vehicle; Inh: inhibitors; OPC: oligodendrocyte progenitor cell. Symbol
16 description: black triangle: skull injury; blue square: uninjured volume; red triangle: vehicle;
17 light blue triangle: double inhibitors (NBI 74330 and CU CPT22); black square: control
18 primary OPCs; red circle: double inhibitor (NBI 74330 and CU CPT22) treated primary OPCs.

19

20 **Figure 6. Cerebrospinal fluid-derived molecules induce proliferation of OPCs and scar-**
21 **like phenotype.**

22 (**A**) Graph depicting the size of the injured volume after skull, nostril, and small skull injury at
23 1 dpi. p-values are based on Welch one-way ANOVA (unequal variances; p-value= 3.034e-4)
24 with post-hoc Dunnett T3 test with unequal variances (all pairs). (**B**) Scheme depicting the
25 small skull injury model. Nostril and small skull injuries were performed with a glass capillary.
26 The red line indicates the dorso-ventral injury through the skull and blue indicates the location
27 of the telencephalic ventricle. (**C**) Image illustrating the reactivity of Olig2:GFP⁺ and 4C4⁺
28 cells 7 days after small skull injury. (**D**) Magnification of the oligodendroglial accumulation
29 boxed in C. (**E**) Design of the experimental workflow to analyze the effect of human CSF
30 administration. (**F**) Image illustrating the reactivity of Olig2:GFP⁺ cells 3 days after nostril
31 injury and hCSF treatment. White line delineates the injury site. (**G**) Experimental design to
32 analyze the proliferative capacity (BrdU incorporation) of Sox10⁺ cells after nostril injury at 3

1 dpi and hCSF or heat-inactivated hCSF administration. **(H-I')** Images showing the
2 accumulation of Sox10⁺ and BrdU⁺ cells at the nostril injury site after hCSF **(H, H')** or heat-
3 inactivated human CSF **(I, I')** administration. White lines delineate the injury site and white
4 arrowheads the colocalization of BrdU and Sox10. **(J)** Dot-plot depicting the proportion of
5 Sox10⁺ and BrdU⁺ cells accumulating at the nostril injury site after hCSF or heat-inactivated
6 hCSF administration. p-value is based on Student's t-test with equal variances. **(K)** Workflow
7 to study the effect of the Tlr1/2 and Cxcr3 inhibitor treatment after human CSF injection. **(L)**
8 Micrograph of a nostril-injured telencephalon at 3 dpi depicting Olig2:GFP⁺ cell reactivity
9 following human CSF and inhibitor treatment. **(M)** Graph showing the Olig2:GFP⁺ cell density
10 at the injury site after nostril injury at 3 dpi, with hCSF and double-inhibitor treatment after
11 hCSF administration. White line delineates the injury site. p-values are based on one-way
12 ANOVA (p-value= 1.042e-06) with post-hoc Tukey Test (all pairs). Data are shown as mean
13 ± SEM; each data point represents one animal. All images are full z-projections of confocal
14 stack. Scale bar in C= 100 µm; scale bars in D, F, H, H', I, I' and L= 20 µm. Abbreviations:
15 dpi: days post-injury; hCSF: human cerebrospinal fluid; Inh: inhibitors; N3d; nostril 3 dpi.
16 Symbol description: black triangle: skull injury; black circle: nostril injury; black rectangle:
17 small skull injury; red circle: human CSF administration; blue circle: heat-inactivated hCSF
18 treatment; light blue circle: double inhibitors (NBI 74330 and CU CPT22).

19

20 **Figure 7. Identification of cerebrospinal fluid-containing cytokines inducing scarring**
21 **process.**

22 **(A-C)** Micrographs illustrating the proportion of proliferating (pH3⁺) cells in control wildtype
23 (WT) **(A, B)** and Tlr2 and Cxcr3-deficient **(C)** OliNeu oligodendrocyte progenitor cell line in
24 basal conditions **(A)** and in response to the CSF treatment **(B, C)**. **(D)** Dot-plot depicting the
25 proportion of proliferating WT and Tlr2 and Cxcr3-deficient OliNeu cells after CSF treatment.
26 The line indicates corresponding linear data-fit. Data are shown as mean ± SEM; each data
27 point represents one independent experiment. Adjusted p-values assess the quality of the linear
28 fit for the WT clone (black) and difference in the slopes of the linear fits (color-coded) using
29 the linear regression model. **(E)** Table showing the array map. Color-code illustrates the
30 presence of each cytokine in CSF samples (White: negative in all samples; Green: positive in
31 all samples; Blue: positive in 3 out of 4 samples; Orange: positive in 2 out of 4 samples; Magenta:
32 Positive in 1 out of 4 samples). Cytokines names colored in red or yellow were selected for the

1 screening in **G**. **(F)** Representative image of a cytokine antibody array depicting the cytokine
2 composition of a donor-derived CSF. **(G)** Dot plot depicting proliferation of OliNeu cells after
3 treatment with different cytokines and CSF. Scale bars in A, B, C= 50µm Abbreviations: hCSF:
4 human cerebrospinal fluid. Symbol description: black diamond: control OliNeu cells; green
5 square: Tlr2&Cxcr3-deficient clone 1; red square Tlr2&Cxcr3-deficient clone 2; red circle:
6 human CSF administration.

7

1 **Expanded View Figure Legends**

2 **Figure EV1. Activation of Tlr1/2 innate immunity pathways induces long-term**
3 **accumulation of Olig2⁺ cells after nostril injury.**

4 (A) Histogram illustrating the expression level of *Tlr2* in the intact and injured adult zebrafish
5 telencephalon measured by qPCR. Data are shown as mean \pm SEM (n=3 animals). (B) Scheme
6 of the experimental design to identify receptor mediating zymosan A effect. (C, E)
7 Micrographs of zymosan A-treated telencephalic sections of the *Tg(Olig2:GFP)* line 5 days
8 after nostril injury and vehicle (C) or Tlr1/2 inhibitor (E) treatment. D and F are magnifications
9 of the boxed areas in C and E, respectively. (G) Graph depicting the number of Olig2:GFP⁺
10 cells located at the injured area after aCSF, zymosan A, and zymosan A and Tlr1/2 treatment.
11 Data are shown as mean \pm SEM, each data point represents one animal. p-values are based on
12 one-way ANOVA (p-value= 1.312e-05) with post-hoc Tukey Test. All images are full z-
13 projections of confocal stack. Inlets indicate the rostro-caudal levels of the sections. Scale bars
14 in C and D = 100 μ m; scale bars in D and F = 20 μ m. Abbreviations: N3d: nostril 3 days post-
15 injury; S3d: skull 3 days post-injury; aCSF: artificial cerebrospinal fluid; Inh: inhibitor. Symbol
16 description: black circle: nostril injury; red circle: intraperitoneal injection of vehicle; dark blue
17 circle: intraperitoneal injection of Tlr1/2 inhibitor, CU CPT22; orange circle: ventricular
18 zymosan A injection; orange rectangle: aCSF.

19

20 **Figure EV2. Innate immunity pathways and glial reactivity 4 days after skull and nostril**
21 **injury.**

22 (A) Experimental outline to assess the reaction of 4C4⁺ cells after skull injury with vehicle,
23 Tlr1/2 inhibitor (CU CPT22), Cxcr3 inhibitor (NBI 74330) and Cxcr3 and Tlr1/2 inhibitor
24 (NBI 74330 and CU CPT22) treatment. (B-E) Micrographs depicting telencephalic sections 4
25 days after skull injury stained for 4C4 after vehicle (B), Tlr1/2 inhibitor (C), Cxcr3 inhibitor
26 (D) and double Tlr1/2 and Cxcr3 inhibitor (E) treatment. Cyan line delineates telencephalic
27 hemisphere. (F) Graph illustrating the proportion of area covered by 4C4 signal after vehicle,
28 single-inhibitor, and double-inhibitor treatments. p-values are based on One-way ANOVA (p-
29 value= 7.021e-05) with post-hoc Dunnett Test (many-to-one). (G) Scheme of the experimental
30 workflow to analyze the effect of the additional inhibitor combination (CU CPT22 + AMG-

1 487) on glial scar formation. **(H, I)** Images of injured *Tg(Olig2:GFP)* section at 4 dpi stained
2 for GFP and Sox10 after vehicle **(H)** and CU CPT22 + AMG-487 inhibitor **(I)** treatment. **(J)**
3 Dot-plot showing the accumulation of Olig2:GFP⁺ cells at the injury site after vehicle and two
4 different inhibitor combinations. Note that both double-inhibitor combinations reduced
5 oligodendroglia accumulation to the same extent. p-values are based on One-way ANOVA (p-
6 value= 1.221e-03) with post-hoc Dunnett Test (many-to-one). **(K)** Scheme depicting the
7 experimental design to analyze oligodendroglial reaction after nostril injury and vehicle or
8 double Tlr1/2 and Cxcr3 inhibitor (NBI 74330 and CU CPT22) treatment. **(L-M')** Micrographs
9 illustrating accumulation of oligodendroglia (Olig2:GFP⁺ cells) at the injury site 3 days after
10 nostril injury and vehicle **(L, L')** or double inhibitor treatment **(M, M')**. White lines delineate
11 the injury site. **(N)** Graph depicting the number of Olig2:GFP⁺ cells located at the injury area
12 as a function of Tlr1/2 and Cxcr3 pathways. p-values are based on One-way ANOVA (p-value=
13 3.674e-01) with post-hoc Dunnett Test (many-to-one). All images are full z-projections of
14 confocal stack. Insets indicate the rostro-caudal levels of the sections. Data are shown as mean
15 ± SEM; each data point represents one animal. Scale bars in B, C, D, and E = 100 μm; scale
16 bars in H, I, L, L', M and M' = 20 μm. Abbreviations: dpi: days post-injury; N3d: nostril 3
17 days post-injury; Veh: vehicle; Inh: inhibitor. Symbol description: red triangle: vehicle; dark
18 blue triangle: Tlr1/2 inhibitor (CU CPT22); green triangle: Cxcr3 inhibitor (NBI 74330); light
19 blue triangle: double inhibitors (NBI 74330 and CU CPT22); orange triangle: intraperitoneal
20 CU CPT22 + AMG-487 injection; black circle: nostril injury; red circle: vehicle; light blue
21 circle: double inhibitors (NBI 74330 and CU CPT22).

22

23 **Figure EV3. Tlr1/2 and Cxcr3 pathways regulate oligodendroglia scar formation**
24 **independently from microglial and monocyte activation.**

25 **(A)** Scheme of the experimental setting to address the role of Cxcr3 and Tlr1/2 in glial scar
26 formation 4 days after injury. **(B)** Graph showing the volume of the injured tissue after different
27 treatments. p-value is based on one-way ANOVA (p-value = 1.801e-01) with post-hoc Dunnett
28 test. **(C)** Image of an uninjured section stained for two immune cell markers (L-plastin and
29 4C4). **(D)** Scheme of the experimental setting to eliminate microglia and infiltrating monocytes
30 using Clodrosome to deplete resident microglia and Ccr2 inhibitor to block the extravasation
31 of monocytes. **(E)** Micrograph illustrating the depletion of L-plastin⁺ and 4C4⁺ cells in intact
32 brain. **(F)** Graph depicting the proportion of section covered with 4C4 signal in untreated and

1 treated brains; 95% of 4C4⁺ cells were depleted after combined Clodrosome and Ccr2 inhibitor
2 treatment. p-value is based on Welch's t-test with unequal variances. (G) Scheme of the
3 experimental setting to analyze 4C4 reactivity upon skull injury and microglia and monocyte
4 depletion. (H, I) Micrographs illustrating 4C4 depletion 1 (H) and 2 (I) days after skull injury.
5 White lines depict the injury site and section profiles are delimited by yellow and blue lines.
6 (J) Scheme of the experimental design to analyze glial scar formation after injecting empty
7 control liposomes used as vehicle for Clodrosome (Encapsome). (K) Image depicting the
8 Olig2:GFP⁺ cell accumulation at the injury site in Encapsome-treated brains. Note that
9 repetitive ventricular injections did not alter oligodendroglial scar formation. (L) Graph
10 illustrating the expression levels of Cxcr3 (Cxcr3.1, Cxcr3.2, Cxcr3.3) and Tlr2 (Tlr2, Tlr18)
11 zebrafish orthologs in Olig2:dsRed⁺ cells analyzed by RNA sequencing. (M-P) Micrographs
12 with orthogonal projections illustrating the expression of Cxcr3.2 (M), Tlr8b (N), MYD88 (O)
13 and Mxc (P) genes in the Olig2:GFP⁺ cells 3 days after skull injury. (Q, R) Images showing
14 the RNAscope negative controls for the Cy3 (Q) and Cy5 (R) channels. All images are full z-
15 projections of confocal stack. The level of the cross-section is indicated in the inset. Data are
16 shown as mean ± SEM and each data point represents one animal. Scale bars in C, E, H, and I
17 = 100 μm; scale bar in K = 20 μm; scale bar in M, N, O, P, Q, R = 10 μm. Abbreviations: TPM:
18 transcripts per million reads; dpi: days post-injury; Inh: inhibitor. Symbol description: red
19 triangle: vehicle; dark blue triangle: Tlr1/2 inhibitor (CU CPT22); green triangle: Cxcr3
20 inhibitor (NBI 74330); light blue triangle: double inhibitors (NBI 74330 and CU CPT22); black
21 rectangle: intact; orange square: ventricular injection of clodrosome; purple square:
22 intraperitoneal injection of Ccr2 inhibitor; black triangle: skull injury; gray triangle:
23 encapsome; Orange triangle: ventricular injection of clodrosome; purple triangle:
24 intraperitoneal injection of Ccr2 inhibitor.

25

26 **Figure EV4. Oligodendrocyte lineage cells respond to injury by activation of innate**
27 **immunity, cell proliferation and cell migration pathways.**

28 (A) Dot plot depicting up- and down-regulated genes in FACS-purified Olig2:GFP⁺ cells
29 isolated from the injured zebrafish telencephalon after vehicle treatment. Lines indicate cut-off
30 borders (p-value <0.05 and fold change ≥2). (B) Pie chart showing the proportion of injury-
31 regulated genes in zebrafish Olig2⁺ cells belonging to different pathways based on Panther
32 analysis. (C) Histogram depicting GO term biological process significantly enriched (p-values

1 indicated on bars) in a gene set upregulated after brain injury in zebrafish Olig2⁺ cells. GO
2 terms related to inflammatory response are shown by gray bars; patterned bars indicate
3 processes previously reported to be activated in response to injury. Note that both toll-like
4 receptor signaling and response to cytokine are induced by the injury. **(D)** Dot plot depicting
5 coregulation of ECM-related genes in the entire telencephalon and Olig2⁺ cells 3 days after
6 skull injury. Lines indicate cut-off borders (p-value <0.05 and fold change ≥2). **(E)** Dot plot
7 depicting up- and downregulated genes in FACS-purified Olig2:dsRed⁺ cells isolated from the
8 injured zebrafish telencephalon after Tlr1/2 and Cxcr3 inhibitor treatment. **(F)** Experimental
9 design to analyze the density and maturation rate of oligodendrocytes after skull injury. **(G-I')**
10 Images depicting the distribution of Mbp:nls-GFP⁺ cells and BrdU⁺ cells in intact condition
11 **(G-H')** and 7 days after skull injury **(I, I')**. Double positive Mbp:nls-GFP and BrdU cells (white
12 arrow) represent oligodendrocyte progenitor cells that differentiated into mature
13 oligodendrocyte. **(J, K)** Dot plots showing the total density of Mbp:nls-GFP⁺ cells **(J)** and the
14 proportion of newly matured oligodendrocytes **(K)** in intact brains and 7 days after skull injury.
15 Data are shown as mean ± SEM; each data point represents one animal. p-values are based on
16 Student's t-test with equal variances. All images are full z-projections of confocal stack. Scale
17 bars in G, I, I' = 100 μm; scale bars in H, H' = 20 μm. Abbreviations: dpi: days post-injury;
18 Veh: vehicle; Int: intact; Inh: inhibitor. Symbol description: black rectangle: intact; black
19 triangle: skull injury.

20

21 **Figure EV5. Generation of the Tlr2 and Cxcr3 OliNeu knockout line.**

22 **(A, B)** Sequence alignment of the Cxcr3 **(A)** and Tlr2 **(B)** locus depicting the Cas9-mediated
23 bi-allelic deletions (green blocks) leading to the premature STOP codon generation (red
24 asterisk) in oligodendrocyte progenitor OliNeu cell line. The position of gRNAs is indicated
25 with grey boxes. **(C, D)** Micrographs depicting Ki67-positive cells in WT OliNeu cell clone
26 (only transfected with Cas9) **(C)** and Cxcr3/Tlr2 mutant clone 1 **(D)**. **(E)** Dot plot depicting the
27 proportion of pH3 positive cells in WT OliNeu cells and two mutant cell clones (Clone 1, Clone
28 2). Data are shown as mean ± SEM; each data point represent single coverslip. p-value is based
29 on one-way ANOVA (p-value= 2.473e-03) and Dunnett Test (many-to-one). Scale bars in C,
30 D = 50μm. Symbol description: black diamond: control OliNeu cells; green square:
31 Tlr2&Cxcr3-deficient clone 1; red square Tlr2&Cxcr3-deficient clone 2.

32

33

1 **Extended View Movie Legend**

2 **Movie EV1**

3 3D reconstruction of cleared intact telencephalic tissue stained for Sox10 (magenta), 4C4
4 (cyan) and DAPI (blue).

5 **Movie EV2**

6 3D reconstruction of cleared telencephalic tissue stained for Sox10 (magenta), 4C4 (cyan)
7 and DAPI (blue) 3 days after nostril injury.

8 **Movie EV3**

9 3D reconstruction of cleared telencephalic tissue stained for Sox10 (magenta), 4C4 (cyan)
10 and DAPI (blue) 7 days after nostril injury.

11 **Movie EV4**

12 3D reconstruction of *Tg(fli1:eGFP)* transgenic line 28 days after nostril and skull injury.
13 Ependymogial cells were labeled by electroporation of a plasmid encoding for membrane
14 localized tdTomato 21 days after injury.

15 **Movie EV5**

16 3D reconstruction of cleared infarct tissue stained for Sox10 and DAPI 7 days after skull
17 injury and vehicle treatment.

18 **Movie EV6**

19 3D reconstruction of cleared infarct tissue stained for Sox10 and DAPI 7 days after skull
20 injury and double inhibitor treatment.

1 References and Notes:

- 2 1. Gurtner, G. C., Werner, S., Barrandon, Y. & Longaker, M. T. Wound repair and regeneration.
3 *Nature* **453**, 314–321 (2008).
- 4 2. Sofroniew, M. V. Molecular dissection of reactive astrogliosis and glial scar formation. *Trends*
5 *Neurosci.* **32**, 638–647 (2009).
- 6 3. Hol, E. M. & Pekny, M. Glial fibrillary acidic protein (GFAP) and the astrocyte intermediate
7 filament system in diseases of the central nervous system. *Curr Opin Cell Biol* **32**, 121–130
8 (2015).
- 9 4. Pekny, M. & Pekna, M. Astrocyte intermediate filaments in CNS pathologies and regeneration.
10 *J. Pathol.* **204**, 428–437 (2004).
- 11 5. Li, L. *et al.* Protective role of reactive astrocytes in brain ischemia. *J Cereb Blood Flow Metab*
12 **28**, 468–481 (2008).
- 13 6. Dimou, L. & Gotz, M. Glial cells as progenitors and stem cells: new roles in the healthy and
14 diseased brain. *Physiol Rev* **94**, 709–737 (2014).
- 15 7. Silver, J. & Miller, J. H. Regeneration beyond the glial scar. *Nat Rev Neurosci* **5**, 146–156
16 (2004).
- 17 8. Busch, S. A. & Silver, J. The role of extracellular matrix in CNS regeneration. *Curr Opin*
18 *Neurobiol* **17**, 120–127 (2007).
- 19 9. Fitch, M. T. & Silver, J. CNS injury, glial scars, and inflammation: Inhibitory extracellular
20 matrices and regeneration failure. *Exp Neurol* **209**, 294–301 (2008).
- 21 10. Pekny, M. & Nilsson, M. Astrocyte activation and reactive gliosis. *Glia* **50**, 427–434 (2005).
- 22 11. Anderson, M. A. *et al.* Astrocyte scar formation AIDS central nervous system axon
23 regeneration. *Nature* (2016) doi:10.1038/nature17623.
- 24 12. Reimer, M. M. *et al.* Motor neuron regeneration in adult zebrafish. *J Neurosci* **28**, 8510–8516
25 (2008).
- 26 13. Reimer, M. M. *et al.* Sonic hedgehog is a polarized signal for motor neuron regeneration in
27 adult zebrafish. *J Neurosci* **29**, 15073–15082 (2009).
- 28 14. Baumgart, E. V. V *et al.* Stab wound injury of the zebrafish telencephalon: a model for
29 comparative analysis of reactive gliosis. *Glia* **60**, 343–357 (2012).
- 30 15. Zambusi, A. & Ninkovic, J. Regeneration of the central nervous system-principles from brain
31 regeneration in adult zebrafish. *World J. Stem Cells* **12**, (2020).
- 32 16. Thored, P. *et al.* Persistent production of neurons from adult brain stem cells during recovery
33 after stroke. *Stem Cells* **24**, 739–747 (2006).
- 34 17. Arvidsson, A., Collin, T., Kirik, D., Kokaia, Z. & Lindvall, O. Neuronal replacement from
35 endogenous precursors in the adult brain after stroke. *Nat Med* **8**, 963–970 (2002).
- 36 18. Brill, M. S. S. *et al.* Adult generation of glutamatergic olfactory bulb interneurons. *Nat Neurosci*
37 **12(12)**, 1524–1533 (2009).
- 38 19. Ayari, B., Elhachimi, K. H., Yanicostas, C., Landoulsi, A. & Soussi-Yanicostas, N. Prokineticin
39 2 expression is associated with neural repair of injured adult zebrafish telencephalon. *J*
40 *Neurotrauma* (2010) doi:10.1089/neu.2009.0972.
- 41 20. Colak, D. *et al.* Adult neurogenesis requires Smad4-mediated bone morphogenic protein
42 signaling in stem cells. *J Neurosci* **28**, 434–446 (2008).
- 43 21. Willis, E. F. *et al.* Repopulating Microglia Promote Brain Repair in an IL-6-Dependent Manner.
44 *Cell* (2020) doi:10.1016/j.cell.2020.02.013.
- 45 22. Kroehne, V., Freudenreich, D., Hans, S., Kaslin, J. & Brand, M. Regeneration of the adult
46 zebrafish brain from neurogenic radial glia-type progenitors. *Development* **138**, 4831–4841
47 (2011).
- 48 23. Marz, M., Schmidt, R., Rastegar, S. & Strahle, U. Regenerative response following stab injury
49 in the adult zebrafish telencephalon. *Dev Dyn* **240**, 2221–2231 (2011).
- 50 24. Soehnlein, O. & Lindbom, L. Phagocyte partnership during the onset and resolution of
51 inflammation. *Nature Reviews Immunology* vol. 10 (2010).
- 52 25. Bernut, A. *et al.* Mycobacterium abscessus cording prevents phagocytosis and promotes
53 abscess formation. *Proc Natl Acad Sci U S A* **111**, E943-52 (2014).
- 54 26. Shin, J., Park, H. C., Topczewska, J. M., Mawdsley, D. J. & Appel, B. Neural cell fate analysis
55 in zebrafish using olig2 BAC transgenics. *Methods Cell Sci* **25**, 7–14 (2003).
- 56 27. März, M. *et al.* Heterogeneity in progenitor cell subtypes in the ventricular zone of the zebrafish

- 1 adult telencephalon. *Glia* **58**, 870–888 (2010).
- 2 28. Adolf, B. *et al.* Conserved and acquired features of adult neurogenesis in the zebrafish
3 telencephalon. *Dev Biol* **295**, 278–293 (2006).
- 4 29. Barbosa, J. S. S. *et al.* Single-cell in vivo imaging of adult neural stem cells in the zebrafish
5 telencephalon. *Nat Protoc* **11**, 1360–1370 (2016).
- 6 30. Barbosa, J. S. S. & Ninkovic, J. Adult neural stem cell behavior underlying constitutive and
7 restorative neurogenesis in zebrafish. *Neurogenesis*. **3**, e1148101 (2016).
- 8 31. Chen, J., Poskanzer, K. E., Freeman, M. R. & Monk, K. R. Live-imaging of astrocyte
9 morphogenesis and function in zebrafish neural circuits. *Nat. Neurosci.* **23**, (2020).
- 10 32. Bernardos, R. L. & Raymond, P. A. GFAP transgenic zebrafish. *Gene Expr Patterns* **6**, 1007–
11 1013 (2006).
- 12 33. Simon, C., Dimou, L. & Gotz, M. Progenitors in the adult cerebral cortex - cell cycle properties
13 and regulation by physiological stimuli and injury . *Glia* **59(6)**, 869–881 (2011).
- 14 34. Frik, J. *et al.* Cross-talk between monocyte invasion and astrocyte proliferation regulates
15 scarring in brain injury. *EMBO Rep* **19**, (2018).
- 16 35. Barbosa, J. S. S. *et al.* Live imaging of adult neural stem cell behavior in the intact and injured
17 zebrafish brain. *Science (80-.)*. **348**, 789–793 (2015).
- 18 36. Horvat, A. *et al.* A novel role for protein tyrosine phosphatase SHP1 in controlling glial
19 activation in the normal and injured nervous system. *J. Neurosci.* **21**, (2001).
- 20 37. Zhu, Y. M. *et al.* Sevoflurane postconditioning attenuates reactive astrogliosis and glial scar
21 formation after ischemia–reperfusion brain injury. *Neuroscience* **356**, (2017).
- 22 38. Liddelow, S. A. & Barres, B. A. Reactive Astrocytes: Production, Function, and Therapeutic
23 Potential. *Immunity* vol. 46 (2017).
- 24 39. Hsu, J. Y. C. *et al.* Matrix metalloproteinase-9 facilitates glial scar formation in the injured
25 spinal cord. *J. Neurosci.* **28**, (2008).
- 26 40. Schachtrup, C. *et al.* Fibrinogen triggers astrocyte scar formation by promoting the availability
27 of active TGF- β after vascular damage. *J. Neurosci.* **30**, (2010).
- 28 41. Runger, T. M., Quintanilla-Dieck, M. J. & Bhawan, J. Role of cathepsin K in the turnover of the
29 dermal extracellular matrix during scar formation. *J. Invest. Dermatol.* **127**, (2007).
- 30 42. Li, X. *et al.* Cathepsin B Regulates Collagen Expression by Fibroblasts via Prolonging
31 TLR2/NF- κ B Activation. *Oxid. Med. Cell. Longev.* **2016**, (2016).
- 32 43. Lalmanach, G., Saidi, A., Marchand-Adam, S., Lecaille, F. & Kasabova, M. Cysteine
33 cathepsins and cystatins: From ancillary tasks to prominent status in lung diseases. *Biological*
34 *Chemistry* vol. 396 (2015).
- 35 44. Pan, Z. *et al.* MFAP4 deficiency alleviates renal fibrosis through inhibition of NF- κ B and TGF-
36 β /Smad signaling pathways. *FASEB J.* **34**, (2020).
- 37 45. Sulimai, N. & Lominadze, D. Fibrinogen and Neuroinflammation During Traumatic Brain Injury.
38 *Molecular Neurobiology* vol. 57 (2020).
- 39 46. Dietrich, N., Lienenklaus, S., Weiss, S. & Gekara, N. O. Murine Toll-Like Receptor 2 Activation
40 Induces Type I Interferon Responses from Endolysosomal Compartments. *PLoS One* (2010)
41 doi:10.1371/journal.pone.0010250.
- 42 47. Owens, B. M. J., Moore, J. W. J. & Kaye, P. M. IRF7 regulates TLR2-mediated activation of
43 splenic CD11chi dendritic cells. *PLoS One* (2012) doi:10.1371/journal.pone.0041050.
- 44 48. Liljeroos, M. *et al.* Bacterial ligand of TLR2 signals Stat activation via induction of IRF1/2 and
45 interferon- α production. *Cell. Signal.* (2008) doi:10.1016/j.cellsig.2008.06.017.
- 46 49. Nomiyama, H., Osada, N. & Yoshie, O. The evolution of mammalian chemokine genes.
47 *Cytokine and Growth Factor Reviews* (2010) doi:10.1016/j.cytogfr.2010.03.004.
- 48 50. Portou, M. J., Baker, D., Abraham, D. & Tsui, J. The innate immune system, toll-like receptors
49 and dermal wound healing: A review. *Vasc. Pharmacol* **71**, 31–36 (2015).
- 50 51. Mann, D. L., Topkara, V. K., Evans, S. & Barger, P. M. Innate immunity in the adult
51 mammalian heart: for whom the cell tolls. *Trans Am Clin Clim. Assoc* **121**, 31–34 (2010).
- 52 52. Burda, J. E. & Sofroniew, M. V. Reactive gliosis and the multicellular response to CNS
53 damage and disease. *Neuron* **81**, 229–248 (2014).
- 54 53. Griffiths, M. R., Gasque, P. & Neal, J. W. The regulation of the CNS innate immune response
55 is vital for the restoration of tissue homeostasis (repair) after acute brain injury: a brief review.
56 *Int J Inflam* **2010**, 151097 (2010).
- 57 54. Kyritsis, N. *et al.* Acute inflammation initiates the regenerative response in the adult zebrafish
58 brain. *Science (80-.)*. **338**, 1353–1356 (2012).

- 1 55. Sato, M. *et al.* Direct Binding of Toll-Like Receptor 2 to Zymosan, and Zymosan-Induced NF-
2 κ B Activation and TNF- α Secretion Are Down-Regulated by Lung Collectin Surfactant Protein
3 A. *J. Immunol.* (2003) doi:10.4049/jimmunol.171.1.417.
- 4 56. Marcel, L., Pius, L., Nicole, B., Eckart, M. & Bernhard, M. Lymphocyte-specific chemokine
5 receptor CXCR3: regulation, chemokine binding and gene localization. *Eur. J. Immunol.*
6 (1998).
- 7 57. Wijtmans, M. *et al.* Chemical subtleties in small-molecule modulation of peptide receptor
8 function: the case of CXCR3 biaryl-type ligands. *J Med Chem* **55**, 10572–10583 (2012).
- 9 58. Cheng, K., Wang, X., Zhang, S. & Yin, H. Discovery of small-molecule inhibitors of the
10 TLR1/TLR2 complex. *Angew. Chemie - Int. Ed.* (2012) doi:10.1002/anie.201204910.
- 11 59. Torraca, V. *et al.* The CXCR3-CXCL11 signaling axis mediates macrophage recruitment and
12 dissemination of mycobacterial infection. *DMM Dis. Model. Mech.* (2015)
13 doi:10.1242/dmm.017756.
- 14 60. Simon, C., Lickert, H., Gotz, M. & Dimou, L. Sox10-iCreERT2 : a mouse line to inducibly trace
15 the neural crest and oligodendrocyte lineage. *Genesis* **50**, 506–515 (2012).
- 16 61. Zambusi, A., Pelin Burhan, Ö., Di Giaimo, R., Schmid, B. & Ninkovic, J. Granulins Regulate
17 Aging Kinetics in the Adult Zebrafish Telencephalon. *Cells* (2020) doi:10.3390/cells9020350.
- 18 62. Kuroda, M. *et al.* Peripherally derived FGF21 promotes remyelination in the central nervous
19 system. *J. Clin. Invest.* (2017) doi:10.1172/JCI94337.
- 20 63. Yang, J. *et al.* EGF enhances oligodendrogenesis from glial progenitor cells. *Front. Mol.*
21 *Neurosci.* (2017) doi:10.3389/fnmol.2017.00106.
- 22 64. Vinukonda, G. *et al.* Epidermal growth factor preserves myelin and promotes astrogliosis after
23 intraventricular hemorrhage. *Glia* (2016) doi:10.1002/glia.23037.
- 24 65. Pei, D. *et al.* Inhibition of platelet-derived growth factor receptor β reduces reactive glia and
25 scar formation after traumatic brain injury in mice. *Brain Res. Bull.* (2017)
26 doi:10.1016/j.brainresbull.2017.06.020.
- 27 66. Robel, S., Berninger, B., Götz, M. & Gotz, M. The stem cell potential of glia: lessons from
28 reactive gliosis. *Nat. Rev. Neurosci.* **12**(2), 88–104 (2011).
- 29 67. Eugenín-von Bernhardt, J. & Dimou, L. NG2-glia, more than progenitor cells. *Adv. Exp. Med.*
30 *Biol.* (2016) doi:10.1007/978-3-319-40764-7_2.
- 31 68. Karttunen, M. J. *et al.* Regeneration of myelin sheaths of normal length and thickness in the
32 zebrafish CNS correlates with growth of axons in caliber. *PLoS One* **12**, (2017).
- 33 69. von Streitberg, A. *et al.* NG2-Glia Transiently Overcome Their Homeostatic Network and
34 Contribute to Wound Closure After Brain Injury. *Front. Cell Dev. Biol.* **9**, (2021).
- 35 70. Wullmann, M. F. & Rink, E. The teleostean forebrain: a comparative and developmental view
36 based on early proliferation, Pax6 activity and catecholaminergic organization. *Brain Res Bull*
37 **57**, 363–370 (2002).
- 38 71. Mueller, T. & Wullmann, M. F. BrdU-, neuroD (nrd)- and Hu-studies reveal unusual non-
39 ventricular neurogenesis in the postembryonic zebrafish forebrain. *Mech Dev* **117**, 123–135
40 (2002).
- 41 72. Whish, S. *et al.* The inner csf-brain barrier: Developmentally controlled access to the brain via
42 intercellular junctions. *Front. Neurosci.* (2015) doi:10.3389/fnins.2015.00016.
- 43 73. Yu, Y. R. *et al.* Systemic cytokine profiles and splenic toll-like receptor expression during
44 *Trichinella spiralis* infection. *Exp Parasitol* **134**, 92–101 (2013).
- 45 74. Zupanc, G. K. Adult neurogenesis and neuronal regeneration in the brain of teleost fish. *J*
46 *Physiol Paris* **102**, 357–373 (2008).
- 47 75. Zupanc, G. K. Towards brain repair: Insights from teleost fish. *Semin Cell Dev Biol* **20**, 683–
48 690 (2009).
- 49 76. Zupanc, G. K. Neurogenesis and neuronal regeneration in the adult fish brain. *J Comp Physiol*
50 *A Neuroethol Sens Neural Behav Physiol* **192**, 649–670 (2006).
- 51 77. Alunni, A. & Bally-Cuif, L. A comparative view of regenerative neurogenesis in vertebrates.
52 *Development* **143**, 741–753 (2016).
- 53 78. Kizil, C. *et al.* The chemokine receptor cxcr5 regulates the regenerative neurogenesis
54 response in the adult zebrafish brain. *Neural Dev* **7**, 27 (2012).
- 55 79. Labbe, R. M. *et al.* A comparative transcriptomic analysis reveals conserved features of stem
56 cell pluripotency in planarians and mammals. *Stem Cells* **30**, 1734–1745 (2012).
- 57 80. Simkin, J., Gawriluk, T. R., Gensel, J. C. & Seifert, A. W. Macrophages are necessary for
58 epimorphic regeneration in African spiny mice. *Elife* **6**, (2017).

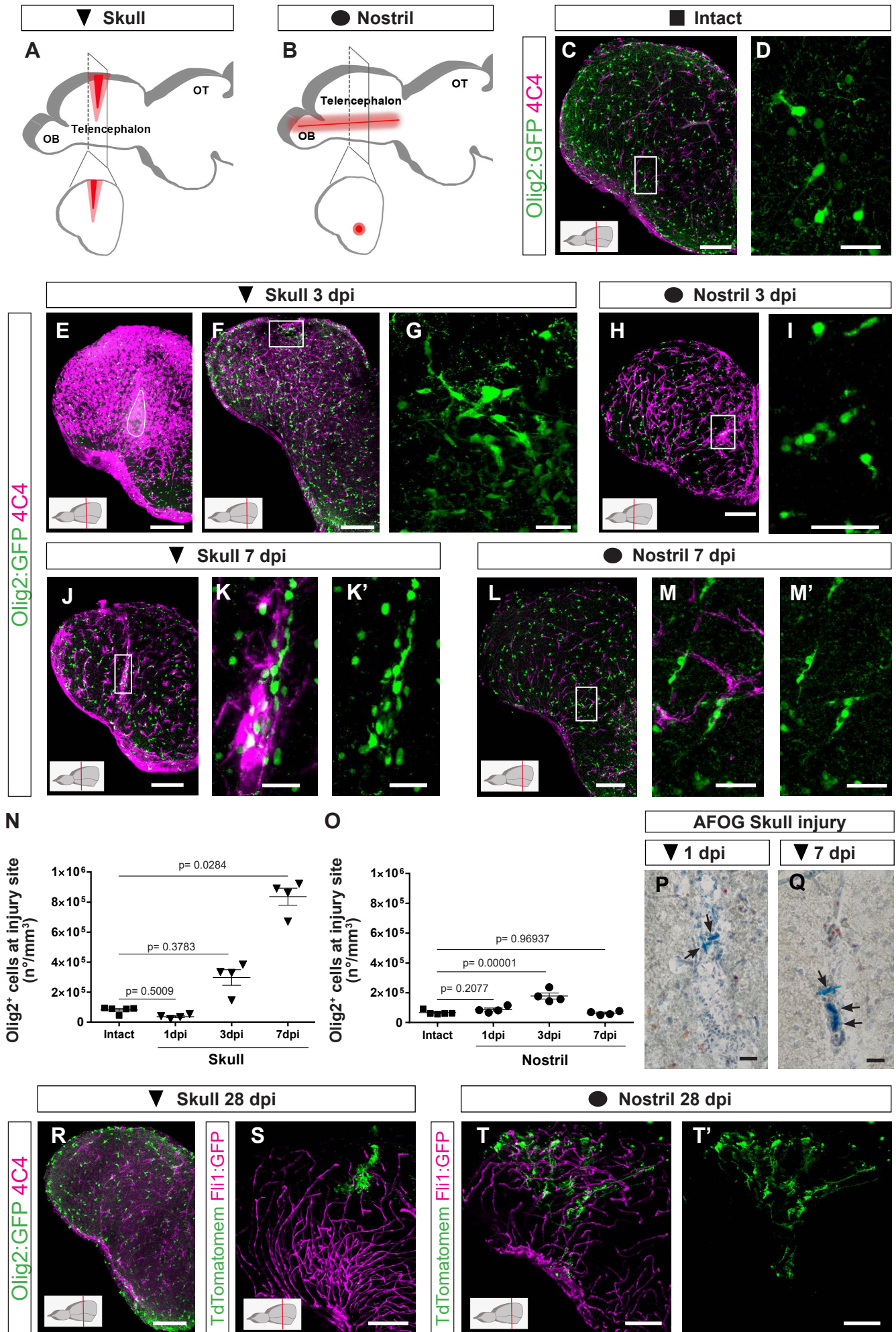
- 1 81. Seifert, A. W. *et al.* Skin shedding and tissue regeneration in African spiny mice (*Acomys*).
2 *Nature* **489**, 561–565 (2012).
- 3 82. Brant, J. O., Yoon, J. H., Polvadore, T., Barbazuk, W. B. & Maden, M. Cellular events during
4 scar-free skin regeneration in the spiny mouse, *Acomys*. *Wound Repair Regen* **24**, 75–88
5 (2016).
- 6 83. Grade, S. & Götz, M. Neuronal replacement therapy: previous achievements and challenges
7 ahead. *Regen Med* (2017).
- 8 84. Grandel, H. & Brand, M. Comparative aspects of adult neural stem cell activity in vertebrates.
9 *Dev Genes Evol* **223**, 131–147 (2013).
- 10 85. Kizil, C., Kaslin, J., Kroehne, V. & Brand, M. Adult neurogenesis and brain regeneration in
11 zebrafish. *Dev Neurobiol* **72**, 429–461 (2012).
- 12 86. Dunkin, C. S. *et al.* Scarring occurs at a critical depth of skin injury: precise measurement in a
13 graduated dermal scratch in human volunteers. *Plast Reconstr Surg* **119**, 1722–1724 (2007).
- 14 87. Bouabe, H., Liu, Y., Moser, M., Bosl, M. R. & Heesemann, J. Novel highly sensitive IL-10-beta-
15 lactamase reporter mouse reveals cells of the innate immune system as a substantial source
16 of IL-10 in vivo. *J Immunol* **187**, 3165–3176 (2011).
- 17 88. Hsieh, C. L. *et al.* CCR2 deficiency impairs macrophage infiltration and improves cognitive
18 function after traumatic brain injury. *J Neurotrauma* **31**, 1677–1688 (2014).
- 19 89. Wattananit, S. *et al.* Monocyte-Derived Macrophages Contribute to Spontaneous Long-Term
20 Functional Recovery after Stroke in Mice. *J Neurosci* **36**, 4182–4195 (2016).
- 21 90. Rothhammer, V. *et al.* Type I interferons and microbial metabolites of tryptophan modulate
22 astrocyte activity and central nervous system inflammation via the aryl hydrocarbon receptor.
23 *Nat Med* **22**, 586–597 (2016).
- 24 91. Rothhammer, V. *et al.* Microglial control of astrocytes in response to microbial metabolites.
25 *Nature* **557**, 724–728 (2018).
- 26 92. Kielian, T. Toll-like receptors in central nervous system glial inflammation and homeostasis. *J*
27 *Neurosci Res* **83**, 711–730 (2006).
- 28 93. Krauthausen, M. *et al.* CXCR3 modulates glial accumulation and activation in cuprizone-
29 induced demyelination of the central nervous system. *J Neuroinflammation* **11**, 109 (2014).
- 30 94. Goldberg, S. H. *et al.* CXCR3 expression in human central nervous system diseases.
31 *Neuropathol Appl Neurobiol* **27**, 127–138 (2001).
- 32 95. Bsibsi, M., Ravid, R., Gveric, D. & van Noort, J. M. Broad expression of Toll-like receptors in
33 the human central nervous system. *J Neuropathol Exp Neurol* **61**, 1013–1021 (2002).
- 34 96. Dzamko, N. *et al.* Toll-like receptor 2 is increased in neurons in Parkinson’s disease brain and
35 may contribute to alpha-synuclein pathology. *Acta Neuropathol* **133**, 303–319 (2017).
- 36 97. Mestre, H. *et al.* Cerebrospinal fluid influx drives acute ischemic tissue swelling. *Science* (80-
37). (2020) doi:10.1126/science.aaw7462.
- 38 98. Lepko, T. *et al.* Choroid plexus-derived miR-204 regulates the number of quiescent neural
39 stem cells in the adult brain. *EMBO J.* **38**, (2019).
- 40 99. Sirko, S. *et al.* Reactive glia in the injured brain acquire stem cell properties in response to
41 sonic hedgehog. [corrected]. *Cell Stem Cell* **12**, 426–439 (2013).

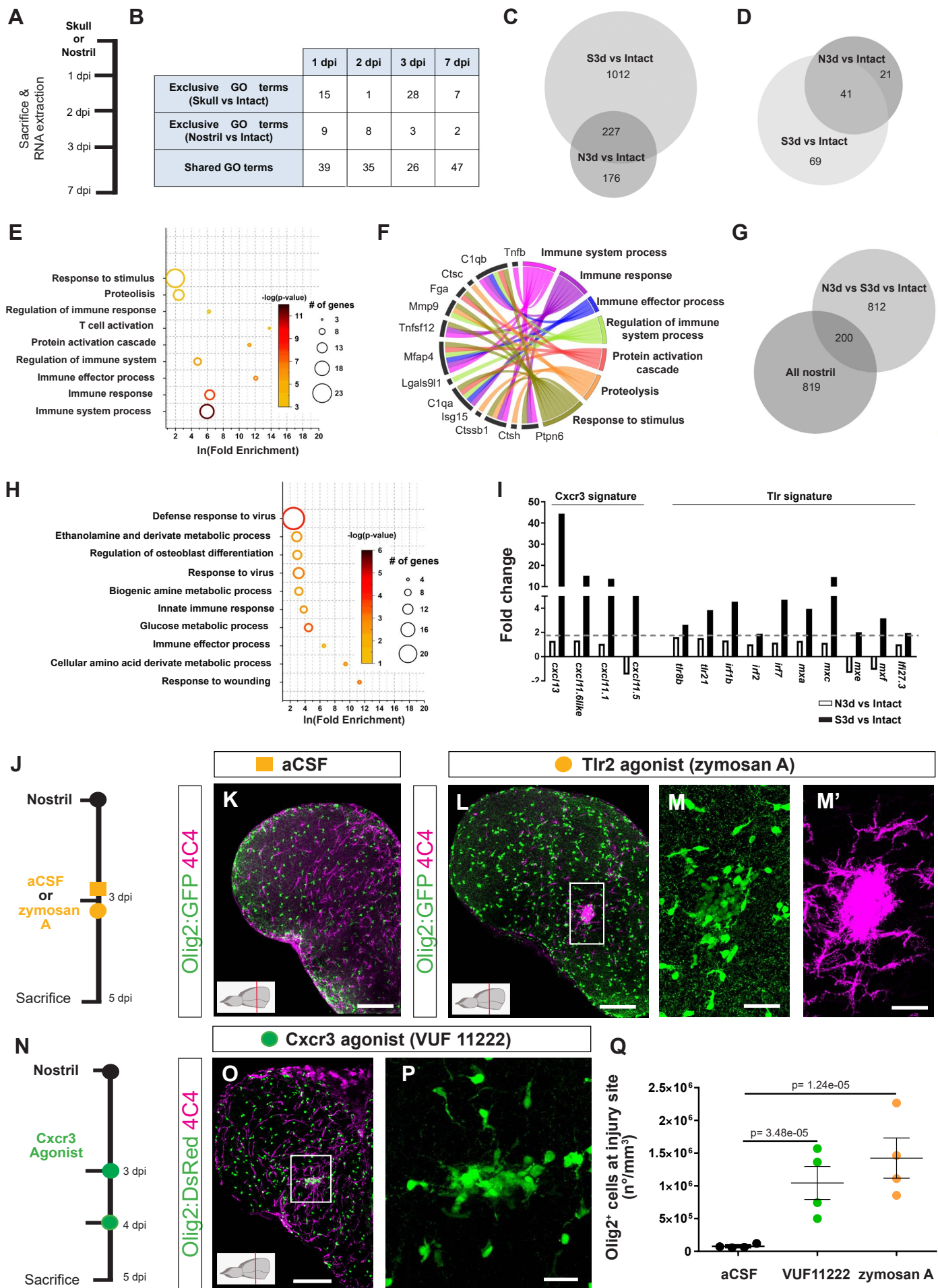
42

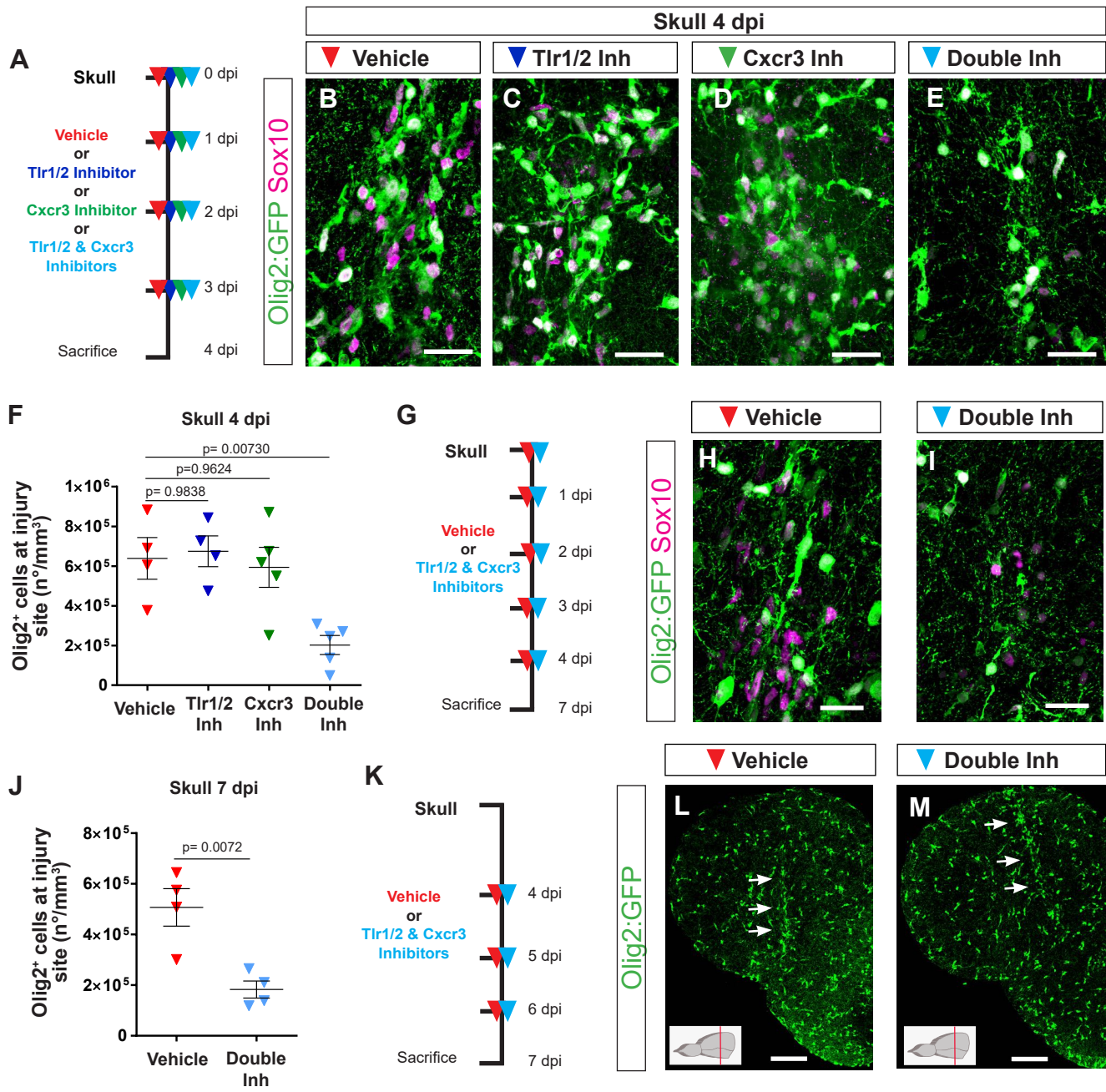
43 **Acknowledgments:**

44 We want to thank Pamela Raymonds for sharing the *Tg(gfap:GFP)mi2001* fish line and Bruce
45 Apple for sharing *Tg(Olig2:GFP)* and *Tg(Olig2:DsRed)* fish lines. We are thankful to Andrea
46 Steiner-Mazzardi, Sarah Hübinger and Beate Stiening for excellent technical help, and to Sofia
47 Grade and Clayton Gordy for critical reading of the manuscript. We also gratefully acknowledge
48 funding to JN from the German Research foundation (DFG) by the SFB 870; SPP1757; TRR 274/1
49 - 408885537; SPP1738 and Thyssen Stiftung, to MG the German Research foundation (DFG) by
50 the SFB 870, and the ERC grant ChroNeuroRepair: GA No. 340793. Work in W. W. lab is by the
51 German Science Foundation Collaborative Research Centre (CRC) 870; funds from the
52 Bayerisches Staatsministerium für Bildung und Kultus, Wissenschaft und Kunst within Bavarian
53 Research Network “Human Induced Pluripotent Stem Cells” (ForIPS) and (in part) by the
54 Helmholtz Portfolio Theme ‘Supercomputing and Modelling for the Human Brain’ (SMHB). H.S.

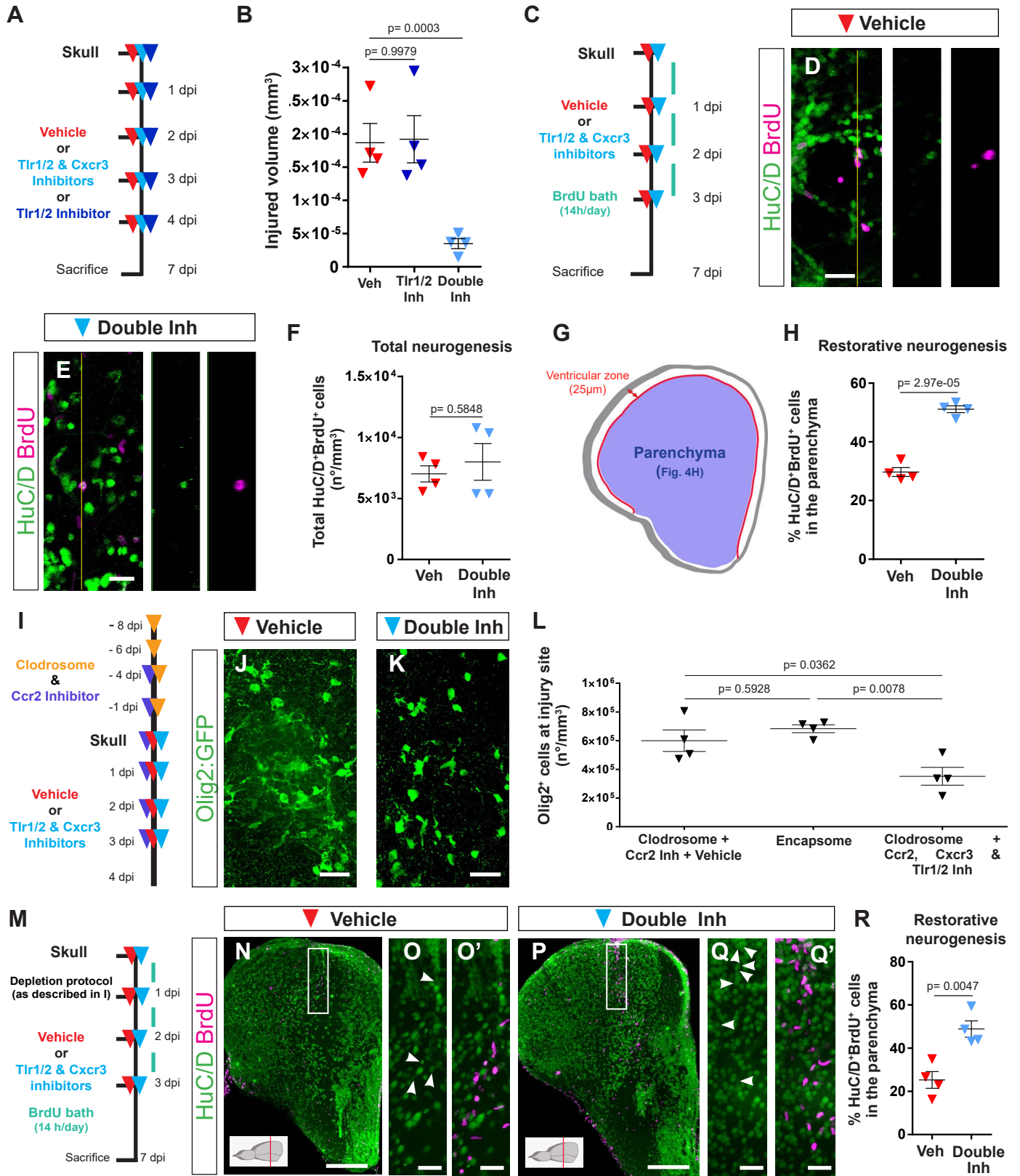
- 1 is supported by the DFG (CRC 870). Dr. Huttner was supported by a research grant from the
- 2 German Research Foundation (DFG-HU1961/2-1).



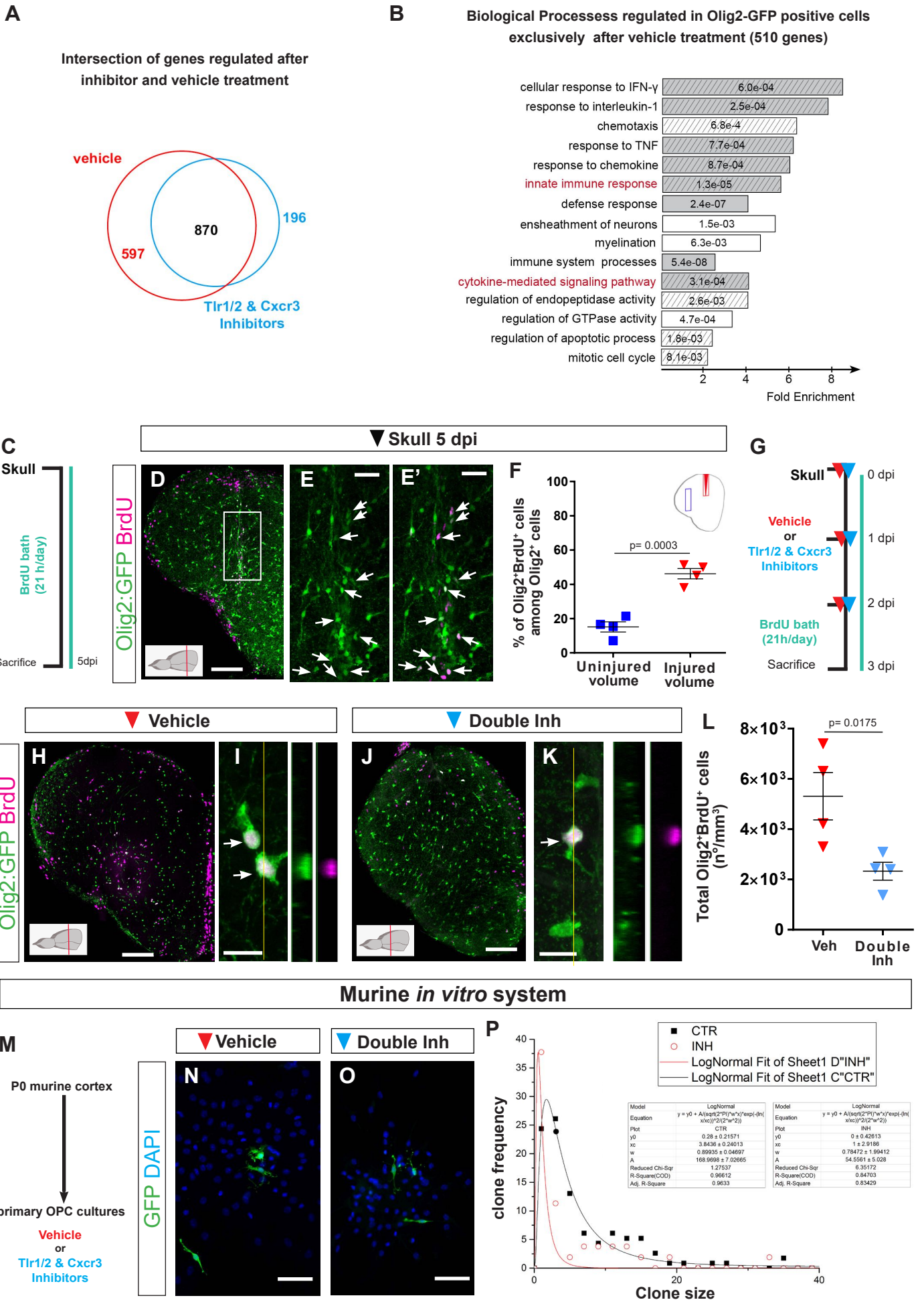


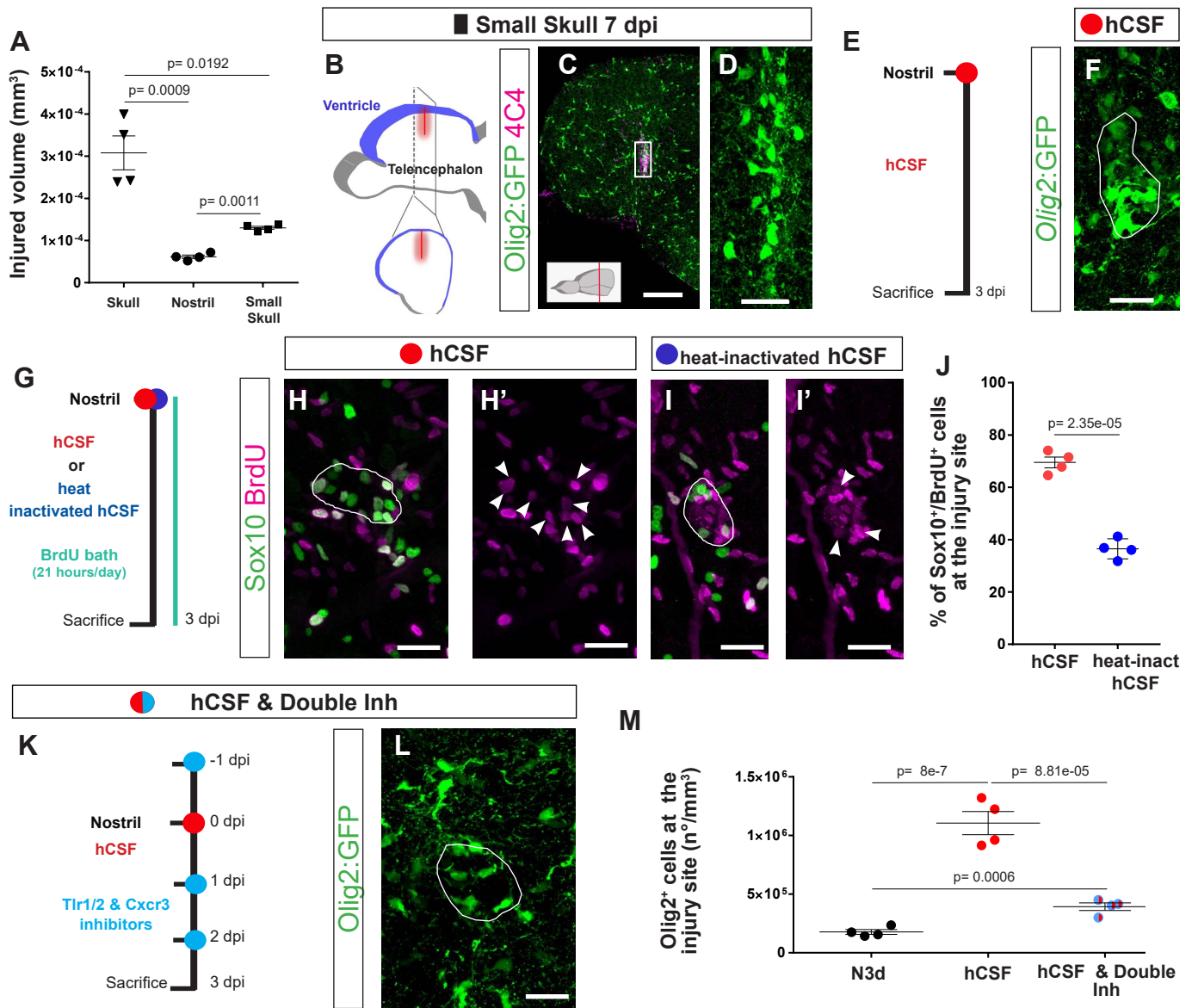


Sanchez-Gonzalez et al., 2021 Figure 3

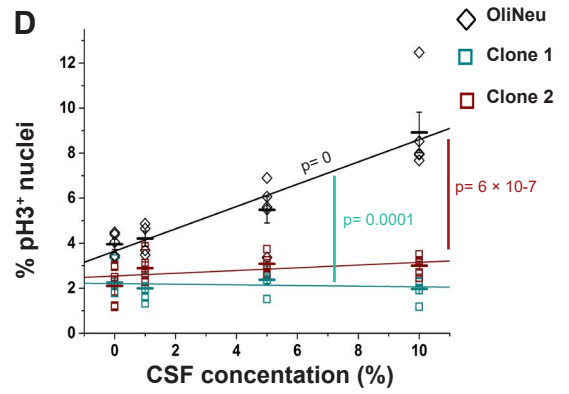
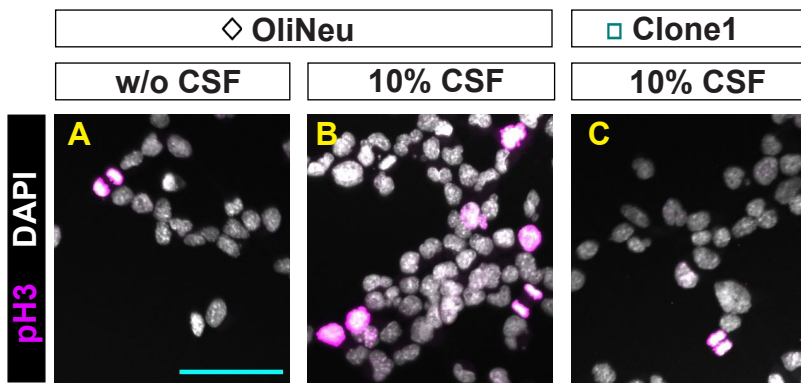


Sanchez-Gonzalez et al., 2021 Figure 4





Sanchez-Gonzalez et al., 2021 Figure 6

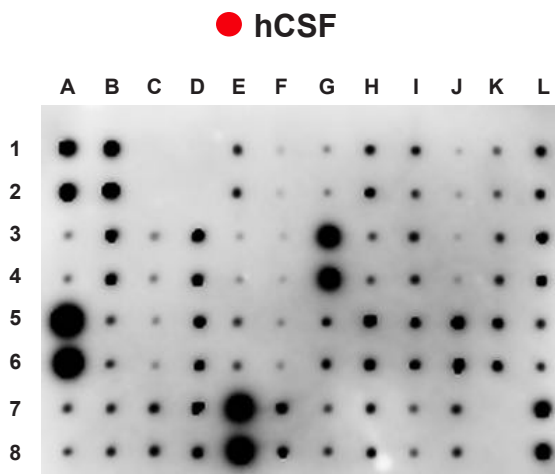


E

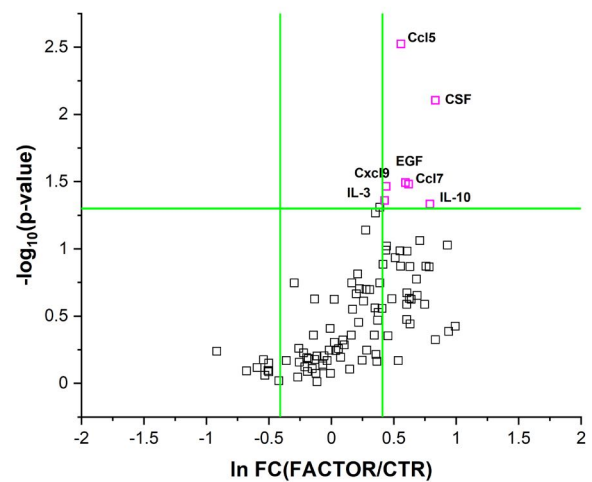
	A	B	C	D	E	F	G	H	I	J	K	L
1	Pos	Pos	Neg	Neg	Cxcl5	G-CSF	GM-CSF	GRO	Cxcl1	Ccl1	IL-1 α	IL-1 β
2	Pos	Pos	Neg	Neg	Cxcl5	G-CSF	GM-CSF	GRO	Cxcl1	Ccl1	IL-1 α	IL-1 β
3	IL-2	IL-3	IL-4	IL-5	IL-6	IL-7	IL-8	IL-10	IL-12	IL-13	IL-15	IFN- γ
4	IL-2	IL-3	IL-4	IL-5	IL-6	IL-7	IL-8	IL-10	IL-12	IL-13	IL-15	IFN- γ
5	Ccl2	Ccl8	Ccl7	MCSF	Ccl22	Cxcl9	Ccl15	Ccl5	SCF	SDF-1	Ccl17	TGF- β 1
6	Ccl2	Ccl8	Ccl7	MCSF	Ccl22	Cxcl9	Ccl15	Ccl5	SCF	SDF-1	Ccl17	TGF- β 1
7	TNF- α	TNF- β	EGF	IGF-I	ANG	MOSM	THPO	VEGF	PDGF BB	Leptin	Neg	Pos
8	TNF- α	TNF- β	EGF	IGF-I	ANG	MOSM	THPO	VEGF	PDGF BB	Leptin	Neg	Pos

Legend:
 □ Negative
 ■ Positive (4 samples)
 ■ Positive (3 samples)
 ■ Positive (2 samples)
 ■ Positive (1 sample)

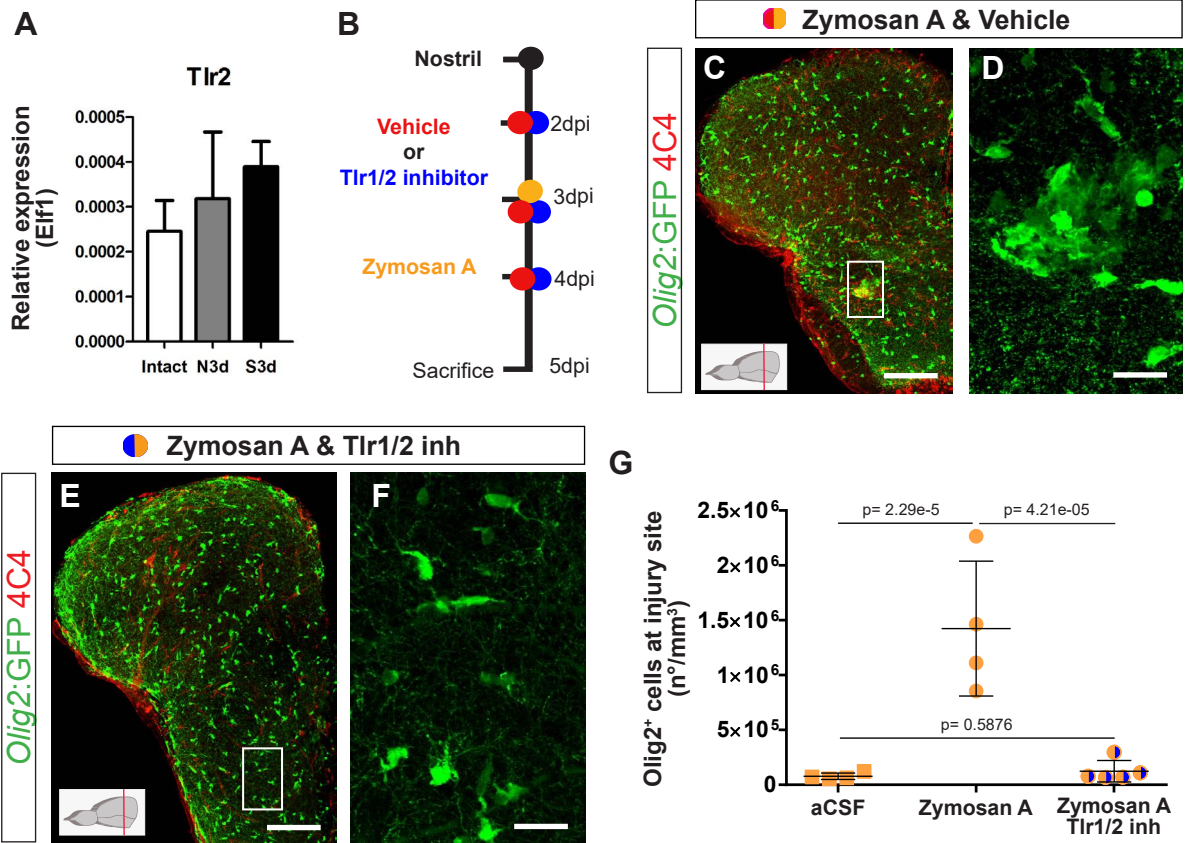
F



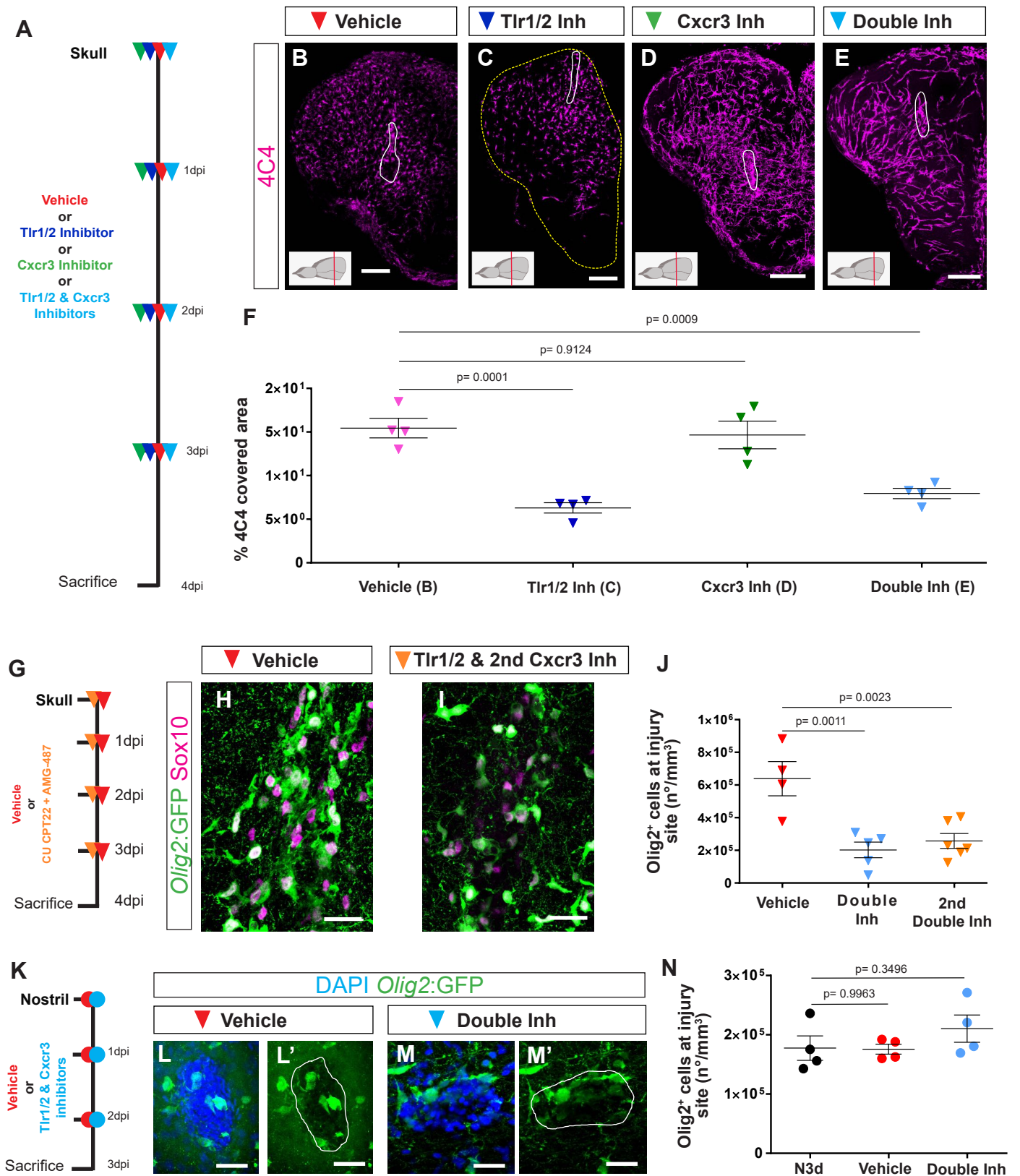
G



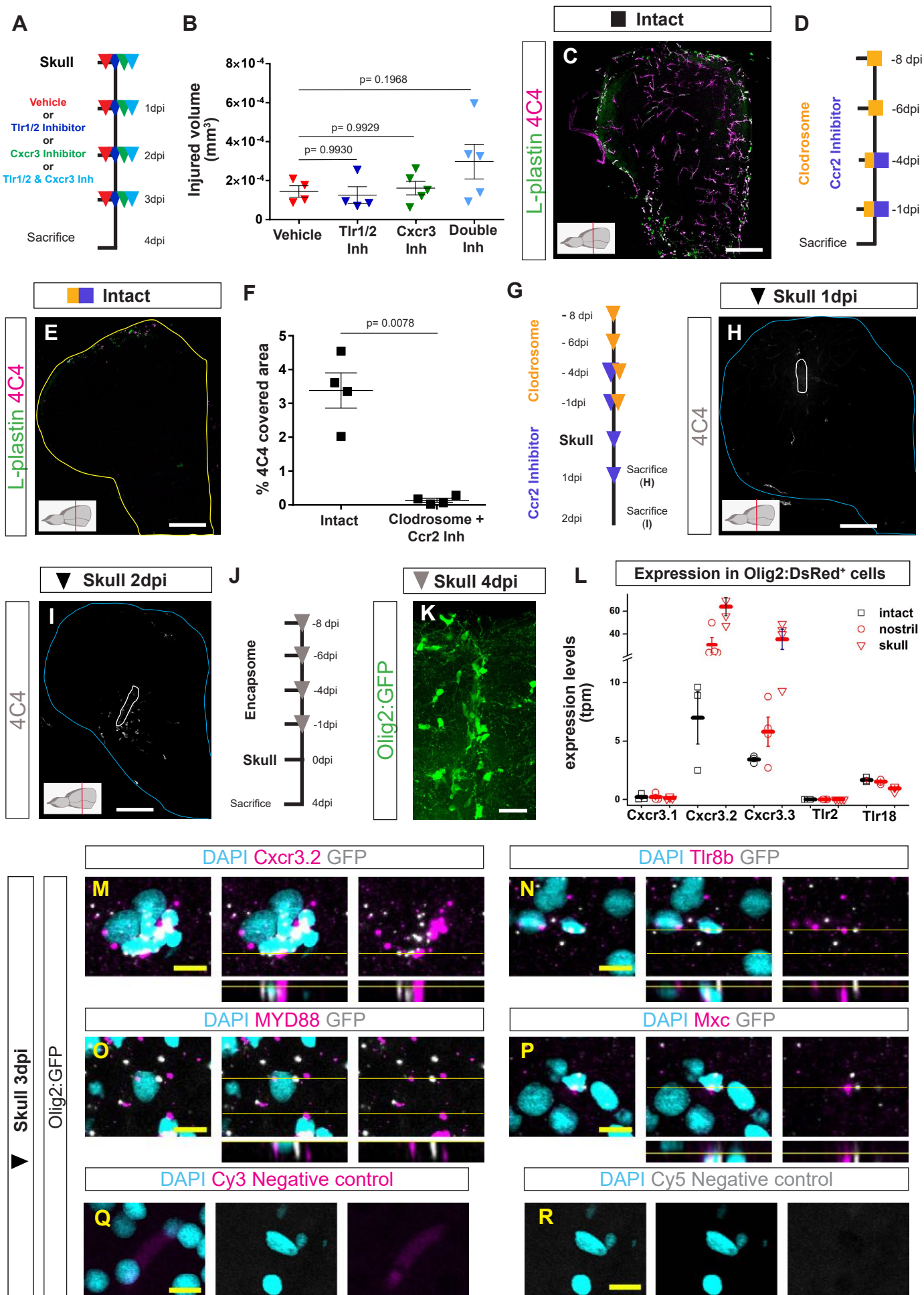
Sanchez-Gonzalez et al., 2021 Figure 7



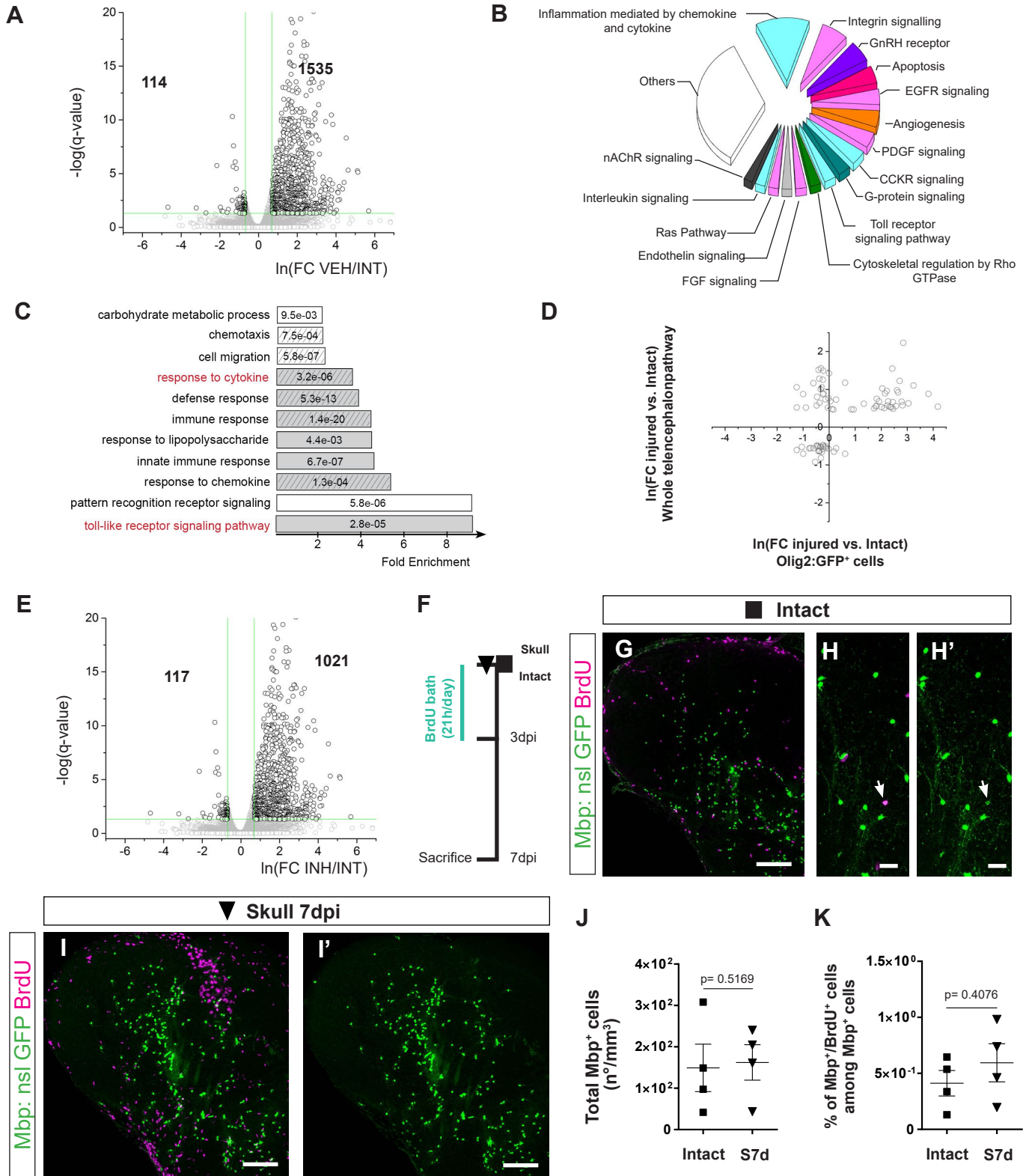
Sanchez-Gonzalez et al., 2021 Figure EV1



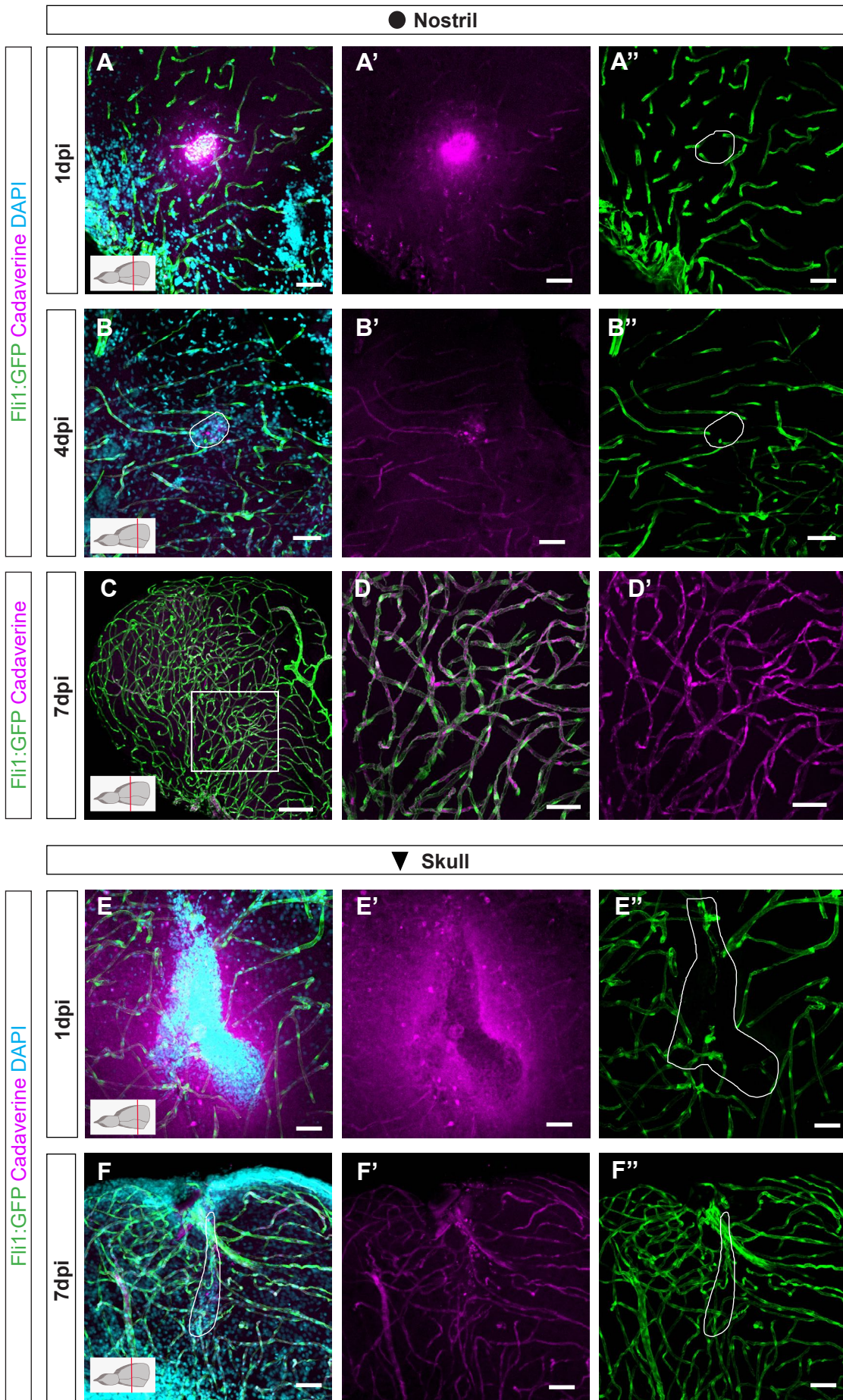
Sanchez-Gonzalez et al., 2021 Figure EV2



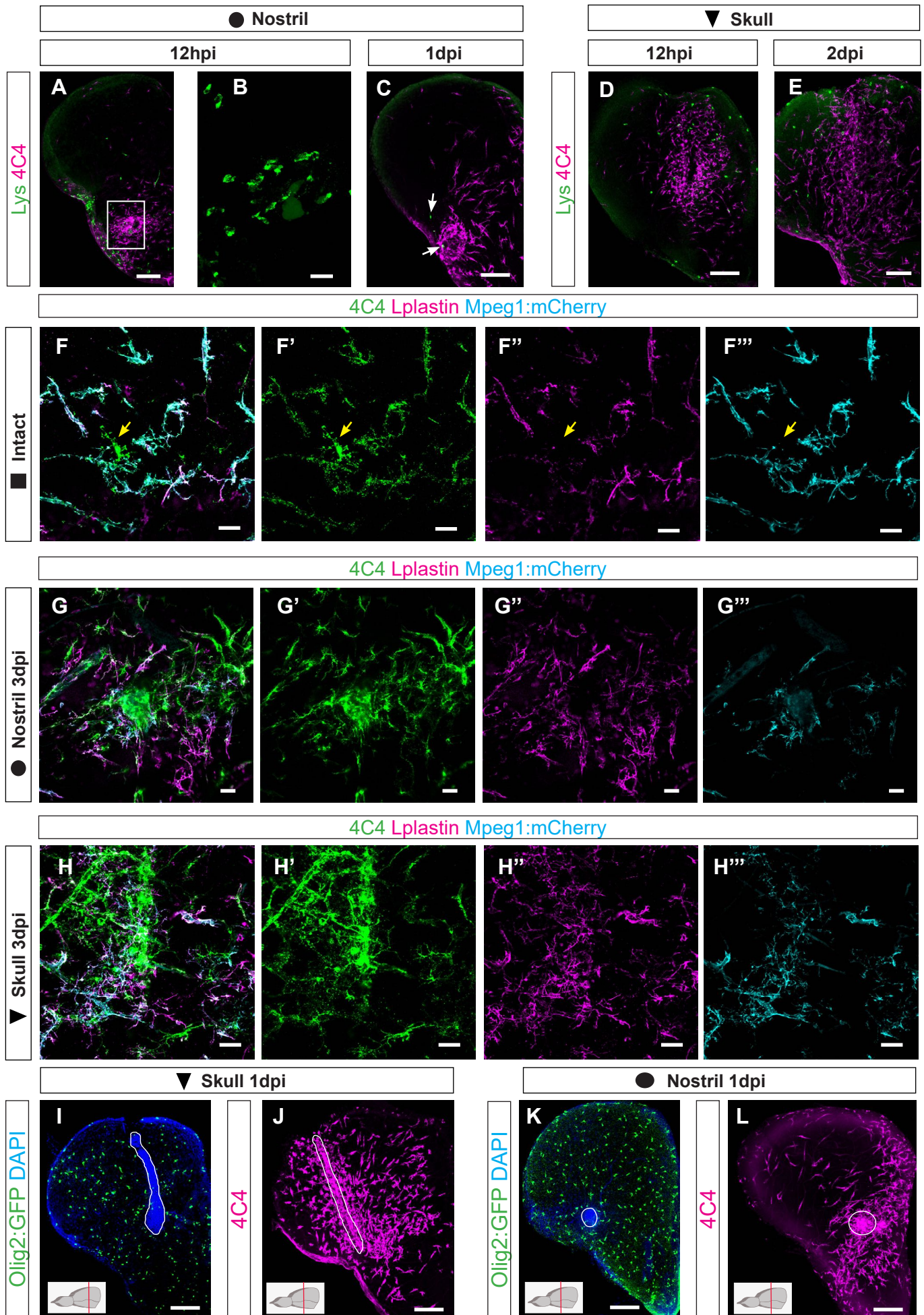
Sanchez-Gonzalez et al., 2021 Figure EV3



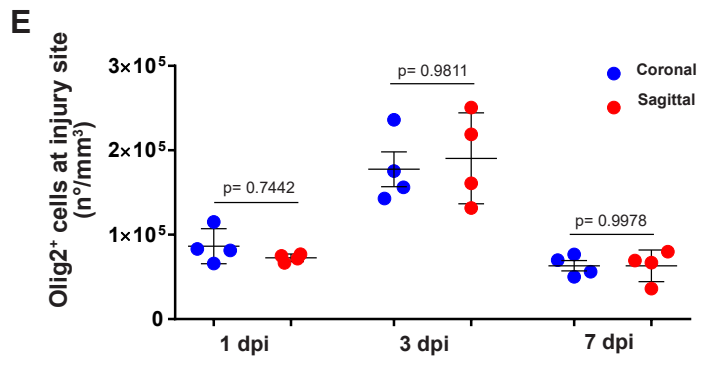
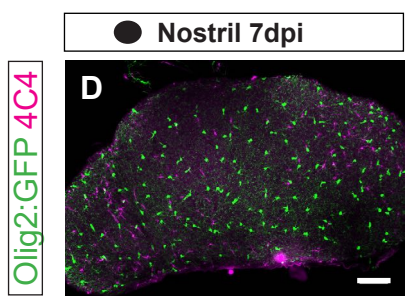
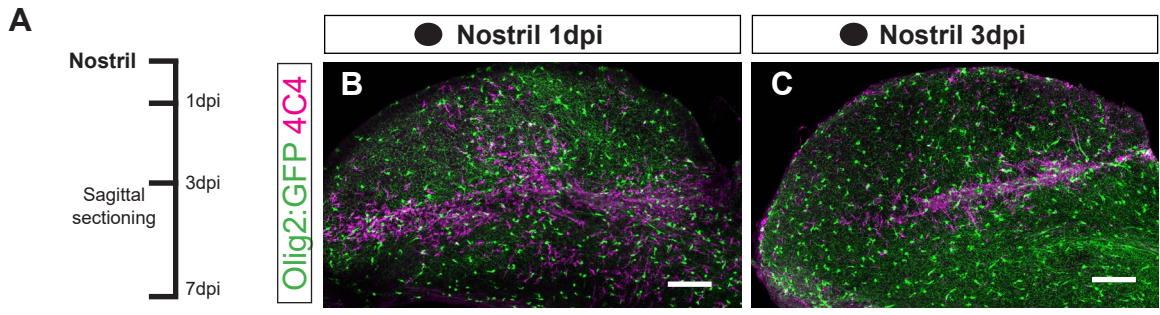
Sanchez-Gonzalez et al., 2021 Figure EV4



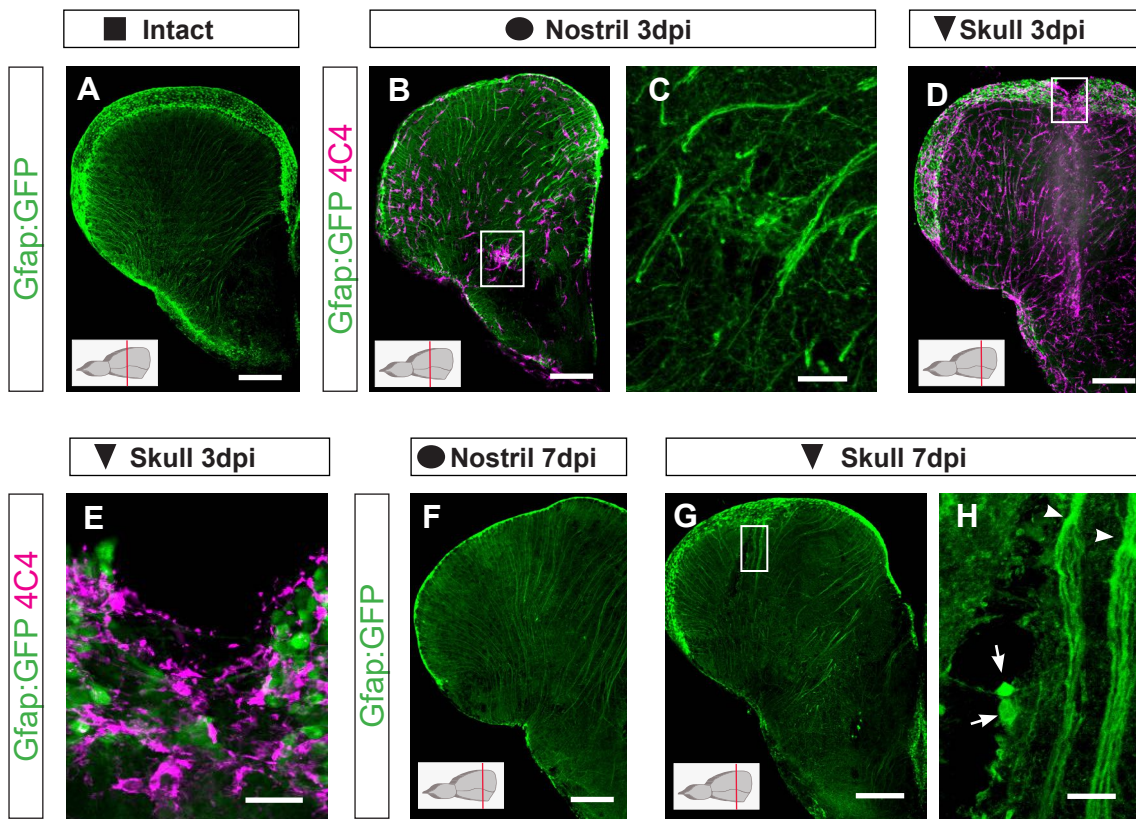
Appendix Figure S1



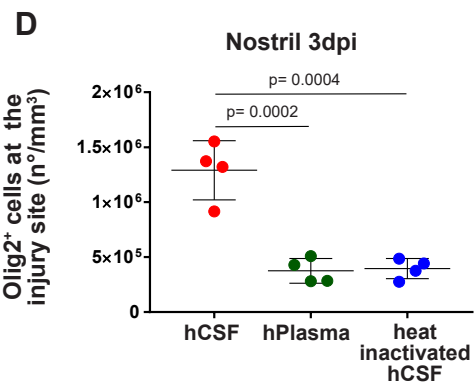
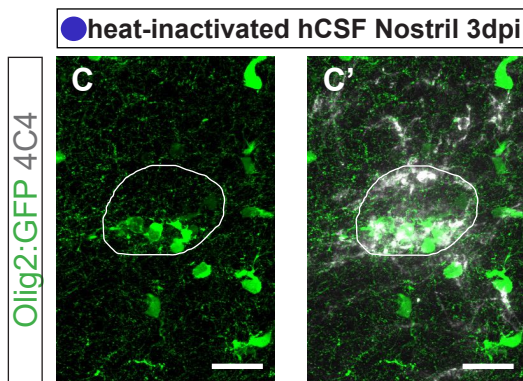
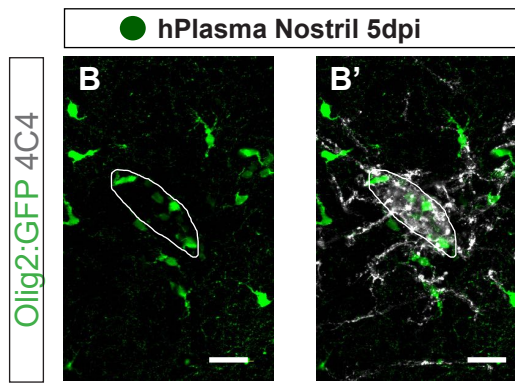
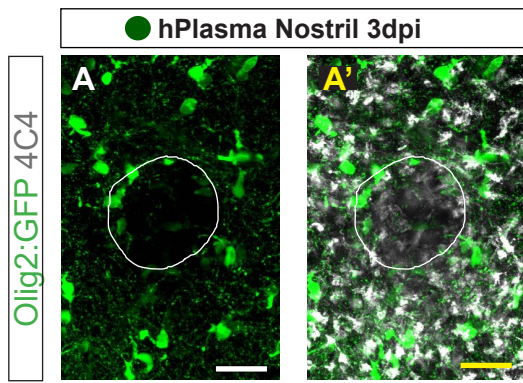
Appendix Figure S2



Appendix Figure S3



Appendix Figure S4



Appendix figure S5

Discussion

Aging is considered the primary risk factor for the onset of neurodegenerative diseases, such as Alzheimer's disease (AD), Parkinson's disease (PD) and frontotemporal dementia (FTD) (Hou et al., 2019; Mattson and Arumugam, 2018). Moreover, a correlation between traumatic brain injuries (TBI) and increased rate of neurodegeneration associated with abnormal accumulation of proteins, including tau, amyloid- β and TDP-43, has been established (Cruz-Haces et al., 2017; Graham and Sharp, 2019). However, the direct link between TBI and neurodegenerative diseases has not yet been fully understood.

Interestingly, neuroinflammation is a common thread between aging, TBI and neurodegenerative diseases (Simon et al., 2017). Indeed, aberrant activation of both innate and adaptive immunity, and transition of homeostatic microglial cells to disease-associated microglia (DAMs) characterized by increased production of pro-inflammatory cytokines and complement factors, are common neuroinflammatory changes observed in the mammalian CNS in response to TBI or during aging. Moreover, several studies have demonstrated the correlation between high levels of neuroinflammation and increased risk for neurodegenerative diseases (Guzman-Martinez et al., 2019; Hou et al., 2019; McKenzie et al., 2017). Therefore, the identification of factors contributing to the regulation of neuroinflammation during aging and in response to TBI in the CNS and the characterization of the mechanisms of action of these factors would represent a turning point for the development of new therapies aimed to ameliorate the quality of life of aging individuals and patients affected by TBI. Furthermore, these discoveries may help to prevent the onset or slow the progression of neurodegeneration in the human CNS.

To this goal, during my PhD, I identified and characterized granulins (Grns) as key factors involved in the regulation of neuroinflammation in the aging CNS and in response to TBI in the zebrafish telencephalon (*Zambusi et al., 2020, Zambusi, Novoselc et al., in revision*). As previously introduced, in contrast to mammals, zebrafish genome harbors four different granulin

genes: *grna*, *grnb*, *grn1* and *grn2*. Due to the high similarity between *Grna* and *Grnb* (orthologs of the mammalian *PGRN* originated by genome duplication), I used a composite knockout model for *Grna* and *Grnb* to avoid any possible compensatory effect (Solchenberger et al., 2015; *Zambusi et al., 2020, Zambusi, Novoselec et al., in revision*).

The results described in my PhD thesis provide novel mechanisms of action of granulins in the context of the CNS, highlight the importance of tightly regulating neuroinflammation, describe a link between liquid-liquid phase separation (LLPS) and microglial cell activation *in vivo*, and describe for the first time the consequences of dysregulated LLPS on CNS regeneration of the adult zebrafish.

Altogether, these new findings strengthen the validity of zebrafish as model to study aging and regeneration in the CNS and demonstrate the regulatory role of granulins in tuning neuroinflammation, proposing their use as therapeutic targets to ameliorate the regenerative outcome in the human CNS.

Granulins regulate aging kinetics and neuroinflammatory state in the adult zebrafish telencephalon

Several studies have focused on the identification of potential candidates associated with aging progression in humans. Interestingly, *PGRN* variants have been discovered to increase the rate of biological aging in the human cerebral cortex (Rhinn and Abeliovich, 2017). However, the molecular mechanisms and the direct consequences of *PGRN* genetic variants on the aging kinetics of the CNS remain elusive.

To address this question, I analyzed the typical age-related hallmarks in the telencephalon of young and old, wildtype (wt) and *Grna;Grnb*-deficient (*Grn*-deficient) zebrafish (*Zambusi et al., 2020*).

The first approach I took was to further validate zebrafish as model to study the typical age-related hallmarks within the CNS. Notably, when young and old wt zebrafish were compared, I detected significant changes in several processes associated with aging, similarly to what has been demonstrated in

the aging mammalian CNS (Mattson and Arumugam, 2018), supporting the value of the results described in this thesis.

More specifically, similarly to the decline of activated stem cells and the reduced neurogenic potential in the mammalian dentate gyrus (DG) and subependymal zone (SEZ) during aging (Bast et al., 2018; Kalamakis et al., 2019; Lazarov et al., 2010; Villeda et al., 2011), I detected a significant reduction in the proportion of proliferating cells located at the ventricular zone (VZ) of old animals. The majority of proliferating cells located at the VZ of adult zebrafish telencephalon are ependymogial cells (a proportion of these cells possess neurogenic potential) (Barbosa et al., 2015). Therefore, it is tempting to speculate that the reduction of proliferating cells in the VZ may represent a reduction of activated stem cells in the aging zebrafish telencephalon. This hypothesis was supported by the lower number of newly generated neurons deposited in the subventricular zone (SVZ) in the telencephalon of old animals. This set of data implies a reduction of the neurogenic potential in the aging zebrafish CNS and is in line with previous observations (Edelmann et al., 2013; *Obermann et al., 2019*). However, it remains to be assessed whether the increased proportion of quiescent adult neural stem cells (aNSCs) and the reduction of constitutive neurogenesis observed in the telencephalon of old animals is caused by age-related cell intrinsic changes (mitochondria dysfunction and telomere shortening) (Molofsky et al., 2006), age-related systemic changes affecting the neurogenic niches (i.e. neuroinflammation) (Kalamakis et al., 2019) or the combinatory effect of both age-related cell intrinsic and extrinsic changes.

Along with a decline in stem cell activation and neurogenesis, aging caused a significant reduction of proliferating oligodendroglial cells in the telencephalon of old animals, suggesting that oligodendrogenesis is also affected during aging in the zebrafish CNS. Notably, a similar impairment has been observed in the aging mouse brain (Miyamoto et al., 2013; Waly et al., 2014), strengthening the translational value of the results obtained in zebrafish in the context of brain aging.

To further investigate the age-related changes in the zebrafish telencephalon, the analyses of telomeres and genes involved in telomere protection were performed. During aging in the mammalian CNS, telomeres are susceptible to shortening with each round of cell division and mutations in telomere-protective genes lead to accelerated onset of age-related hallmarks (Armanios et al., 2009; López-Otín et al., 2013; Mattson and Arumugam, 2018). Furthermore, it has been demonstrated that a strong correlation between telomere shortening rate and life span exists in numerous species (Whittemore et al., 2019).

Similarly, telomere length was significantly reduced in the telencephalon of old zebrafish. This result was complemented by the lower expression of genes encoding for enzymes actively protecting telomeres in physiological conditions, including telomerase reverse transcriptase (Tert), tumor protein p53 (Tp53) and tripeptidyl peptidase 1 (Tpp1).

These data are in agreement with previous studies describing the similarities between telomeres in humans and zebrafish, and identifying the process of telomere shortening in zebrafish during aging (Carneiro et al., 2016).

In summary, these data validate zebrafish as model to study aging kinetics in the CNS and to identify new factors regulating aging and aging-associated neuroinflammation in the CNS.

Based on these observations, I addressed the functional roles of Grns in the context of brain aging in zebrafish, comparing the typical age-related hallmarks between and young/old wt and young/old Grn-deficient animals. Interestingly, the proportion of proliferating cells in the VZ (active aNSCs) of young Grn-deficient animals was significantly reduced, similarly to the number of newborn neurons generated and deposited in the SVZ. Therefore, it is tempting to speculate that Grn-deficient aNSCs are affected by accelerated aging kinetics, entering prematurely into quiescence and causing a significant impairment of neurogenesis already during young adulthood.

Comparably to the decline of active aNSCs, the number of BrdU-incorporating oligodendrocyte cells was also reduced in the telencephalon of young Grn-deficient animals. To distinguish between lower proliferation rate of oligodendrocyte precursor cells (OPCs) or impaired oligodendrogenesis, I

compared the transcriptome of FACS-isolated wt and Grn-deficient oligodendroglial cells and detected lower expression of molecular programs associated with oligodendroglial cell differentiation and myelination, such as negative regulation of BMP, Hedgehog, Notch, TGF- β and ErbB signaling pathways (Bartus et al., 2019; Grinspan, 2015; López-Juárez et al., 2017; Palazuelos et al., 2014). Altogether, these results suggest that Grn deficiency affects the differentiation and maturation processes of OPCs during young adulthood, causing premature deficits in oligodendrogenesis that are normally detected during aging in wt animals.

Surprisingly, the decline in neurogenesis and oligodendrogenesis in the telencephalon of young Grn-deficient animals was comparable to the decline detected in old wt animals and did not worsen in old Grn-deficient animals, supporting the concept that granulin deficiency promotes accelerated aging kinetics in the telencephalon of young adult animals.

To gain further insights on the correlation between aging kinetics and granulin levels in the zebrafish CNS, the telomere length and the expression of telomere-protective genes (same as above) were analyzed. Interestingly, young/old Grn-deficient and old wt telencephali displayed higher rate of telomere shortening and lower expression of telomere-protective genes when compared to the group of young wt animals. Collectively, these results provide new evidence supporting the role of Grns in regulating aging kinetics in the CNS and demonstrate for the first time that Grn-deficient zebrafish are affected by accelerated onset of age-related hallmarks in the CNS.

Encouraged by these observations, I compared the transcriptomic signatures of young/old Grn-deficient and young/old wt animals and showed that the accelerated aging kinetics in young Grn-deficient telencephali was also reflected at the transcriptome level, with numerous genes being upregulated and downregulated in a similar manner to old wt animals. Surprised by the high degree of similarity, I isolated the commonly regulated genes in young Grn-deficient and old wt animals (young wt group was used as reference) to detect possible shared age-related programs. Gene Ontology (GO) analysis revealed significant enrichment of genes associated with regulation of

apoptosis, extracellular matrix composition, cell adhesion, and neuroinflammation. Several of these programs have been previously identified in *N. furzeri*, a well-established aging model (Baumgart et al., 2014), supporting our previous data and confirming the importance of granulins to regulate aging kinetics in the zebrafish CNS.

Neuroinflammation is a typical age-related hallmark in the CNS, associated with changes that include modifications in microglial cell morphology, elevated secretion of pro-inflammatory cytokines and chemokines, and exacerbated production of complement factors (Cribbs et al., 2012; Franceschi et al., 2000; Lucin and Wyss-Coray, 2009; Lui et al., 2016).

As our main research goal coincided with the identification of key factors regulating neuroinflammation in the context of brain aging and TBI, and as significant changes in the expression level of neuroinflammatory genes were detected in the telencephalon of young Grn-deficient and old wt animals, I further characterized the neuroinflammatory state in the telencephalon of Grn-deficient animals.

To this end, I isolated via FACS and compared Grn-deficient and wt microglial cells and identified a large cohort of upregulated inflammatory genes associated with tumor necrosis factor (TNF), MAPK and Janus kinases/signal transducer and activator of transcription protein (JAK/STAT) signaling pathways, programs actively stimulating the production of pro-inflammatory cytokines (Lim et al., 2014; Perner et al., 2019). Moreover, Grn-deficient microglial cells displayed significant downregulation of genes belonging to the peroxisome proliferator-activated receptor (PPAR) signaling, a pathway shown to counteract the secretion of pro-inflammatory cytokines (Heming et al., 2018).

In accordance with these results, Grn-deficient microglial cells expressed higher mRNA levels of pro-inflammatory cytokines, such as *il6*, *tnfa*, *il12* and *cxcl8a* and lower mRNA levels of anti-inflammatory cytokines, such as *tgfb3*, *igf1* and *il10*.

In addition to their pro-inflammatory signature, Grn-deficient microglia displayed altered morphology characterized by larger somata, hyper-ramification and shorter processes, similarly to the microglial cell

morphology detected in old wt animals and considered as established hallmark of immune cell activation (Hart et al., 2012; Olah et al., 2018).

These results provide proof of the direct link between granulins and regulation of neuroinflammation in the aging zebrafish CNS. In fact, Grn-deficient microglial cells are characterized by pro-inflammatory signature and morphological changes reminiscent of those in DAMs in the aging mammalian brain and in patients with neurodegenerative diseases (Deczkowska et al., 2018; Götzl et al., 2019).

To assess the translational potential of these findings, I compared the differentially expressed genes (DEGs) in Grn-deficient microglial cells isolated from young adult animals with a previously published dataset of genes identified in aged (~95-years-old) human microglial cells, enriched in susceptibility genes for AD and multiple sclerosis (MS), increasing with advancing age (Olah et al., 2018). Notably, ~10% of all human genes identified in the dataset published by Olah et al., with an existing zebrafish ortholog, were also found in Grn-deficient microglial cells isolated from young adult zebrafish. Moreover, GO analysis of commonly regulated genes in aged human microglia and Grn-deficient microglia in zebrafish revealed over-representation of programs associated with AD, MS and aging. This set of data is particularly important because it demonstrates for the first time the accelerated aging kinetics in Grn-deficient microglia also during young adulthood and the degree of conservation between Grn-deficient zebrafish microglia and human DAMs enriched for genes associated with neurodegenerative diseases.

Altogether, the results obtained provide new insights on the functional roles of granulins in the CNS, with possible implications for their use as therapeutic targets to reduce neuroinflammation and to slow the progression of additional age-related hallmarks that could contribute to the higher risk for neurodegenerative diseases.

However, how the age-related hallmarks are interconnected in the context of granulin deficiency, and the specific mechanisms through which granulins regulate both cell intrinsic and cell extrinsic features remain to be investigated.

Granulin-mediated regulation of phase-separated TDP-43 controls the activation states of microglia after TBI and promotes CNS regeneration

Chronic neuroinflammation is a well-established aging hallmark and is considered a major hindrance to regeneration in the mammalian CNS after injury.

Generating new neurons in a timely manner coinciding with the resolution of the inflammatory response activated after injury appears to be a crucial event for the CNS regeneration in zebrafish. This feature allows immune cells to initially perform their functions and promote the activation/de-activation of additional programs positively regulating aNSC activation and neurogenesis (Kizil et al., 2012a, 2012b; Kyritsis et al., 2012). To avoid neuronal cell death and inefficient integration into the pre-existing circuitry as observed in the mammalian CNS due to the presence of long-lasting glial scar and neuroinflammation (Adams and Gallo, 2018; Frik et al., 2018), the generation of new neurons during the inflammatory period is blocked by regulation specific programs, including the AhR signaling (Di Giaimo et al., 2018). The inflammatory response is terminated and the accumulation of glial cells at injury sites is resolved shortly after TBI. NSCs are subsequently activated and new neurons are generated, surviving in a permissive environment (Barbosa et al., 2015; Baumgart et al., 2012; Di Giaimo et al., 2018).

In addition to the programs regulating NSC activation and neurogenesis in the adult zebrafish telencephalon in response to TBI, it is essential to better characterize the cellular dynamics of immune cells responding to injury and to identify signaling pathways and key factors underlying the transient activation and resolution of the inflammatory response in the zebrafish CNS. These results would be crucial to ameliorate the regenerative outcome in the human CNS, targeting and limiting long-lasting neuroinflammation, thus improving neuronal survival and integration into the pre-existing circuitry, and preventing possible secondary damages and increased risk for neurodegenerative diseases.

To address this, I investigated the cellular and molecular mechanisms activated in response to TBI in the adult zebrafish telencephalon (*Sanchez et al., in revision; Zambusi, Novoselec et al., in revision*). The major focus of this

research project was the characterization of microglial cell dynamics in response to injury and the identification of key factors involved in the transition of microglial cells back to homeostasis. As a result, I demonstrated the existence of a transient state of pro-regenerative microglia returning to their homeostatic state in a granulin-dependent manner in response to injury. More importantly, I provided new evidence on the importance of granulin-dependent regulation of LLPS and clearance of TDP-43 condensates to promote microglial de-activation when the wound healing period is over, thus achieving scarless regeneration in the adult zebrafish CNS.

More specifically, I analyzed microglial cell dynamics in response to injury in the zebrafish telencephalon and reported the accumulation of reactive microglia at injury sites at 3 days post injury (dpi). In accordance with previous observations of scarless regeneration in the zebrafish CNS (Barbosa et al., 2015; Baumgart et al., 2012), the accumulation of microglial cells was quickly resolved at 7 dpi. Notably, signs of microglial activation were restricted to injury sites, consistently with recent observations that specific microglial populations emerge in response to TBI or neurodegenerative diseases in the mammalian brain, having distinct dynamics and functions in regulating neuroinflammation and modulating other scar-forming cells (Li et al., 2020; Masuda et al., 2019).

By comparing the transcriptome of single microglial cells over the regenerative time course (obtained using a droplet-based single cell RNA-sequencing (scRNA-seq)), I confirmed the activation of microglial cells at 3 dpi, as I detected enrichment of numerous genes associated with innate immunity (TLR signaling), neuroinflammation (cytokine-cytokine receptor interaction), lipid metabolism and extracellular matrix remodeling.

To further gain insights into microglial cell kinetics in response to TBI, I performed RNA velocity-based analysis (Bergen et al., 2020; La Manno et al., 2018) and revealed three non-overlapping trajectories of six distinct microglial clusters. Notably, microglial cells belonging to the three independent trajectories were characterized by distinct inflammatory signatures, with IL1-dependent signaling pathway enriched in Wt-MG3, and

TNF- and TLR-dependent signaling pathways enriched in Wt-MG0. Conversely, Wt-MG4 displayed significant downregulation of genes associated with pro-inflammatory programs, including TNF-, TLR- and NOD-signaling pathways, thus suggesting that microglial cells belonging to this trajectory could display anti-inflammatory properties.

All three microglial trajectories converged on Wt-MG2 cluster, characterized by under-representation of pro-inflammatory cytokines and enrichment for genes indicative of *in vivo* homeostatic microglia (Bernier et al., 2020; Dou et al., 2012; Lauro and Limatola, 2020).

Altogether, these results confirm that, similarly to the mammalian brain, in the adult zebrafish brain specific subpopulations of activated microglia emerge in response to injury. Their unique inflammatory signatures (distinct pro-inflammatory and anti-inflammatory programs in specific microglial clusters) could represent a key determinant for their timed return to homeostatic state when the wound healing period is over, thus avoiding long-lasting neuroinflammation.

Because of the kinetics characterized by a significant increase in proportion at 3 dpi and a phase of normalization at 7 dpi, I focused on microglial cells belonging to Wt-MG0 cluster. Interestingly, microglial cells belonging to this specific cluster expressed numerous genes previously identified in pro-regenerative microglia emerging after injury in the spinal cord of neonatal mice (Li et al., 2020). These results open new avenues for the understanding of cellular and molecular mechanisms underlying the capacity of zebrafish to efficiently regenerate the CNS. Moreover, they suggest that mammals and zebrafish share programs necessary for the stimulation of microglial cell activation in response to injury (Adams and Gallo, 2018; Burda and Sofroniew, 2014). Lastly, this set of data suggest that the regulatory programs promoting the return of microglial cells to homeostatic state observed in regeneration-competent species, such as zebrafish, were possibly not lost during evolution but rather during mammalian development and aging.

Pro-regenerative microglia (Wt-MG0) were characterized by high mRNA levels of genes associated with lipid-droplet accumulating microglia in the aging brain of mice (Marschallinger et al., 2020). As previously mentioned, lipid droplets (LDs) are intracellular defenses promoting innate immunity activation and sequestering compounds that may become cytotoxic for other cells (Bosch et al., 2020). However, excessive production of LDs and failure to clear LDs have been found to be detrimental for microglial cell functionality (Childs et al., 2016; Marschallinger et al., 2020). Furthermore, *grna* was among the most significantly enriched genes in Wt-MG0 microglial cells and it has been previously demonstrated that granulins are key regulators of inflammation and lipid metabolism in microglial cells (Marschallinger et al., 2020). Therefore, it is tempting to speculate that Wt-MG0 represents a population of activated microglia accumulating at injury sites and promoting regeneration in the adult zebrafish CNS. When the wound healing period is over and neuroinflammation needs to be terminated not to hinder neuronal survival and integration, activated microglia require the activation of specific genes, including granulins, to promote their transition back to homeostatic state after clearance of LDs, thus avoiding long-lasting neuroinflammation. Strengthening this hypothesis, all members of the granulin family (*grna*, *grnb* and *grn1-2*) were upregulated at 3 dpi, coinciding with the peak of microglial activation, and returned to basal levels at 7 dpi, coinciding with the termination of the regeneration process.

To further test whether granulins are required for the de-activation of pro-regenerative microglia (contributing to the clearance of LDs in microglial cells) and the resolution of the glial scar in response to injury in the adult zebrafish telencephalon, I characterized the wound healing progression in Grn-deficient brains. No major differences in reactivity were detected between wt and Grn-deficient microglial and oligodendroglial cells at 3 dpi, confirming that the injury-induced activation of neuroinflammation and the glial cell accumulation at injury sites are granulin-independent. However, both the glial cell accumulation and the presence of lipid-droplet containing microglia at injury sites were not resolved in Grn-deficient animals at 21 dpi, demonstrating that granulins are necessary to promote regeneration in the

adult zebrafish telencephalon. The presence of activated microglial and oligodendroglial cells at injury sites of Grn-deficient animals reproduces the glial scar formed in response to TBI in the mammalian brain (Adams and Gallo, 2018). For this reason, I verified the impact of the prolonged glial cell accumulation on the neurogenic potential of the zebrafish CNS and detected a significant reduction of newly generated neurons in the zebrafish parenchyma of Grn-deficient animals. These results prove that granulin deficiency is sufficient to hinder the resolution of both neuroinflammation and glial cell accumulation, subsequently impairing neurogenesis and turning a scarless model into a scarring one. Moreover, I showed that long-lasting neuroinflammation was the underlying cause for impaired regeneration of Grn-deficient animals. In fact, treatment with dexamethasone, an anti-inflammatory drug blocking microglial activation in the adult zebrafish telencephalon in response to TBI (Kyritsis et al., 2012), was sufficient to completely rescue the phenotype.

Indeed, chronic neuroinflammation is a pathological response to TBI in the mammalian brain and a significant factor contributing to inefficient regeneration and neuronal survival in the mammalian CNS (Burda and Sofroniew, 2014; Frik et al., 2018). The importance of tightly regulating neuroinflammation in response to brain injuries is highlighted by the fact that Grn-associated exacerbated neuroinflammation is sufficient to cause a cascade of detrimental events leading to impaired regeneration in zebrafish, completely disrupting its regenerative potential.

To further characterize the neuroinflammatory state in the Grn-deficient telencephalon and identify the molecular mechanisms underlying this pathological state, I analyzed the behavior of Grn-deficient microglial cells with scRNA-seq during the wound healing period. In agreement with our previous observations, Grn-deficient microglia failed to transition back to homeostatic state, displayed enrichment of genes associated with innate immunity, phagosome maturation and apoptosis, and were characterized by elevated mRNA levels of genes previously identified in lipid-droplet accumulating microglia. Furthermore, I detected elevated levels of stress-related genes, including numerous members of the heat shock protein (HSP)

family 70, and higher expression of *g3bp1*, a gene associated with stress granule (SG) formation by LLPS (Yang et al., 2020).

SGs can be transiently induced via LLPS in the cytoplasm by multiple signals, including TBI (Anderson et al., 2018; Panas et al., 2016; Wiesner et al., 2018). Failure to remove the stress signal and to disassemble SGs may subsequently contribute to the onset of pathologies and neurodegeneration in the CNS (Yu et al., 2020).

Inflammation has been found to enhance the formation of SGs, which in turn can affect microglial cell functionality, limiting their phagocytic activity, thus suggesting the existence of a positive feed-forward loop between inflammation and SG formation.

TDP-43 is known to re-localize to the cytoplasm in several neurodegenerative diseases, such as amyotrophic lateral sclerosis (ALS) and FTD (Bentmann et al., 2012; Wolozin and Ivanov, 2019), forming condensates or aggregates via LLPS and co-localizing with SGs. Furthermore, granulins have been demonstrated to directly alter the solubility and the LLPS properties of TDP-43 (Beel et al., 2018; Bhopatkar et al., 2020; Salazar et al., 2015). Therefore, I hypothesized that dysregulated LLPS and impaired capacity of clearing TDP-43 condensates in the cytoplasm would be a major source of cellular stress, locking Grn-deficient microglial cells into an activated state, subsequently causing a cascade of events leading to long-lasting neuroinflammation, prolonged glial cell accumulation at injury sites and impaired regeneration in the zebrafish CNS. To confirm this hypothesis, I showed that TDP-43 condensates were generated both in wt and Grn-deficient animals. However, Grn-deficient animals failed to clear extranuclear TDP-43 condensates in microglial cells due to the dysregulation of the LLPS of TDP-43. Injection of excessive LLPS-competent TDP-43 was sufficient to reproduce the phenotype in wt animals. Furthermore, treating Grn-deficient animals during the wound healing period with lipoamide, a newly identified agent inhibiting SG formation by LLPS (Wheeler et al., 2019), was sufficient to reduce the exacerbated neuroinflammation and to clear extranuclear TDP-43 condensates. These results were supported by scRNA-seq analysis demonstrating that blocking SG formation via lipoamide

administration was sufficient to promote the transition of Grn-deficient microglial cells back to homeostasis.

In summary, I demonstrated that clearance of SGs formed via LLPS in microglial cells is required to prevent long-lasting neuroinflammation and that granulins are necessary to tightly regulate this process. Failure to clear SGs leads to a cascade of events locking microglial cells in their pro-inflammatory state thus hindering zebrafish brain regeneration.

Importantly, the translation value of these results was supported by the analysis of patients with stroke. More specifically, similarly to the phenotype observed in Grn-deficient brains after TBI, I detected increased microglial reactivity accompanied by high lipid-droplet content, TDP-43 condensates and SGs in brain tissue of patients with stroke, supporting the concept that similar regulatory mechanisms of neuroinflammation may be conserved in the mammalian and zebrafish brain, and may be targeted to enhance regeneration in the human CNS.

Collectively, I identified and described for the first time the association between regulation of LLPS, neuroinflammation and regeneration in the adult zebrafish CNS. More specifically, I discovered that the granulin-mediated clearance of cytoplasmic TDP-43 condensates in microglial cells in response to TBI is required to promote their inactivation, thus contributing to the resolution of neuroinflammation and glial cell accumulation at injury sites when the wound healing period is over. This set of data describe a novel mechanism functionally contributing to CNS regeneration in zebrafish.

Although the exact mechanism through which LLPS-mediated TDP-43 condensates impair microglial functionality remains elusive, these findings represent an important step towards the future development of new therapeutic treatments aimed to ameliorate the regenerative outcome in human patients affected by TBI and neurodegenerative diseases.

Bibliography

- Adams, K.L., and Gallo, V. (2018). The diversity and disparity of the glial scar. *Nat. Neurosci.* *21*, 9–15.
- Adav, S.S., Park, J.E., and Sze, S.K. (2019). Quantitative profiling brain proteomes revealed mitochondrial dysfunction in Alzheimer's disease. *Mol. Brain* *12*, 8.
- Adolf, B., Chapouton, P., Lam, C.S., Topp, S., Tannhauser, B., Strahle, U., Gotz, M., and Bally-Cuif, L. (2006). Conserved and acquired features of adult neurogenesis in the zebrafish telencephalon. *Dev Biol* *295*, 278–293.
- Alam, A., Thelin, E.P., Tajsic, T., Khan, D.Z., Khellaf, A., Patani, R., and Helmy, A. (2020). Cellular infiltration in traumatic brain injury. *J. Neuroinflammation* *17*, 1–17.
- Alberti, S., and Hyman, A.A. (2021). Biomolecular condensates at the nexus of cellular stress, protein aggregation disease and ageing. *Nat. Rev. Mol. Cell Biol.* *22*, 196–213.
- Alberti, S., Gladfelter, A., and Mittag, T. (2019). Considerations and Challenges in Studying Liquid-Liquid Phase Separation and Biomolecular Condensates. *Cell* *176*, 419–434.
- Alexander, G.E., Ryan, L., Bowers, D., Foster, T.C., Bizon, J.L., Geldmacher, D.S., and Glisky, E.L. (2012). Characterizing cognitive aging in humans with links to animal models. *Front. Aging Neurosci.* *4*.
- Almaida-Pagán, P.F., Lucas-Sánchez, A., and Tocher, D.R. (2014). Changes in mitochondrial membrane composition and oxidative status during rapid growth, maturation and aging in zebrafish, *Danio rerio*. *Biochim. Biophys. Acta - Mol. Cell Biol. Lipids* *1841*, 1003–1011.
- Alunni, A., and Bally-Cuif, L. (2016). A comparative view of regenerative neurogenesis in vertebrates. *Development* *143*, 741–753.
- Alunni, A., Krecsmarik, M., Bosco, A., Galant, S., Pan, L., Moens, C.B., and Bally-Cuif, L. (2013). Notch3 signaling gates cell cycle entry and limits neural stem cell amplification in the adult pallium. *Dev.* *140*, 3335–3347.
- Anderson, P., and Kedersha, N. (2002). Visibly stressed: The role of eIF2, TIA-1, and stress granules in protein translation. *Cell Stress Chaperones* *7*, 213–221.
- Anderson, E.N., Gochenaur, L., Singh, A., Grant, R., Patel, K., Watkins, S., Wu, J.Y., and Pandey, U.B. (2018). Traumatic injury induces stress granule formation and enhances motor dysfunctions in ALS/FTD models. *Hum. Mol. Genet.* *27*, 1366–1381.
- Armanios, M., Alder, J.K., Parry, E.M., Karim, B., Strong, M.A., and Greider, C.W. (2009). Short Telomeres are Sufficient to Cause the Degenerative Defects Associated with Aging. *Am. J. Hum. Genet.* *85*, 823–832.
- Ayari, B., Elhachimi, K.H., Yanicostas, C., Landoulsi, A., and Soussi-Yanicostas, N. (2010). Prokineticin 2 expression is associated with neural repair of injured adult zebrafish telencephalon. *J Neurotrauma*.

- Baker, M., Mackenzie, I.R., Pickering-Brown, S.M., Gass, J., Rademakers, R., Lindholm, C., Snowden, J., Adamson, J., Sadovnick, A.D., Rollinson, S., et al. (2006). Mutations in progranulin cause tau-negative frontotemporal dementia linked to chromosome 17. *Nature* *442*, 916–919.
- Barbosa, J.S.S., Sanchez-Gonzalez, R., Di Giaimo, R., Baumgart, E.V. V, Theis, F.J.J., Götz, M., Ninkovic, J., Gotz, M., Ninkovic, J., Gonzalez-Sanchez, R., et al. (2015). Live imaging of adult neural stem cell behavior in the intact and injured zebrafish brain. *Science* (80-.). *348*, 789–793.
- Bartus, K., Burnside, E.R., Galino, J., James, N.D., Bennett, D.L.H., and Bradbury, E.J. (2019). ErbB receptor signaling directly controls oligodendrocyte progenitor cell transformation and spontaneous remyelination after spinal cord injury. *Glia* *67*, 1036–1046.
- Bast, L., Calzolari, F., Strasser, M.K., Hasenauer, J., Theis, F.J., Ninkovic, J., and Marr, C. (2018). Increasing Neural Stem Cell Division Asymmetry and Quiescence Are Predicted to Contribute to the Age-Related Decline in Neurogenesis. *Cell Rep.* *25*, 3231-3240.e8.
- Bateman, A., and Bennett, H.P.J. (2009). The granulin gene family: From cancer to dementia. *BioEssays* *31*, 1245–1254.
- Baumgart, E.V. V, Barbosa, J.S.S., Bally-Cuif, L., Gotz, M., Ninkovic, J., Götz, M., and Ninkovic, J. (2012). Stab wound injury of the zebrafish telencephalon: a model for comparative analysis of reactive gliosis. *Glia* *60*, 343–357.
- Baumgart, M., Groth, M., Priebe, S., Savino, A., Testa, G., Dix, A., Ripa, R., Spallotta, F., Gaetano, C., Ori, M., et al. (2014). RNA-seq of the aging brain in the short-lived fish *N. furzeri* - conserved pathways and novel genes associated with neurogenesis. *Aging Cell* *13*, 965–974.
- Beckervordersandforth, R., Ebert, B., Schäffner, I., Moss, J., Fiebig, C., Shin, J., Moore, D.L., Ghosh, L., Trincherro, M.F., Stockburger, C., et al. (2017). Role of Mitochondrial Metabolism in the Control of Early Lineage Progression and Aging Phenotypes in Adult Hippocampal Neurogenesis. *Neuron* *93*, 560-573.e6.
- Beel, S., Herdewyn, S., Fazal, R., De Decker, M., Moisse, M., Robberecht, W., Van Den Bosch, L., and Van Damme, P. (2018). Progranulin reduces insoluble TDP-43 levels, slows down axonal degeneration and prolongs survival in mutant TDP-43 mice. *Medical and Health Sciences 1109 Neurosciences. Mol. Neurodegener.* *13*.
- Bellver-Landete, V., Bretheau, F., Mailhot, B., Vallières, N., Lessard, M., Janelle, M.E., Vernoux, N., Tremblay, M.È., Fuehrmann, T., Shoichet, M.S., et al. (2019). Microglia are an essential component of the neuroprotective scar that forms after spinal cord injury. *Nat. Commun.* *10*, 1–18.
- Bentmann, E., Neumann, M., Tahirovic, S., Rodde, R., Dormann, D., and Haass, C. (2012). Requirements for stress granule recruitment of fused in sarcoma (FUS) and TAR DNA-binding protein of 43 kDa (TDP-43). *J. Biol. Chem.* *287*, 23079–23094.
- Bentmann, E., Haass, C., and Dormann, D. (2013). Stress granules in

neurodegeneration - Lessons learnt from TAR DNA binding protein of 43 kDa and fused in sarcoma. *FEBS J.* 280, 4348–4370.

Bergen, V., Lange, M., Peidli, S., Wolf, F.A., and Theis, F.J. (2020). Generalizing RNA velocity to transient cell states through dynamical modeling. *Nat. Biotechnol.*

Bernardes de Jesus, B., Vera, E., Schneeberger, K., Tejera, A.M., Ayuso, E., Bosch, F., and Blasco, M.A. (2012). Telomerase gene therapy in adult and old mice delays aging and increases longevity without increasing cancer. *EMBO Mol. Med.* 4, 691–704.

Bernier, L.P., York, E.M., Kamyabi, A., Choi, H.B., Weilinger, N.L., and MacVicar, B.A. (2020). Microglial metabolic flexibility supports immune surveillance of the brain parenchyma. *Nat. Commun.*

Bhattarai, P., Thomas, A.K., Cosacak, M.I., Papadimitriou, C., Mashkaryan, V., Froc, C., Reinhardt, S., Kurth, T., Dahl, A., Zhang, Y., et al. (2016). IL4/STAT6 Signaling Activates Neural Stem Cell Proliferation and Neurogenesis upon Amyloid- β 42 Aggregation in Adult Zebrafish Brain. *Cell Rep.* 17, 941–948.

Bhattarai, P., Thomas, A.K., Zhang, Y., and Kizil, C. (2017). The effects of aging on Amyloid- β 42-induced neurodegeneration and regeneration in adult zebrafish brain. *Neurogenesis* 4, e1322666.

Bhopatkar, A.A., Uversky, V.N., and Rangachari, V. (2020). Granulins modulate liquid–liquid phase separation and aggregation of the prion-like C-terminal domain of the neurodegeneration-associated protein TDP-43. *J. Biol. Chem.* 295, 2506–2519.

Bhowmick, S., D’Mello, V., Caruso, D., Wallerstein, A., and Abdul-Muneer, P.M. (2019). Impairment of pericyte-endothelium crosstalk leads to blood-brain barrier dysfunction following traumatic brain injury. *Exp. Neurol.* 317, 260–270.

Blasco, M.A. (2007). Telomere length, stem cells and aging. *Nat. Chem. Biol.* 3, 640–649.

Boldrini, M., Fulmore, C.A., Tartt, A.N., Simeon, L.R., Pavlova, I., Poposka, V., Rosoklija, G.B., Stankov, A., Arango, V., Dwork, A.J., et al. (2018). Human Hippocampal Neurogenesis Persists throughout Aging. *Cell Stem Cell* 22, 589-599.e5.

Bosch, M., Sánchez-Álvarez, M., Fajardo, A., Kapetanovic, R., Steiner, B., Dutra, F., Moreira, L., López, J.A., Campo, R., Marí, M., et al. (2020). Mammalian lipid droplets are innate immune hubs integrating cell metabolism and host defense. *Science* (80-.). 370.

Bramlett, H.M., and Dietrich, W.D. (2015). Long-Term Consequences of Traumatic Brain Injury: Current Status of Potential Mechanisms of Injury and Neurological Outcomes. *J. Neurotrauma* 32, 1834–1848.

Brawek, B., Skok, M., and Garaschuk, O. (2021). Changing functional signatures of microglia along the axis of brain aging. *Int. J. Mol. Sci.* 22, 1–22.

Buffo, A., Vosko, M.R., Erturk, D., Hamann, G.F., Jucker, M., Rowitch, D.,

- and Gotz, M. (2005). Expression pattern of the transcription factor Olig2 in response to brain injuries: implications for neuronal repair. *Proc Natl Acad Sci U S A* *102*, 18183–18188.
- Burda, J.E., and Sofroniew, M. V (2014). Reactive gliosis and the multicellular response to CNS damage and disease. *Neuron* *81*, 229–248.
- Burda, J.E., Bernstein, A.M., and Sofroniew, M. V. (2016). Astrocyte roles in traumatic brain injury. *Exp. Neurol.* *275*, 305–315.
- Cadieux, B., Chitramuthu, B.P., Baranowski, D., and Bennett, H.P.J. (2005). The zebrafish progranulin gene family and antisense transcripts. *BMC Genomics* *6*, 156.
- Caldwell, L.J., Davies, N.O., Cavone, L., Mysiak, K.S., Semenova, S.A., Panula, P., Armstrong, J.D., Becker, C.G., and Becker, T. (2019). Regeneration of dopaminergic neurons in adult zebrafish depends on immune system activation and differs for distinct populations. *J. Neurosci.* *39*, 4694–4713.
- Calvo-Rodriguez, M., Hou, S.S., Snyder, A.C., Kharitonova, E.K., Russ, A.N., Das, S., Fan, Z., Muzikansky, A., Garcia-Alloza, M., Serrano-Pozo, A., et al. (2020). Increased mitochondrial calcium levels associated with neuronal death in a mouse model of Alzheimer’s disease. *Nat. Commun.* *11*, 1–17.
- Campbell, C.A., Fursova, O., Cheng, X., Snella, E., McCune, A., Li, L., Solchenberger, B., Schmid, B., Sahoo, D., Morton, M., et al. (2021). A zebrafish model of granulin deficiency reveals essential roles in myeloid cell differentiation. *Blood Adv.* *5*, 796–811.
- Carneiro, M.C., De Castro, I.P., and Ferreira, M.G. (2016). Telomeres in aging and disease: Lessons from zebrafish. *DMM Dis. Model. Mech.* *9*, 737–748.
- Carrillo, S.A., Anguita-Salinas, C., Peña, O.A., Morales, R.A., Muñoz-Sánchez, S., Muñoz-Montecinos, C., Paredes-Zúñiga, S., Tapia, K., and Allende, M.L. (2016). Macrophage Recruitment Contributes to Regeneration of Mechanosensory Hair Cells in the Zebrafish Lateral Line. *J. Cell. Biochem.* *117*, 1880–1889.
- Cenik, B., Sephton, C.F., Cenik, B.K., Herz, J., and Yu, G. (2012). Progranulin: A proteolytically processed protein at the crossroads of inflammation and neurodegeneration. *J. Biol. Chem.* *287*, 32298–32306.
- Chapouton, P., Jagasia, R., and Bally-Cuif, L. (2007). Adult neurogenesis in non-mammalian vertebrates. *Bioessays* *29*, 745–757.
- Chapouton, P., Skupien, P., Hesl, B., Coolen, M., Moore, J.C., Madelaine, R., Kremmer, E., Faus-Kessler, T., Blader, P., Lawson, N.D., et al. (2010). Notch Activity Levels Control the Balance between Quiescence and Recruitment of Adult Neural Stem Cells. *J. Neurosci.* *30*, 7961–7974.
- Chen, J., Poskanzer, K.E., Freeman, M.R., and Monk, K.R. (2020). Live-imaging of astrocyte morphogenesis and function in zebrafish neural circuits. *Nat. Neurosci.* *23*, 1297–1306.
- Chicco, A.J., and Sparagna, G.C. (2007). Role of cardiolipin alterations in mitochondrial dysfunction and disease. *Am. J. Physiol. - Cell Physiol.* *292*.

- Childs, B.G., Baker, D.J., Wijshake, T., Conover, C.A., Campisi, J., and Van Deursen, J.M. (2016). Senescent intimal foam cells are deleterious at all stages of atherosclerosis. *Science* (80-.). *354*, 472–477.
- Chitramuthu, B.P., Bennett, H.P.J., and Bateman, A. (2017). Progranulin: A new avenue towards the understanding and treatment of neurodegenerative disease. *Brain* *140*, 3081–3104.
- Cohen, S.M., Li, B., Tsien, R.W., and Ma, H. (2015). Evolutionary and functional perspectives on signaling from neuronal surface to nucleus. *Biochem. Biophys. Res. Commun.* *460*, 88–99.
- Cooper, J.A. (2013). Mechanisms of cell migration in the nervous system. *J. Cell Biol.* *202*, 725–734.
- Cribbs, D.H., Berchtold, N.C., Perreau, V., Coleman, P.D., Rogers, J., Tenner, A.J., and Cotman, C.W. (2012). Extensive innate immune gene activation accompanies brain aging, increasing vulnerability to cognitive decline and neurodegeneration: A microarray study. *J. Neuroinflammation* *9*, 1–18.
- Cruts, M., Gijselinck, I., Van Der Zee, J., Engelborghs, S., Wils, H., Pirici, D., Rademakers, R., Vandenberghe, R., Dermaut, B., Martin, J.J., et al. (2006). Null mutations in progranulin cause ubiquitin-positive frontotemporal dementia linked to chromosome 17q21. *Nature* *442*, 920–924.
- Cruz-Haces, M., Tang, J., Acosta, G., Fernandez, J., and Shi, R. (2017). Pathological correlations between traumatic brain injury and chronic neurodegenerative diseases. *Transl. Neurodegener.* *6*, 1–10.
- D’Adda Di Fagagna, F., Reaper, P.M., Clay-Farrace, L., Fiegler, H., Carr, P., Von Zglinicki, T., Saretzki, G., Carter, N.P., and Jackson, S.P. (2003). A DNA damage checkpoint response in telomere-initiated senescence. *Nature* *426*, 194–198.
- Davalos, D., Grutzendler, J., Yang, G., Kim, J. V., Zuo, Y., Jung, S., Littman, D.R., Dustin, M.L., and Gan, W.B. (2005). ATP mediates rapid microglial response to local brain injury in vivo. *Nat. Neurosci.*
- Deczkowska, A., Keren-Shaul, H., Weiner, A., Colonna, M., Schwartz, M., and Amit, I. (2018). Disease-Associated Microglia: A Universal Immune Sensor of Neurodegeneration. *Cell*.
- Dimou, L., and Gotz, M. (2014). Glial cells as progenitors and stem cells: new roles in the healthy and diseased brain. *Physiol Rev* *94*, 709–737.
- Diotel, N., Beil, T., Strähle, U., and Rastegar, S. (2015). Differential expression of id genes and their potential regulator *znf238* in zebrafish adult neural progenitor cells and neurons suggests distinct functions in adult neurogenesis. *Gene Expr. Patterns* *19*, 1–13.
- Diotel, N., Lübke, L., Strähle, U., and Rastegar, S. (2020). Common and Distinct Features of Adult Neurogenesis and Regeneration in the Telencephalon of Zebrafish and Mammals. *Front. Neurosci.* *14*.
- Dorrier, C.E., Aran, D., Haenelt, E.A., Sheehy, R.N., Hoi, K.K., Pintarić, L., Chen, Y., Lizama, C.O., Cautivo, K.M., Weiner, G.A., et al. (2021). CNS fibroblasts form a fibrotic scar in response to immune cell infiltration. *Nat. Neurosci.* *24*, 234–244.

- Dou, Y., Wu, H.J., Li, H.Q., Qin, S., Wang, Y.E., Li, J., Lou, H.F., Chen, Z., Li, X.M., Luo, Q.M., et al. (2012). Microglial migration mediated by ATP-induced ATP release from lysosomes. *Cell Res.*
- Dray, N., Bedu, S., Vuillemin, N., Alunni, A., Coolen, M., Krecsmarik, M., Supatto, W., Beaurepaire, E., and Bally-Cuif, L. (2015). Large-scale live imaging of adult neural stem cells in their endogenous niche. *Dev.* *142*, 3592–3600.
- Edelmann, K., Glashauser, L., Sprungala, S., Hesl, B., Fritschle, M., Ninkovic, J., Godinho, L., and Chapouton, P. (2013). Increased radial glia quiescence, decreased reactivation upon injury and unaltered neuroblast behavior underlie decreased neurogenesis in the aging zebrafish telencephalon. *J Comp Neurol* *521*, 3099–3115.
- Ekdahl, C.T., Claasen, J.H., Bonde, S., Kokaia, Z., and Lindvall, O. (2003). Inflammation is detrimental for neurogenesis in adult brain. *Proc. Natl. Acad. Sci. U. S. A.* *100*, 13632–13637.
- Evers, B.M., Rodriguez-Navas, C., Tesla, R.J., Prange-Kiel, J., Wasser, C.R., Yoo, K.S., McDonald, J., Cenik, B., Ravenscroft, T.A., Plattner, F., et al. (2017). Lipidomic and Transcriptomic Basis of Lysosomal Dysfunction in Progranulin Deficiency. *Cell Rep.* *20*, 2565–2574.
- Farmer, B.C., Walsh, A.E., Kluemper, J.C., and Johnson, L.A. (2020). Lipid Droplets in Neurodegenerative Disorders. *Front. Neurosci.* *14*, 742.
- Farr, S.A., Niehoff, M.L., and Nguyen, A.D. (2020). Progranulin improves memory in normal aging and Alzheimer’s disease. *Alzheimer’s Dement.* *16*, e046374.
- Ferrón, S., Mira, H., Franco, S., Cano-Jimenez, M., Bellmunt, E., Ramírez, C., Fariñas, I., and Blasco, M.A. (2004). Telomere shortening and chromosomal instability abrogates proliferation of adult but not embryonic neural stem cells. *Development* *131*, 4059–4070.
- Folgueira, M., Bayley, P., Navratilova, P., Becker, T.S., Wilson, S.W., and Clarke, J.D.W. (2012). Morphogenesis underlying the development of the everted teleost telencephalon. *Neural Dev.* *7*, 32.
- Franceschi, C., Bonafè, M., Valensin, S., Olivieri, F., De Luca, M., Ottaviani, E., and De Benedictis, G. (2000). Inflamm-aging. An evolutionary perspective on immunosenescence. In *Annals of the New York Academy of Sciences*, (New York Academy of Sciences), pp. 244–254.
- Frik, J., Merl-Pham, J., Plesnila, N., Mattugini, N., Kjell, J., Kraska, J., Gomez, R.M., Hauck, S.M., Sirko, S., and Gotz, M. (2018). Cross-talk between monocyte invasion and astrocyte proliferation regulates scarring in brain injury. *EMBO Rep* *19*.
- Galluzzi, L., Baehrecke, E.H., Ballabio, A., Boya, P., Bravo-San Pedro, J.M., Cecconi, F., Choi, A.M., Chu, C.T., Codogno, P., Colombo, M.I., et al. (2017). Molecular definitions of autophagy and related processes. *EMBO J.* *36*, 1811–1836.
- Gant, J.C., Sama, M.M., Landfield, P.W., and Thibault, O. (2006). Early and simultaneous emergence of multiple hippocampal biomarkers of aging is

- mediated by Ca²⁺-induced Ca²⁺ release. *J. Neurosci.* *26*, 3482–3490.
- Ghosh, S., and Geahlen, R.L. (2015). Stress Granules Modulate SYK to Cause Microglial Cell Dysfunction in Alzheimer's Disease. *EBioMedicine*.
- Di Giaimo, R., Durovic, T., Barquin, P., Kociaj, A., Lepko, T., Aschenbroich, S., Breunig, C.T.T., Irmeler, M., Cernilogar, F.M.M., Schotta, G., et al. (2018). The Aryl Hydrocarbon Receptor Pathway Defines the Time Frame for Restorative Neurogenesis. *Cell Rep* *25*, 3241-3251 e5.
- Götzl, J.K., Mori, K., Damme, M., Fellerer, K., Tahirovic, S., Kleinberger, G., Janssens, J., Van Der Zee, J., Lang, C.M., Kremmer, E., et al. (2014). Common pathobiochemical hallmarks of progranulin-associated frontotemporal lobar degeneration and neuronal ceroid lipofuscinosis. *Acta Neuropathol.* *127*, 845–860.
- Götzl, J.K., Colombo, A.V., Fellerer, K., Reifschneider, A., Werner, G., Tahirovic, S., Haass, C., and Capell, A. (2018). Early lysosomal maturation deficits in microglia triggers enhanced lysosomal activity in other brain cells of progranulin knockout mice. *Mol. Neurodegener.* *13*, 1–16.
- Götzl, J.K., Brendel, M., Werner, G., Parhizkar, S., Sebastian Monasor, L., Kleinberger, G., Colombo, A., Deussing, M., Wagner, M., Winkelmann, J., et al. (2019). Opposite microglial activation stages upon loss of PGRN or TREM 2 result in reduced cerebral glucose metabolism . *EMBO Mol. Med.* *11*.
- Graciarena, M., Dambly-Chaudière, C., and Ghysen, A. (2014). Dynamics of axonal regeneration in adult and aging zebrafish reveal the promoting effect of a first lesion. *Proc. Natl. Acad. Sci. U. S. A.* *111*, 1610–1615.
- Graham, N.S.N., and Sharp, D.J. (2019). Understanding neurodegeneration after traumatic brain injury: From mechanisms to clinical trials in dementia. *J. Neurol. Neurosurg. Psychiatry* *90*, 1221–1233.
- Grandel, H., Kaslin, J., Ganz, J., Wenzel, I., and Brand, M. (2006). Neural stem cells and neurogenesis in the adult zebrafish brain: origin, proliferation dynamics, migration and cell fate. *Dev Biol* *295*, 263–277.
- Grinspan, J.B. (2015). Bone Morphogenetic Proteins: Inhibitors of Myelination in Development and Disease. In *Vitamins and Hormones*, (Vitam Horm), pp. 195–222.
- Guzman-Martinez, L., Maccioni, R.B., Andrade, V., Navarrete, L.P., Pastor, M.G., and Ramos-Escobar, N. (2019). Neuroinflammation as a common feature of neurodegenerative disorders. *Front. Pharmacol.* *10*, 1008.
- Hamilton, L.K., Dufresne, M., Joppé, S.E., Petryszyn, S., Aumont, A., Calon, F., Barnabé-Heider, F., Furtos, A., Parent, M., Chaurand, P., et al. (2015). Aberrant Lipid Metabolism in the Forebrain Niche Suppresses Adult Neural Stem Cell Proliferation in an Animal Model of Alzheimer's Disease. *Cell Stem Cell* *17*, 397–411.
- Hanisch, U.-K., and Kettenmann, H. (2007). Microglia: active sensor and versatile effector cells in the normal and pathologic brain. *Nat Neurosci* *10*, 1387–1394.
- Hart, A.D., Wyttenbach, A., Hugh Perry, V., and Teeling, J.L. (2012). Age related changes in microglial phenotype vary between CNS regions: Grey

- versus white matter differences. *Brain. Behav. Immun.* **26**, 754–765.
- Haynes, S.E., Hollopeter, G., Yang, G., Kurpius, D., Dailey, M.E., Gan, W.B., and Julius, D. (2006). The P2Y₁₂ receptor regulates microglial activation by extracellular nucleotides. *Nat. Neurosci.* **9**, 1512–1519.
- He, Z., Ong, C.H.P., Halper, J., and Bateman, A. (2003). Progranulin is a mediator of the wound response. *Nat. Med.*
- Heming, M., Gran, S., Jauch, S.L., Fischer-Riepe, L., Russo, A., Klotz, L., Hermann, S., Schäfers, M., Roth, J., and Barczyk-Kahlert, K. (2018). Peroxisome proliferator-activated receptor- γ modulates the response of macrophages to lipopolysaccharide and glucocorticoids. *Front. Immunol.* **9**.
- Herman, A.B., Silva Afonso, M., Kelemen, S.E., Ray, M., Vrakas, C.N., Burke, A.C., Scalia, R.G., Moore, K., and Autieri, M. V. (2019). Regulation of stress granule formation by inflammation, vascular injury, and atherosclerosis. *Arterioscler. Thromb. Vasc. Biol.*
- Hofweber, M., Hutten, S., Bourgeois, B., Spreitzer, E., Niedner-Boblenz, A., Schifferer, M., Ruepp, M.D., Simons, M., Niessing, D., Madl, T., et al. (2018). Phase Separation of FUS Is Suppressed by Its Nuclear Import Receptor and Arginine Methylation. *Cell* **173**, 706-719.e13.
- Hou, Y., Dan, X., Babbar, M., Wei, Y., Hasselbalch, S.G., Croteau, D.L., and Bohr, V.A. (2019). Ageing as a risk factor for neurodegenerative disease. *Nat. Rev. Neurol.* **15**, 565–581.
- Van houcke, J., De Groef, L., Dekeyster, E., and Moons, L. (2015). The zebrafish as a gerontology model in nervous system aging, disease, and repair. *Ageing Res. Rev.* **24**, 358–368.
- Jaskelioff, M., Muller, F.L., Paik, J.H., Thomas, E., Jiang, S., Adams, A.C., Sahin, E., Kost-Alimova, M., Protopopov, A., Cadiñanos, J., et al. (2011). Telomerase reactivation reverses tissue degeneration in aged telomerase-deficient mice. *Nature* **469**, 102–107.
- Jassam, Y.N., Izzy, S., Whalen, M., McGavern, D.B., and El Khoury, J. (2017). Neuroimmunology of Traumatic Brain Injury: Time for a Paradigm Shift. *Neuron* **95**, 1246–1265.
- Jian, J., Konopka, J., and Liu, C. (2013). Insights into the role of progranulin in immunity, infection, and inflammation. *J. Leukoc. Biol.* **93**, 199–208.
- Johnson, V.E., Weber, M.T., Xiao, R., Cullen, D.K., Meaney, D.F., Stewart, W., and Smith, D.H. (2018). Mechanical disruption of the blood–brain barrier following experimental concussion. *Acta Neuropathol.* **135**, 711–726.
- Jurisch-Yaksi, N., Yaksi, E., and Kizil, C. (2020). Radial glia in the zebrafish brain: Functional, structural, and physiological comparison with the mammalian glia. *Glia* **68**, 2451–2470.
- Kalamakis, G., Brüne, D., Ravichandran, S., Bolz, J., Fan, W., Ziebell, F., Stiehl, T., Catalá-Martinez, F., Kupke, J., Zhao, S., et al. (2019). Quiescence Modulates Stem Cell Maintenance and Regenerative Capacity in the Aging Brain. *Cell* **176**, 1407-1419.e14.
- Kao, A.W., McKay, A., Singh, P.P., Brunet, A., and Huang, E.J. (2017).

- Progranulin, lysosomal regulation and neurodegenerative disease. *Nat. Rev. Neurosci.* *18*, 325–333.
- Karlseder, J., Broccoli, D., Yumin, D., Hardy, S., and De Lange, T. (1999). p53- and ATM-dependent apoptosis induced by telomeres lacking TRF2. *Science* (80-.). *283*, 1321–1325.
- Kaslin, J., Ganz, J., and Brand, M. (2008). Proliferation, neurogenesis and regeneration in the non-mammalian vertebrate brain. *Philos Trans R Soc L. B Biol Sci* *363*, 101–122.
- Kaslin, J., Ganz, J., Geffarth, M., Grandel, H., Hans, S., and Brand, M. (2009). Stem cells in the adult zebrafish cerebellum: initiation and maintenance of a novel stem cell niche. *J Neurosci* *29*, 6142–6153.
- Kedersha, N., Ivanov, P., and Anderson, P. (2013). Stress granules and cell signaling: More than just a passing phase? *Trends Biochem. Sci.* *38*, 494–506.
- Keil, U., Bonert, A., Marques, C.A., Scherping, I., Weyermann, J., Strosznajder, J.B., Müller-Spahn, F., Haass, C., Czech, C., Pradier, L., et al. (2004). Amyloid β -induced changes in nitric oxide production and mitochondrial activity lead to apoptosis. *J. Biol. Chem.* *279*, 50310–50320.
- Kim, N.W., Piatyszek, M.A., Prowse, K.R., Harley, C.B., West, M.D., Ho, P.L.C., Coviello, G.M., Wright, W.E., Weinrich, S.L., and Shay, J.W. (1994). Specific association of human telomerase activity with immortal cells and cancer. *Science* (80-.). *266*, 2011–2015.
- Kindler, S., and Kreienkamp, H.J. (2012). Dendritic mRNA targeting and translation. *Adv. Exp. Med. Biol.* *970*, 285–305.
- Kishimoto, N., Shimizu, K., and Sawamoto, K. (2012). Neuronal regeneration in a zebrafish model of adult brain injury. *Dis Model Mech* *5*, 200–209.
- Kizil, C., Kyritsis, N., Dudczig, S., Kroehne, V., Freudenreich, D., Kaslin, J., and Brand, M. (2012a). Regenerative Neurogenesis from Neural Progenitor Cells Requires Injury-Induced Expression of Gata3. *Dev. Cell* *23*, 1230–1237.
- Kizil, C., Dudczig, S., Kyritsis, N., Machate, A., Blaesche, J., Kroehne, V., and Brand, M. (2012b). The chemokine receptor *cxc5* regulates the regenerative neurogenesis response in the adult zebrafish brain. *Neural Dev* *7*, 27.
- Kroehne, V., Freudenreich, D., Hans, S., Kaslin, J., and Brand, M. (2011). Regeneration of the adult zebrafish brain from neurogenic radial glia-type progenitors. *Development* *138*, 4831–4841.
- Kyritsis, N., Kizil, C., Zocher, S., Kroehne, V., Kaslin, J., Freudenreich, D., Iltzsche, A., and Brand, M. (2012). Acute inflammation initiates the regenerative response in the adult zebrafish brain. *Science* (80-.). *338*, 1353–1356.
- Kyritsis, N., Kizil, C., and Brand, M. (2014). Neuroinflammation and central nervous system regeneration in vertebrates. *Trends Cell Biol.* *24*, 128–135.
- De Lange, T. (2005). Shelterin: The protein complex that shapes and safeguards human telomeres. *Genes Dev.* *19*, 2100–2110.
- Lauro, C., and Limatola, C. (2020). Metabolic Reprogramming of Microglia in the Regulation of the Innate Inflammatory Response. *Front. Immunol.*

- Lazarov, O., Mattson, M.P., Peterson, D.A., Pimplikar, S.W., and van Praag, H. (2010). When neurogenesis encounters aging and disease. *Trends Neurosci.* *33*, 569–579.
- LeBert, D.C., and Huttenlocher, A. (2014). Inflammation and wound repair. *Semin. Immunol.* *26*, 315–320.
- Levin, O., Fujiyama, H., Boisgontier, M.P., Swinnen, S.P., and Summers, J.J. (2014). Aging and motor inhibition: A converging perspective provided by brain stimulation and imaging approaches. *Neurosci. Biobehav. Rev.* *43*, 100–117.
- Li, Y., Du, X.F., Liu, C.S., Wen, Z.L., and Du, J.L. (2012). Reciprocal Regulation between Resting Microglial Dynamics and Neuronal Activity In Vivo. *Dev. Cell* *23*, 1189–1202.
- Li, Y., He, X., Kawaguchi, R., Zhang, Y., Wang, Q., Monavarfeshani, A., Yang, Z., Chen, B., Shi, Z., Meng, H., et al. (2020). Microglia-organized scar-free spinal cord repair in neonatal mice. *Nature* *587*, 613–618.
- Libbing, C.L., McDevitt, A.R., Azcueta, R.-M.P., Ahila, A., and Mulye, M. (2019). Lipid Droplets: A Significant but Understudied Contributor of Host–Bacterial Interactions. *Cells* *8*, 354.
- Lim, F.T., Ogawa, S., and Parhar, I.S. (2016). Spred-2 expression is associated with neural repair of injured adult zebrafish brain. *J. Chem. Neuroanat.* *77*, 176–186.
- Lim, M.X., Png, C.W., Tay, C.Y.B., Teo, J.D.W., Jiao, H., Lehming, N., Tan, K.S.W., and Zhang, Y. (2014). Differential regulation of proinflammatory cytokine expression by mitogen-activated protein kinases in macrophages in response to intestinal parasite infection. *Infect. Immun.* *82*, 4789–4801.
- López-Juárez, A., Titus, H.E., Silbak, S.H., Pressler, J.W., Rizvi, T.A., Bogard, M., Bennett, M.R., Ciruolo, G., Williams, M.T., Vorhees, C. V., et al. (2017). Oligodendrocyte Nf1 Controls Aberrant Notch Activation and Regulates Myelin Structure and Behavior. *Cell Rep.* *19*, 545–557.
- López-Otín, C., Blasco, M.A., Partridge, L., Serrano, M., and Kroemer, G. (2013). The hallmarks of aging. *Cell* *153*, 1194.
- Lucin, K.M., and Wyss-Coray, T. (2009). Immune Activation in Brain Aging and Neurodegeneration: Too Much or Too Little? *Neuron* *64*, 110–122.
- Lui, H., Zhang, J., Makinson, S.R., Cahill, M.K., Kelley, K.W., Huang, H.Y., Shang, Y., Oldham, M.C., Martens, L.H., Gao, F., et al. (2016). Progranulin Deficiency Promotes Circuit-Specific Synaptic Pruning by Microglia via Complement Activation. *Cell*.
- Luo, P., Li, X., Wu, X., Dai, S., Yang, Y., Xu, H., Jing, D., Rao, W., Xu, H., Gao, X., et al. (2019). Preso regulates NMDA receptor-mediated excitotoxicity via modulating nitric oxide and calcium responses after traumatic brain injury. *Cell Death Dis.* *10*, 1–14.
- La Manno, G., Soldatov, R., Zeisel, A., Braun, E., Hochgerner, H., Petukhov, V., Lidschreiber, K., Kastrioti, M.E., Lönnerberg, P., Furlan, A., et al. (2018). RNA velocity of single cells. *Nature*.

- Marschallinger, J., Iram, T., Zardeneta, M., Lee, S.E., Lehallier, B., Haney, M.S., Pluvinage, J. V., Mathur, V., Hahn, O., Morgens, D.W., et al. (2020). Lipid-droplet-accumulating microglia represent a dysfunctional and proinflammatory state in the aging brain. *Nat. Neurosci.*
- Martens, L.H., Zhang, J., Barmada, S.J., Zhou, P., Kamiya, S., Sun, B., Min, S.W., Gan, L., Finkbeiner, S., Huang, E.J., et al. (2012). Progranulin deficiency promotes neuroinflammation and neuron loss following toxin-induced injury. *J. Clin. Invest.* *122*, 3955–3959.
- Marz, M., Schmidt, R., Rastegar, S., Strahle, U., März, M., Schmidt, R., Rastegar, S., and Strähle, U. (2010). Expression of the transcription factor *Olig2* in proliferating cells in the adult zebrafish telencephalon. *Dev Dyn* *239*, 3336–3349.
- Marz, M., Schmidt, R., Rastegar, S., and Strahle, U. (2011). Regenerative response following stab injury in the adult zebrafish telencephalon. *Dev Dyn* *240*, 2221–2231.
- März, M., Chapouton, P., Diotel, N., Vaillant, C., Hesel, B., Takamiya, M., Lam, C.S., Kah, O., Bally-Cuif, L., Strähle, U., et al. (2010). Heterogeneity in progenitor cell subtypes in the ventricular zone of the zebrafish adult telencephalon. *Glia* *58*, 870–888.
- Masuda, T., Sankowski, R., Staszewski, O., Böttcher, C., Amann, L., Sagar, Scheiwe, C., Nessler, S., Kunz, P., van Loo, G., et al. (2019). Spatial and temporal heterogeneity of mouse and human microglia at single-cell resolution. *Nature* *566*, 388–392.
- Mattson, M.P. (2000). Apoptosis in neurodegenerative disorders. *Nat. Rev. Mol. Cell Biol.* *1*, 120–129.
- Mattson, M.P. (2012). Energy intake and exercise as determinants of brain health and vulnerability to injury and disease. *Cell Metab.* *16*, 706–722.
- Mattson, M.P., and Arumugam, T. V. (2018). Hallmarks of Brain Aging: Adaptive and Pathological Modification by Metabolic States. *Cell Metab.* *27*, 1176–1199.
- Mattson, M.P., Gleichmann, M., and Cheng, A. (2008). Mitochondria in Neuroplasticity and Neurological Disorders. *Neuron* *60*, 748–766.
- McKenzie, J.A., Spielman, L.J., Pointer, C.B., Lowry, J.R., Bajwa, E., Lee, C.W., and Klegeris, A. (2017). Neuroinflammation as a Common Mechanism Associated with the Modifiable Risk Factors for Alzheimer’s and Parkinson’s Diseases. *Curr. Aging Sci.* *10*.
- Menzel, L., Kleber, L., Friedrich, C., Hummel, R., Dangel, L., Winter, J., Schmitz, K., Tegeder, I., and Schäfer, M.K.E. (2017). Progranulin protects against exaggerated axonal injury and astrogliosis following traumatic brain injury. *Glia* *65*, 278–292.
- Michinaga, S., and Koyama, Y. (2019). Dual roles of astrocyte-derived factors in regulation of blood-brain barrier function after brain damage. *Int. J. Mol. Sci.* *20*.
- Miyamoto, N., Pham, L.D.D., Hayakawa, K., Matsuzaki, T., Seo, J.H., Magnain, C., Ayata, C., Kim, K.W., Boas, D., Lo, E.H., et al. (2013). Age-

related decline in oligodendrogenesis retards white matter repair in mice. *Stroke* *44*, 2573–2578.

Mizoguchi, Y., and Monji, A. (2017). Microglial intracellular Ca²⁺ signaling in synaptic development and its alterations in neurodevelopmental disorders. *Front. Cell. Neurosci.* *11*, 69.

Molliex, A., Temirov, J., Lee, J., Coughlin, M., Kanagaraj, A.P., Kim, H.J., Mittag, T., and Taylor, J.P. (2015). Phase Separation by Low Complexity Domains Promotes Stress Granule Assembly and Drives Pathological Fibrillization. *Cell* *163*, 123–133.

Molofsky, A. V., Slutsky, S.G., Joseph, N.M., He, S., Pardal, R., Krishnamurthy, J., Sharpless, N.E., and Morrison, S.J. (2006). Increasing p16INK4a expression decreases forebrain progenitors and neurogenesis during ageing. *Nature* *443*, 448–452.

Moore, E.E., Moore, H.B., Kornblith, L.Z., Neal, M.D., Hoffman, M., Mutch, N.J., Schöchl, H., Hunt, B.J., and Sauter, A. (2021). Trauma-induced coagulopathy. *Nat. Rev. Dis. Prim.* *7*, 30.

Del Moral, M.O., Asavapanumas, N., Uzcátegui, N.L., and Garaschuk, O. (2019). Healthy brain aging modifies microglial calcium signaling in vivo. *Int. J. Mol. Sci.* *20*.

Moritz, C., Berardi, F., Abate, C., and Peri, F. (2015). Live imaging reveals a new role for the sigma-1 (σ 1) receptor in allowing microglia to leave brain injuries. *Neurosci. Lett.* *591*, 13–18.

Mosher, K.I., and Wyss-Coray, T. (2014). Microglial dysfunction in brain aging and Alzheimer's disease. *Biochem. Pharmacol.* *88*, 594–604.

Moyzis, R.K., Buckingham, J.M., Cram, L.S., Dani, M., Deaven, L.L., Jones, M.D., Meyne, J., Ratliff, R.L., and Wu, J.R. (1988). A highly conserved repetitive DNA sequence, (TTAGGG)(n), present at the telomeres of human chromosomes. *Proc. Natl. Acad. Sci. U. S. A.* *85*, 6622–6626.

Neumann, M., Sampathu, D.M., Kwong, L.K., Truax, A.C., Micsenyi, M.C., Chou, T.T., Bruce, J., Schuck, T., Grossman, M., Clark, C.M., et al. (2006). Ubiquitinated TDP-43 in frontotemporal lobar degeneration and amyotrophic lateral sclerosis. *Science* (80-.). *314*, 130–133.

Nimmerjahn, A., Kirchhoff, F., and Helmchen, F. (2005). Resting microglial cells are highly dynamic surveillants of brain parenchyma in vivo. *Science* (80-.). *308*, 1314–1318.

Obermann, J., Wagner, F., Kociaj, A., Zambusi, A., Ninkovic, J., Hauck, S.M.S.M., and Chapouton, P. (2019). The Surface Proteome of Adult Neural Stem Cells in Zebrafish Unveils Long-Range Cell-Cell Connections and Age-Related Changes in Responsiveness to IGF. *Stem Cell Reports* *12*.

Olah, M., Patrick, E., Villani, A.C., Xu, J., White, C.C., Ryan, K.J., Piehowski, P., Kapasi, A., Nejad, P., Cimpean, M., et al. (2018). A transcriptomic atlas of aged human microglia. *Nat. Commun.* *9*, 1–8.

Oosterhof, N., Boddeke, E., and van Ham, T.J. (2015). Immune cell dynamics in the CNS: Learning from the zebrafish. *Glia* *63*, 719–735.

- Palazuelos, J., Klingener, M., and Aguirre, A. (2014). TGF β signaling regulates the timing of CNS myelination by modulating oligodendrocyte progenitor cell cycle exit through SMAD3/4/FoxO1/Sp1. *J. Neurosci.* *34*, 7917–7930.
- Panas, M.D., Ivanov, P., and Anderson, P. (2016). Mechanistic insights into mammalian stress granule dynamics. *J. Cell Biol.* *215*, 313–323.
- Park, B., Buti, L., Lee, S., Matsuwaki, T., Spooner, E., Brinkmann, M.M., Nishihara, M., and Ploegh, H.L. (2011). Granulin Is a Soluble Cofactor for Toll-like Receptor 9 Signaling. *Immunity* *34*, 505–513.
- Paul, A., Belton, A., Nag, S., Martin, I., Grotewiel, M.S., and Duttaroy, A. (2007). Reduced mitochondrial SOD displays mortality characteristics reminiscent of natural aging. *Mech. Ageing Dev.* *128*, 706–716.
- Pennetta, G., and Welte, M.A. (2018). Emerging Links between Lipid Droplets and Motor Neuron Diseases. *Dev. Cell* *45*, 427–432.
- Peri, F., and Nüsslein-Volhard, C. (2008). Live Imaging of Neuronal Degradation by Microglia Reveals a Role for v0-ATPase $\alpha 1$ in Phagosomal Fusion In Vivo. *Cell* *133*, 916–927.
- Perner, F., Perner, C., Ernst, T., and Heidel, F.H. (2019). Roles of JAK2 in Aging, Inflammation, Hematopoiesis and Malignant Transformation. *Cells* *8*.
- Petkau, T.L., Neal, S.J., Orban, P.C., MacDonald, J.L., Hill, A.M., Lu, G., Feldman, H.H., MacKenzie, I.R.A., and Leavitt, B.R. (2010). Progranulin expression in the developing and adult murine brain. *J. Comp. Neurol.* *518*, 3931–3947.
- Petrie, T.A., Strand, N.S., Tsung-Yang, C., Rabinowitz, J.S., and Moon, R.T. (2014). Macrophages modulate adult zebrafish tail fin regeneration. *Dev.* *141*, 2581–2591.
- Piccin, D., Tufford, A., and Morshead, C.M. (2014). Neural stem and progenitor cells in the aged subependyma are activated by the young niche. *Neurobiol. Aging* *35*, 1669–1679.
- Pickford, F., Marcus, J., Camargo, L.M., Xiao, Q., Graham, D., Mo, J.R., Burkhardt, M., Kulkarni, V., Crispino, J., Hering, H., et al. (2011). Progranulin is a chemoattractant for microglia and stimulates their endocytic activity. *Am. J. Pathol.* *178*, 284–295.
- De Preux Charles, A.S., Bise, T., Baier, F., Marro, J., and Jaźwińska, A. (2016). Distinct effects of inflammation on preconditioning and regeneration of the adult zebrafish heart. *Open Biol.* *6*.
- Protter, D.S.W., and Parker, R. (2016). Principles and Properties of Stress Granules. *Trends Cell Biol.* *26*, 668–679.
- Qin, L., Liu, Y., Hong, J.S., and Crews, F.T. (2013). NADPH oxidase and aging drive microglial activation, oxidative stress, and dopaminergic neurodegeneration following systemic LPS administration. *Glia* *61*, 855–868.
- Rhinn, H., and Abeliovich, A. (2017). Differential Aging Analysis in Human Cerebral Cortex Identifies Variants in TMEM106B and GRN that Regulate Aging Phenotypes. *Cell Syst.* *4*, 404-415.e5.

- Roden, C., and Gladfelter, A.S. (2021). RNA contributions to the form and function of biomolecular condensates. *Nat. Rev. Mol. Cell Biol.* *22*, 183–195.
- Ruhl, T., Jonas, A., Seidel, N.I., Prinz, N., Albayram, O., Bilkei-Gorzo, A., and Von Der Emde, G. (2015). Oxidation and Cognitive Impairment in the Aging Zebrafish. *Gerontology* *62*, 47–57.
- Salazar, D.A., Butler, V.J., Argouarch, A.R., Hsu, T.Y., Mason, A., Nakamura, A., McCurdy, H., Cox, D., Ng, R., Pan, G., et al. (2015). The progranulin cleavage products, granulins, exacerbate TDP-43 toxicity and increase TDP-43 levels. *J. Neurosci.* *35*, 9315–9328.
- Shimoda, N., Izawa, T., Yoshizawa, A., Yokoi, H., Kikuchi, Y., and Hashimoto, N. (2014). Decrease in cytosine methylation at CpG island shores and increase in DNA fragmentation during zebrafish aging. *Age (Omaha)*. *36*, 103–115.
- Shin, Y., and Brangwynne, C.P. (2017). Liquid phase condensation in cell physiology and disease. *Science (80-.)*. *357*.
- Shoyab, M., McDonald, V.L., Byles, C., Todaro, G.J., and Plowman, G.D. (1990). Epithelins 1 and 2: Isolation and characterization of two cysteine-rich growth-modulating proteins. *Proc. Natl. Acad. Sci. U. S. A.* *87*, 7912–7916.
- Sieger, D., Moritz, C., Ziegenhals, T., Prykhozhiy, S., and Peri, F. (2012). Long-Range Ca²⁺ Waves Transmit Brain-Damage Signals to Microglia. *Dev. Cell* *22*, 1138–1148.
- Simon, D.W., McGeachy, M.J., Bayır, H., Clark, R.S.B., Loane, D.J., and Kochanek, P.M. (2017). The far-reaching scope of neuroinflammation after traumatic brain injury. *Nat. Rev. Neurol.* *2017* *13*, 171–191.
- Smith, K.R., Damiano, J., Franceschetti, S., Carpenter, S., Canafoglia, L., Morbin, M., Rossi, G., Pareyson, D., Mole, S.E., Staropoli, J.F., et al. (2012). Strikingly different clinicopathological phenotypes determined by progranulin-mutation dosage. *Am. J. Hum. Genet.* *90*, 1102–1107.
- Snowden, J.S., Pickering-Brown, S.M., Mackenzie, I.R., Richardson, A.M.T., Varma, A., Neary, D., and Mann, D.M.A. (2006). Progranulin gene mutations associated with frontotemporal dementia and progressive non-fluent aphasia. *Brain* *129*, 3091–3102.
- Sochocka, M., Diniz, B.S., and Leszek, J. (2017). Inflammatory Response in the CNS: Friend or Foe? *Mol. Neurobiol.* *54*, 8071–8089.
- Solchenberger, B., Russell, C., Kremmer, E., Haass, C., and Schmid, B. (2015). Granulin Knock Out Zebrafish Lack Frontotemporal Lobar Degeneration and Neuronal Ceroid Lipofuscinosis Pathology. *PLoS One* *10*, e0118956.
- Stahon, K.E., Bastian, C., Griffith, S., Kidd, G.J., Brunet, S., and Baltan, S. (2016). Age-related changes in axonal and mitochondrial ultrastructure and function in white matter. *J. Neurosci.* *36*, 9990–10001.
- Stephan, A.H., Madison, D. V., Mateos, J.M., Fraser, D.A., Lovelett, E.A., Coutellier, L., Kim, L., Tsai, H.H., Huang, E.J., Rowitch, D.H., et al. (2013). A dramatic increase of C1q protein in the CNS during normal aging. *J. Neurosci.* *33*, 13460–13474.

- Stocchetti, N., and Zanier, E.R. (2016). Chronic impact of traumatic brain injury on outcome and quality of life: A narrative review. *Crit. Care* 20.
- Szepesi, Z., Manouchehrian, O., Bachiller, S., and Deierborg, T. (2018). Bidirectional Microglia–Neuron Communication in Health and Disease. *Front. Cell. Neurosci.* 12, 323.
- Tai, H.C., and Schuman, E.M. (2008). Ubiquitin, the proteasome and protein degradation in neuronal function and dysfunction. *Nat. Rev. Neurosci.* 9, 826–838.
- Tanaka, Y., Matsuwaki, T., Yamanouchi, K., and Nishihara, M. (2013a). Exacerbated inflammatory responses related to activated microglia after traumatic brain injury in progranulin-deficient mice. *Neuroscience*.
- Tanaka, Y., Matsuwaki, T., Yamanouchi, K., and Nishihara, M. (2013b). Increased lysosomal biogenesis in activated microglia and exacerbated neuronal damage after traumatic brain injury in progranulin-deficient mice. *Neuroscience* 250, 8–19.
- Tang, W., Lu, Y., Tian, Q.Y., Zhang, Y., Guo, F.J., Liu, G.Y., Muzaffar Syed, N., Lai, Y., Alan Lin, E., Kong, L., et al. (2011). The growth factor progranulin binds to tnfr receptors and is therapeutic against inflammatory arthritis in mice. *Science* (80-.). 332, 478–484.
- Tsuruma, K., Saito, Y., Okuyoshi, H., Yamaguchi, A., Shimazawa, M., Goldman, D., and Hara, H. (2018). Granulin 1 promotes retinal regeneration in zebrafish. *Investig. Ophthalmol. Vis. Sci.* 59, 6057–6066.
- Valdez, C., Wong, Y.C., Schwake, M., Bu, G., Wszolek, Z.K., and Krainc, D. (2017). Progranulin-mediated deficiency of cathepsin D results in FTD and NCL-like phenotypes in neurons derived from FTD patients. *Hum. Mol. Genet.* 26, 4861–4872.
- Viales, R.R., Diotel, N., Ferg, M., Armant, O., Eich, J., Alunni, A., Marz, M., Bally-Cuif, L., Rastegar, S., and Strahle, U. (2015). The helix-loop-helix protein id1 controls stem cell proliferation during regenerative neurogenesis in the adult zebrafish telencephalon. *Stem Cells* 33, 892–903.
- Villeda, S.A., Luo, J., Mosher, K.I., Zou, B., Britschgi, M., Bieri, G., Stan, T.M., Fainberg, N., Ding, Z., Eggel, A., et al. (2011). The ageing systemic milieu negatively regulates neurogenesis and cognitive function. *Nature* 477, 90–96.
- Waly, B. El, Macchi, M., Cayre, M., and Durbec, P. (2014). Oligodendrogenesis in the normal and pathological central nervous system. *Front. Neurosci.* 8, 145.
- Wang, X., Saegusa, H., Huntula, S., and Tanabe, T. (2019). Blockade of microglial Cav1.2 Ca²⁺ channel exacerbates the symptoms in a Parkinson’s disease model. *Sci. Rep.* 9, 1–13.
- Wang, Y., Moges, H., Bharucha, Y., and Symes, A. (2007). Smad3 null mice display more rapid wound closure and reduced scar formation after a stab wound to the cerebral cortex. *Exp. Neurol.* 203, 168–184.
- Wheeler, R.J., Lee, H.O., Poser, I., Pal, A., Doeleman, T., Kishigami, S., Kour, S., Anderson, E.N., Marrone, L., Murthy, A.C., et al. (2019). Small molecules

for modulating protein driven liquid-liquid phase separation in treating neurodegenerative disease. *BioRxiv*.

Whittemore, K., Vera, E., Martínez-Nevado, E., Sanpera, C., and Blasco, M.A. (2019). Telomere shortening rate predicts species life span. *Proc. Natl. Acad. Sci. U. S. A.* *116*, 15122–15127.

Wiesner, D., Tar, L., Linkus, B., Chandrasekar, A., olde Heuvel, F., Dupuis, L., Tsao, W., Wong, P.C., Ludolph, A., and Roselli, F. (2018). Reversible induction of TDP-43 granules in cortical neurons after traumatic injury. *Exp. Neurol.* *299*, 15–25.

Wils, H., Kleinberger, G., Pereson, S., Janssens, J., Capell, A., Van Dam, D., Cuijt, I., Joris, G., De Deyn, P.P., Haass, C., et al. (2012). Cellular ageing, increased mortality and FTLD-TDP-associated neuropathology in progranulin knockout mice. *J. Pathol.* *228*, 67–76.

Winblad, B., Amouyel, P., Andrieu, S., Ballard, C., Brayne, C., Brodaty, H., Cedazo-Minguez, A., Dubois, B., Edvardsson, D., Feldman, H., et al. (2016). Defeating Alzheimer's disease and other dementias: A priority for European science and society. *Lancet Neurol.* *15*, 455–532.

Wolozin, B., and Ivanov, P. (2019). Stress granules and neurodegeneration. *Nat. Rev. Neurosci.* *20*, 649–666.

Wu, Y., Dissing-Olesen, L., MacVicar, B.A., and Stevens, B. (2015). Microglia: Dynamic Mediators of Synapse Development and Plasticity. *Trends Immunol.* *36*, 605–613.

Xia, X., and Serrero, G. (1998). Identification of cell surface binding sites for PC-cell-derived growth factor, PCDGF, (Epithelin/Granulin precursor) on epithelial cells and fibroblasts. *Biochem. Biophys. Res. Commun.* *245*, 539–543.

Yang, P., Mathieu, C., Kolaitis, R.M., Zhang, P., Messing, J., Yurtsever, U., Yang, Z., Wu, J., Li, Y., Pan, Q., et al. (2020). G3BP1 Is a Tunable Switch that Triggers Phase Separation to Assemble Stress Granules. *Cell* *181*, 325–345.e28.

Yin, F., Banerjee, R., Thomas, B., Zhou, P., Qian, L., Jia, T., Ma, X., Ma, Y., Iadecola, C., Beal, M.F., et al. (2010). Exaggerated inflammation, impaired host defense, and neuropathology in progranulin-deficient mice. *J. Exp. Med.*

Yu, H., Lu, S., Gasiior, K., Singh, D., Vazquez-Sanchez, S., Tapia, O., Toprani, D., Beccari, M.S., Yates, J.R., Cruz, S. Da, et al. (2020). HSP70 chaperones RNA-free TDP-43 into anisotropic intranuclear liquid spherical shells. *Science* (80-.).

Zambusi, A., and Ninkovic, J. (2020). Regeneration of the central nervous system-principles from brain regeneration in adult zebrafish. *World J. Stem Cells*.

Zambusi, A., Pelin Burhan, Ö., Di Giaimo, R., Schmid, B., and Ninkovic, J. (2020). Granulins Regulate Aging Kinetics in the Adult Zebrafish Telencephalon. *Cells*.

Zhang, J., Velmeshev, D., Hashimoto, K., Huang, Y.H., Hofmann, J.W., Shi, X., Chen, J., Leidal, A.M., Dishart, J.G., Cahill, M.K., et al. (2020). Neurotoxic

microglia promote TDP-43 proteinopathy in progranulin deficiency. *Nature* *588*.

Zhou, R., Yazdi, A.S., Menu, P., and Tschopp, J. (2011). A role for mitochondria in NLRP3 inflammasome activation. *Nature* *469*, 221–226.

Zhu, J., Nathan, C., Jin, W., Sim, D., Ashcroft, G.S., Wahl, S.M., Lacomis, L., Erdjument-Bromage, H., Tempst, P., Wright, C.D., et al. (2002). Conversion of proepithelin to epithelins: Roles of SLPI and elastase in host defense and wound repair. *Cell* *111*, 867–878.

Publications

- **Zambusi, A.**; Pelin Burhan, Ö.; Di Giaimo, R.; Schmid, B.; Ninkovic, J. **Granulins Regulate Aging Kinetics in the Adult Zebrafish Telencephalon.**
Cells 2020; 9, 350. doi.org/10.3390/cells9020350.
- **Zambusi, A.***; Novoselc, K.T.*; Koupourtidou, C.; Kalpazidou, S.; Hutten, S.; Silva, L.; Schmid, B.; Delbridge, C.; Schlegel, J.; Aliee, H.; Theis, F.; Dormann, D.; Ninkovic, J. **Phase-separated TDP-43 regulates the activation states of microglia after traumatic brain injury.**
The paper is currently in revision in Nature Neuroscience.
- (Review) **Zambusi, A.**; Ninkovic, J. **Regeneration of the central nervous system-principles from brain regeneration in adult zebrafish.**
World J Stem Cells 2020; 12(1): 8-24. doi: 10.4252/wjsc.v12.i1.8.
- Obermann, J.; Wagner, F.; Kociaj, A.; **Zambusi, A.**; Ninkovic, J.; Hauck, S. M.; Chapouton, P. **The Surface Proteome of Adult Neural Stem Cells in Zebrafish Unveils Long-Range Cell-Cell Connections and Age-Related Changes in Responsiveness to IGF.**
Stem Cell Reports (2019). <https://doi.org/10.1016/j.stemcr.2018.12.005>.
- Sanchez-Gonzalez, R.; Koupourtidou, C.; Lepko, T.; **Zambusi, A.**; Novoselc, K.T.; Durovic, T.; Aschenbroich, S.; Schwarz, V.; Breunig, C.; Straka, H.; Huttner, H.; Irmeler, M.; Beckers, J.; Wurst, W.; Zwergal, A.; Schauer, T.; Straub, T.; Czopka, T.; Trümbach, D.; Götz, M.; Stricker, S.; Ninkovic, J. **Activation of innate immune pathways after brain injury promotes scar formation and impairs tissue recovery.**
The paper has been resubmitted after revision to EMBO Journal.

Eidesstattliche Versicherung/Affidavit

Hiermit versichere ich an Eides statt, dass ich die vorliegende Dissertation *“The role of granulins in regulating adult zebrafish brain homeostasis and regeneration”* selbstständig angefertigt habe, mich außer der angegebenen keiner weiteren Hilfsmittel bedient und alle Erkenntnisse, die aus dem Schrifttum ganz oder annähernd übernommen sind, als solche kenntlich gemacht und nach ihrer Herkunft unter Bezeichnung der Fundstelle einzeln nachgewiesen habe.

I hereby confirm that the dissertation *“The role of granulins in regulating adult zebrafish brain homeostasis and regeneration”* is the result of my own work and that I have only used sources or materials listed and specified in the dissertation.

München, den
Munich, date
16th August, 2021

Unterschrift
Signature
Alessandro Zambusi

Declaration of author contributions

1. **Zambusi, A.**; Pelin Burhan, Ö.; Di Giaimo, R.; Schmid, B.; Ninkovic, J. **Granulins Regulate Aging Kinetics in the Adult Zebrafish Telencephalon.** *Cells* (2020).

The contribution of authors is as follows:

Conceptualization, A.Z., R.D.G., J.N.; methodology, A.Z., Ö.P.B.; software, A.Z.; validation, A.Z., J.N.; visualization, A.Z., J.N.; formal analysis, A.Z., J.N.; investigation, A.Z., Ö.P.B., B.S., J.N.; data curation, A.Z., Ö.P.B., J.N.; writing, A.Z., J.N.; supervision, B.S., J.N.; funding acquisition, B.S., J.N.

For this paper I was involved in performing and analyzing all the experiments, with the exception for the measurement of telomere length (Figure 9, Panel B), performed by Özge Pelin Burhan.

I was also involved in writing, editing and reviewing the paper, together with Prof. Dr. Jovica Ninkovic.

As an open access article distributed under the Creative Commons Attribution License and as author of this publication, I have the right to include it in a thesis or dissertation.

Confirmation of author contributions:

Prof. Dr. Jovica Ninković

Alessandro Zambusi

2. Obermann, J.; Wagner, F.; Kociaj, A.; **Zambusi, A.**; Ninkovic, J.; Hauck, S. M.; Chapouton, P. **The Surface Proteome of Adult Neural Stem Cells in Zebrafish Unveils Long-Range Cell-Cell Connections and Age-Related Changes in Responsiveness to IGF.** *Stem Cell Reports* (2019).

The contribution of authors is as follows:

J.O. performed the gene ontology analysis, generated all graphs representing the proteomics dataset, and wrote the proteomics methods; F.W. produced the SFRP-EGFP construct; A.K. contributed to the FACS experiments; **A.Z. performed the RNA-seq experiments on FACS isolated cells**; J.N. analyzed the RNA-seq results; S.M.H. designed the biotinylation protocols and analyzed the mass spectrometry data; P.C. conceived the study, performed the experiments, prepared the figures, and wrote the manuscript.

For this paper I was involved in preparing RNA-Seq libraries from FACS isolated cells.

Confirmation of author contributions:

Prof. Dr. Jovica Ninković

Alessandro Zambusi

3. **Zambusi, A.***; Novoselec, K.T.*; Koupourtidou, C.; Kalpazidou, S.; Hutten, S.; Silva, L.; Schmid, B.; Delbridge, C.; Schlegel, J.; Aliee, H.; Theis, F.; Dormann, D.; Ninkovic, J. **Phase-separated TDP-43 regulates the activation states of microglia after traumatic brain injury.** *The paper is currently in revision in Nature Neuroscience.*

* The authors contributed equally to the manuscript

The contribution of authors is as follows:

A.Z., K.T.N. and J.N. conceived the project and experiments. A.Z., K.T.N., S.K., S.H., L.S., C.D. performed the experiments and analyzed the data; A.Z., K.T.N., C.K., H.A. and F.T. performed the bioinformatic analyses. A.Z., K.T.N., and J.N. wrote the manuscript with inputs from B.S., J.S., and D.D. J.N. and D.D. supervised research and acquired funding.

For this paper I was involved in performing and analyzing all the experiments, with the exception for staining of brain tissues from patients with stroke (Figure 7), performed by Sofia Kalpazidou and Dr. Claire Delbridge. All the materials required to study the phase-separation of TDP-43 and FUS were provided by Dr. Saskia Hutten, Lara Silva and Prof. Dr. Dorothee Dormann.

I was also involved in writing, editing and reviewing the paper, together with Prof. Dr. Jovica Ninkovic and Klara Tereza Novoselec.

Confirmation of author contributions:

Prof. Dr. Jovica Ninković

Alessandro Zambusi

Klara Tereza Novoselec

4. Sanchez-Gonzalez, R.; Koupourtidou, C.; Lepko, T.; **Zambusi, A.**; Novoselec, K.T.; Durovic, T.; Aschenbroich, S.; Schwarz, V.; Breunig, C.; Straka, H.; Huttner, H.; Irmeler, M.; Beckers, J.; Wurst, W.; Zwergal, A.; Schauer, T.; Straub, T.; Czopka, T.; Trümbach, D.; Götz, M.; Stricker, S.; Ninkovic, J. **Activation of innate immune pathways after brain injury promotes scar formation and impairs tissue recovery.** *The paper has been resubmitted after revision to EMBO Journal.*

For this paper I was involved in performing FACS sorting and preparing RNA-Seq libraries.

I was also involved in editing and reviewing the paper.

Confirmation of author contributions:

Prof. Dr. Jovica Ninković

Dr. Rosario Sanchez-Gonzalez

Alessandro Zambusi

Acknowledgements

When I arrived in Munich in 2014 as a Master's student, I would have never imagined living this journey. I was not sure whether the PhD would have been the right choice for me. Now that I see the end of it and think about all the moments spent, I can say that I do not regret it. I grew as a person and as scientist, and for this I must thank all the people that accompanied me during these 6 years. I really hope that I gave you all something in return for everything you granted me.

The first person I feel the need to acknowledge is Jovica. You were a great mentor and supervisor. You gave me several chances to prove myself even during the toughest times when I was not confident about myself. You encouraged me and guided me throughout my PhD, and I would like to thank you for giving me the freedom to think and try on my own, facing failures and successes. I will always be grateful to you for giving me the opportunity to work here...and for keeping me even if, for some months, the PCR was not working.

The second person that I would like to acknowledge is Magdalena. I still remember the first thing you told me when we met: "Oh another Italian in the lab". I hope I convinced you that we need more of those messy Italians around. Your passion is contagious and your energy really pushed me to give a little bit more every time. You were always supportive even though I was not one of your students and for this I cannot thank you enough.

A special mention goes to Emily Baumgart. I spent a lot of time with you when I joined the lab and you were a key part for my decision to stay and do a PhD. You guided me and taught me everything I know. You were not only a teacher but also a dear friend. I could not have wished for someone better than you to take my first steps around.

Many thanks go to Klara. You made the crazy choice to work with me, and it is not an easy task, so I hope you do not regret it. You motivated me when I was lazy and made me laugh when I was tired. You were an instrumental part for what I achieved in the last few years. And the trips to Slovenia were memorable.

Thanks to all the core members of the group, with whom I spent most of my life in these 6 years, and thanks to the new people that recently joined. Specifically, thanks to Joana, Anita, Tamara, Tjasa, Christina, Sven, Veronika, Finja, Sofia, Priya, Silvija, Viviane and Julia. Thank you all not only for your help but also for creating a wonderful environment. It was always a pleasure to come to work and spend some good time with you. I also wanted to apologize for my awful singing skills. I hope you can find in your heart the strength to forgive me.

Thanks to all the people I collaborated with, thanks to my TAC members for all the precious inputs and suggestions, thanks to the GSN for all the support provided during my PhD and thank to Michaelone for taking care of the fish.

As I also had a lot of fun outside the lab, I would like to thank all the friends I met during these years. Without you this journey would not have been the same.

Among them, I would like to specifically thank three people that were extremely important to me during my stay in Munich: Namone, Campone e Marcone. Even though destiny divided us, we are still in touch after all these years. I consider you among my best friends and I hope we will meet again for some exciting weekends around the world...do not forget that you still owe me a Michelin star dinner.

Special thanks to my parents that encouraged me to follow my dream of trying new experiences abroad. It is thanks to them that this journey started in the first place and I will be forever grateful to them.

Lastly, a special mention for Sabrina. They say that behind a great man there is a great woman, and this could not be truer. You made me a better person without limiting my personality. You were always there when I needed you and I cannot express how grateful I am to have your unconditional love and support. I hope you will never get tired of us.